DOCTORAL THESIS

Various Modulated Hybrid Pulse Compression for Advanced Ultrasound Technology and Its Non-destructive Testing Applications

A Thesis submitted to Brunel University London
in accordance with the requirements
for award of the degree of Doctor of Philosophy

in

the department of "Electronic and Electrical Engineering"

Zeng Fan

February 1, 2022

Declaration of Authorship

I, Student Name, declare that the work in this dissertation was carried out in accordance with the requirements of the University's Regulations and Code of Practice for Research Degree Programmes and that it has not been submitted for any other academic award. Except where indicated by specific reference in the text, the work is the candidate's own work. Work done in collaboration with, or with the assistance of, others, is indicated as such. Any views expressed in the dissertation are those of the author.

SIGNED: ..... DATE: .....

(Signature of student)

Abstract

Ultrasound is a sound wave with a frequency greater than 20 kHz. It obeys the propagation laws of reflection, refraction, diffraction, and scattering. Because of its excellent physical properties, ultrasound has been used in a variety of fields, including industry and medicine. There are many techniques that use ultrasound as detection methods in the field of non-destructive testing (NDT) and medical treatment. In a typical ultrasound system, a sine wave or pulse signal with a fit window is considered as the transmitted signal. This results in low accuracy in some special situations, such as testing high attenuation material. The signal-to-noise ratio (SNR) is an important parameter for evaluating the performance of an echo signal or imaging. However, under high attenuation materials or noisy conditions, SNR will significantly decrease. Under these conditions, valid information in the received signal will be obscured by noise. This situation can cause errors in the detection system. In an ultrasound system, increasing the SNR of the echo signal can reduce detection errors and improve accuracy.

First, in ultrasound systems, a noise reduction method based on pulse compression has been investigated and applied. Convolution and modulation were used in the proposed method to generate new hybrid emission signals. The hybrid codes can only be distinguished by a special matched filter that is related to the emission signals. The echo signals processed by a special matched filter have a high main lobe and a very low side lobe, implying that the side lobe level and SNR will increase. When compared to traditional denoising methods, the proposed method can significantly improve SNR while only requiring a change in the transmission code without requiring any hardware changes.

Second, in a low voltage ultrasonic testing (UT) system, a hybrid phase modulated code excitation method based on the Barker and Golay code pairs was proposed and implemented. In a UT system, the lower the pulsing voltage, the lower the SNR of the signal. Attempting to reduce the pulsing voltage will result in noisy and unusable results. The proposed hybrid method can increase main lobe power in low average power transmitted and received signals. The proposed method has been theoretically examined and then tested in simulation studies. The experimental results showed that the main lobe level of the code produced by convolution of Barker code and Golay code pairs is around 30 dB higher than the simple pulse, and the main lobe of the combined code is around 15 dB higher than the traditional Barker code, with the sidelobe being the same as the Baker code that constitutes this combined code. As a result, the combined code's peak sidelobe

level (PSL) is approximately 5 dB lower than the traditional Barker code. Because of this, UT devices can be used in real-world applications, even in low-voltage situations.

Third, the torsional wave mode T(0,1) hybrid phase modulated code excitation method has been proposed and applied in a long range guided wave testing (GWT) system. The proposed hybrid method combines the Barker and Golay code pair and is modulated by a fitted sine wave. This method combines the benefits of these two coding methods and increases code length flexibility. The SNR and PSL of the processed signal are used to assess the method's performance. The proposed method has been tested in GWT using both finite element method (FEM) simulation and real-world testing. The results of pipeline laboratory testing revealed that the best increasing SNR of BCG is around 33.5 dB when compared to a simple pulse at 40 kHz, and the peak sidelobe level is around -24 dB. The proposed method, as well as other traditional methods, were used for pipeline defect detection testing. The results of the tests showed that the hybrid coded excitation method can detect notches that are difficult to detect with other methods and effectively improve the SNR. The applied method's increasing SNR is around 6 dB, which agrees with the simulation and laboratory testing results. In UGW testing, the proposed coded excitation method was highly regarded.

Finally, the non-linear frequency modulated (NLFM) hybrid pulse compression method has been proposed and implemented in an ultrasound imaging (UI) system. The proposed code combines the Barker and Golay codes and is modulated using a non-linear frequency method based on the Zak transform. Theoretical research on signal generation and decoding has been presented, as well as cyst phantom simulation. The simulation analysis shows that the novel code method can improve the contrast ratio by 15.96 dB and the SNR by 36.64 dB when compared to a simple pulse signal. Overall, this study demonstrated that the proposed novel method can be effectively used in ultrasound detection methods to improve performance.

Acknowledgements

I would like to express my sincere gratitude to my supervisor, Dr Hongying Meng for providing the opportunity to carry out the research and his excellent guidance and supervision throughout the work process. His scientific vision, research attitude and enthusiasm for research have always inspired me. It was my great privilege and honour to be supervised by him.

I would like to thank my parents Zhongjun Fan, Chunbo Xu and my wife Xinyu Zhang for their continuous support, patience and understanding, which I will forever cherish. I can not do this without them. This thesis is dedicated to them.

I would like to thank Dr John Rudlin and Mr. Giorgos Asfis from TWI Ltd for their support the research. Their guidance has really benefited me a lot. My sincere appreciation goes to Dr Xudong Niu from University of Bristol, Dr Shengrun Shi from University of Birmingham and Dr Longjie Wang from Brunel University London for their helpful suggestions for this work. I would also like to thank all my colleagues in the NDT team for their help and making the working environment pleasant.

Last but not the least, my warm thanks to Dr Lu Gan and Dr Juvaria Syeda for their valuable assistance.

Contents

List of Figures

List of Tables

List of Abbreviations

ACF Autocorrelation function

ACUT Air-coupled ultrasonictesting

AE Acoustic Emission

AMR Anisotropic Magneto-resistive

ASIC Application specificintegrated circuit

BCG Barker-sequence combined Golay code

BMG Barker-sequence-modulated Golay

CE coded excitation

CNR Contrast to noise ratio

CT Computedtomography

DDF Dynamic depth focusing

DOF Depth of field

DW Diverging wave

ECG Electrocardiogram

ECT Eddy current testing

ET Electromagnetic Testing

FEM Finite element method

GFRP Glass fibre reinforced plastics

GMR Giant magneto-resistance

GPR Ground Penetrating Radar

GWT Guided wave testing

HFR High Frame rate

ILI In-lineInspection

IR Infrared Testing

LFM Linear frequency modulated

LM Laser Testing Method

LT Leak Testing

MBN Magnetic Barkhausen noise

MFL Magnetic Flux Leakage

MMM Metal magnetic memor

MT Magnetic Particle Testing

NDT Non-destructive testing

NLFM Non linear frequency modulation

NR Neutron Radiographic Testing

PACE Photoacoustic coding excitation

PCBG Pseudo Chirp-Barker-Golay

PIGs Pipeline Inspection Gauges

PMP Permanent magnet perturbation

PRF Pulse repetition frequency

PSL Peak sidelobe level

PT Liquid Penetrant Testing

RF Radio-frequency

RSLL range side lobe level

RT Radiographic Testing

SLL Side lobe level

SNR Signal-to-noise ratio

SVD Singular value decomposition

SVM Support vector machine

TECO Transien eddy current oscillations

TMR Tunneling Magneto-resistive

TOFD Time-of-flight diffraction

TX transmitter

UFT Ultrasonic fatigue testing

UI Ultrasound imaging

UT Ultrasonic testing

VA Vibration Analysis

VHCF Very high cycle fatigue

VT Visual Testing

WT Wavelet transform

XBT X-ray backscatter technique

Chapter 1

Introduction

1.1 Background

The inspection industry is critical in both daily life and industrial production. Material or tissue, such as pipelines, railway networks, and human organs, may have defects as a result of the stresses and environmental conditions they are subjected to. Internal or external defects in these materials might damage their structure, limiting their service life or producing hazardous circumstances. On December 11, 2012, a 20-inch diameter underground natural gas pipeline of the Columbia Gas Transmission Corporation ruptured. The spilled high pressure natural gas was immediately burned, resulting in a loss of millions of dollars. The investigation determined that the primary cause of the accident was external corrosion of the pipeline and a lack of recent inspections [1]. Figure 1.1 depicts the accident scene. As a result, inspection is vital for the safety of both humans and the environment.

Non-destructive testing (NDT) is an essential and effective tool for industrial development in the inspection industry, and it reflects a country's level of industrial development. The NDT industry's application areas have gradually expanded, and the NDT market has also expanded. According to a new MarketsandMarkets research report, the NDT market value in 2018 was 11.4 billion British pounds and is expected to reach 16.8 billion British pounds by 2024, with a compound annual growth rate of 6.7% from 2019 to 2024. In this massive market, ultrasonic inspection will hold a significant market share, accounting for approximately 30-40% of the NDT market. According to the British Institute of NDT, over 25,000 non-destructive inspections are performed in factories and on-sites every day in the UK to detect defects and damages in various products and structures. It is estimated

Figure 1.1: The accident scene of pipeline rupture [1].

that there are over 120,000 inspectors in the world.

Because NDT has excellent market prospects and can be used in a variety of fields, it is critical to research NDT in the industrial field. There are many NDT method by using different physical properties. Because of its excellent physical properties, ultrasound has been widely used as a detection method in engineering, biology, chemistry, materials sciences, and other fields. The majority of these areas covered by ultrasound are depicted in Figure 1.2. High sensitivity, fast speed, low cost, human body safety, and the capacity to discover and quantify flaws are all advantages of ultrasonic detection systems. Ultrasound wave is a kind of mechanical wave and it can propagate in the material at a certain speed and direction. When an ultrasound wave encounters heterogeneous interfaces with different acoustic impedance, it can produce reflection, refraction, and waveform conversion (such as defects or the bottom surface of the object, etc.). According to the principle, the ultrasonic detection method can be classified as ultrasonic pulse echo technique, Time-of-flight diffraction (TOFD), phased array ultrasonic testing, guided wave testing, and so on.

1.2 Motivation

Since NDT is very important in industry and daily life, it can detect and monitor the health of materials. Ultrasound detection technique is the most extensively utilised method in NDT. However, several ultrasonic technologies have drawbacks that lead to erroneous detection results and low efficiency. To improve axial resolution in ultrasonic testing systems, high-frequency short ultrasonic pulses are frequently used as the transmitted signal. The signal has the ability to avoid echoes overlapping, but this results in poor signal-to-

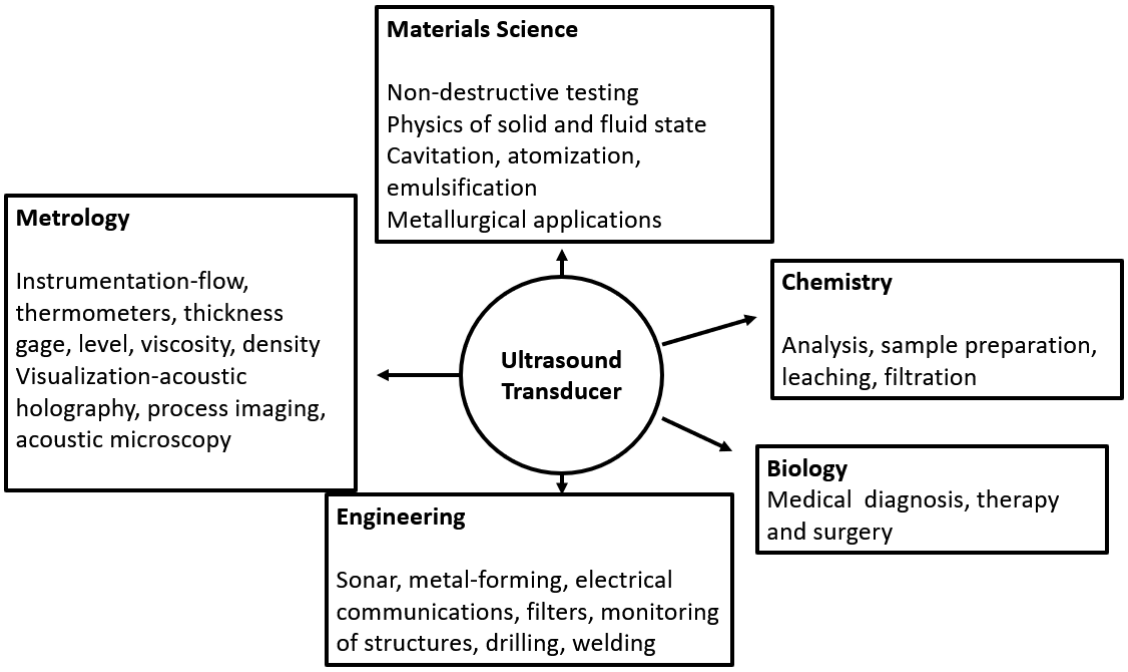

Figure 1.2: The most area covered by ultrasound transducers.

noise ratio (SNR) and depth penetration [4].

In a guided wave testing system, guided waves can propagate over a long range in an elongated structure while guided by its boundaries. This technique has high susceptibility to interference on a propagation path [5]. Depending on the SNR, guided wave testing has a high sensitivity [6]. Increasing performance in pipe inspection by changing transducers, on the other hand, will raise testing costs.

There are several ways to improve the penetration depth of high resolution imaging in an ultrasound imaging system. Cannata [7] increased the sensitivity of the transmitted sensor, which improved the quality of ultrasonic imaging. However, this technique is constrained by transducer material and technological level [8], making it difficult to break through by improving transducer sensitivity. The power of the ultrasound transducer can be increased to improve signal intensity, but it is limited by the safety threshold of human body.

Traditional ultrasonic detection methods and equipment have the inherent problem of being extremely sensitive to unwanted external noise. As a consequence, it is imperative to use some specific analysis methods to distinguish the signals depending on the noise and the defect in echo signal, furthermore, to reduce the influence of the noise on the echo signal.

1.3 Aim and objectives

Ultrasonic detection techniques are widely used in the industrial and medical field, but they have limitations in certain situations. The main aim of this study is to solve the existing problems by using different modulation methods in ultrasound detection techniques. The specific problems include the improvement of SNR for low voltage ultrasonic testing systems, the improvement of the performance for long range guided wave testing systems and the enhancement of imaging performance for ultrasound imaging systems.

The following objectives have been established in order to achieve the aims of this study.

- A review of the literature on NDT, ultrasonic testing, and signal processing methods was conducted in order to determine the current research status. The limitations of commonly used methods are discovered through analysis, and solutions to these limitations are discussed. As a result, the groundwork for future research has been established.
- To address the limitations of current methods, an alternative method based on the pulse compression technique was proposed and implemented. The feasibility of the hybrid modulation method has been demonstrated theoretically.
- As transmitted signals, different bits of the Barker code, Golay code pair, and various Barker code convoluted Golay code pair sequences are used to improve the SNR of low-voltage ultrasonic testing systems. The modulation methods will be verified theoretically and their results will be validated with the Matlab Field II simulation results.
- To improve the SNR of the guided wave testing system, torsional wave mode T(0,1) of the Barker code and the Barker code convoluted Golay coded pair sequence are applied as transmitted signals. The hybrid modulation method needs to be theoretically verified, and the FEM simulation results in Abaqus should be validated with the theoretical results. To demonstrate the feasibility of this method, laboratory tests on the pipeline at various frequencies are required. Field tests on faulty pipelines are required to demonstrate the superiority of this method.
- To improve the SNR and resolution of the ultrasound imaging system, the nonlinear frequency modulated hybrid coded excitation method will be applied as transmitted signals. This method necessitates theoretical validation as well as cyst simulation. To determine the superiority of this method, the improved SNR and resolution of the applied method need to be compared.

1.4 Thesis structure

This thesis has six chapters overall.

Chapter 1 provides an overview of the background of the research. The market for NDT is very large, and the ultrasound detection method is an important part of NDT. This chapter also discusses the motivations and aims of this research.

In Chapter 2, a review of the literature on NDT, ultrasound methods, and pulse compression techniques is provided. Firstly, traditional detection methods, such as electromagnetic detection, optical detection, and acoustic detection, are briefly described. Following that, various ultrasound methods and the judging indicator are discussed. Finally, a pulse compression technique involving frequency modulation and phase modulation is presented.

In Chapter 3, the convolution of Barker and Golay codes for low voltage UT systems is introduced. In a low voltage UT system, a new hybrid coded excitation method has been presented and used. This section introduces the generation and compression process of the hybrid coded excitation method and the theoretical study of the present method. The system performance has been compared with the traditional coded excitation method. The present method has the advantage that the processed echo signal has higher SNR and lower side lobe level than others. The simulation which uses the Field II toolbox in MATLAB is also presented in this section.

In Chapter 4, the long range guided wave testing method based on different modulation and hybrid coded excitation methods is investigated. Firstly, the guided wave testing method was introduced. In this research, the pulse and frequency modulated methods based on the torsional wave mode T(0,1) are implemented in a guided wave testing system. The system applies commonly used methods and proposed methods for transmitting signals. Secondly, the proposed method is applied in Abaquse, which is a finite element method (FEM) software. A pipeline module was modelled to compare the performance of different excitation methods. Thirdly, the laboratory tests in the pipeline have been implemented. The experiment used various transmitted signals, including the proposed method, on different frequencies to find out the performance of this method. Finally, the proposed methods are applied in pipeline with defected field experiments.

Chapter 5 presents a study on ultrasound imaging systems by using non-linear frequency modulated coded excitation methods. A non-linear frequency modulation method based on the Zak transform is applied in this section. The hybrid transmitted signal has the

ability to improve SNR and resolution, which can be used in ultrasound imaging systems. In order to verify the feasibility of this method, the theoretical study is presented in this section. Different modulation methods are compared in Matlab and cyst simulations are present to prove the performance of the proposed method.

The last chapter concludes this thesis, providing future directions for the proposed hybrid pulse compression technique in the ultrasound detection method.

1.5 Thesis contributions

This dissertation presents contributions in the area of pulse compression technique for different ultrasound detection methods, such as ultrasonic testing, guided wave testing, and ultrasound imaging.

- To improve SNR and side lobe level (SLL) in a low voltage ultrasonic testing system with high accuracy and efficiency, a novel hybrid coded excitation code has been generated and compressed. Chapter 3 describes the generation and compression specifications, as well as the simulation results.
- To achieve long-range ultrasound detection, different modulation methods are used to modulate the hybrid coded excitation methods, and they are applied to guided wave testing. The methods include the following: frequency modulated Barker code and Barker convolution Golay code, and pulse modulated Baker code. The detailed information about each method is presented in Chapter 4. The best performance method is applied in pipeline field detection experiments.
- For an ultrasound imaging system, a non-linear frequency modulation method based on the Zak transform is modulated with hybrid coded excitation. By altering the proposed transmission signal, this study improves the SNR and contrast ratio of the ultrasound imaging system, resulting in significantly improved imaging performance when compared to traditional methods. Through simulations, this study validates the performance. The detailed description of the system is presented in Chapter 5.

1.6 Publication list

Journal paper

- Fan, Z., Niu,X., & Meng, H. 'Hybrid coded excitation of the torsional guided wave mode T(0,1) in pipes' Mechanical Systems and Signal Processing (Submited)
- Fan, Z., Rudlin, J., Asfis, G., & Meng, H. (2019). 'Convolution of Barker and Golay Codes for Low Voltage Ultrasonic Testing.' Technologies, 7(4), 72. https://www.mdpi.com/2227-7080/7/4/72/htm

Conference paper

- Fan, Z.& Meng, H.'Coded excitation with Nonlinear Frequency Modulation Carrier in Ultrasound Imaging System' FENDT 2020, China. https://ieeexplore.ieee.org/document/9337517
- Fan, Z., Rudlin, J.& Meng, H.'Odd Length Barker Code In Ultrasonic Testing To Improve Signal-to-noise Ratio' ECEBPS 2019, London

Poster

- Fan, Z. 'Low voltage coded excitation for in intrinsically safe environment' 2017,London
- Fan, Z. 'A new coded excitation technique to improve SNR in ultrasonic testing' NSIRC conference 2018, Cambridge

Chapter 2

Literature Review

2.1 Non-destructive testing

In both industry and civil engineering, testing and quality inspection are required.Industrial materials often suffer from extreme temperature, high pressure, corrosion, flammable, explosive, and so on. Surface defect or internal defects will seriously affect the mechanical properties of materials and structures. The stress concentration could impact the mechanical properties of the material significantly. Once the material is abnormal, it has the potential to cause a catastrophic accident, resulting in property damage and personal injury. To find out the stages during the life of a material accurately, engineers should have a new method of inspection. For our deteriorating infrastructure, better inspection techniques are required [9].

Traditional inspection methods use artificial methods to detect material defects with the naked eye or a magnifying glass. However, there are some limitations to experience recognition, particularly when dealing with complex defects. Manual classification becomes more difficult when the size and shape of the material vary greatly. It's also difficult to detect defects in the material with the naked eye. Therefore, traditional detection methods have been unable to adapt to modern industrial production and requirements for rapid detection and real-time detection. To overcome these limitations, non-destructive testing (NDT) methods have been developed with the development of computer science, such as optics, acoustics, and computer graphics.

NDT is a broad category of analysis techniques used in the science and technology industries. NDT can assess the properties of materials, components, or systems without

causing any damage. Test method names often refer to the type of penetrating medium or the equipment used to perform that test [10]. The common NDT methods are: Acoustic Emission Testing (AE), Ultrasonic Testing (UT), Guided Wave Testing (GW), Ultrasound imaging (UI) Electromagnetic Testing (ET), Eddy Current Testing (ECT), Magnetic Flux Leakage (MFL), Permanent Magnet Perturbation (PMP), Laser Testing Methods (LM), Leak Testing (LT), Neutron Radiographic Testing (NR), and Radiographic Testing (RT).

Due to the diversity of testing methods, NDT can be used in testing practices in a variety of situations. These methods meet the requirements for rapid detection and real-time detection. Non-destructive techniques are useful for evaluating the condition of structures.The primary benefit of NDT is the avoidance of structure damage during evaluation, which has improved in recent years. Several researchers performed NDT tests to evaluate the condition of structures. The rest of this chapter introduces NDT methods and the recent work of these methods. By reviewing these existing technologies and applications, the advantages and disadvantages of these methods can be understood and inspired for future work.

2.1.1 Electromagnetic method

Magnetostriction and piezomagnetic effects have received more attention in the NDT field because of the fundamental feature of ferromagnetic materials, which is the coupling between stress and magnetic field and the change in magnetization of ferromagnetic materials with stress. There have been a lot of non-destructive magnetic techniques being proposed in recent years. The most popular magnetic NDT technologies can be assorted into active magnetic methods such as MFL, ECT, PMP, magnetic Barkhausen noise (MBN) and passive magnetic methods such as recently developed metal magnetic memory (MMM) [11].

The MFL technique is based on an increase in magnetic refraction leakage and is characterized by peaks in the test signal. Nabighian *et al*. [12] introduced the MFL device, which was built by Rudolf Eickemeyer in 1889 to detect section changes or magnetic penetration in ferrous metals. Nestleroth [13] combined high-magnetization and low-magnetization MFL technology for stress to detect axial and circumferential. By orienting the magnetic field around the pipe, the magnetized axial defect can affect more of the magnetic field and is easier to detect. As a non-contact sensing method, the MFL method has the advantages of powerful penetration and detection capabilities. This method is effective for both internal and external defects, and has immunity to non-ferromagnetic objects. However,

the limitation of this method is that it can only detect ferromagnetic material, and the detection device is heavy, leading to inconvenient testing. Figure 2.1 shows the fundamental principles of the MFL. The basic idea is to magnetise the steel with a strong magnet. The magnetic field ”leaks” from the steel in areas where there is corrosion or missing metal.

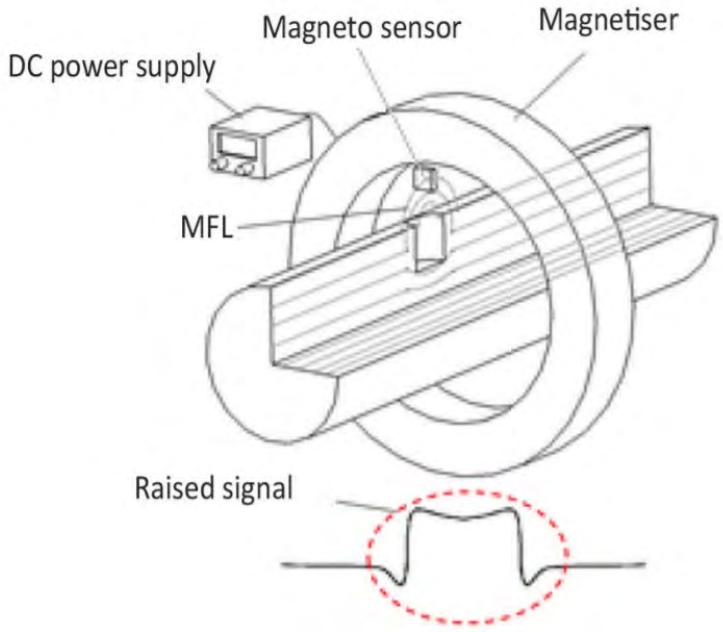

Figure 2.1: The fundamental principles of the MFL [2].

The secondary magnetic field of ECT based on the eddy current is interrupted due to the defects of the test object, thereby generating troughs in the test signal. The origin of ECT methods can be attributed to Hans Christian Ørsted, who demonstrated that a magnetic field is developed when an electric current passes through a wire and discovered Oersted's Law [11]. Although the electric current he used was direct current from a battery, this discovery led the Englishman Michael Faraday to discover electromagnetic induction in 1831, which is the operating principle of ECT. This method is used to detect near-surface cracks and corrosion in metallic objects such as tubes and aircraft fuselage structures. Figure 2.2 shows the fundamental principles of the ECT. This technology uses electromagnetic induction to discover and characterise surface and subsurface defects in conductive materials.

As a non-contact sensing method, the ECT method has the advantage that it is suitable for automatic detection of all metal materials. The equipment using this technology is easy to install and carry, and the sensor is light in weight. However, it can only detect the surface and subsurface. James *et al*. [14] applied ECT in carbon fiber reinforced polymer composite structures because of these advantages. The structure of this material is

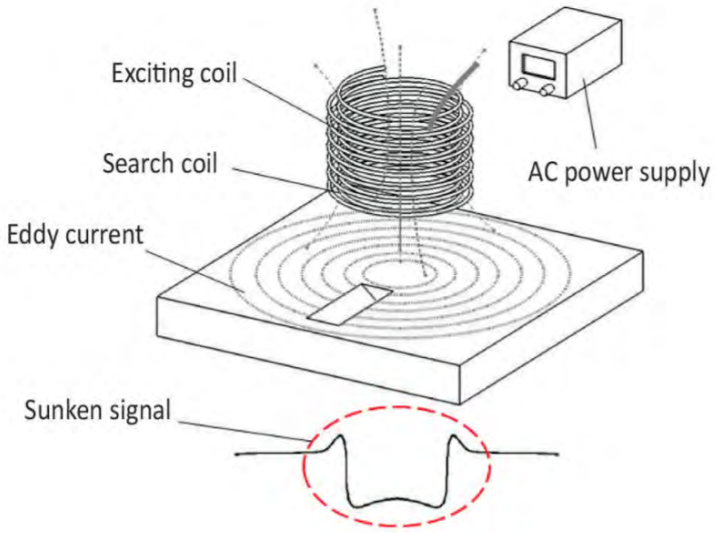

Figure 2.2: The fundamental principles of the ECT [2].

usually detected using UT and X-ray methods. Eddy currents can be generated by ECT because of the inherent conductivity of carbon fibre. FEM simulation was used to simulate the defects of composite materials and the high frequency ECT method was used as a detecting method. Rifai *et al*. [15] designed and applied a novel ECT probe for ferromagnetic pipes. This new probe was combined with the ECT inspection system to improve the transducers by optimizing the number of excitation coils and GMR sensors. Zhu *et al*. [16] combined ECT and deeply learned ECT to improve the recognition rate. It was verified through eddy current inspection experiments that the recognition rate of this novel machine learning model based on CNN for defects is close to 100%. Dmitriev *et al*. [17] applied ECT in titanium sheets joined by a welded joint.The correlation of the ECT response at different depths is determined by examining the detection depth of the two titanium sheets. This study has a big impact on how we judge the quality of titanium board welding.

The principle of PMP is that it is generated by the permanent magnet and the test object in the magnetic field, and the spatial magnetic disturbance caused by the defect of the object will produce a distorted test signal. Figure 2.3 shows the fundamental principles of the PMP. According to the magnetic perturbation mechanism, magnetic field perturbation represents information such as a change in the boundary of the magnetic interaction field.

Xiao and Zhang [18] used small permanent magnets to magnetize ferromagnetic materials and the signal measured by the Hall sensor is the component of the vertical amplitude magnetic flux density to detect material defects. The method is simple and easy to implement, suitable for detecting small defects. Due to its high sensitivity and spatial resolu-

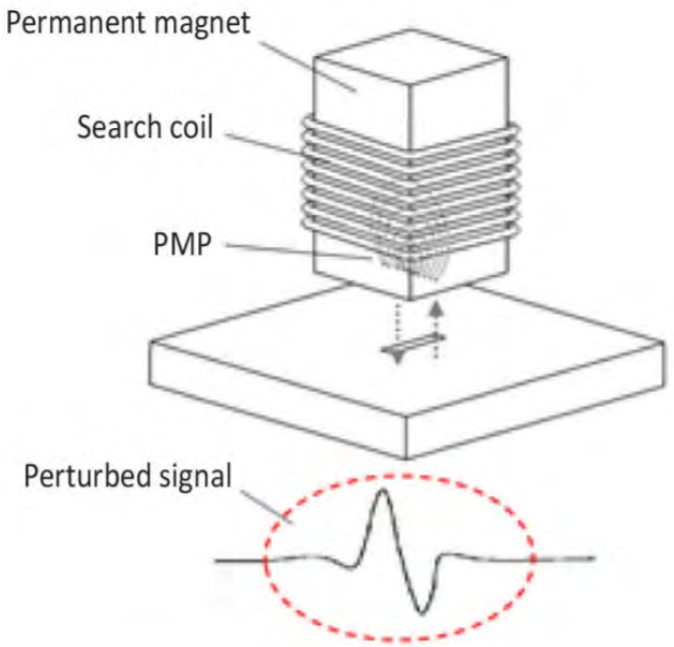

Figure 2.3: The fundamental principles of the PMP [2].

tion, it can provide information about the shape of defects. Fei *et al*. [19] improved the ability of pulsed magnetic flux leakage to test shallow defects by analyzing the signals in pulsed magnetic flux leakage.

As a non-contact sensing method, the PMP method has the advantage of not requiring an additional current source for excitation. It is, however, only for ferromagnetic materials and is not appropriate for internal defects.

Ricci *et al*. [20] built an on-line inspection system for stainless steel strips which can enlarge the set of detectable defects by exploiting machine vision and magnetic imaging apparatuses to improve the detection and classification tasks. Xiuli and Yang *et al*. [21] presented a new type of steel wire rope NDT detector apparatus which is composed of a magnetizer and sensor array, using the highly sensitive and giant magneto-resistance (GMR) micro sensor to inspect the inner and outer flaws of the steel wire rope. Evanson *et al*. [22] had developed a DC magnetic NDT technique using a SQUID (superconducting quantum interference device) coupled to a planar gradiometer for the inspection of structures such as flat steel plates and steel pipes. Pasha and Kahn [23] found that the low-cost shelf Anisotropic Magneto-resistive (AMR) and Tunneling Magneto-resistive (TMR) magnetometers, coupled with permanent magnets, can detect flaws in ferromagnetic pipelines that can replace the traditional expensive Pipeline Inspection Gauges (PIGs) and In-Line Inspection (ILI) methods. Angani and Ramos [24] used a new NDT method called transient eddy current oscillations (TECO) which uses a probe that consists of a capacitor

and an induction coil discharging in a free oscillation fashion, while the resultant magnetic field is detected by using a Hall-effect sensor. And to improve the accuracy of the experiment, a model-based support vector machine (SVM) analysis was used on the experimental data. Qiao *et al*. [25] developed a new type of intelligent sensor based on MMM technology to solve the early diagnosis problem of fatigue fracture caused by stress concentration.

Based on the magnetic-stress coupling effect, various magnetic NDT techniques have been used in the NDT area and applied in a lot of research. However, due to the high sensitivity of magnetic stress to the microstructure of complex materials, this technology still faces challenges.

2.1.2 Optical method

Due to its non-destructive imaging characteristics with high accuracy and sensitivity, optical NDT has received more and more attention in recent years [26]. The main types of optical NDT are surface measurements. There are many optical NDT methods, such as fibre optics, electronic speckle, infrared thermography, and X-ray. X-ray as an effective method has been applied in NDT of social and infrastructures due to its high performance that an attenuating map in 2-D can be generated by penetrating thick structures [27]. Figure 2.4 shows the fundamental principles of X-Ray testing. This method inspects materials and components with ionising radiation with the goal of locating and quantifying defects and degradation in material properties.

Degrieck *et al*. [28] embedded optical fibres with a Bragg sensor in a simple composite laminate and tested it. It was found that the strain of the optical fibres with a Bragg sensor had a linear relationship with the pressure on the material, which proved the feasibility of optical fibres with a Bragg sensor in NDT testing. Peng *et al*. [29] proposed a method to detect internal defects based on laser speckle shearing interference. The method achieved the relevant image information from speckle pattern to measure the depth of defect. Inagaki *et al*. [30] evaluated the detection mechanism and quantitative limits under various conditions by conducting related experimental research on infrared thermal imaging cameras.

Kolkoori *et al*. [31] presented a new X-ray backscatter technique (XBT) which uses a special twisted slit collimator to inspect the whole object by changing the viewing direction of the X-ray backscatter camera. It can be used for aerospace materials with only single-

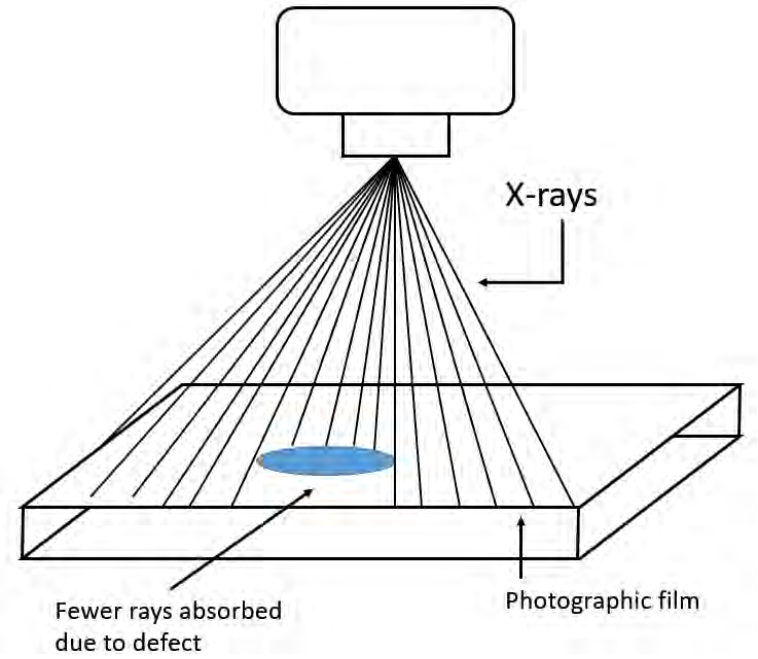

Figure 2.4: The fundamental principles of the X-Ray testing.

sided access. Cho *et al*. [32] studied the compressed-sensing (CS)-based deblurring and implemented the proposed algorithm to provide the feasibility of the deblurring in x-ray non-destructive testing. Tian *et al*. [27] developed a photon counting imaging detector system which uses high energy X-rays for testing thick objects. The application specific integrated circuit (ASIC) has been used in the system as high instant counter. Rometsch *et al*. [33] used polychromatic X-ray absorption radiography to detect the selective laser melting and the experimental data suggested that the method was in good agreement with theoretical expectations. Plessis *et al*. [34] compared the industrial X-ray computed tomography (CT) with the medical CT scanners, and found that the industrial CT is better for applications such as quick scout-scans, high throughput applications and larger objects.

Optical sensing and detection methods have a wide range of advantages, such as anti-electromagnetic interference, non-contact, higher sensitivity and resolution. However, optical NDT methods are high cost and have poor permeability, which have certain limitations.

2.1.3 Acoustics method

A sound wave is the form of mechanical vibration (or energy) of the object. The vibration frequency of ultrasound is greater than 20 kHz or more. People call these inaudible sound

waves ”ultrasound” because the frequency of vibration per second is very high, exceeding the general upper limit of human hearing. Ultrasound has a variety of characteristics due to its high frequency. Firstly, ultrasound has a lot of power; its energy is much higher than the average sound wave. As a result, it can be used for a variety of tasks such as cutting, welding, and drilling. Furthermore, industrial and medical ultrasound is commonly used for ultrasonic detection due to its high frequency, short wavelength, low diffraction, and good orientation. Ultrasound and audible sound are essentially the same. Their essence is a mechanical vibration, usually in the form of longitudinal wave propagation in the elastic medium. They are a form of energy transmission. The difference between them is the frequency of ultrasound is high, the wavelength is short and it has good beam and directional property within a certain distance along a straight line.

The propagation law of ultrasonic reflection is not fundamentally different from the law of audible acoustic waves such as refraction, diffraction, scattering and so on. But the wavelength of the ultrasound is very short, only a few centimetres or even a few thousandths of a millimetre. Compared with audible acoustic waves, ultrasound has many singular properties. The ultrasonic wavelength is very short in propagation characteristics, and the size of the obstacle is frequently many times larger than the ultrasonic wavelength. So the ultrasonic diffraction ability is poor, it is in the uniform medium can be directed linear transmission. The shorter the wavelength of ultrasound, the more significant the propagation characteristics. In power characteristics, when the sound is in the air, the particles in the air promote the reciprocating vibration of particles and work. Sonic power is the physical quantity that represents the speed of the sound. At the same intensity, the higher the frequency of the sound waves, the greater the power it has. As the ultrasonic frequency is very high, so the power of the ultrasonic wave is larger compared with the general sound.

In order to understand the origin and inspiration of acoustic testing method, the history of this method needs to be studied. On April 14, 1912, the Titanic, dubbed the ”unsinkable ship,” capsized in the Atlantic Ocean after colliding with an iceberg. There were 1,519 people on board who died as a result of the shipwreck. The news of the Titanic’s sinking shocked the entire world. So far, it has piqued the scientific community’s interest. Lewis Richardson applied for a patent for ultrasound echolocation/ranging after only one week, kicking off modern ultrasound research [35]. In the First World War in 1916, a team led by French physicist Paul Langevin conducted research on underwater submarine sonar technology to detect submarines [36]. The researchers investigated the vibration of quartz piezoelectric crystals and successfully recorded ultrasonic waves propagating in water. They detect and locate underwater submarines by using ultrasound.

Sokolov [37] published an article in the 1930s on the propagation of ultrasonic oscillations in various objects, proposing the use of ultrasonic wave penetration to detect internal defects in opaque objects. Later, he published an article on internal flaw detection in metallic materials, in which he described the ultrasonic echo test results. The transmitting and receiving probes of the testing instrument should be placed on both sides of the test piece and always maintain the corresponding relationship between the probe positions. The defect detection sensitivity and detection efficiency of the proposed system are very low in this case.

Firestone [36] pioneered pulsed ultrasonic testing using a pulse-echo technique in the 1940s. The detector works by transmitting and receiving ultrasound waves from the same side of the object, and it can detect small defects inside the object. It is capable of accurately determining the location of the defect as well as measuring the defect size.

After 1950, the A-scan pulse reflection ultrasonic detector was widely used in steel smelting, machinery manufacturing, shipbuilding, and other fields to detect cast and forged steel parts, as well as thick-walled steel plates. Simultaneously, the medical diagnostic capabilities of ultrasound were investigated in Japan. With the advancement of electronic technology and the invention of microprocessors in the 1970s, the performance of ultrasonic testing instruments was greatly improved. Researchers have introduced a computer-aided automatic ultrasonic inspection device that is mainly used for objects with relatively regular shapes. At the same time, signal processing technology have been successively carried out.

Due to the directionality and penetration of ultrasound waves, it has been widely used for NDT application [38]. Ramadas *et al*. [39] designed a conformal mapping technique based on the popular 2-D ultrasonic phased arrays. Experimental results demonstrated a working sparse array transducer capable of performing volumetric imaging. Guo *et al*. [40] designed an automatic ultrasonic testing system which is applicable for the detecting of typical defected polyethylene (PE) material by using the phased array ultrasonic technique. Legendre *et al*. [41] presented a wavelet transform (WT) of inspection signals method which is based on neural network. They suggested that the weld recognition quality can be improved by this method. Moallemi *et al*. [42] used an array-based immersion ultrasonic testing method to detect an ultrasonic array and solid samples in water, which can result in a strong interference signal. The results showed that the proposed approach yields a lower root mean squared error for the parameter estimates, compared to the root mean squared velocity technique. Ricci *et al*. [43] built an application of a pulse-compression procedure which can enhance the signal-to-noise ratio. The paper discussed the procedure to reduce quantization noise and the possibility of reconstructing signal

based on pseudorandom m-sequences. Camacho *et al*. [44] studied auto-focusing along with dynamic depth focusing (DDF), which can get the best resolution at all depths and avoid the burden of calculation when detecting any shape of the parts. Li and Zhou [45] found that using the pulse compression techniques based on P4 polyphase codes can improve the SNR of air-coupled ultrasonic testing systems. They proposed that this technique can generate lower noise of compressed signal and higher peak side lobe (PSL) ratio. This experiment showed that the SNR raised up to 12.11 dB. Flore *et al*. [46] found ultrasonic fatigue testing (UFT) can be applied for cyclic tension testing of glass fibre reinforced plastics (GFRP) which are rarely investigated in the very high cycle fatigue (VHCF) regime. The testing time could be reduced by using UFT and fatigue data which were generated by using a conventional servo-hydraulic device at a low frequency of 10Hz. Similar results were obtained by Cavuto and Martarelli under the condition of using a laser-ultrasonic diagnostic measurement procedure to detect the integrity of the wheel for the safety of the railway [47]. The ultrasonic wave generated by a high energy pulsed laser spreads in the train wheel. It is more flexible than the standard technology applied to wheel-rail diagnostics.

2.2 Ultrasound technology in NDT

Section 2.1 reviewed the most widely used NDT methods, such as the electromagnetic NDT method, optical NDT method, and acoustics NDT method. Because the acoustic NDT method has a wide range of technical applications, it can detect the structure of a variety of materials, and has comprehensive advantages over other NDT methods for determining the parameters of internal defects. And this technology has high sensitivity, the equipment is light and can be used for on-site detection.

The transmitting probes are used to transmit ultrasonic waves to the surface of the structure. When ultrasonic waves propagate inside the structure, they will have different reflected signals when they encounter different interfaces. The reflected signals are used to observe the time difference between different signals being delivered to the probe. This method can check the internal defects of the structure. The height and position of the echo signal displayed on the screen can be used to judge the size, position and general nature of the defect. The sine wave is commonly used as a transmitted signal. The quality of the echo signal is critical for obtaining accurate detection results. The following section discusses commonly used acoustic methods.

2.2.1 High frequency ultrasonic testing

Ultrasonic NDT technology is one of the conventional detection technologies. Compared with other conventional NDT technology, it has a wide range of measured objects. This technology has the characteristics of large depth of detection, accurate positioning of defects, high detection sensitivity, low cost, convenient use, fast speed, harmless to the human body and easy to use on site.

At present, many metal materials and components are used in the quality of online monitoring and product inspection, such as steel plate, pipe, welding, surfacing layer, composite layer, pressure vessel and high-pressure pipe, rail and motorcycle parts, ribs and integrated circuit lead detection. This technology can also be used for the detection of new materials, such as organic composite materials, metal-based composite materials, structural ceramic materials, ceramic-based composite materials. Ultrasonic testing technology has become a pillar of composite materials.

This technology is used for non-metallic testing, such as concrete, rock, pile and pavement and other quality inspection. The applications, including its internal defects, internal stress, strength are gradually increased.

This technology can be used to test large structures, pressure vessels and complex equipment. In particular, ultrasound imaging has the advantages of intuitiveness, ease of detection and higher accuracy. This technology can be used for ultrasonic testing in the nuclear power industry.

This technique can be used for other aspects of ultrasonic testing. For example, ultrasound detection technology has been widely used in the field of medical diagnosis. People are currently trying to use ultrasound detection technology to open other new areas and industries, such as people trying to use ultrasonic testing technology for blood pressure control in non-contact detection systems, for identification performance analysis and also for fault diagnosis systems [48].

The Pulse reflection method is the use of ultrasonic pulse wave incident on two different media interface reflection on the principle of detection. This method uses the same transducer as a transmitter and receiver. The received signal is displayed on the screen.

The basic principles and waveform are shown in Figure 2.5. When there is no defect in the structure, the received waveform is shown on the left of Figure 2.5. The screen only shows the beginning of wave T and bottom of wave B. When there is a defect that is

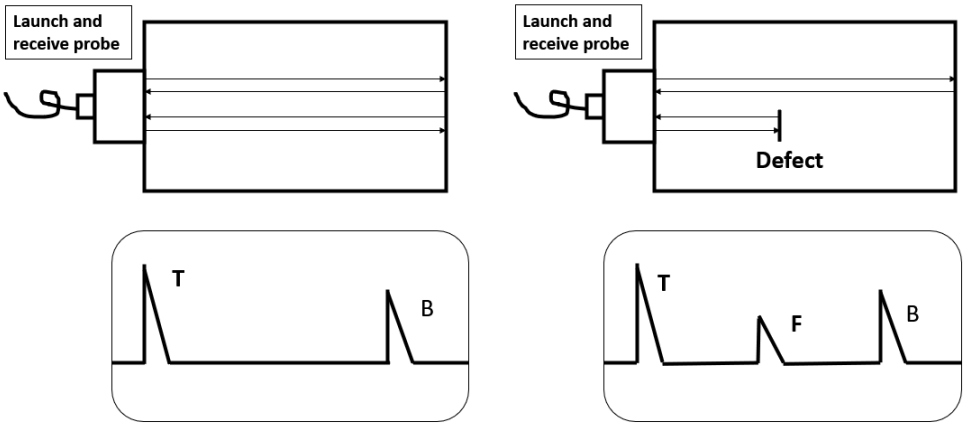

Figure 2.5: The fundamental principles of the ultrasound pulse echo technique.

smaller than the cross section of the beam, the defective wave F appears and the position of the F wave on the time base axis depends on the defective sound path Lf. The position of the defect in the specimen can be determined by this method. The intensity of the defective echo depends on the size of the defect and the magnitude of the direction angle, whereby the equivalent size of the defect can be evaluated. Due to defects in the acoustic energy reflection, the bottom wave height decreased.

As shown in the right of Figure 2.5, when there is a defect larger than the beam cross section, all acoustic energy will be reflected by the defect. There will be only the beginning of the signal and large defects signal appear on the screen.

Compared to other transmission methods, the pulse reflection method has many advantages. This method is highly sensitive and can be tested when the reflected sound pressure reaches 1% of the starting sound pressure of the wafer. So that smaller defects can be found. This method has high defect positioning accuracy. It is the use of defective wave propagation time, by adjusting the scanning speed to modify the time base and the proportion of the sound path to finally locate the defect. So if the instrument has horizontal linearity, defect positioning is accurate. This method adapts to a wide range of applications, by means of changing the coupling, the probe and the wave can achieve different methods of detection. This method is easy to operate. The pulse reflection wave generally does not need a special scanning device, making great contribute to convenience and flexibility of detection operation for a variety of occasions [49].

But the pulse reflection method also has some shortcomings. This method has a certain blind spot, near the surface defects and thin-walled work is not applicable. This method for the beam axis is not perpendicular to the defect surface, due to the refraction of the

results, so that the probe often cannot receive defect echo signal, likely to cause miss. This method is not suitable for the detection of high attenuation materials due to the propagation of sound waves.

The launch and receive probes of the pulse transmission method are placed on both sides of the test specimen and the two probes of the sound axis on the same line, while ensuring the sound coupling between probe and specimen. When there is no defect in the specimen, the phosphor screen shows the initial wave T and a certain amplitude of the echo pulse B. When there is a small defect, the sound waves are blocked by the defect, the received echo signal amplitude decreases. And when the defect area caused by the defect area in the specimen is larger than that of the beam section, only the starting pulse T and no echo signal are displayed on the phosphor screen as shown in Figure 2.6.

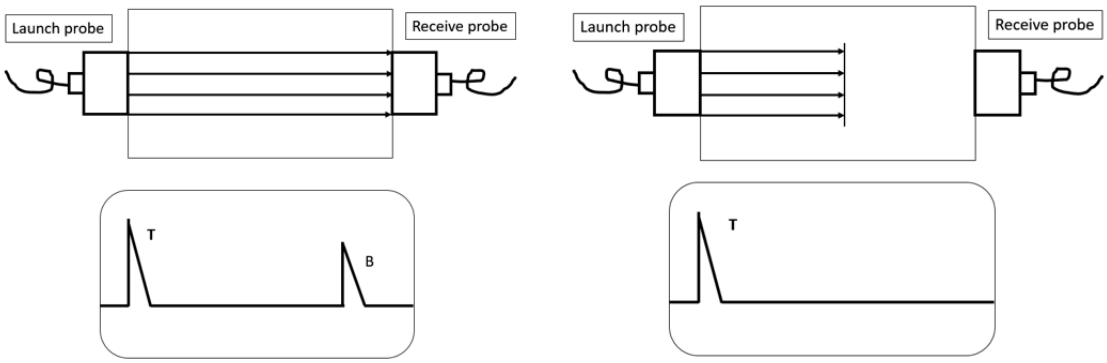

Figure 2.6: The fundamental principles of the pulse transmission technique.

Compared to other transmission methods, the pulse transmission method has many advantages. This method does not exist in the detection of blind spots, suitable for detection of thin-walled parts. This detection method can neglect the effects of defect orientation. Regardless of the defect orientation, if it blocks the beam propagation path, the receiver can be found. This method of detection in the transmission method, the sound wave is a single sound transmission, it is suitable for detecting high attenuation of the material [50].

But the pulse transmission method also has some shortcomings. This detection method has low detection sensitivity. The incident sound pressure can be detected by the receiver probe when pressure changes greater than 20% or more. This detection method cannot determine the depth of the defect location, can only determine the presence or absence of defects. This detection method requires strict positioning of the probe and the relative position of the probe and requires a special probe support device, which is inconvenient

to operate.

Time of Flight Diffraction (TOFD) is a method of detecting defects by means of diffraction energy which is obtained from the ”end angle” and ”end point” of the internal structure of the specimen to be inspected (mainly refers to the defect) for the detection, quantification and positioning of the defect. TOFD requires the probe to receive a weak signal to achieve a sufficient signal to noise ratio. The instrument can record A scan waveform and the formation of D scan map, as well as can be used to solve the triangle method. A scan time value into the depth value. TOFD technology in the 20th century, 70 years by the United Kingdom Ka Weier National Nondestructive Testing Center Dr. Silk first proposed the principle of Dr. Silk from the crack tip diffraction signal research [51].

The diffraction phenomenon is the basic physical principle adopted by TOFD technology. The diffraction phenomenon explanation is that waves encounter obstacles or holes through the scattering continue to spread the phenomenon. According to the Huygens principle, the media on the wave front of the points can be the wave of the launch wave, then the envelope of these waves at any moment is the new wave front at that moment. TOFD technology uses a two-band wide-band narrow pulse probe for detection, the probe relative to the weld centerline symmetrical layout. The transmitting probe generates a non-focused longitudinal wave beam to be incident on theworkpiece to be inspected at an angle in which a portion of the beam propagates along the near surface and is received by the receiving probe, and the portion of the beam is reflected by the bottom and then received by the probe. The receiving probe determines the position and the height of the defect by receiving the diffractive signal at the tip of the defect and its time difference as shown in Figure 2.7.

TOFD technology are usually used a pressure probe as transmitter and receiver, the reflection angle range of main pressure wave is 45° to 70°. The diffractive signal is received by the receiving probe and judged using an ultrasonic pattern system that can generate a B-scan pattern.

When the ultrasonic wave is incident on a linear defect, it will be diffracted at both ends except for the ordinary reflected wave. Diffraction energy propagates over a wide range of angles and assumes that it is derived from the end of the defect. This is completely different from traditional ultrasound. Traditional ultrasound mainly relies on the size of the energy reflected from the defect to determine the defect.

The TOFD method has many advantages. This detection method can scan almost the entire weld area (except the upper and lower surface blind area). It can also achieve a very

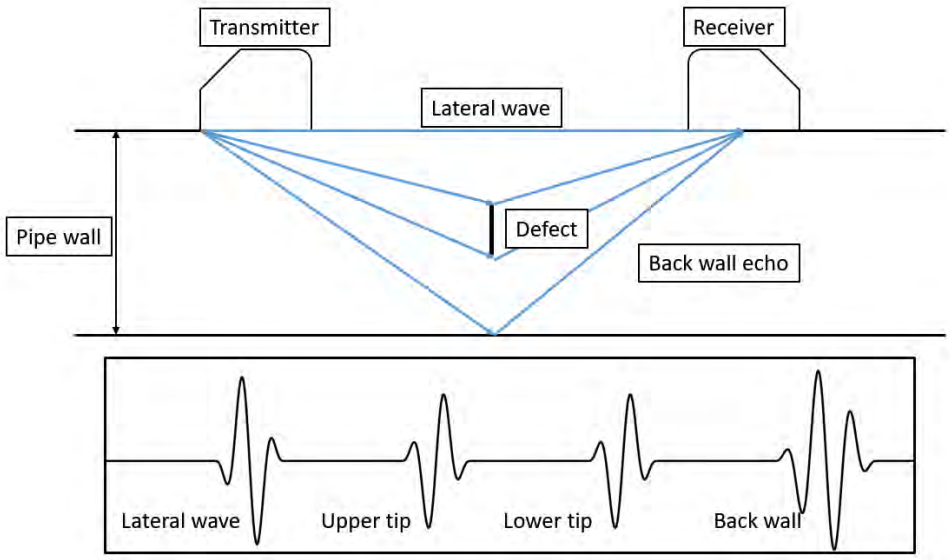

Figure 2.7: The fundamental principles of the TOFD technique.

high detection speed. The reliability of this method is better, for the middle of the weld defect detection rate is high. This detection method can detect various types of defects, not sensitive to the direction of the defect. This detection method can identify defects that extend to the surface. This method of detection using D-scan imaging, defect interpretation is more intuitive. This method of detection of the vertical direction of the defect and positioning is very accurate. The accuracy error is less than 1 mm. This detection method can be combined with the pulse reflection method, when the detection effect is better. The coverage rate of this method is 100%. This detection method is not suitable for T-type weld inspection [52].

But TOFD method also has some shortcomings. There is a blind spot near the surface in this method, the detection of the region is not enough reliability. This detection method is more difficult to qualify the defect. This detection method requires extensive experience in image interpretation. This detection method is more difficult to detect lateral defects. This detection method is difficult to detect coarse grain material. This detection method is more difficult to measure complex geometric shapes of the workpiece.

2.2.2 Low frequency long range guided wave testing

Guided wave testing is very cost-effective for long-range inspection of inaccessible from a signal point of testing. This method has the powerful function of remote inspection of the structure and detection of defects under low frequency. The frequency of conventional

GWT system is dependent on the thickness of the structure. The frequency range of UT system is high for deep penetration into structure thickness. However, the UT system has limitations that can only detect a short range structure at one time. GWT system has the ability to detect long-range structures. Figure 2.8 shows the difference between the UT system and the GWT system.

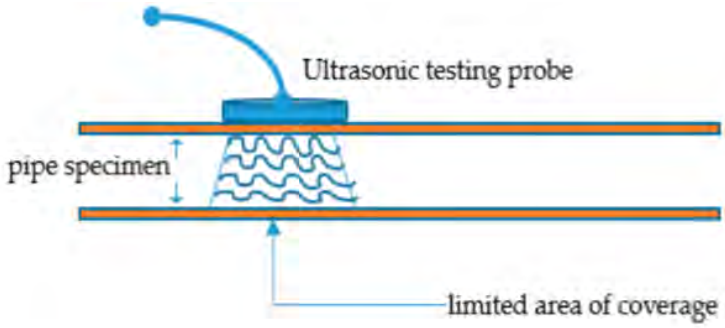

(a) UT system probe detects a short range structure.

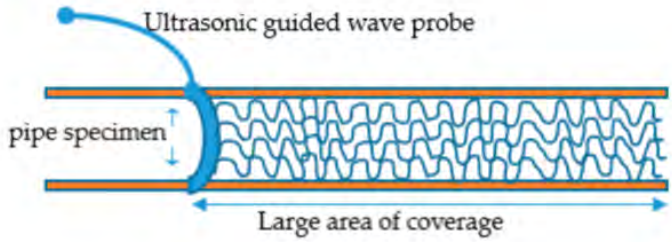

(b) Guided wave testing system detects a long-range structure.

Figure 2.8: The different between UT system and GWT system [3].

Cawley [53] proposed using guided waves to detect large structures in order to improve detection efficiency. Guided waves with frequencies below 100 kHz are mainly used for experimental analysis, and relevant effective information is extracted through their wave mode structures. Because of this advantage of GWT, it is used in many long-range detection applications. Loveday and Long [54] built an experimental monitoring system to monitor the health of an operational rail track. The system used two transducers to transmit and receive ultrasonic guided waves. A small mass was gluing under the head of the rail as an artificial defect. This experiment continued to detect and collect data for two weeks. Experimental results show that GWT has a good ability to identify defects in long-range rails. El-Hussein *et al*. [55] used low-frequency guided wave to detect long pipeline. The pipeline FEM simulation results show that the low-frequency (under 10 kHz) guided waves have the ability to defect notch from long-range pipeline. Guided waves have a lower attenuation during the detection process. Lowe *et al*. [56] investigated the GWT system for thermoplastic pipes. The results of experiments and simulations show that guided wave detection can be applied to this material. In the experiment, the attenuation

at low frequencies can be reduced by increasing the number of sensors on the circumference. Niu *et al*. [57] used T(0,1) mode guided waves to simulate and test pipeline defects. The experimental results of defects in different positions show that changing the position of the transducers can improve the sensitivity and accuracy of detection. Fromme *et al*. [58] designed a prototype of a guided ultrasonic wave array system. The system used the first anti-symmetric Lamb wave mode A0 to monitor the integrity of structural. The array, which is a ring of 32 transducers, is used to detect different kinds of defects on the plate. Experiment results and theoretical results are in good agreement in the dynamic test. Leinov *et al*. [59] studied guided wave propagation in an 8-inch pipe buried in soil. They found that the attenuation values of the torsion mode and the longitudinal mode are in the range of 1.65–5.5 dB/m and 0.98–3.2 dB/m, respectively at the frequency of 11–34 kHz. The experiment results showed great agreement with the Disperse software model. Raišutis *et al*. [60] applied guided wave testing for multi-wire rope structures. They obtained the optimal excitation area through finite element analysis and detected the defect of multi-wire ropes with polymer cores in the experiment. Cawley *et al*. [61] used a sparse-array structural health monitoring system based on guided wave testing to monitor the commercial shipping container. They established a database of healthy shipping container inspection results through FEM analysis and three weeks of test results combined with temperature changes. After that, the defective shipping container was detected and the result was verified. Howard Matt *et al*. [62] used S0 mode ultrasonic guided waves to detect the wing skin-to-spar bonds of unmanned aerial vehicles. FEM simulation and small piezoelectric transducer disks experiment are studied to detect two different kinds of defects. The findings revealed that defected bonds resulted in increased transmission strength. Alleyne *et al*. [63] studied the difference between the L(0,2) mode and T(0,1) mode guided waves. T(0,1) mode guided waves are more commonly used in industrial testing as the T(0,1) mode guided wave testing system required is simpler and lighter. They analysed through experiment results that L(0,2) mode guided waves may not be applicable in liquid-filled pipes. Mahal *et al*. [64] directly processed the signals of all the conductive arrays instead of the signals that process a single ring. They did a pipeline detection experiment which had two defects at different locations, wherein the size of the first defect was 2% and 3%, respectively, and the size of the second defect was 4% and 5%, respectively. The test proved the advantages of using information received from all elements instead of a single signal. Yücel *et al*. [65] combined linear chirp excitation and guided wave testing to improve SNR and resolution. It is quantitatively validated from simulation and experiment from an aluminium rod that this technology significantly improves the signal-to-noise ratio of the guided wave response. Taheri *et al*. [66] applied guided wave to phase array in composite materials. Due to the optimal detection frequency, the optimal detection frequency needs to be selected. Multi-element and time control are provided by using a guided wave phase array tests.

The various applications of guided waves indicate that this technology can be applied to the inspection of plates and pipelines.

2.2.3 Ultrasound imaging

Ultrasound imaging has been widely used for clinical. The most important underpinning technologies include transducers, beam forming, pulse compression, tissue harmonic imaging, contrast agents, techniques for measuring blood flow and tissue motion, and three-dimensional imaging. Specialized and emerging technologies include tissue characterization and image segmentation, micro scanning and intravascular scanning, elasticity imaging, reflex transmission imaging, computed tomography, Doppler tomography, photoacoustic and thermoacoustic. Phantoms and quality assurance are necessary to maintain imaging performance. Contemporary ultrasonic imaging procedures seem to be safe, but studies of bioeffects are continuing. It is concluded that advances in ultrasonic imaging have primarily been pushed by the application of physics and innovations in engineering, rather than being pulled by the identification of specific clinical objectives in need of scientific solutions. Moreover, the opportunities for innovation to continue into the future are both challenging and exciting.

Since Dr. Karl Theo Dussik, an Austrian neurologist, was the first to apply ultrasound as a medical diagnostic tool to image the brain [67]. There are a lot of applications in ultrasound imaging. Jeffries and Couture [68] applied super-resolution ultrasound imaging in medical imaging. This technique is inspired by optical microscopes. Through the positioning of individually injected microbubbles and tracking their displacement with sub-wavelength resolution, blood vessel and velocity maps can be generated at the level of a micrometre. Demi *et al*. [69] proposed an image formation protocol that can capture the frequency dependence of the well-known artifact (B-line) and visualize it in real-time, ultimately providing a quantitative assessment of the signal received from the lungs. The results show that the image forming process can work on lung tissue. Tai and Khairalseed [70] proposed a novel non-invasive, low-cost, real-time Hermite scan ultrasound technology. The purpose of the research is to develop a new attenuation correction method based on adaptive K-means clustering. This method has the ability to improve the ability of H-scan US imaging to estimate the size of acoustic scatterers. It can also improve the clinical application of tissue characterization when imaging complex tissues. Khan and Huh [71] applied deep learning in ultrasound imaging system to improve the performance of delay-and-sum beamformer. They designed a deep neural network for a

single data-driven adaptive beamformer which can process various detector channel configurations to generate a high performance figure. The experiment results show that this method can significant performance gain for ultrasound imaging systems.

2.2.4 Signal to noise ratio

The commonly used ultrasound detection methods have been introduced before. In order to obtain accurate detection results, the quality of the echo signal is very important. SNR is an important measure parameter in engineering area that reflects the level of a desired signal. The SNR is defined as the ratio of desired signal power to the background noise power, and is generally expressed in dB. The SNR can be improved by improving transmission means and enhancing equipment capabilities. Equation 2.1 shows the defining of SNR, where P is average power.

$$SNR = \frac{P_{signal}}{P_{noise}} \tag{2.1}$$

The sources of noise are generally divided into internal and external sources. The internal noise is mainly caused by factors such as circuit design, manufacturing process and the equipment itself. The external noise is caused by the electronic environment and the physical and chemical environment where the equipment is located. Since many signals have a very wide dynamic range, the logarithmic decibel scale is usually used to represent the signal. Equation 2.2 shows the express of SNR in dB.

$$SNR_{dB} = 10log_{10}(\frac{P_{signal}}{P_{noise}}) \tag{2.2}$$

Since SNR is an important parameter to measure the influence of noise on the signal. Many researchers have focused on improving SNR. Boer *et al*. [72] presented SNR improvement in the optical coherence tomography system which can measure light reflected from within tissue. They derived an expression for the SNR in the time domain and spectral domain. The results have shown that SNR achieved significant improvement. Firbank *et al*. [73] estimated the noise of background pixels by acquisition in a magnetic resonance imaging system. The double acquisition method was more accurate, but the execution speed was slower. They found that the single-shot acquisition method is suitable for practical applications by comparing the two methods. Yan *et al*. [74] presented a new method to improve SNR in inductive coil which is used as a NDT sensor to detect the pipe or wire ropes. An extra iron core was placed in the inductive coil to concentrate the

magnetism. Experiments proved that the SNR of the proposed method was improved by nearly six times. Bilik *et al*. [75] proposed a new method to improve the SNR of ground penetrating radar remote sensing equipment. They scanned the tested soil, and then a special algorithm performed subsequent processing on the received electromagnetic wave signals. Compared with the traditional methods, the proposed method can improve the SNR from 10 dB to several 10's dB. Tiwari *et al*. [76] applied wavelet transform, cross-correlation and Hilber-Huang in ultrasonic non-destructive testing to improve SNR. The wind turbine blade, which was made of glass fibre reinforced plastic, was used as the sample and several artificially defects were made on it. The results showed that the hybrid method can improve SNR significantly. Bernieri *et al*. [77] compared the performance of various UT excitation, filtering and diagnostic techniques through experiments. They found that the combination of detective methods, the type of defect and its position relative to the inspection instrument were closely related through the inspection test on the aluminium rod.

SNR is used in many applications as a judging indicators. In engineering area, it is important to improve SNR. Pulse compression technique is an effective method to improve SNR.

2.3 Pulse compression technique

To explore the possibility of improving the SNR of low voltage ultrasonic testing by using long, complementary code excitation, pulse trains, the study of coded excitation signal should be carried out. Pulse compression has been used to increase the SNR and resolution in sonar, radar, medical and industrial ultrasound. It contains the frequency modulated excitation signals or binary coded excitation, which is associated with the received signal so that the received echo becomes shorter in duration and higher in intensity, thereby increasing system resolution and SNR. The most well-known frequency modulated excitation signal is the chirp signal, which is obtained by the frequency modulating the excitation. By adjusting the length and bandwidth of the chirp signal, the SNR and resolution can be controlled. Coded excitation sequences operate in a little different way. The most common is the bursts cascade coding according to the polarity of the binary sequence, i.e., a sequence composed of 1 and 0 or -1. Under any condition, when correlating the received signal with the transmitted sequence, the approximation to the signal initial burst can be obtained. Figure 2.9 shows an example of a pulse compression technique.

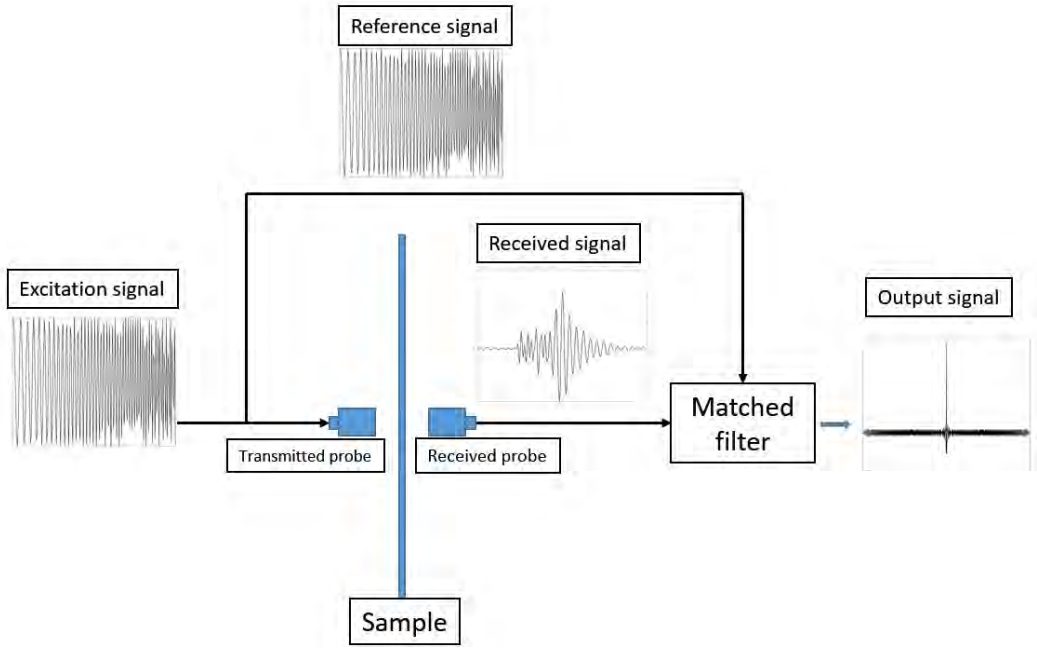

Figure 2.9: The example of pulse compression technique. After being excited by the sensor, the transmitted signal passes through the sample. Following reference signal processing, the results can be obtained.

Coded excitation is the established technology of radar technology. Many kinds of coded signals have been proposed [78]. lashkari and Zhang [79] has used a mismatched coded excitation based on Golay codes to improve the frame rate of ultrasound imaging. The new family of mismatched coded which can be separated from multiple elements has the same identical duration and centre frequency. In their proposed experiment, a set of codes (PRF=625 Hz) was sent every 1.6 ms, and each image was generated by four measurements (20 CEs). Therefore, taking into account the acquisition time, the new system can be 156.25 Hz frame rate imaging. Shen *et al*. [80] found that the dual-frequency harmonic imaging can improve SNR by Golay excitation. The conventional Golay decoding was affected by spectral crosstalk of 3f0 and DC interference. However, for orthogonal Golay, the output of the switched filter can be subtracted from the original filter to eliminate crosstalk. The results showed that the level of side lobes are reduced in hydrophone measurement and B-mode imaging. Li and Zhou [45] first used P4 codes pulse compression technique which is divided by polyphase code in the field of air-coupled ultrasonic testing (ACUT). They studied the principle of selecting parameters of P4 codes pulse compression and proposed a signal processing method for reducing the noise. Shen *et al*. [81] have found a method which use third order harmonic Golay codes to improve the SNR. The third harmonic (3f0) emission phase can be achieved by increasing the harmonic SNR at the fundamental (2.25 MHz) and 3f0 (6.75 MHz) frequencies to achieve the mutual enhancement between the frequency and frequency components. To further increase the SNR without excessive transmission pressure, the coding excitation can be incorporated

into the 3f0 emission phase to improve the occurrence of tissue harmonics. The analysis showed that, due to its excellent transmit bandwidth efficiency, phase-coded Golay excitation is suitable for 3f0 emission phasing. The combined frequency and frequency components of the combined harmonic signal can be simultaneously subjected to Golay coding to improve SNR. The increasing in the main wave signal and the Golay excitation in the 3f0 emission phase was consistent between the tissue harmonic measurements and the simulation. The B-mode images of the spot-generated phantom also showed an increase in tissue harmonic SNR of about 11 dB without significant compression artifacts. Zhou *et al*. [82] presented a phase-coded pulse compression hybrid method to improve the SNR in air-coupled ultrasonic testing technique. The air-coupled ultrasonic testing technique is considered as a viable solution for advanced composite material defect detection in the aerospace industry. However, the huge mismatch of the acoustic impedance causes the transmission efficiency of the ultrasonic wave to be reduced, resulting in a SNR difference of the received signal. Kim *et al*. [83] proposed a new Barker-sequence-modulated Golay (BMG) coded excitation technique for ultrasound imaging. The sequence of BMG techniques is generated by the Barker code modulation Golay code, which can lead to further improvements in signal strength and code length flexibility compared to conventional Golay codes. The improvement in SNR is determined by the code length. They demonstrated that BMG technology has a higher contrast than other technologies. Isla *et al*. [84] proposed a new method of coding excitation. By introducing the receiving interval or pause in the excitation itself, the reception is carried out at these time intervals. As a result, the code length is no longer limited by the distance of the nearest reflector and a higher SNR can be achieved. In addition, the excitation can be encoded in a manner that is possible to continuously transmit, which reduced the overall duration of the system's response to media changed. Zhou *et al*. [85] presented a method which introduce Golay complementary coding excitation and decoding compression into ophthalmic ultrasound biometrics instead of using a conventional method of pulse excitation. By using this method, the excitation voltage can be reduced from 60 V to $\pm$15 V. Thus, the ultrasonic instantaneous excitation power was greatly reduced, while the average excitation power increased. Sanchez *et al*. [86] used the technique of converting non-binary FM codes into binary frequency modulated codes. To convert non-binary to binary code, a second-order one-bit sigma-delta modulator is used. The sigma-delta modulation code was generated in MATLAB and then stored in a double data rate synchronous dynamic random-access memory. A field programmable gate array can access the memory device transmits binary waveforms and record them using an oscilloscope. Lahav *et al*. [87] have proposed a high-quality, low-cost method for CE imaging by integrating pulse compression into the recently developed frequency-domain beamforming framework. This approach reduced the computational complexity by a factor of 26 without affecting image quality. This reduction allowed CE to be effectively implemented in array imaging, increasing

SNR, improving imaging depth, and getting higher frame rates. Fu *et al*. [88] studied the limitations of conventional Barker coding excitation and proposed a new Barker coding excitation which called linear frequency modulated (LFM) Barker with LFM carrier. The LFM-Barker's pulse compression scheme has been developed to suppress side lodes and compared with the traditional Barker coding stimulus. The simulation results showed a significant increase in SNR and axial resolution.

Zhao and Tong [89] have tested the feasibility of applying coding excitation in DW imaging to improve the corresponding SNR, contrast and penetration depth. To this end, two types of codes, the linear frequency modulation chirp code and a set of complementary Golay codes were tested in three different DW imaging schemes, i.e., no composite 1-angle DW transmission, with coherently mixed 3 And 5 angles DW. The performance (SNR, contrast (CR), contrast noise ratio (CNR) and transmittance) of different imaging schemes were studied by simulation and in vitro experiments. For benchmarks, there was also a corresponding DW imaging scheme with conventional pulse excitation and a conventional focus imaging scheme. Peng *et al*. [90] proposed a computational method to construct the sector pattern image and improve the SNR of the HFR system. The method uses orthogonal complementary Golay coding excitation to implement two transmit and receive events. Each emission simultaneously emits two plane waves with different transmission angles. Then, according to the orthogonality of the Golay code, the received echo signals associated with different angles are separated and used to construct two images of different imaging regions by the HFR method. Finally, the two images were combined into one frame mode image. Peng *et al*. [91] used the Golay codes to apply elastic imaging to improve its quality. They used the phase zero algorithm as the displacement estimator and used the amplitude modulation correction position estimation method as the position estimator. By comparing the traditional methods, the Golay code can obtain a higher elastic SNR than the short pulse at low echo SNR, since the echo SNR gain using the Golay code improves the displacement estimate. Zhang *et al*. [92] were inspired by chirp code which is a reference to the chirping sound made by birds. They provided a tutorial on a new RF steganography scheme for concealing digital communications in linear chirped radar signals. They first provided a review of the linear chirp signal and the existing communication system which used chirped waveform. Next, they discussed how to implement RF steganography and hide the digital modulation communication information within the linear chirped radar signal to prevent the enemy from detecting the presence of such hidden information. The modulation chirp waveform was almost identical to the unmodulated chirp signal using a new modulation method called phase shift keying. In addition, the variable symbol duration is used to eliminate the cyclostationary characteristics that could otherwise be exploited by the enemy to detect the presence of hidden information. Lasaygues *et al*. [93] compared chirp coding with excitation methods to de-

termine the time-of-flight and evaluated the accuracy of the measurement at several time intervals. The method was used to measure the apparent thickness and the ultrasonic velocity in the parallelepiped plates of the resin and the wood material, and the pulse mode method was used as a reference. The result showed that the relative error of the thickness measurement is 0.1%to 6.81% compared to the caliper measurement. For the speed, the chirp coding excitation method showed a difference from the reference method from 0.78% to 3.64%. Peng *et al*. [94] applied chirped pulse impulse excitation to ultrasonic strain imaging and studied the effects of various factors. Chirped pulses are much better at low echo SNR than traditional short pulses. Some chirp schemes can obtain higher elasticity SNR than short pulses under high echo SNR conditions. The performance of the chirped pulse depended primarily on the RSLL and the main lobe width under high echo SNR conditions. There is a trade-off between energy, RSLL and the width of the main lobe when designing a strain imaging chirp scheme. Yoon *et al*. [95] proposed an efficient chirp-coded excitation pulse compression method to reduce the burden of complexity. In the proposed method, the pulse compression method was carried out using the extracted of complex baseband data instead of a beamformed radio-frequency (RF) data. Although the complex data has been used for compression, due to the implementation of the L-fold to reduce the number of data and filter coefficients. So, the total computational complexity reduced by 4 times the factor.

Merilainen *et al*. [96] have developed a high frequency coded signal based on orthogonally modulated ultrasound imaging. The device allowed pulse-echo operation at 300 MHz. They presented an improved design with new RF components. Compared to the traditional method, the new design increases SNR by 16 dB. They also investigated the use of dual-frequency chirp code to further reduce local oscillator interference. They used any TX code to test a device with a GHz ultrasonic sensor in the 0.9-1.1 GHz band. Toosi *et al*. [97] used adaptive beamforming to suppress the sidelobe effect, thereby increasing the resolution of the coded excitation ultrasound imaging system. The simulation results show that the SNR and the resolution can be improved significantly by applying the minimum variance adaptive beamformer to the chirped laser ultrasound imaging system. The purpose of Mamou *et al*. [98] study is to use modern ring sensor technology and coding excitation to simultaneously improve depth of field (DOF) and penetration depth. A 20 MHz five-membered ring array with a focal length of 18 mm and a total pore size of 6 mm was customized using a 25-micron thick polyvinylidene fluoride film. The ring array is excited by an 8-micron coded signal to image a phantom made of seven regularly spaced 25-micron lines. The coded signal is a chirp pulse with a frequency range of 40 MHz. The results of this study show that DOF can be improved by 3 times, and the SNR can be improved by coding excitation by more than 24 dB. Increased SNR provides the potential to increase penetration depth during in vivo imaging. Dackermann *et al*. [99]

presented a comparative study of the properties of wood orthorhombic materials which use static and ultrasonic tests. In the literature, the nature of the material is usually only available in the longitudinal direction and most international standards do not provide details of the test on two other secondary directions (radial and tangential). They discussed the use of static testing and ultrasonic-based alternative testing methods to determine the properties of all twelve orthotropic materials of the two-hardwood species. Kumar *et al*. [100] proposed an inter-frame and intra-frame correlation technique for the electrocardiogram (ECG) signal based on the singular value decomposition (SVD) and adaptive scanning wavelet difference reduction technique. In this method, the corresponding beat segments are arranged in an array of N×M and processed with the proposed compression technique. Li *et al*. [101] proposed a coding algorithm for lossless compression of audio signals. The proposed algorithm consists of a loss coding part and a lossless coding part. The loss coding part is based on the code excitation method in which the excitation gains and the short-term prediction coefficients are adjusted in a sampling mode to cope with the fast time varying nature of the audio signal. The error between the input and code-induced composite signals is encoded by the arithmetic encoder to achieve lossless compression. The excitation code book has been searched as a search condition by using the arithmetic error of the minimum error energy and the minimum code length of the M-L tree search strategy. The proposed encoder has a very low decoding complexity due to its simple code-driven structure and achieves comparable compression performance to other advanced lossless encoders for encoding CD-quality audio. Peng *et al*. [102] developed a new method of using the clutter signal in the coding excitation to determine the displacement of the object or the desired region of the object with a greatly improved resolution. The method included sending a pair of Golay complementary sequences, receiving an echo from a region of an object or object, compressing the pulse, eliminating the main lobe, and determining the displacement of the object between the two transmissions from the residual clutter signal around the main lobe. Computer simulation results showed that the new method improves the resolution by several orders of magnitude, which is more robust than the traditional pulse echo method. Mienkina *et al*. [103] evaluated the advantages of photoacoustic coding excitation (PACE). The performance of unipolar Golay code was analyzed and verified experimentally. Successfully demonstrated the use of 1 MHz PRF laser diodes and modified clinical ultrasound scans of copper plates. Triger *et al*. [104] described the development of an integrated miniaturized ultrasound system which is designed for low voltage piezoelectric transducer arrays. The aim of this technology was for low frequency NDT and sonar applications with a frequency of 1.2 MHz. They have built a flexible, reconfigurable, low-cost building block that can perform 3-D beamforming. The mosaic of multiple building blocks allows the formation of scalable 2D macro arrays with increased size and varying shape. This is different from traditional ultrasonic solutions by integrating the entire system into a single module. Huang and

Li [105] present a new coding scheme for efficient synthesis of arbitrary waveform codes using a bipolar square wave pulse generator. They proposed a bipolar pulse generator which maintains a low-cost advantage. While the pulse generator can achieve roughly the same compression performance as an arbitrary waveform generator. The key idea of the proposed method is that the conversion of a non-binary code (ie, requires an arbitrary waveform generator) has good compression performance into binary code (ie only bipolar pulse generator) and code tuning. The results obtained under the same setting are the same as simulation. The results showed that arbitrary waveform coding can be achieved using bipolar square wave pulser in medical applications for ultrasound. Malo *et al*. [106] presented a 2-D compression pulse analysis to improve the performance of the guided wave. This novel technology combines the use of pulse compression and dispersion compensation to improve the SNR. The ability of the technology to distinguish between different waveform modes is also highlighted. In addition, an iterative algorithm has been developed to use adaptive peak detection to identify the wave of interest in order to achieve automatic wave pattern discrimination.

2.4 Summary

This chapter has reviewed the most commonly used NDT methods, such as the electromagnetic method, optical method, and acoustics method. Each method has advantages and disadvantages. The acoustic method is discussed after examining the benefits and drawbacks of each method. Among the acoustic methods, the main review objects are UT, GWT, and UI. The applications of pulse compression are reviewed in order to improve detection accuracy. Frequency modulation and phase modulation are both used in the pulse compression method.

Through literature review research, it has been shown that the performance of the UT system is closely related to the characteristics of the input signal. There are many studies to improve the performance of the UT system by increasing the energy of the input signal and by a variety of noise reduction methods. Attempting to reduce the pulsing voltage in a UT system can result in noisy and unusable results. Guided waves suffer in GWT systems when they propagate through high attenuation materials and multiple modes as a result of excitation, which reduces the power of echo signals and induces corruption caused by coherent noise. The ultrasound imaging system has a low axial resolution due to the high bandwidth of the sidelobe. SNR can be improved using pulse compression without increasing average power. These issues will be addressed in the following chap-

ters. Despite the aforementioned theoretical inferences, no study to date has provided empirical support for the hybrid pulse compression method on different ultrasound detection systems. Therefore, in a series of experiments, we explored the direct effects of the proposed hybrid pulse compression method on ultrasound signals. The results not only provide support for the theory, but also have practical significance for the industry.

Chapter 3

Sine Modulated Hybrid Pulse Compression for Low Voltage Ultrasonic Testing

3.1 Introduction

Ultrasonic Testing (UT) is an important technology in non-destructive testing (NDT) methods that is often used for obtaining parameters related to the durability, the physical and mechanical properties of a material by using ultrasound waves. The traditional pulse-echo and transmission techniques were applied
laws in the material [107]. In the case of certain hazardous flammable and explosive atmospheres, traditional high-voltage UT equipment cannot be used. The main reason for making UT equipment unsuitable is the high voltage used by the pulsing circuitry. It has enough energy to ignite a gas and the potential to generate a spark in the event of a failure. However, the lower the pulsing voltage is, the lower the SNR of the signal is. Attempting to reduce the pulsing voltage can lead to noisy and unusable results. In order to ensure high SNR of signals in low-voltage ultrasonic testing equipment, a method without changing the hardware of UT device should be considered.

The technique of coded excitation has been used to improve the SNR in ultrasonic testing [83]. The technique of coded excitation has been used in radar for about 60 years, but

it was successfully introduced for clinical ultrasound only within the last 10 years [108]. Coded excitation refers to the technique of using a series of pulses following a calculated width and pause structure. These pulse trains follow a mathematically described code sequence and are used as complementary pairs whose auto-correlation coefficients sum to zero in most cases. The most well-known and studied pairs of coded sequences are the Golay code and the Barker code [109]. The result of such an excitation is a long sequence and must be associated with a transmitted signal, so that the received echo becomes shorter in duration and higher in intensity, thereby increasing the system SNR. By using the compressed signal, clearer A-scan can be reconstructed. The long duration of the pulse trains allows for a significant amount of ultrasonic energy to be transmitted in the material. Thus, this technique is quite suitable for testing highly attenuated materials by using low-voltage pulse signals since the maximum amount of energy is not limited by the amplitude of the pulse [110].

In this chapter, a coded excitation method which uses convolution of Barker code and Golay code pair is applied to a low voltage ultrasonic testing system. The Barker code sequence has the ability to increase the intensity of the main lobe. The Golay code pair has an extraordinary advantage. The sidelobes are completely eliminated after passing through the matched filter. The method combines the advantages of these two coding methods and increases the diversity of code lengths. The method can be used in low-voltage ultrasonic testing devices without changing the internal hardware. The main contributions of this chapter are presented below.

- The combined coded excitation technique is applied to low-voltage ultrasonic testing devices, not like other existing work for high-voltage situations.
- The extensive theoretical analysis and simulation results are provided for all the possible combinations of coded excitation for ultrasonic testing, not like other works on selected coding methods.
- Current combined coded excitation techniques are applied to ultrasonic imaging systems only. This work opens the door for all ultrasonic testing devices for many other applications in low-voltage situations.

The rest of this chapter is organized as follows. In section 3.2, the related work of ultrasonic testing and coded excitation has been reviewed. In section 3.3, our methodology for analyzing its superiority is proposed . The theoretical analysis results are described in section 3.4 and the simulation results are described in section 3.5. Finally, the summary and discussion is given in section 3.6.

3.2 Related works

Coded excitation applied to medical ultrasound imaging systems was first proposed by Takeuchi [111] in 1979. However, due to the time-bandwidth limitation of this technique, there were rare studies on coded excitation in the literature in the following years. O'Donnell [112] considered to use coded excitation to improve the SNR of the ultrasound system. A signal which has been compressed on the digital beamformer was used in the ultrasound system. Later, Jedwab and Parker [113] gave a general construction for an odd length binary Golay sequence pair of length 26 from a Barker sequence of length 13 and a related Barker sequence of length 11. This work lays the theoretical foundation for coded excitation. Kim *et al*. [83] proposed a new coded excitation method for ultrasound imaging by modulating Golay code pairs with the Barker sequence. However, they only used finite types of codes, which are 3-bit Barker code, 8-bit Golay code pair and 3-bit Barker code modulated 4-bit Golay code pair in their experiment [83]. Recently, Wang and Cong [114] proposed a new pseudo Chirp-Barker-Golay (PCBG) coded excitation method in ultrasound imaging. They use the Field II toolbox to simulate phantoms and cyst phantoms in B-mode images.

Methodology-wise, there are two pulse compression methods. The first one is frequency modulated excitation signals which include linear chirp code and pseudo-chirp excitation. The other one is binary coded excitation signals which include Barker code such as m-sequences, orthogonal Golay sequences. Coded excitation sequences operate in a slightly different way compared to frequency modulated excitation signals. The most common way of using this technique is the burst cascade coding according to the polarity of a binary sequence, such as a sequence composed of 1 and 0 or -1 [43].

The limitation is the length of the sequences of the coded excitation. The improvement in SNR is related to the length of the sequences, but there are only a few lengths of Barker codes available, although there is no limit for conventional Golay codes [108]. Even if the length of the selected codes is not the required length, one of the codes with a known length is inevitably selected. Therefore, this may lead to inefficiency.

So far, the combined code excitation methods are only applied in ultrasound imaging under high-voltage situations, and the selection of the combined code is limited. However, for other ultrasound devices operating under low-voltage situations, there is no existing study on them. Here, the task of both complete theoretical analysis and extensive simulation experiments are investigated.

3.3 Methodology

3.3.1 Matched filter

Matched filters, which are electrical tools for detecting a known piece of signal, are widely used in radar, mobile communication systems, and ultrasound imaging as an important filter [115]. The optimal criterion for the matched filter is that the output SNR is the largest when it is in the white noise background and noise bandwidth is wider than signal bandwidth. Since the transmitted signal spans a wide frequency range, the matched filter cuts out some of the signal as well as some background noise because it has a finite bandwidth [116]. The frequency response of the matched filter is the conjugate of the frequency response of the input signal.

The basic problem that often arises in ultrasonic testing systems is that detecting a pulse transmitted over a channel is corrupted by channel noise. The Equation 3.1 shows the ideal receiving structure of Barker code signal $B(t)$ though matched filter.

$$\begin{aligned} y(t) &= x(t) * h(t) \\ x(t) &= B(t) + w(t) \\ h(t) &= B(T-t) \end{aligned} \tag{3.1}$$

where $w(t)$ is the white noise and $x(t)$ is the filter input, which is the sum of $B(t)$ and $w(t)$. $y(t)$ is the filter output which is the convolution of filter input $x(t)$ and matched filter $h(t)$ when T is the length of $B(t)$ [117].

From amplitude-frequency characteristics, the amplitude-frequency characteristics of a matched filter are related to the amplitude-frequency characteristics of the input signal. At the stronger signal frequency point, the amplification factor of the filter is also larger. The matched filters allow the received signal to pass as much as possible regardless of the characteristics of the noise. Since one of the preconditions of the matched filter is white noise, the power spectrum of the noise is flat. In this case, this technique can reduce the passage of noise.

From phase-frequency characteristics, phase-frequency characteristics of the matched filter are conjugated to the input signal. Thus, the phase of the signal is zero by matching the filter. This can achieve a coherent superposition of the signal in the time domain. The phase of the noise is random and only non-coherent superposition can be achieved. This

technique ensures the maximum SNR of the output signal in the time domain. In fact, the name of the matched filter indicates its distinctive feature. The matched filters match the input signals. Once the input signal changes, the original matched filter also changes.

3.3.2 Barker code

The Barker code is one of the binary phase codes that produce a compressed waveform with a constant sidelobe level equal to one. The auto-correlation coefficients are defined and should all be small [118]:

$$\left| \sum_{i=1}^{N-k} b_i b_{i+k} \right| \leq 1 \tag{3.2}$$

In the Equation 3.2, b_i is an element of Barker code B_N and $b_i = \pm 1$. N is the length of the Barker code.N ≥ 2 and $1 \leq k < N$. There are Barker codes of lengths of 2, 3, 4, 5, 7, 11, and 13, and it is conjectured that there is no longer a Barker code [119]. The optimal binary sequence is that whose auto-correlation peak sidelobe is the minimum possible for a given code length. The advantage is that the self-correlation or matched filtering of these codes gives the main lobe peak of N and the minimum peak sidelobe of 1. Table 3.1 lists all known Barker codes and the side lobes level of these codes. Ideally, if there is a long length, these codes can be used for pulse compression radar. However, the longest known Barker code length is 13, so the pulse compression radar using these Barker codes will be limited to the maximum compression ratio of 13. Figure 3.1 shows a 5-bit Barker code and the compression result after the matched filter. It can be seen that the frequency characteristics of the matched filter are exactly the same as the input signal, and there are little changes in the frequency characteristics of the compression signal.

Table 3.1: Barker code of various lengths

Code symbol	Length	Code	SLL(dB)
B2	2	(+1,-1),(+1,+1)	-6
B3	3	+1,+1,-1	-9.5
B4	4	(+1,-1,+1,+1),(+1,-1,-1,-1)	-12
B5	5	+1,+1,+1,-1,+1	-14
B7	7	+1,+1,+1,-1,-1,+1,-1	-16.9
B11	11	+1,+1,+1,-1,-1,-1,+1,-1,-1,+1,-1	-20.8
B13	13	+1,+1,+1,+1,+1,-1,-1,+1,+1,-1,+1,-1,+1	-22.3

Barker code has a good performance of inhibiting the auto-correlation side lobe. Due to the property of the Barker code which can improve the SNR, it is considered as the transmission code for the low-voltage ultrasonic device.

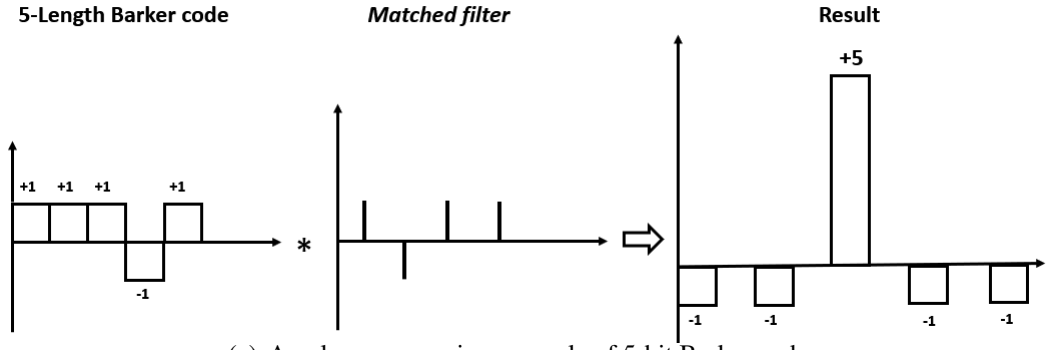

(a) A pulse compression example of 5-bit Barker code.

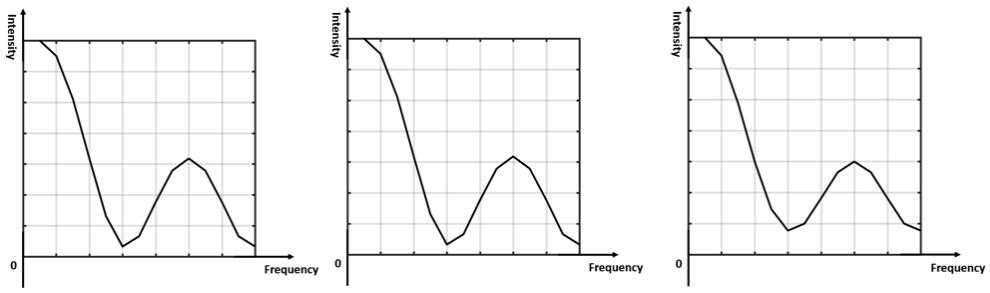

(b) Frequency response of 5-bit Barker code,matched filter and compressed result

Figure 3.1: Illustration of 5-bit Barker code compression. (**a**) An pulse compression example of 5-bit Barker code compression. (**b**) Frequency response of the 5-bit Barker code, matched filter and compressed result.

3.3.3 Golay code

Golay code is defined as a pair of equal-finite length composed elements, and the number of identical element pairs in one sequence is equal to the number of distinct element pairs in another sequence at any given interval [120]. An ideal pulse compression result without sidelobes is obtained by adding matched pairs of echoes which are generated by transmitting a pair of complementary sequences.

Defined there are a pair of Golay complementary pair sequence G_a(n) and sequence G_b(n). Each element of G_a(n) and G_b(n) is either 1 or -1. Due to the property of Golay code pair, the auto-correlations of sequence G_a(n) and sequence G_b(n) are shown in Equation 3.3. $\delta(n)$ is a Dirac delta function. $*$ is the symbol of convolution.

$$G_a(n) * G_a(-n) + G_b(n) * G_b(-n) = 2N * \delta(n) \tag{3.3}$$

When using the coded excitation in ultrasonic testing or imaging, sequence G_a(n) and sequence G_b(n) are used instead of the traditional single-pulse excitation to stimulate the ultrasound transducer sequentially. The echoes from the same stationary object in the ultrasound field are represented by e_a(n) and e_b(n).

$$e_a(n) = y_t(n) * G_a(n) * y_r(n) \tag{3.4}$$

$$e_b(n) = y_t(n) * G_b(n) * y_r(n) \tag{3.5}$$

Where y_t(n) and y_r(n) are the impulse response of the ultrasound transmitter and receiver. If the receiver and transmitter have the same element, y_r(n) =y_t (n) the cross-correlation between e_a (n) and sequence G_a(n) is

$$e_a(n) * G_a(-n) = y_t(n) * G_a(n) * G_a(-n) * y_r(n) \tag{3.6}$$

And the cross-correlation between e_b(n) and sequence G_b(n) is

$$e_b(n) * G_b(-n) = y_t(n) * G_b(n) * G_b(-n) * y_r(n) \tag{3.7}$$

Sum the two cross-correlation results,

$$g(n) = e_a(n) * G_a(-n) + e_b(n) * G_b(-n) = 2N(y_t(n) * \delta(n) * y_r(n)) \tag{3.8}$$

$g(n)$ is the result of the pulse compression of the Golay code pair. It shows that the amplitude of $g(n)$ is equal to $2N$ times the echo amplitude of a single-pulse simulation. Figure 3.2 shows a 4-bit Golay code pair and the compressed result after the matched filter.

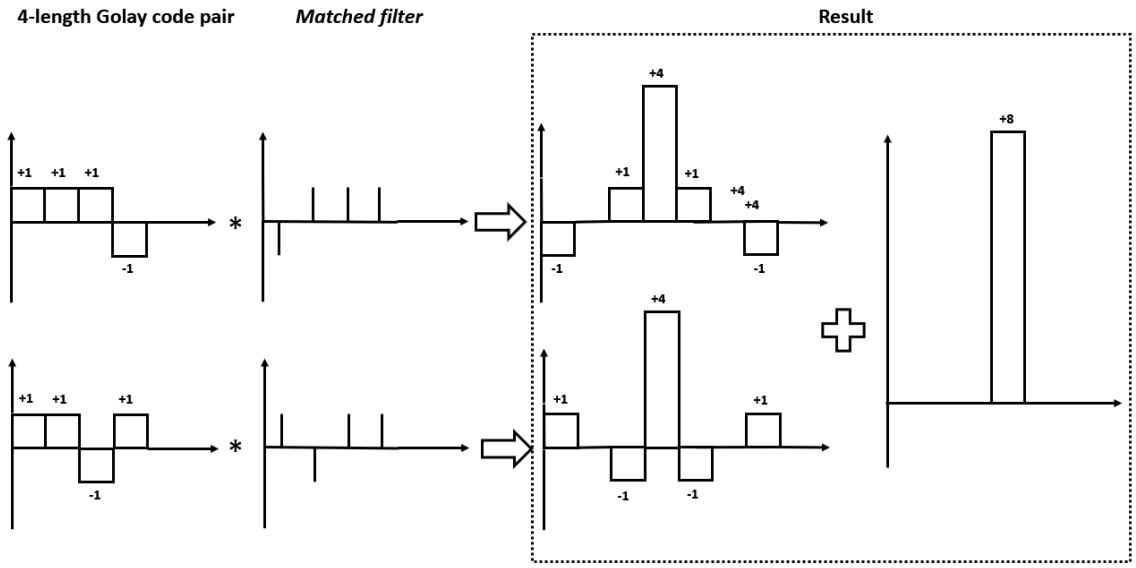

Figure 3.2: An pulse compression example of 4-bit Golay code pair.

Due to the unique properties of this sequences, Golay code pairs can be used as the input signals of an ultrasonic transmitter. The sidelobes of the echo signal after decoding disappear.

3.3.4 Convolution of Barker code and Golay code

Due to the character of the code excitation, the improvement of SNR and resolution is related to the code length. As the length of input code sequence increases, the improvement in SNR also increases significantly [83]. However, since Golay codes and Barker codes are known for their specific sequences, it is only allowed to choose one of the sequences for ultrasonic testing. Barker-sequence combined Golay code (BCG) is convoluted by Golay code and Barker code, which can lead to additional improvements in signal intensity and flexibility for code length compared to conventional Golay code pairs and Barker code. The combined codes have the same sidelobe as the Baker code used, and the main lobe of the combined codes is associated with the main lobe of the Barker code and Golay code pairs. It combines the characteristics of a high main lobe Barker code and no side lobe Golay code pairs.

To excite the ultrasonic signal, the BCG code transmits beamformer and electrical transducer transmit the BCG code ultrasonic signal. The sine-wave modulating signal is gen-

erated by an oscillator and is used to frequency modulate a sine-wave carrier signal to produce frequency-modulated BCG signal [121]. The transducer can receive echo signals from any medium. Figure 3.3 shows the process of generation and compression of BCG codes. The BCG code pair is created by the convolution of the Barker code and the Golay code pair. The BCG code pairs are modulated and transmitted to the medium to obtain a pair of echoes. There are two steps to compress the echos. The first step is to process though a Golay code pair matched filter, and the second step is to process though a Barker code matched filter. The compression result is the sum of the processed pairs.

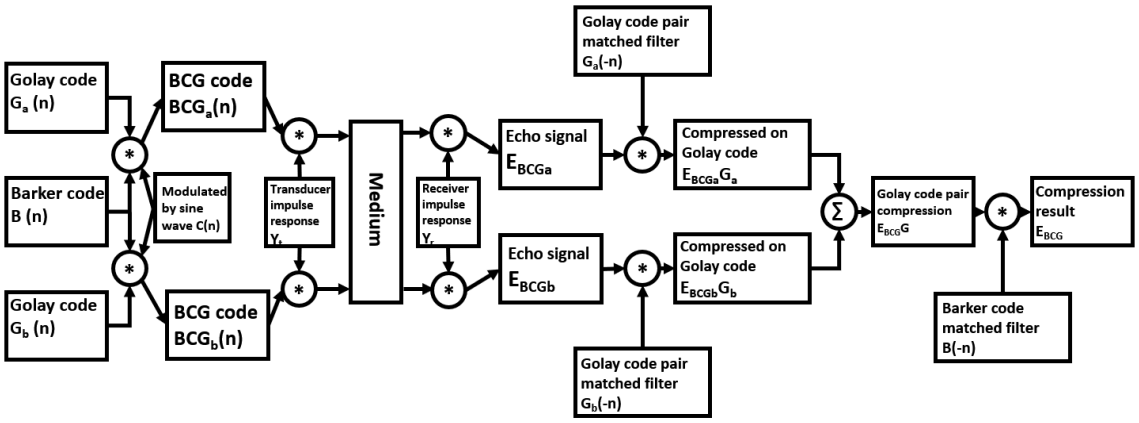

Figure 3.3: The process of generation and compression of BCG codes

As shown in the equations below, a BCG code pair, BCG_a and BCG_b, is constructed by convolution of the Golay and Barker sequences and modulated by a base pulse.

$$BCG_a(n) = G_a(n) * B(n) * C(n) \tag{3.9}$$

$$BCG_b(n) = G_b(n) * B(n) * C(n) \tag{3.10}$$

Where $B(n)$ is a known Barker code sequence, and G_a(n), G_b(n) are the Golay code pairs. Defined the BCG_a (n) and BCG_b(n) as modulated BCG code signal. $C(n)$ is a carrier sine wave.

$$E_{BCGa}(n) = y_t(n) * BCG_a(n) * y_r(n) \tag{3.11}$$

$$E_{BCGb}(n) = y_t(n) * BCG_b(n) * y_r(n) \tag{3.12}$$

y_t(n) and y_r(n) are the impulse response of the ultrasound transmitter and receiver. Then the E_{BCGa}(n) and E_{BCGb}(n) are the beamformed echo signals of BCG_a (n) and BCG_b (n). The received signal will be processed by a matched filter. The composite signal is combined with two types of signal. The received signal should be processed by a matched filter twice. The first step is to process the signal by using corresponding Golay code pair matched filter, the second step is to process the first step signal by using a corresponding Barker sequence matched filter. The echo signals which are processed by the Golay matched filter can be defined as

$$E_{BCGa}G_a = E_{BCGa}(n) * G_a(-n) = y_t(n) * BCG_a(n) * y_r(n) * G_a(-n) \tag{3.13}$$

$$E_{BCGb}G_b = E_{BCGb}(n) * G_b(-n) = y_t(n) * BCG_b(n) * y_r(n) * G_b(-n) \tag{3.14}$$

Where $E_{BCGa}G_a$ (n) and $E_{BCGb}G_b$ (n) are the echo signals processed by Golay matched filter and G_a(-n) and G_b (-n) are known as the matched filter of each Golay code pair. Sum the result of each compressed signal can achieve the Golay code compression of BCG code as:

$$\begin{aligned} E_{BCG}G &= E_{BCGa}G_a + E_{BCGb}G_b \\ &= y_t(n) * y_r(n) * (G_a(-n) * BCG_a(n) + G_b(-n) * BCG_b(n)) \\ &= y_t(n) * y_r(n) * (G_a(-n) * G_a(n) * B(n) + G_b(-n) * G_b(n) * B(n)) \\ &= g(n) * B(n) \end{aligned} \tag{3.15}$$

$E_{BCG}G$ is the result of Golay code pair compression. As mentioned above, g(n) is the result of pulse compression of Golay code pair. The Barker matched filter defined as B (-n). Then the Golay compressed signal should be process by Barker matched filter as:

$$E_{BCG} = E_{BCG}G * B(-n) = p(n) * B(n) * B(-n)) = g(n) * E_B(n) \tag{3.16}$$

E_B (n) is the result of Barker code compression. Therefore, E_{BCG} is the result which is processed by Golay matched filter and Barker matched filter. By using this method, the

length of BCG code can be expressed as

$$N_{BCG} = \sum_{i=1}^{j} N_i - j + 1 \tag{3.17}$$

Where j is the number of the codes used for modulation and N_i is the length of each code.

3.4 Theoretical analysis

To prove the feasibility of the BCG code, the theoretical analysis has been done. All 15 different types of BCG code are used in the analysis. The 15 types of BCG code are combined by 3-bit Barker code with 2-bit 4-bit 8-bit Golay code pair, 5-bit Barker code with 2-bit 4-bit 8-bit Golay code pair, 7-bit Barker code with 2-bit 4-bit 8-bit Golay code pair, 11-bit Barker code with 2-bit 4-bit 8-bit Golay code pair, 13-bit Barker code with 2-bit 4-bit 8-bit Golay code pair, respectively. All Barker codes and commonly used Golay code pairs are included in these codes.

In order to verify the performance of the hybrid code to improve the SNR, a code with a length similar to the hybrid code was found for comparison experiments. Three different types of pulses have been used: a simple pulse, 7-bit Barker code and 4-bit Golay code pairs. Peak sidelobe level (PSL) is a major parameter that describes a code's properties [122] and it can be calculated based on the peak (P_{peak}) and mean (P_{mean}) power of lobe pulse as shown in Equation 3.18.

$$PSL = 20log(\frac{P_{peak}}{P_{mean}}) \tag{3.18}$$

The length of different BCG codes and the peak side lobe level of each code are shown in Table 3.2. Figure 3.4 (a) shows that a 3-bit Barker code modulated 4-bit Golay code compared to simple pulse, 7-bit Barker code and 4-bit Golay code. Figure 3.4 (b) shows the comparison of different theoretical intensities of 15 types of BCG codes. The maximum enhanced SNR of the 15 types of BCG code is 46.36 dB compared to the simple pulse, which is B13G8. The enhanced SNR of B3G4 is 27.6 dB compared to the simple pulse, the enhanced SNR of 7-bit Barker code is 16.9 dB compared to the simple pulse, and the enhanced SNR of 4-bit Golay code pairs is 18.1 dB compared to the simple pulse.

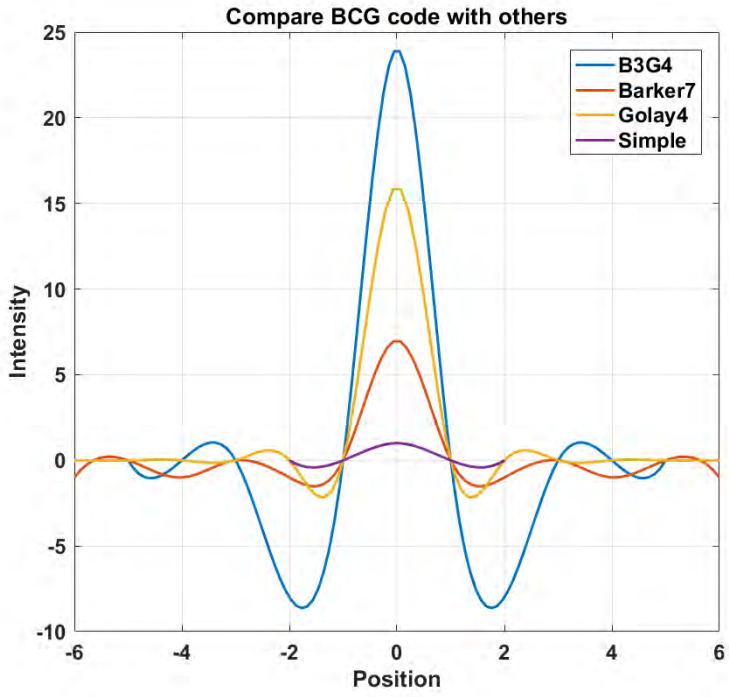

(a) Comparison of BCG code and others

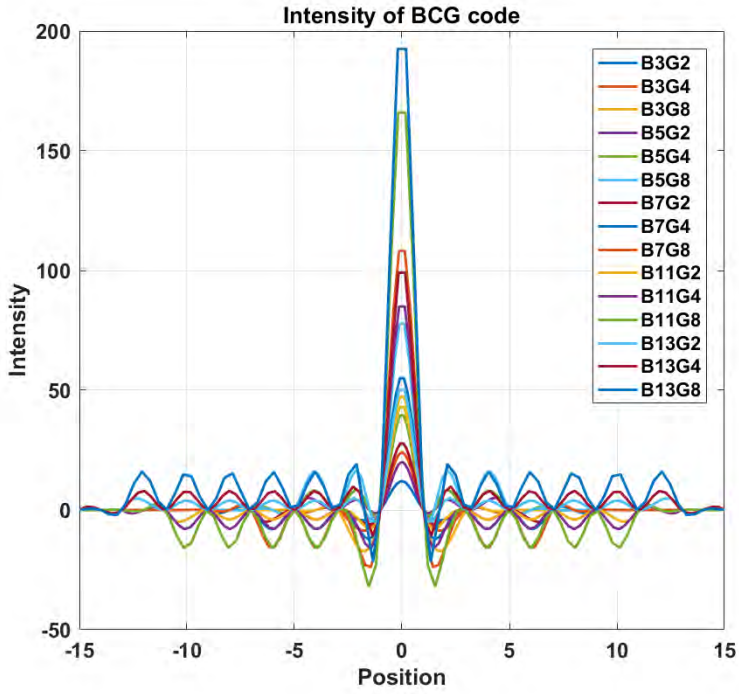

(b) Intensities of different BCG codes after matched filter

Figure 3.4: The theoretical simulation results. (**a**) The 3-bit Barker code combined 4-bit Golay code compared to simple pulse, 7-bit Barker code and 4-bit Golay code. (**b**) the theoretical intensity comparison of 15 different types BCG code.

Table 3.2: Different lengths and peak-sidelobe ratio of BCG code

Code symbol		Code length	PSL(dB)
Barker 3	Golay 2	4	-19
	Golay 4	6	-23.4
	Golay 8	10	-28.6
Barker 5	Golay 2	6	-22
	Golay 4	8	-24.8
	Golay 8	12	-28.8
Barker 7	Golay 2	8	-24.2
	Golay 4	10	-26.4
	Golay 8	14	-29.6
Barker 11	Golay 2	12	-27.6
	Golay 4	14	-29.2
	Golay 8	18	-31.4
Barker 13	Golay 2	14	-29.0
	Golay 4	16	-30.2
	Golay 8	20	-32.2

3.5 Simulation results

The theoretical results show that the BCG codes have better performance than the simple pulse, Barker code and Golay code pairs in SNR and have lower PSL than Barker code. In order to verify the feasibility of this method under actual conditions, the ultrasonic testing simulation needs to be completed. Field II is a program based on linear acoustic in MATLAB. It can be used to simulate the production of the ultrasonic probe and the signal received by the probe to receive the sound field. This program can simulate the pulse generation and recall of various ultrasonic transducers in pulsed or continuous wave operation.

In the simulation, different types of pulse signals have been used as propagation signals through tissue. In order to get the echo signal, a scatterer has been set. The frequency of the signal is 5 MHz and the sample frequency is 100 MHz. The speed of sound is a constant propagation speed of 1540 m/sec. In order to get accurate simulation results, the transducers in the UT system are set. There are 32 elements used in the simulation. The width in the x-direction of elements is 1 mm and the width in the y-direction of elements is 5 mm. The kerf between each two elements is 0.25 mm. The input signals have been modulated by carrier sine waves. The impulse responses of the pulse and receive apertures are a 2-cycle sine wave with a fit Hanning window. The voltage of a simple pulse is 1 V and input voltages of other codes are similar to simple pulses. The purpose is for calculating the received signal from a collection of scatterers and for each combination of

transmitting and receiving elements in the aperture. This corresponds to a full synthetic aperture scan, with each element transmitting and all elements receiving. This simulation experiment set a scatterer at [0,0,100] mm. Figure 3.5 shows the setup of simulation. There is an example of a transmitted 3-bit Barker code convolution 4-bit Golay code pair in Figure 3.6.

Figure 3.7 shows the echo signal of a simple pulse. The top figure shows a composite image of received intensities from the individual elements of a linear array transducer. The bottom figure shows the central element of individual response.

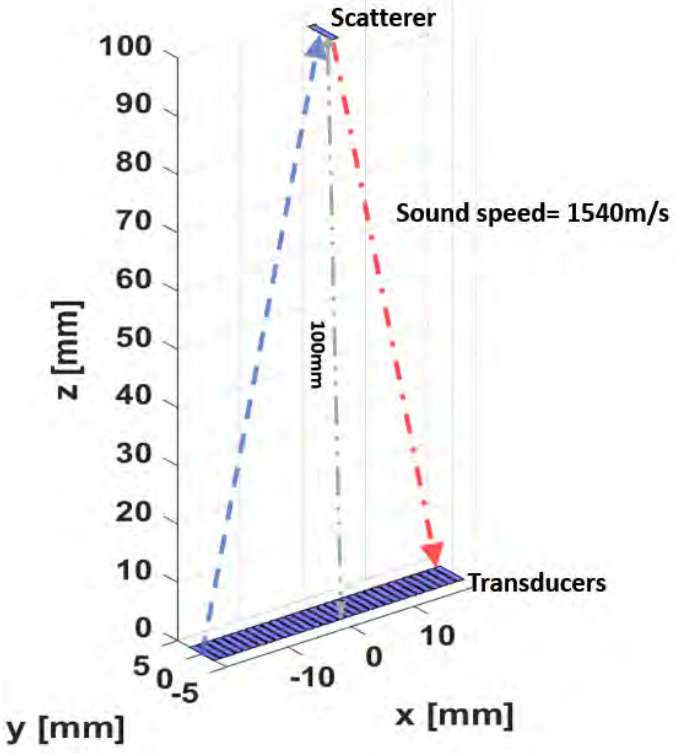

Figure 3.5: The simulation setup

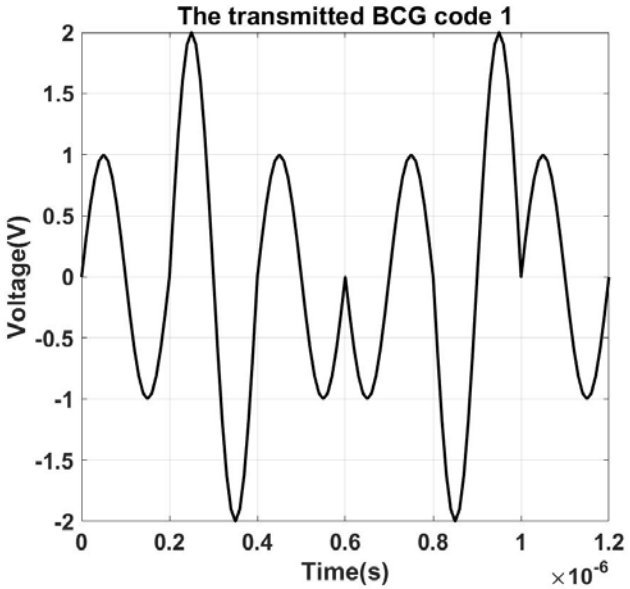

(a) The first transmitted BCG code

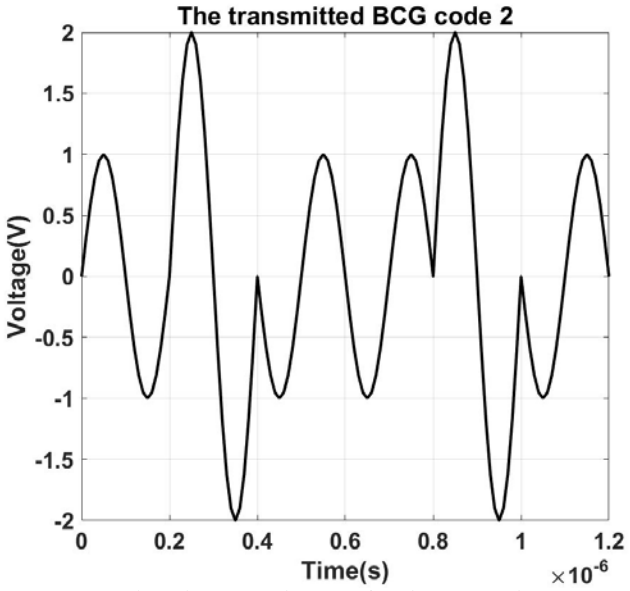

(b) The second transmitted BCG code

Figure 3.6: The transmitted B3G4 code pair in the Filed II simulation (**a**) The first transmitted BCG code (**b**) The second transmitted BCG code

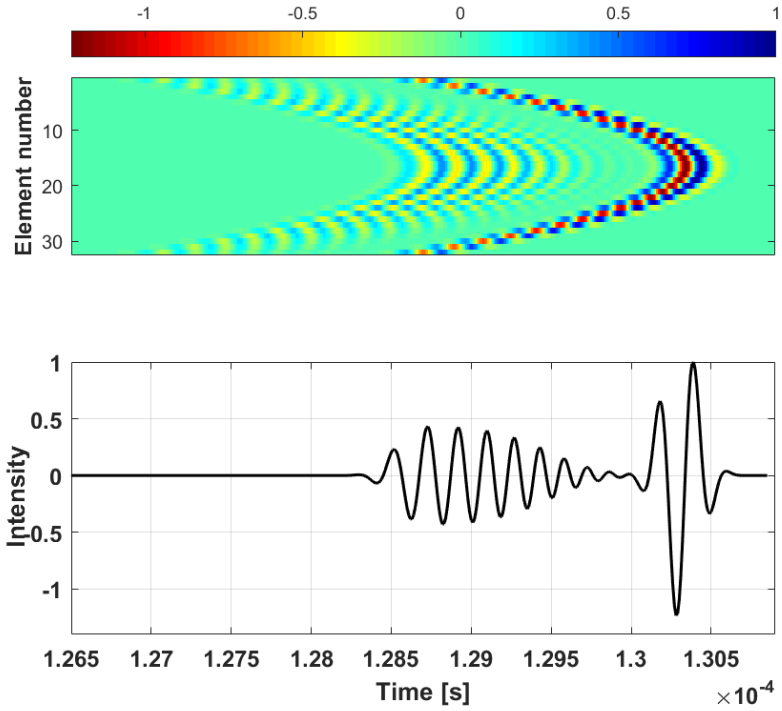

Figure 3.7: Received intensities from the individual elements of a linear array transducer (top) and the individual response of center element (bottom).

3.5.1 Barker code and Golay code pair simulation result

This section shows the simulation results of the Barker code and Golay code pair. The results show that these two traditional coded excitation techniques are successful in improving the SNR by comparing the intensity of the main lobe. The simulation results are compared with the theoretical results. Figure 3.8 shows the received signal and the processed signal by using a 7-bit Barker code signal. Figure 3.8 (a) shows the original received signal, the top shows the composite image of received 7-bit Barker code intensities from the individual elements of a linear array transducer, and the bottom shows the individual response of the central element. Figure 3.8 (b) shows the processed result of the received signal after matched filter. The 7-bit Barker code had an increased intensity of 18.5 dB compared to the simple pulse. In the theoretical study, the increased intensity should be 16.9 dB. Since the echo signal of simple pulse is difficult to distinguish in the simulation, the improvement in SNR of the Barker code sequence in simulation is better than the SNR of the theoretical. That shows a good agreement between the simulation results and theoretical results. The Barker code sequence can significantly improve the echo SNR as expected.

Figure 3.9 shows the echo signals and processed signals of 4-bit Golay code pair signals and Figure 3.9 (a) shows the original received signal, the top shows the composite image of first received 4-bit Golay code intensities from the individual elements of a linear array transducer and the bottom shows the individual response of central element. The Figure 3.9 (b) is the same as (a), it shows the result of the second Golay code pair. Figure 3.9 (c) shows the processed result of received signal after matched filter and compression. The 4-bit Golay code pair had increased intensity of 21.5 dB compared to the simple pulse.

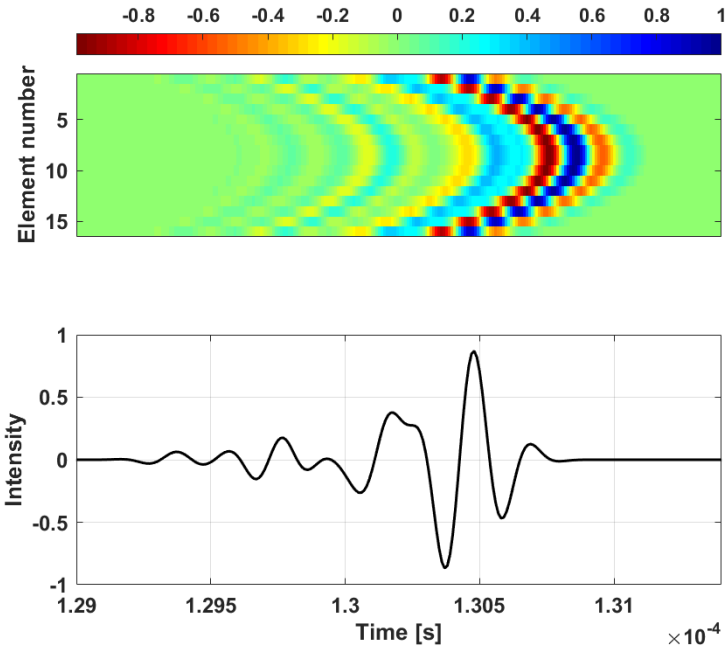

(a) The original received 7-bit Barker code intensities from the individual elements of a linear array transducer (top) and the individual response of center element (bottom).

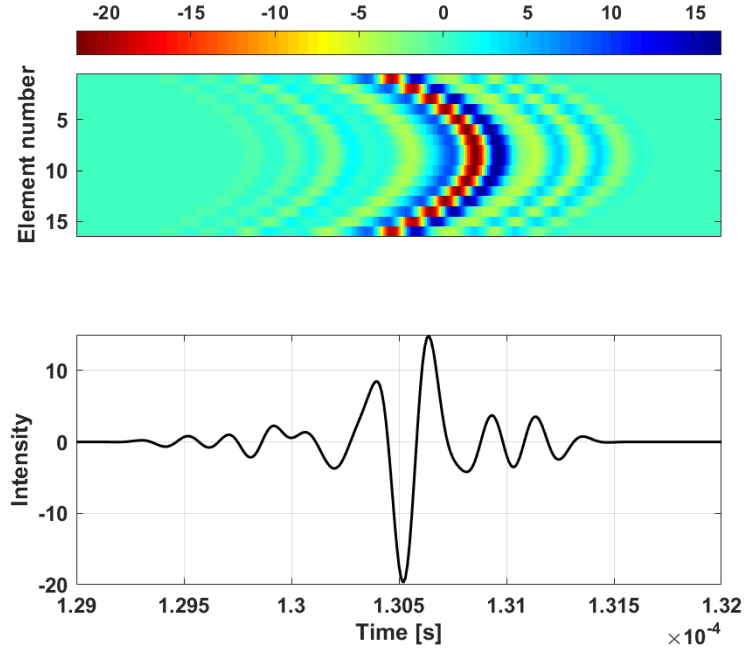

(b) The compressed 7-bit Barker code signals from the individual elements of a linear array transducer (top) and the compressed signal of center element (bottom).

Figure 3.8: The 7-length Barker code simulation result. (**a**) The original received intensities from the individual elements of a linear array transducer (top) and the individual response of center element (bottom). (**b**) The compressed signals from the individual elements of a linear array transducer (top) and the compressed signal of center element (bottom).

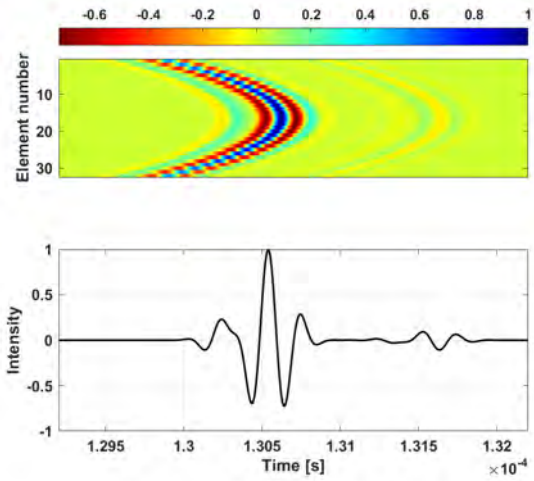

(a) The received 4-bit Golay code 1 intensities.

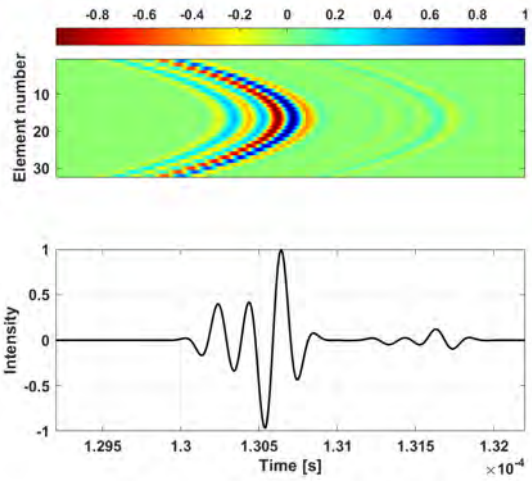

(b) The received 4-bit Golay code 2 intensities.

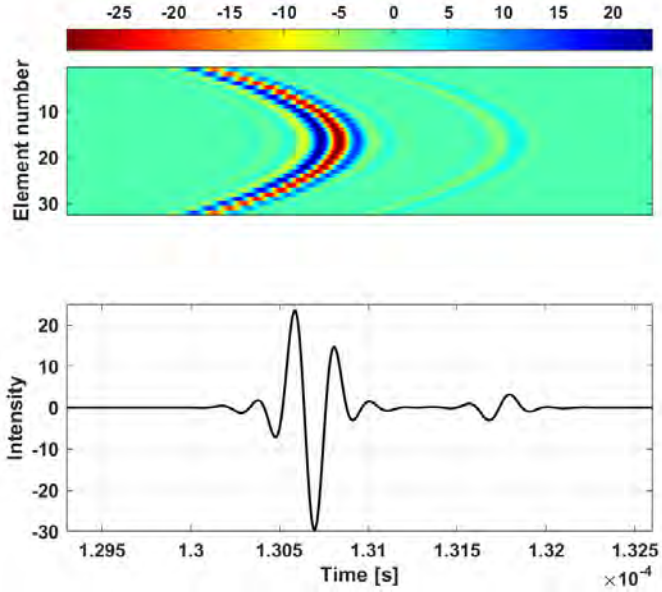

(c) The compressed signals from the individual elements of a linear array transducer (top) and the compressed signal of center element (bottom).

Figure 3.9: The 4-bit Golay code pair simulation results. (a). The original received 4-bit Golay code 1 intensities from the individual elements of a linear array transducer (top) and the individual response of center element (bottom). (b).The original received 4-bit Golay code 2 intensities from the individual elements of a linear array transducer (top) and the individual response of center element (bottom). (c). The compressed signals from the individual elements of a linear array transducer (top) and the compressed signal of center element (bottom).

3.5.2 Convolution of fixed length Barker code and various length Golay code pair

This section shows the simulation results of the convolution of fixed-length Barker codes and various length Golay code pairs. The results show that the techniques are successful in improving the SNR by comparing the intensity of the main lobe. The simulation results are compared with the theoretical results. Figure 3.10 shows the echo signals and processed signals of the convolution of 3-bit Barker code and various lengths of Golay code, which contain 3-bit Barker combined with a 2-bit Golay code pair, 3-bit Barker combined with a 4-bit Golay code pair, and 3-bit Barker combined with an 8-bit Golay code pair.

In both the original received signal part and the processed signal part, the composite images and central elements of individual responses have been posted. By comparing these two parts of the results, the increased intensities can be easily seen. The B3G2 code had an increased intensity of 22.02 dB compared to the simple pulse and the signal side-lobe level is -18.9 dB. The B3G4 code had an increased intensity of 27.1 dB compared to the simple pulse and the signal side-lobe level is -19.2 dB. The B3G8 code had an increased intensity of 30.1 dB compared to the simple pulse and the signal side-lobe level is -23.0 dB.

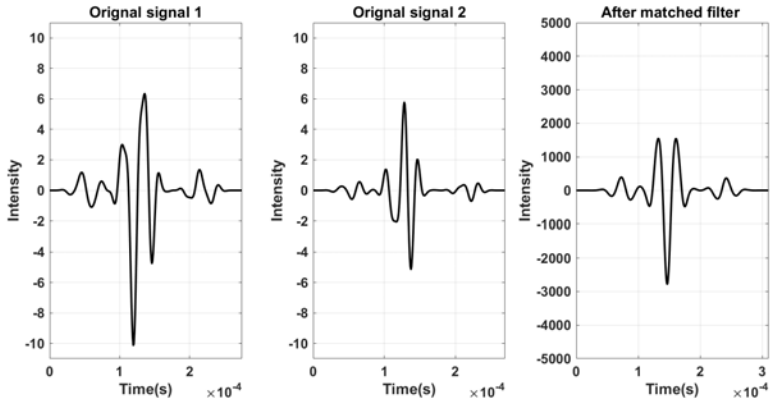

(a) The central line of original B3G2 echo signals and the compressed result after matched filter

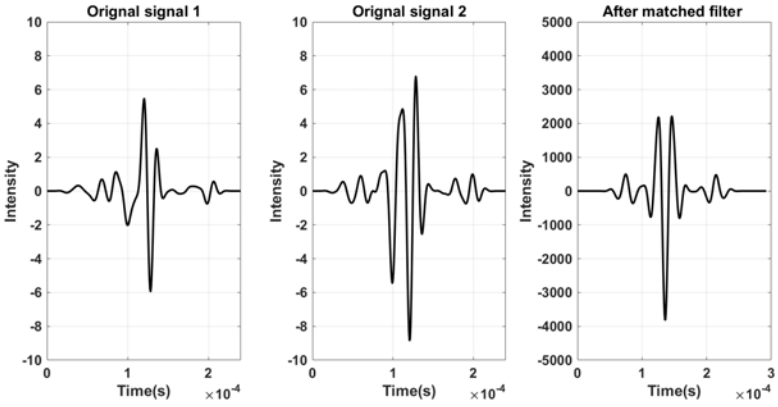

(b) The central line of original B3G4 echo signals and the compressed result after matched filter

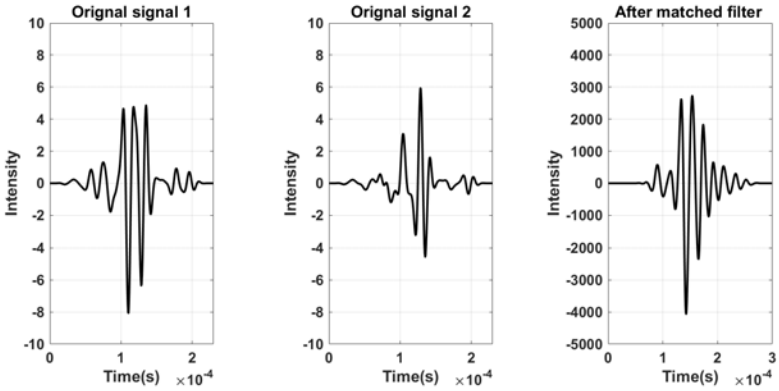

(c) The central line of original B3G8 echo signals and the compressed result after matched filter

Figure 3.10: The central line of 3-bit Barker combine different length Golay code pairs simulation results. (**a**) The original and processed B3G2 pair signals. (**b**)The original and processed B3G4 signals. (**c**) The original and processed B3G8 pair signals.

3.5.3 Convolution of 2-bit Golay code and various length Barker code

This section fixed the length of the Golay code pair at 2 and convoluted the Golay code pair with various lengths of Barker codes. Figure 3.11 and Figure 3.12 show the echo sig-

nals and processed signals of the convolution of 2-bit Golay code and various lengths of Barker code, which contain a 5-bit Barker combined 2-bit Golay code pair, a 7-bit Barker combined 2-bit Golay code pair, an 11-bit Barker combined 2-bit Golay code pair, and a 13-bit Barker combined 2-bit Golay code pair. Each figure contains the original received signal part and the processed signal part.

In both the original received signal part and the processed signal part, the composite images and the central element of individual responses have been posted. By comparing these two parts of the results, the increased intensities can be easily seen. The B5G2 code had an increased intensity of 24 dB compared to the simple pulse and the PSL is -22.6 dB. The B7G2 code had an increased intensity of 27.78 dB compared to the simple pulse and the PSL is -24.2 dB. The B11G2 code had an increased intensity of 31.3 dB compared to the simple pulse and the PSL is -27.4 dB. The B13G2 code had an increased intensity of 35.1 dB compared to the simple pulse and the PSL is -28.2 dB.

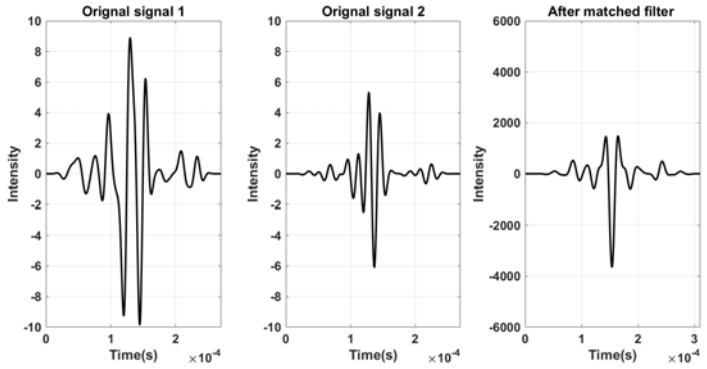

(a) The central line of original B5G2 echo signals and the compressed result after matched filter

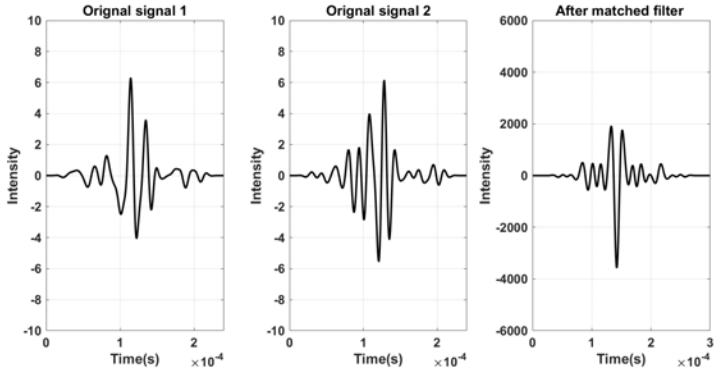

(b) The central line of original B7G2 echo signals and the compressed result after matched filter

Figure 3.11: The central line of 2-bit Golay code combine different length Barker code pairs simulation results(**a**) The original and processed B5G2 pair signals. (**b**)The original and processed B7G2 signals.

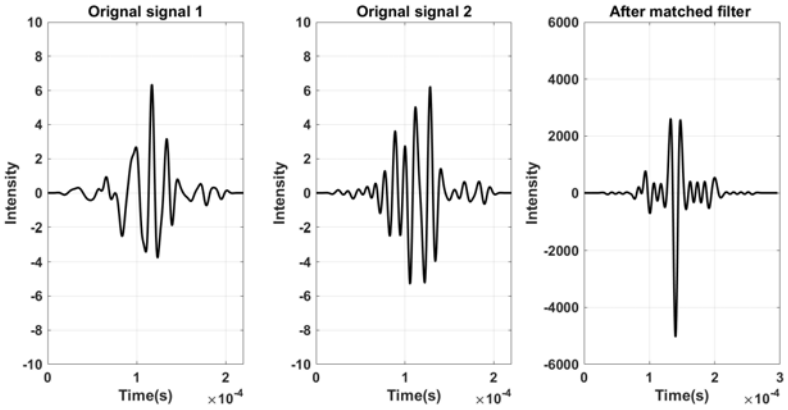

(a) The central line of original B11G2 echo signals and the compressed result after matched filter

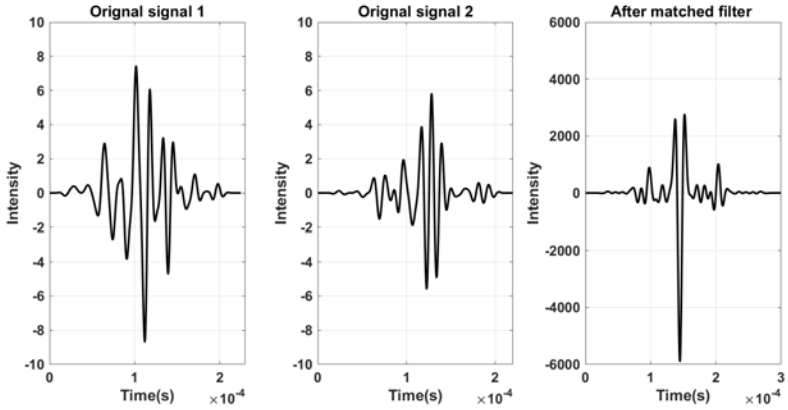

(b) The central line of original B13G2 echo signals and the compressed result after matched filter

Figure 3.12: The central line of 2-bit Golay code combine different length Barker code pairs simulation results(**a**) The original and processed B11G2 pair signals.(**b**) The original and processed B13G2 pair signals.

3.5.4 Convolution of 4-bit Golay code and various length Barker code

This section fixed the length of the Golay code pair at 4 and convoluted the Golay code pair with various lengths of Barker codes. Figure 3.13 and Figure 3.14 show the echo signals and processed signals of the convolution of 4-bit Golay code and various lengths of Barker code which contain a 5-bit Barker combined with a 4-bit Golay code pair, a 7-bit Barker combined with a 4-bit Golay code pair, an 11-bit Barker combined with a 4-bit Golay code pair, and 13-bit Barker combine 4-bit Golay code pair.

In both original received signal part and processed signal part, the composite images and central element of individual responses have been posted. By comparing these two part results, the increased intensities can be obviously seen. The B5G4 code had an increased intensity of 29.6 dB compared to the simple pulse and the PSL is -20.1 dB. The B7G4 code had an increased intensity of 30.7 dB compared to the simple pulse and the PSL is

-18.6 dB. The B11G4 code had an increased intensity of 33.6 dB compared to the simple pulse and the PSL is -25.9 dB. The B13G4 code had an increased intensity of 34.3 dB compared to the simple pulse and the PSL is -23.6 dB.

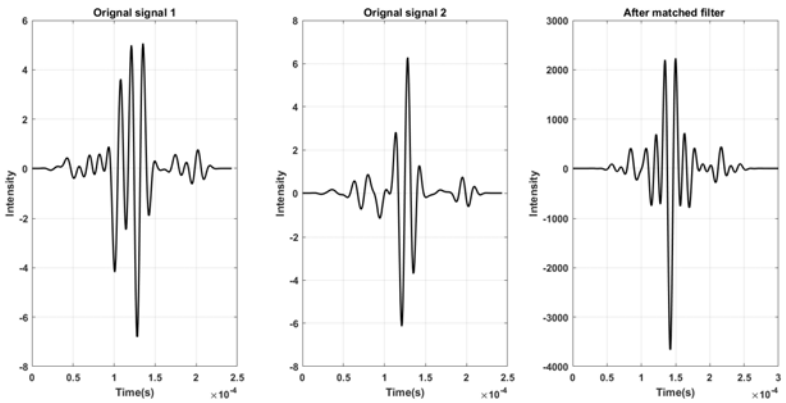

(a) The central line of original B5G4 echo signals and the compressed result after matched filter

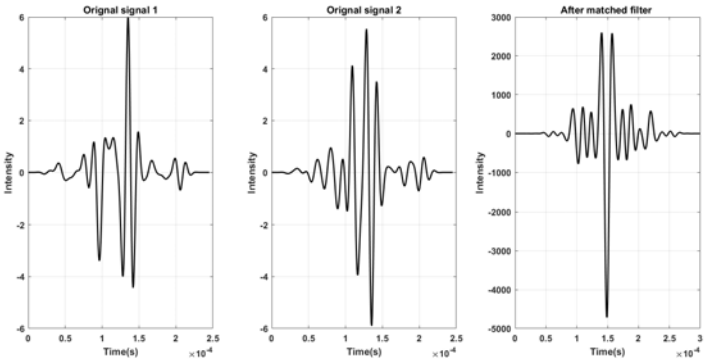

(b) The central line of original B7G4 echo signals and the compressed result after matched filter

Figure 3.13: The central line of 4-bit Golay code combine different length Barker code pairs simulation results(**a**) The original and processed B5G4 pair signals. (**b**)The original and processed B7G4 signals.

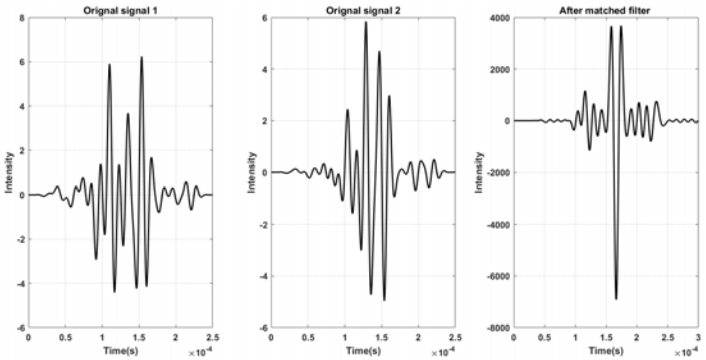

(a) The central line of original B11G4 echo signals and the compressed result after matched filter

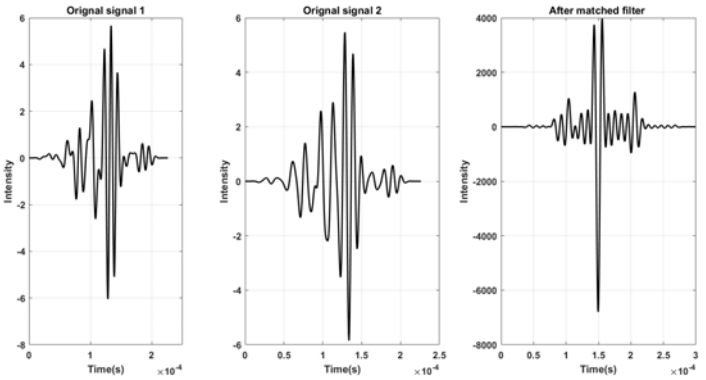

(b) The central line of original B13G4 echo signals and the compressed result after matched filter

Figure 3.14: The central line of 4-bit Golay code combine different length Barker code pairs simulation results (**a**) The original and processed B11G4 pair signals.(**b**) The original and processed B13G4 pair signals.

3.5.5 Convolution of 8-bit Golay code and various length Barker code

This section fixed the length of Golay code pair at 8 and convoluted the Golay code pair with various length of Barker codes. Figure 3.15 and Figure 3.16 show the echo signals and processed signals of convolution of 8-bit Golay code and various lengths Barker code which contain 5-bit Barker combined 8-bit Golay code pair, 7-bit Barker combined 8-bit Golay code pair, 11-bit Barker combined 8-bit Golay code pair and 13-bit Barker combined 8-bit Golay code pair. Each figure contains the original received signal part and the processed signal part.

In both original received signal part and processed signal part, the composite images and central element of individual responses have been posted. By comparing these two part results, the increased intensities can be obviously seen. The B5G8 code had increased intensity of 32.4 dB compared to the simple pulse and the PSL is -24.5 dB. The B7G8 code had an increased intensity of 33.7 dB compared to the simple pulse and the PSL is -21 dB. The B11G8 code had an increased intensity of 38.4 dB compared to the simple pulse and the PSL is -29.4 dB. The B13G8 code had an increased intensity of 38.5 dB compared to the simple pulse and the PSL is -25.4 dB.

As the code length has grown longer, so has the increased intensity. This increase is the same as the result of theoretical research. At the same time, since the intensity of the main lobe increases and the intensity of the side lobes does not change, the performance of the PSL in the result also improves as the code length increases.

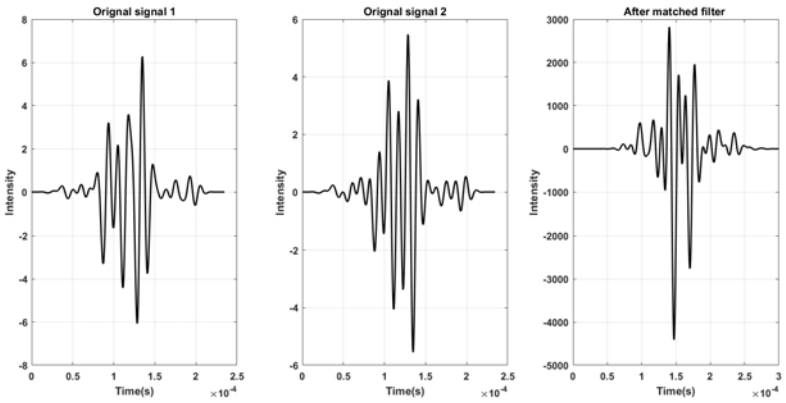

(a) The central line of original B5G8 echo signals and the compressed result after matched filter

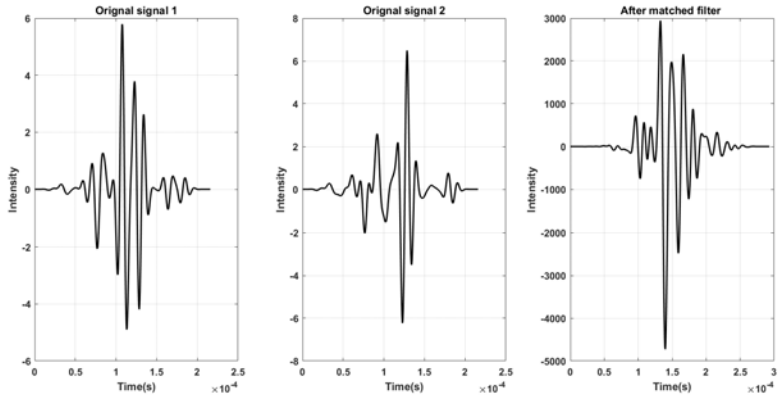

(b) The central line of original B7G8 echo signals and the compressed result after matched filter

Figure 3.15: The central line of 8-bit Golay code combine different length Barker code pairs simulation results(**a**) The original and processed B5G4 pair signals. (**b**)The original and processed B7G8 signals.

3.5.6 Results analysis

Figure 3.17 shows all the results of low voltage UT system simulation. From the simulation results, it is easy to see that the highest intensity of the processing echo signal is 13-bit Barker code convolution 8-bit Golay code pair. The length of 3-bit Barker code convolution 2-bit Golay code pair is the shortest, therefore the intensity of processing signal is the lowest of all. The simulation results have a good agreement with the theoretical results. When the transmitted sequence length is short, the theoretical results and

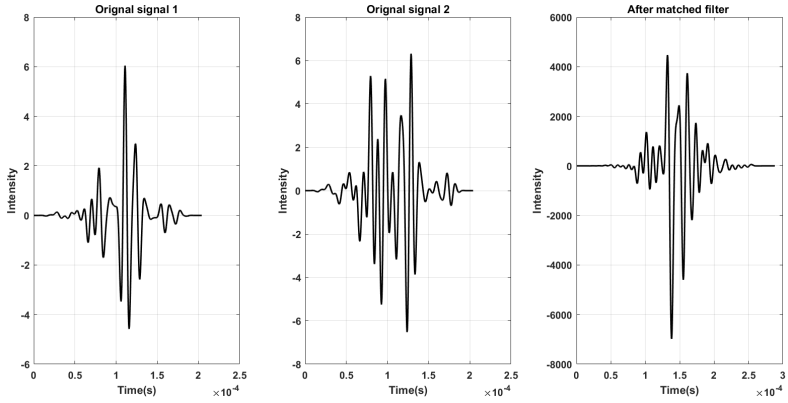

(a) The central line of original B11G8 echo signals and the compressed result after matched filter

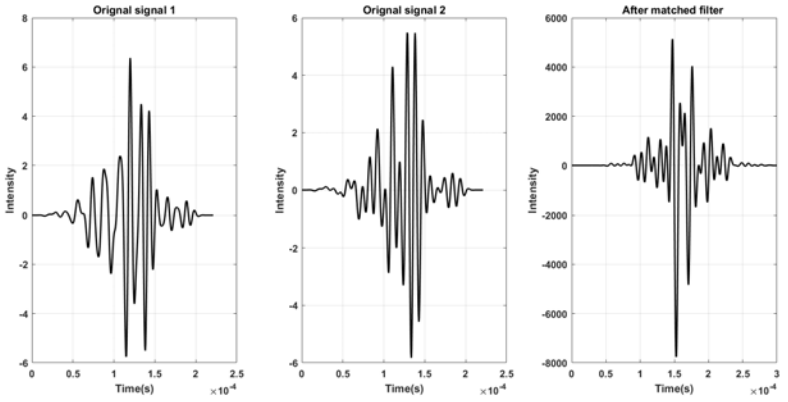

(b) The central line of original B13G8 echo signals and the compressed result after matched filter

Figure 3.16: The central line of 8-bit Golay code combine different length Barker code pairs simulation results(**a**) The original and processed B11G8 pair signals.(**b**) The original and processed B13G8 pair signals.

simulation results are almost the same, and the difference in SNR is 1-2 dB. As the transmitted sequence length increases, the results of theoretical and simulation gradually have larger errors, and the difference in SNR is 5-6 dB. But the trend and rate of change of SNR and PSL are the same. The reason for this problem is that when a long sequence is transmitted, noise and system internal errors will affect the echo signal and reduce SNR. Compared with the traditional method, the proposed BCG method still has a very significant improvement.

Table 3.3 shows all the SNR and PSL results from numerical and theoretical simulations using MATLAB software. In Pilsu Kim 's paper, the SNR of 3-bit Barker code modulated 4-bit code exhibits the improvement of 27.68 dB in SNR and -18.66 dB in sidelobe level [83] which results agree with the simulation results. The 15-bit M-sequences which are commonly used in UT systems in the simulation module increased intensity of 17.8 dB compared to the simple pulse and the signal side-lobe level is -8.66 dB. One of 15-bit Gold sequences in the simulation module increased intensity of 17 dB, and the signal side-lobe level is -7.1 dB.

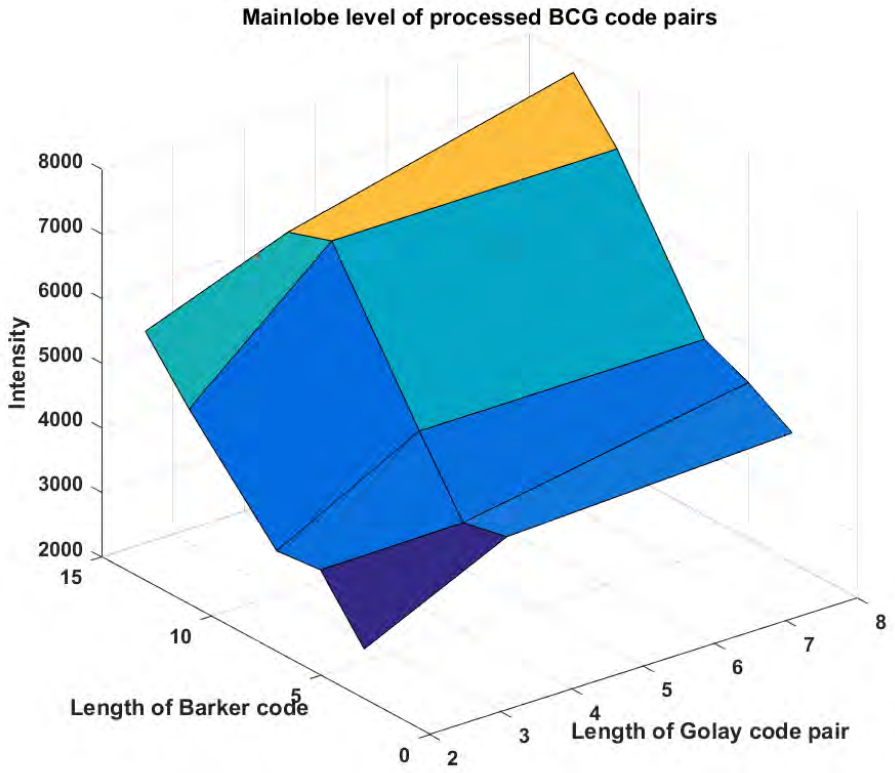

Figure 3.17: The intensity results of all BCG code sequence

3.6 Summary

In this chapter, the convolution of Barker and Golay codes as coded excitation signals is studied for low voltage UT devices. The combined codes have the same sidelobe as the Barker code and its main lobe is associated with one of the Barker code and Golay code pairs used. It combines the characteristics of a high main lobe Barker code and no side lobe Golay code pairs. There is no need to change the hardware of the UT system with this method. The proposed method has been analyzed theoretically and then done in extensive simulation experiments. The experimental results demonstrated that the intensity of the code produced by the convolution of Barker code and Golay is much higher than the simple pulse and the PSL of the code is lower than the traditional Barker code. When the length of the Golay code pair is fixed, increasing the length of the Baker code increases the intensity of the main lobe of the signal and results in a higher SNR. When the length of the Barker code is fixed, increasing the length of the Golay code pair reduces the signal's sidelobe intensity and results in a better PSL. Equipped with this, any UT device can be applied in low voltage situations for a variety of applications.

Table 3.3: The SNR and PSL results from theory and simulation

Code Symbol	Code Bit	Theoretical		Simulation	
		SNR(dB)	PSL(dB)	SNR(dB)	PSL(dB)
Barker 7	7	16.9	-17.0	18.5	-18.1
Golay 4	4	18.1	-	21.5	-
B3G2	4	21.6	-19	22.02	-18.9
B3G4	6	27.6	-23.4	27.1	-19.2
B3G8	10	33.6	-28.6	30.1	-23.0
B5G2	6	26.0	-22.0	24	-22.6
B7G2	8	28.9	-24.2	27.78	-24.2
B11G2	12	32.9	-27.6	31.3	-27.4
B13G2	14	34.3	-29.0	35.1	-28.2
B5G4	8	32	-25.4	29.6	-20.1
B7G4	10	34.9	-26.4	30.7	-18.6
B11G4	14	38.8	-29.1	33.6	-25.9
B13G4	16	40.3	-29.6	34.3	-23.6
B5G8	12	38.1	-28.8	32.4	-24.5
B7G8	16	41.1	-29.6	33.7	-21
B11G8	18	44.9	-31.4	38.4	-29.4
B13G8	**20**	**46.4**	**-32.3**	**38.5**	**-25.4**
M-sequence	15	18.1	-8.6	17.8	-8.66
Gold code	15	18.1	-8.6	17	-7.1

Chapter 4

Hybrid Pulse Compression for Guided Wave Testing Application

4.1 Introduction

Chapter 3 introduced the hybrid pulse compression method in UT system. Theoretical and simulation results prove the feasibility of the new method in a ultrasound system. The UT system has a short wavelength due to the high frequency of ultrasound. This limits the effective distance of ultrasonic testing, which makes it unsuitable in certain situations that require long-distance testing. Chapter 4 proposed the hybrid pulse compression method in ultrasonic guided wave testing, which is a low frequency long range ultrasound detection method.

Ultrasonic guided wave (UGW) testing is a crucial method in NDT technique because of its potential to evaluate the durability, the physical and mechanical properties of long pipes [123]. This method is often used for testing long-range testing of pipelines from a single inspection point [124]. Different types of guided waves can propagate in any bounded medium, such as the well-known Rayleigh (surface) waves or the Lamb waves on plates [125]. An array has many transducers utilized in a pulse-echo mode installed around the pipe circumference to excite signals in low frequencies of ultrasound at any inspection location. The purpose is to generate a single axisymmetric wave pattern. However, guided waves suffer from high attenuation when they propagate in attenuative material pipes and multiple modes due to the excitation, which reduces the power of echo

signals and induces corruption caused by coherent noise [126]. Therefore, the excitation amplitude of input signals needs to be enhanced to acquire featured signal responses.

For industrial purposes, many of these pipelines need to carry explosive and flammable material such as oil or natural gas. The common inspection systems are not suitable due to the high voltage (typical above 50 Volts) used by the pulsing circuitry. It may has high possibility of dangerous to cause high-voltage sparks, even a potential risk to create a fire or explosion [127]. The problem must be solved in a safe manner. Therefore, an inspection system operated by low-voltage ultrasound is required in these specific application environments. Generally, there are many techniques to improve the inspection system performance by increasing the signal-to-noise ratio (SNR), such as wavelet transform, pulse compression and so on. In the case of poor SNR, it is tough for wavelet transform to filter the signal coefficients in every decomposition layer effectively, which may cause the denoising failure [128].

The pulse-compression technique is commonly used by radar, sonar and echography to enhance the echo SNR. This method depends on a combination of cross-correlation with a reference signal [129]. There are two modulation methods in pulse compression, including frequency modulation and phase modulation. Coded excitation is phase modulation on a pulse. Takeuchi firstly proposed the technique applied to medical ultrasound imaging systems in 1979 [111]. However, there are few studies within the literature on coded excitation in recent years due to the time-bandwidth limitation of this technique. O'Donnell considered using coded excitation to ultrasound system for improving the SNR [112]. Afterwards, the digital beamforming with signal compression was used in the ultrasound system. Later, Jedwab and Parker gave a general construction for an odd length binary Golay sequence pair of length 26 from a Barker sequence of length 13 and a related Barker sequence of length 11 [113]. But, their work focused on the theoretical research for coded excitation only.

Kim *et al*. [83] proposed a combined coded excitation method by modulating Golay code sequence with Barker sequence for ultrasound imaging. The combined codes which are 3-bit Barker code, 8-bit Golay code pair and 3-bit Barker code modulated 4-bit Golay code pair are used in their ultrasonic image experiment. Recently, Wang and Cong [114] proposed a new pseudo Chirp-Barker-Golay (PCBG) coded excitation method in ultrasound imaging. They used the Field II toolbox to simulate phantom and cyst phantom of B-mode image. The research into modulated codes is most on ultrasound images.In their research, the combined sequences have relatively low side lobe levels and high main lobe level. At the same time, their length is easily tuned. That means the combined coded pulse compression algorithm is practically promising to reduce coherent noise to increase

SNR.

In this chapter, a hybrid coded excitation method that uses a designed sequence of a Barker code convolution Golay code pair (BCG) is developed to improve the echo SNR of ultrasonic guided wave testing systems. The technique combines the advantages of these two coding methods and increases the diversity of code lengths. The technique performance will be evaluated by SNR and peak sidelobe level (PSL) of the processed signals. The main contributions of this paper are presented as below:

The developed hybrid coded excitation technique is applied to the guided wave mode excitation for pipe inspection for the first time. The proposed method has been theoretically evaluated that has better performance than other common techniques. The experimental results that the proposed method has the best echo SNR and PSL at various frequencies (30 kHz-50 kHz). This work can be extended to other potential applications for a significant SNR improvement. The field test on pipeline with defects has been done. Compared to other methods, the proposed method can detect small defects which cannot be detected by other methods on pipelines.

The rest of this chapter is organised as follows. In Section 4.2, the property of guided waves has been reviewed and code generation and compression also proposed in this section. The methodology and analyse are also described in this section. The results of FEM simulation analysis are described in Section 4.3 and the laboratory testing in pipeline without defect are described in Section 4.4. The experiment set-up and actual testing results are described in Section 4.5. Finally, the summary is given in Section 4.6.

4.2 Methodology

To verify the feasibility of proposed coded excitation method for guided wave testing in pipes, the related dispersion curves of wave modes should be studied first. To obtain the transmitted sequence and estimate the transmitted signal performance, the proposed coded excitation generation and compression need to be investigated.

4.2.1 Property of guided waves

When measuring over a long-range distance with ultrasound guided waves, the wave modes are excited at a low-frequency range between 20 kHz to 100 kHz [130]. Guided waves exist multi-modal orders and dispersed when they propagate along a cylindrical structure [131].

There are three main families of waves exists in pipe, which are Longitudinal, Torsional and Flexural. In these three families of waves, only Longitudinal and Torsional are axisymmetric. Silk and Bainton established a nomenclature of $X(n,m)$ to describe these [132]. The X represents a letter (L, T, or F, for longitudinal, torsional or flexural, respectively) that relates to characteristics of the individual guided wave modes. The n is a positive integer used to identify harmonic changes in displacement around the pipe or the circumference of the pipe and m is an index indicating how it occurs. When testing, the actual results are different from the ideal. Due to the imperfections of equipment and the mode conversion caused by the axisymmetric structure on the internal material, the actual received signal will not be a pure axisymmetric wave but a mixed wave [133]. In addition to the multi-modal nature of guided wave propagation may also exhibit dispersive propagation, but this situation will lead the energy diffusion signal in space and time at the time of propagation [134]. Unlike other waves, the T(0,1) mode is non-dispersive over the entire frequency range, so the T(0,1) mode is often used for detection in practical applications [133].

Figure 4.1 presents the group velocity dispersion curves for an 8-inch (219.1 mm outer diameter) and schedule 40 (8.18 mm wall thickness) steel pipes. Longitudinal axisymmetric modes of L(0,1) and L(0,2) are also a zeroth circumferential order with first and second mode shapes, respectively. Non-axisymmetric flexural modes (up to m=1) of F(1,1), F(1,2) and F(1,3) are a first circumferential order with a first, a second and a third mode shapes, respectively. The effective characteristics of displacement shapes are generated using the semi-analytical finite element method [135].

4.2.2 Code generation and compression

Coded excitation applied in medical ultrasound imaging system was excitation. The improvement of SNR is related to the length of the sequences, but there are only a few lengths of Barker codes available, although there is no limitation for conventional Golay codes [108]. Theoretically, the longer code excitation sequence offers better performance of the SNR but a higher axial resolution depends on a shorter input signal wavelength.

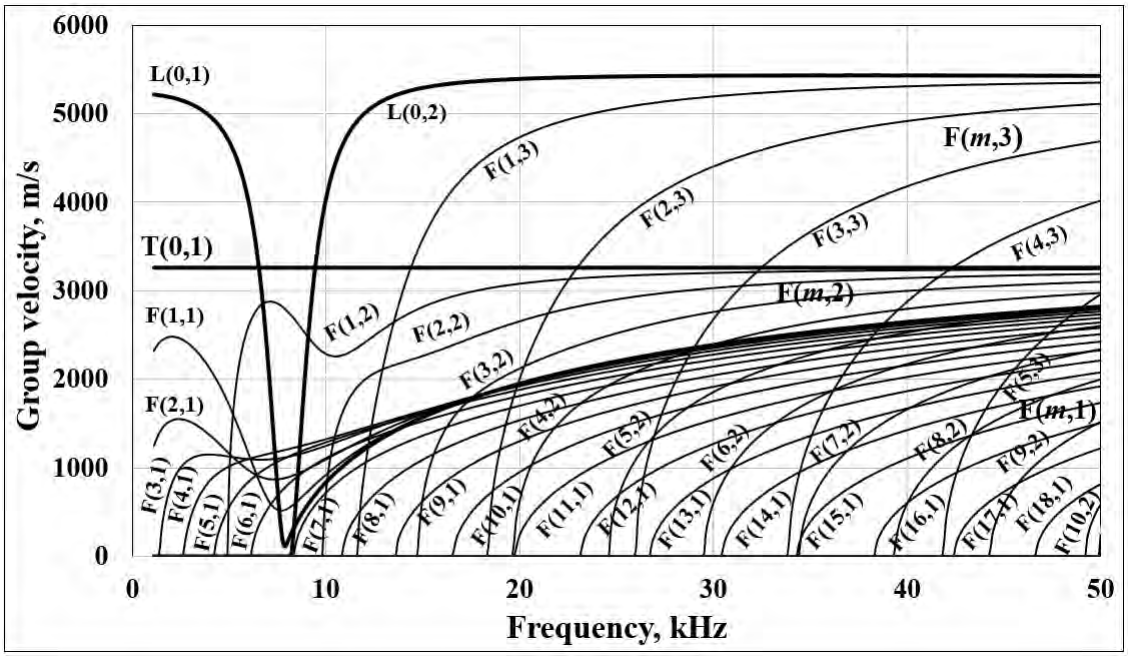

Figure 4.1: Group velocity dispersion curves for a 8-inch, schedule 40 steel pipe

Therefore, the selection of the code excitation sequence length needs to be considered for accuracy and efficiency of defect detection under different applications.

Currently, the combined code excitation methods are only applied in ultrasound imaging, and the selection of the combined code is limited [127]. However, there is no existing literature and usage on the excitation of guided waves for long-range distance detection at low-frequencies. In this paper, this developed technique is successfully achieved to use on the guided wave generation and propagation for pipeline inspection theoretically and experimentally.

Due to the character of the coded excitation, the coded excitation length can influence the improvement of SNR and resolution. However, However, since Golay codes and Barker codes are called out for their specific sequences, it's solely permitted to decide on one among the sequences for ultrasonic testing. BCG is convoluted by Golay code and Barker code, which may result in further improvements in signal intensity and adaptability for code length compared to convention Golay code pairs and Barker code. The combined codes have an equivalent sidelobe of the baker code used and also the main lobe of the combined codes is related to the most lobe of Barker code and Golay code pairs. It combines the characteristics of a high main lobe Barker code and no facet lobe Golay code pairs.

To excite the ultrasonic signal, the BCG code modulates the ultrasonic wave with a wave signal frequency carrier. Transmit beamformer and electrical device transmit the BCG code ultrasonic signal. The electrical device will receive the echo signals from the medium. Figure 4.2 shows the method of generation and compression of BCG codes. The BCG code sequences are made by the convolution of Barker code and Golay code pair. The BCG code sequences are modulated and transmitted to the medium to get a pair of echoes. There are two steps to compress the echoes. The primary step is to compress the Golay code pair sequence, and the second step is to process the Barker code matched filter. The compression result is the addition of the processed echo signal pairs.

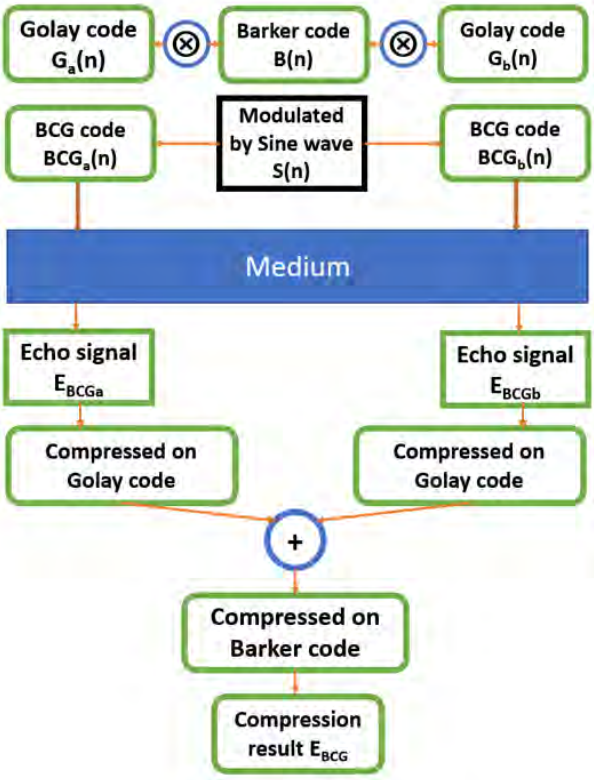

Figure 4.2: The process of generation and compression of Barker-sequence combined Golay codes (BCG).

A BCG code pair, BCG_a and BCG_b, are built by using convolution of Golay sequence and Barker sequence and modulated by a base pulse as shown in following equations.

$$BCG_a(n) = G_a(n) * B(n) * C(n) \tag{4.1}$$

$$BCG_b(n) = G_b(n) * B(n) * C(n) \tag{4.2}$$

where $B(n)$ is a known Barker code sequence and $G_a(n)$, $G_b(n)$ are the Golay code pairs.

Defined the $BCG_a(n)$ and $BCG_b(n)$ as modulated BCG code signal. $C(n)$ is a carrier sine wave. There is an example of transmitted B3G4 code pair in Figure 4.3.

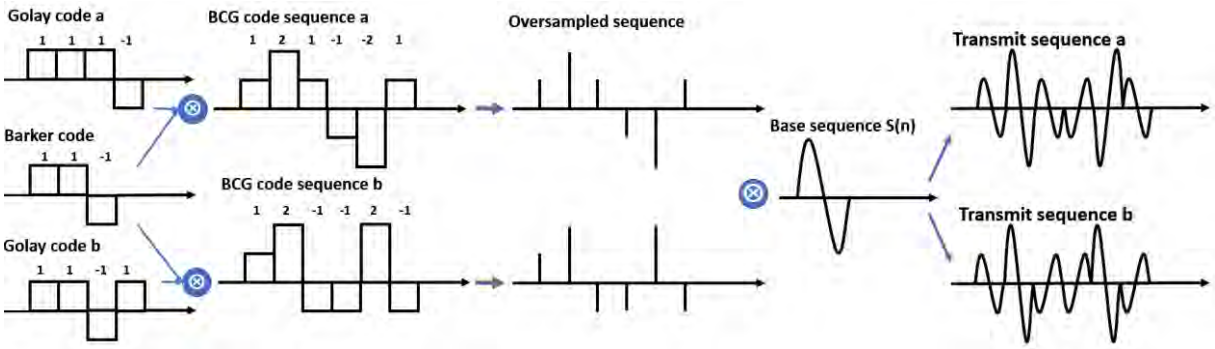

Figure 4.3: The BCG code pair modulated by sine wave.

To prove the feasibility of BCG code, the theoretical analysis based on synthetic input/output signals has been carried out. The 15 different types of BCG code are used in the analysis. Three different types of pulses have been used: a simple pulse, 7-bit Barker code and 4-bit Golay code pairs. PSL is a major parameter that describes a code's properties [122] and it can be calculated based on the peak (P_{peak}) and mean (P_{mean}) power of lobe pulse.

The peak-side lobe level of different sine wave modulated BCG code lengths are shown in Figure 4.4. Figure 4.5 (a) shows the comparison of different theoretical intensities of 9 types of BCG codes. Figure 4.5 (b) shows that a 3-bit Barker code modulated 4-bit Golay code compared to simple pulse, 7-bit Barker code, 11-bit Barker code, 4-bit Golay code and 8-bit Golay code. It can be seen from the Figure 4.5 and Figure 4.4 that the intensity of the same length of sine wave modulated BCG code after processing is significantly higher than other codes. The PSL of different length of BCG codes has been significantly reduced.

4.3 FEM simulation

A commercial finite element software package, Abaqus (version 2016.HF3, Dassault Systèmes Americas Corp., Waltham, MA, USA), has been used to visualise and validate this method. The Abaqus Explicit module was used to produce a transient wave field. The incident signals are Barker code, Golay code, and BCG code modulated with sine waves at a frequency of 40 kHz. The pipe has a thickness of 8.18 mm and length of 7000 mm. The purpose sources are equally distributed, and placed 2600 mm from the front end of

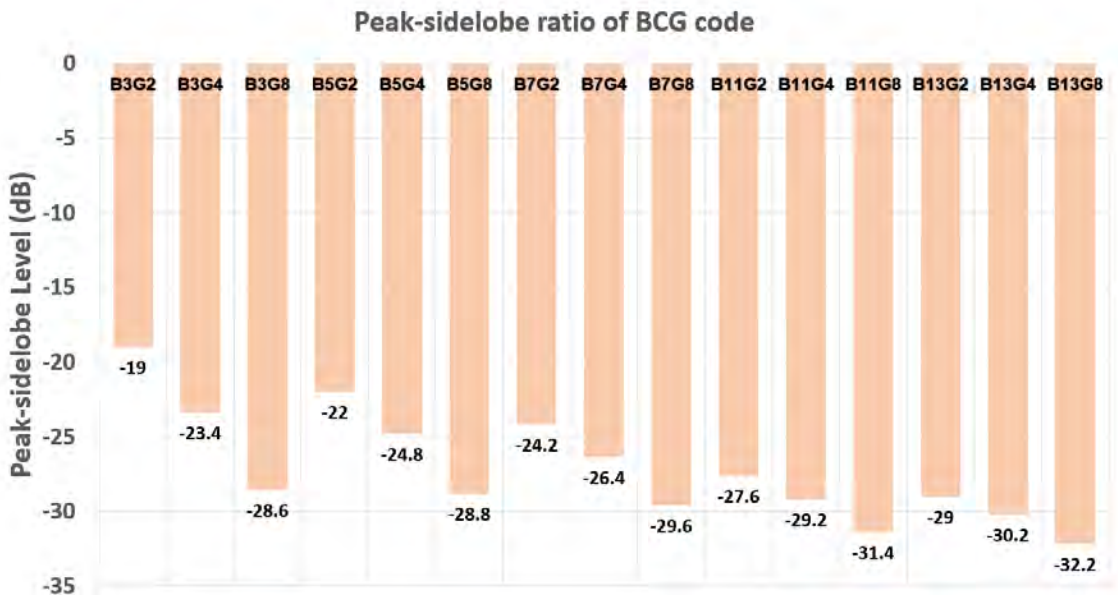

Figure 4.4: The peak-side lobe level of different BCG codes from numerical simulation.

the pipe. Young's Modulus was 210 GPa, Density of 7850 kg/m^3 and Poisson's Ratio of 0.3. The global seed size was set as 0.0025 m, and the time increment was set as 5×10^{-7} s. Figure 4.6 shows the setup of FEM model of a 8-inch steel pipe. As for the hollow cylinder, if the part variety is split into one to three parts in the thickness direction, it'll have achieved sensible accuracy [136].

For simulating the UGW system, one ideal point source is generated around the circumference of the pipe. The system worked within the pulse-echo mode and, therefore, the signals were received from an equivalent number of ideal sources. The received signal is generated from the receiving point and applying an equivalent backward cancellation formula. The signals are generated in MATLAB-R2016a and echo signals are processed in MATLAB as well. The displacement/time plot of Barker code echo signal from the receiver is shown in figure 4.7.

The FEM simulation results are evaluated by increasing SNR and peak sidelobe level. The front and back side increments of SNR from FEM simulation and testing results are compared in Figure 4.48. Due to the character of the Golay code, there is no side lobe in the compressed results of the Golay code pair. The comparison of side lobe level between simulation and testing results is shown in Figure 4.49.

4.4 Laboratory testing

An experiment was carried out on a 7 m long 8-inch schedule 40 steel pipe. The transducers driven by Teletest MK3 system device are located at around 2600 mm from pipe end. A detailed sketch of this experiment has been described, as shown in Figure 4.8. The experiment had been performed by TWI Ltd as shown in Figure 4.9. The steel pipe was placed on roller supports. The received signal gets a signal whose specific part contains only two echoes.

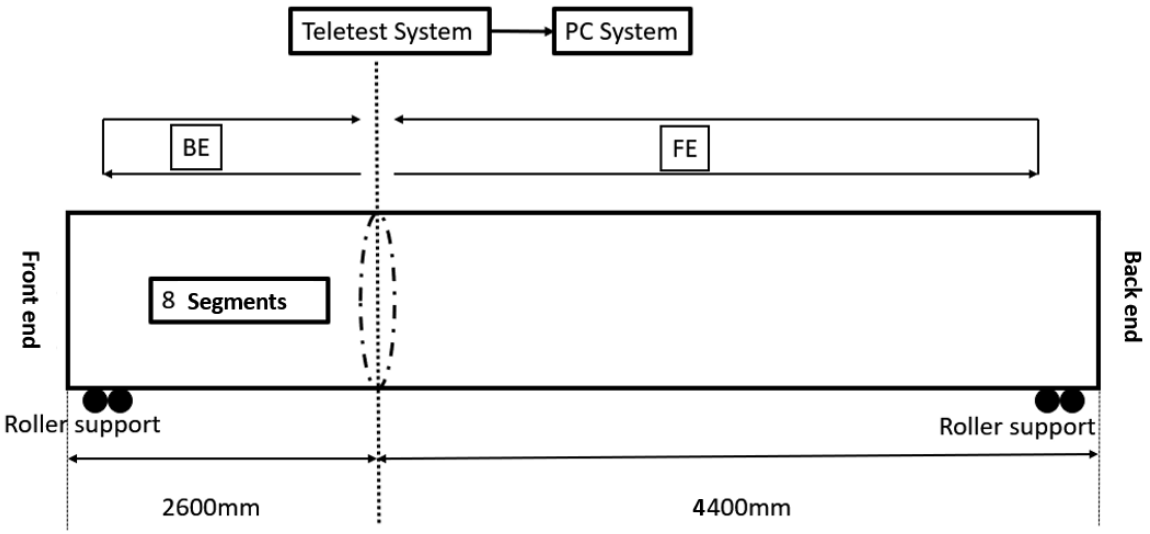

Figure 4.8: Schematic diagram of pipe experiment set-up which contains roller support,Teletest system and PC system.

The experiment used sine waves, different bits of Barker code, different bits of Golay code pair and BCG code pairs as excited signals. There are 8 transmit-receive segments of the system. Each segment has 3 transducers. The amplitude and time of transmitted signal should be created in TXT file for each segment. The TXT file should be coded to TIM file that the supporting software can identify. Then the parameters of the system can be set in the supporting software, including sampling frequency, PRF, capture time and so on. When all 8 segments are set up successfully, the test can be started. Figure 4.10 shows the software used in the GWT system. The code to load the specific code sequence is in the Appendix.

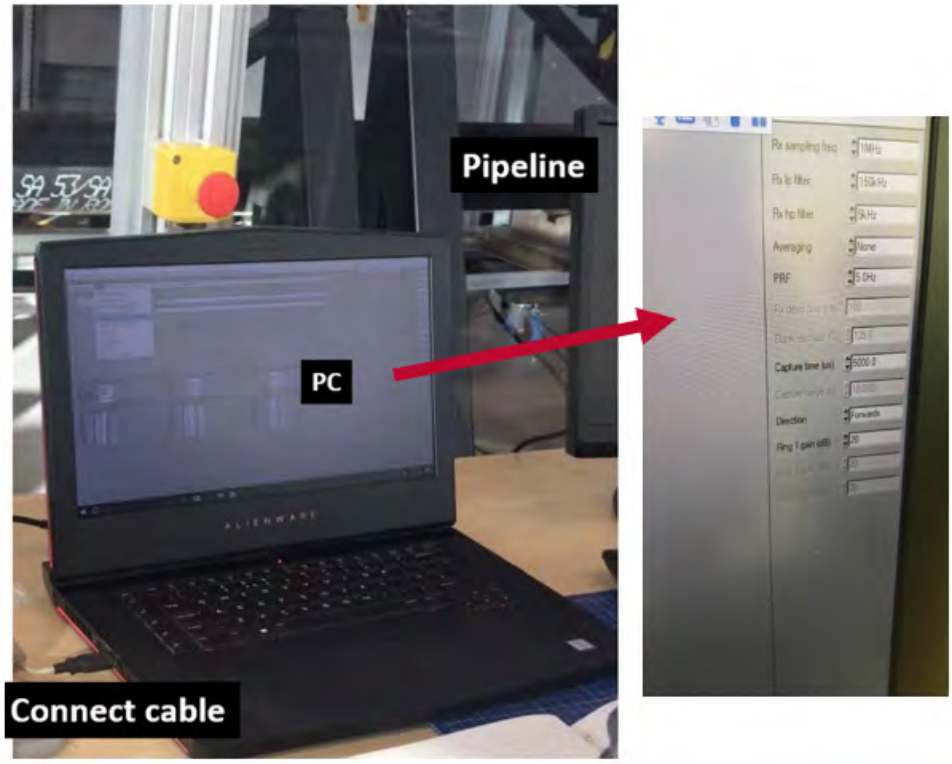

Figure 4.10: The software used in the GWT system.

The transmitted frequency of all of the excited signals is from 30 kHz to 50 kHz and the guided wave mode of T(0,1) was excited by a transmitter. The experimental result was collected from a 7000 mm long steel pipe without any defects, and picked up data from 8 segments using MATLAB software. The details of excited signals are shown in the Table 4.1 and Table 4.2.

Figure 4.11 shows an example of the echo signal that is a 3-bit Barker code at 30 kHz. This figure is a three-dimensional surface plot reconstructed from the echo signals received by eight segments. The echo signals from the front end and the echo signals from the back end have been marked on this figure. The length of the pipe can be calculated from the time of front and back echoes.

4.4.1 Testing of different frequency BCG code

In order to verify the performance of the proposed method at different frequencies, a variety of frequency tests were implemented. Figure 4.12, Figure 4.13, Figure 4.14, Figure 4.15 and Figure 4.16 show the original echo signal pairs and processed results of BCG

Table 4.1: Details of excited signals (Sine wave, Barker code sequence)

Excitation sequence	Frequency (kHz)	Duration(us)	Binary Code
1-cycle sine	30	33	-
	35	29	
	40	25	
	45	22	
	50	20	
3-bit Barker	30	100	+1 +1 -1
	35	87	
	40	75	
	45	66	
	50	60	
5-bit Barker	30	165	+1 +1 +1 -1 +1
	35	145	
	40	125	
	45	110	
	50	100	
7-bit Barker	30	230	+1 +1 +1 -1 -1 +1 -1
	35	203	
	40	175	
	45	154	
	50	140	
11-bit Barker	30	363	+1 +1 +1 1 1 1 +1 1 1 +1 1
	35	319	
	40	275	
	45	242	
	50	220	
13-bit Barker	30	429	+1 +1 +1 +1 +1 1 1 +1 +1 1 +1 1 +1
	35	377	
	40	325	
	45	286	
	50	260	

code from 30 kHz to 50 kHz. After being processed by a fitted matched filter, the intensities of the echo from back and front are significantly increased. By observing the echo signal, the processed echo signal changes as the frequency changes. The processed echo signal from front side and back side is increased by frequency.

The increment of SNR of front side processed BCG code pair signal is 28.9 dB at frequency 30 kHz compared to sine wave and the peak side lobe level of the front side is -13.3 dB. Since the front and back echoes are basically similar, the SNR and peak side lobe level after processing are also basically similar. The increment of SNR of back side processed BCG code pair signal is 30.1 dB compared to sine wave and the peak side lobe level is -10.5 dB at 30 kHz. The increment of SNR of front side at frequency 35 kHz is

Table 4.2: Details of excited signals (Golay code pair, BCG code pair)

Excitation sequence	Frequency (kHz)	Duration(us)	Binary Code
2-bit Golay	30	66	+1 +1 & +1 -1
	35	58	
	40	50	
	45	44	
	50	40	
4-bit Golay	30	132	+1 +1 +1 -1 & +1 +1 -1 +1
	35	116	
	40	100	
	45	88	
	50	80	
8-bit Golay	30	264	+1 +1 +1 -1 +1 +1 -1 +1 & +1 +1 +1 -1 -1 -1 +1 -1
	35	232	
	40	200	
	45	176	
	50	160	
6-bit BCG	30	198	+1 +2 +1 -1-+2 +1 & +1 +2 -1 -1 +2 -1
	35	174	
	40	150	
	45	132	
	50	120	

2.5 dB higher than increased frequency at 30 kHz and the increment of SNR of back side at frequency 35 kHz is 2.3 dB higher than increased frequency at 30 kHz. The front and back peak side lobe level of the 35 kHz processed signal is -27.9 dB and -24.3 dB, respectively. The echo signal at 40 kHz shows the best performance among all signals. The increment of SNR of front side is 32 dB at frequency 40 kHz and the side lobe level of the front side signal is -28.5 dB. The increment of SNR of back side is 33.5 dB at frequency 40 kHz and the side lobe level of the back side signal is -19.5 dB. The performance of processed signal declined at frequency 45 kHz and 50 kHz. The SNR of front side at frequency 45 kHz and 50 kHz decreased 2.7 dB and 5.3 dB compared to the processed signal at frequency 40 kHz, respectively. The SNR of back side at frequency 45 kHz and 50 kHz decreased 3.7 dB and 5.4 dB compared to the processed signal at frequency 40 kHz, respectively. The side lobe level of the front side signals were increased 6.5 dB and 6.8 dB compared to the processed signal at frequency 40 kHz, respectively.

Table 4.3 shows the SNR and side lobe level of the 3-bit Barker code convolution 4-bit Golay code pair at different frequency. Through the experimental data, it can be found that the 40 kHz frequency BCG code pair is the best frequency for measuring an 8-inch schedule 40 steel pipe.

Table 4.3: SNR and PSL of BCG code from front and back side at different frequencies

Frequency	Front SNR (dB)	Front PSL(dB)	Back SNR(dB)	Back PSL(dB)
30 kHz	28.9	-13.3	30.1	-10.5
35 kHz	31.4	-27.9	32.4	-24.3
40 kHz	**32**	**-28.5**	**33.5**	**-19.5**
45 kHz	29.3	-22	29.8	-22.9
50 kHz	26.7	-21.7	28.1	-16.9

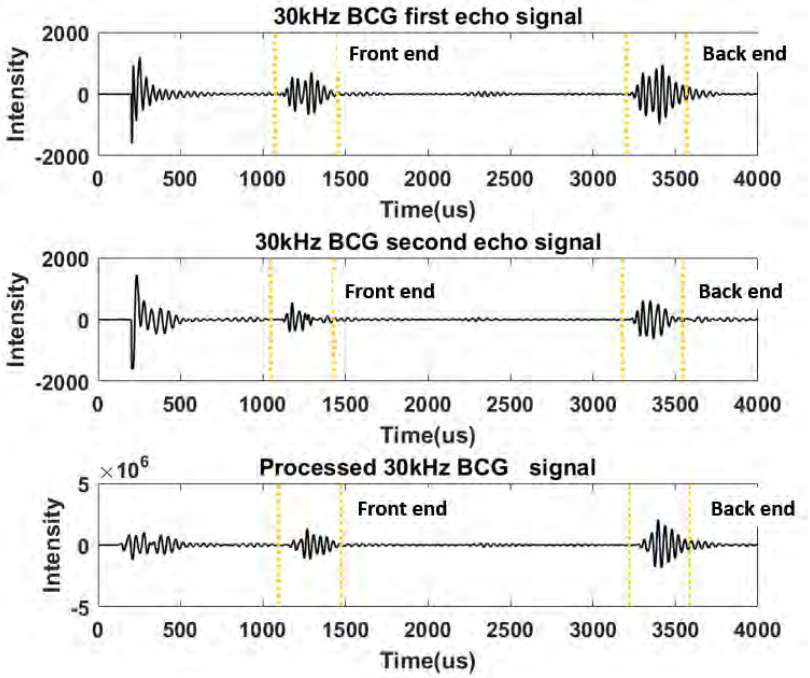

Figure 4.12: 30 kHz BCG code pair original echo signal pairs and processed result.

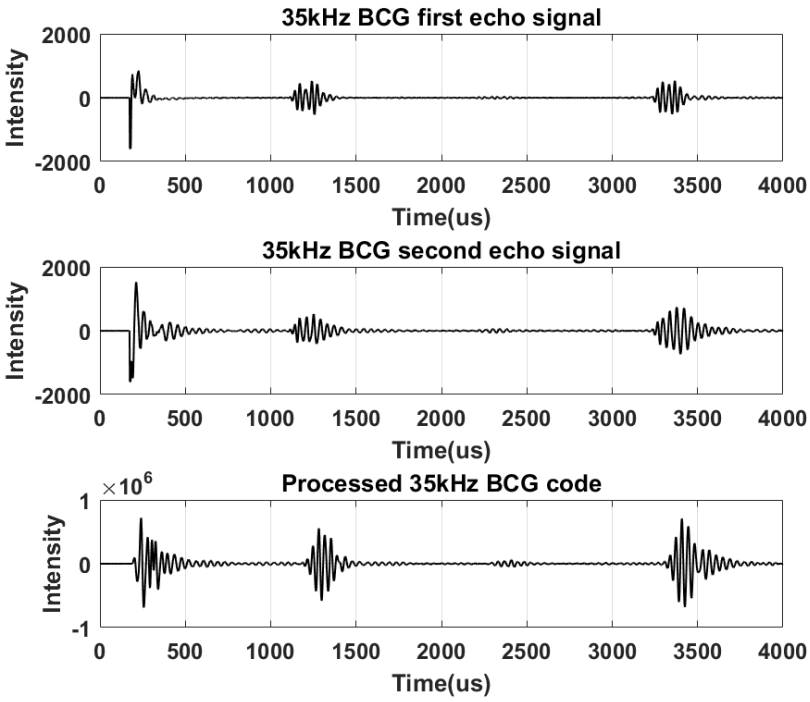

Figure 4.13: 35 kHz BCG code pair original echo signal pairs and processed result.

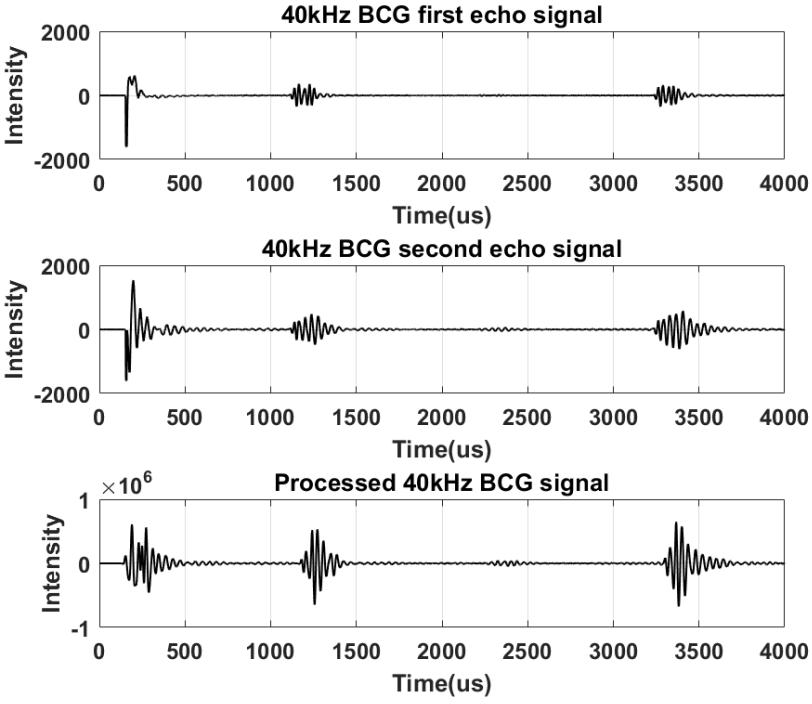

Figure 4.14: 40 kHz BCG code pair original echo signal pairs and processed result.

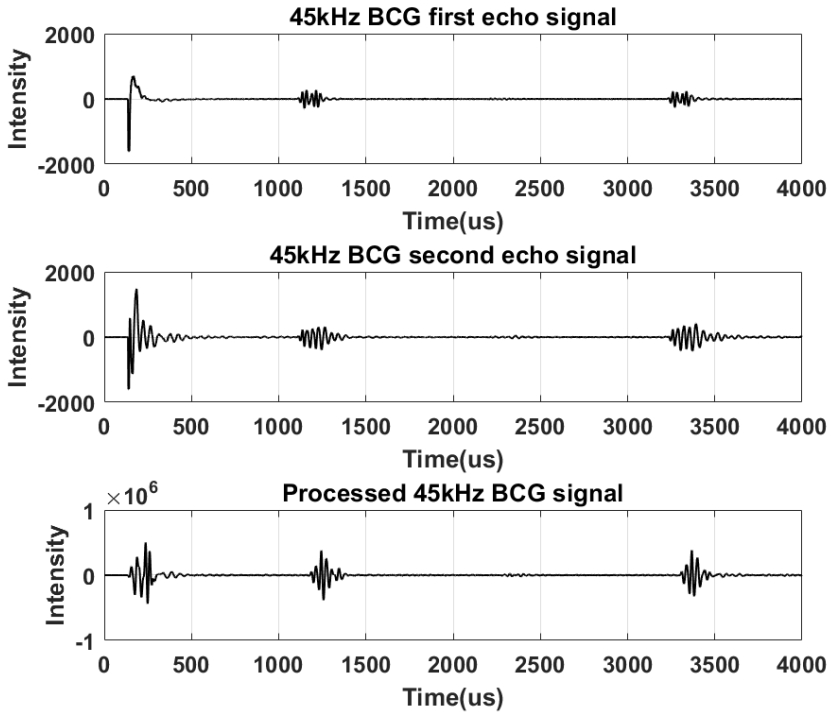

Figure 4.15: 45 kHz BCG code pair original echo signal pairs and processed result.

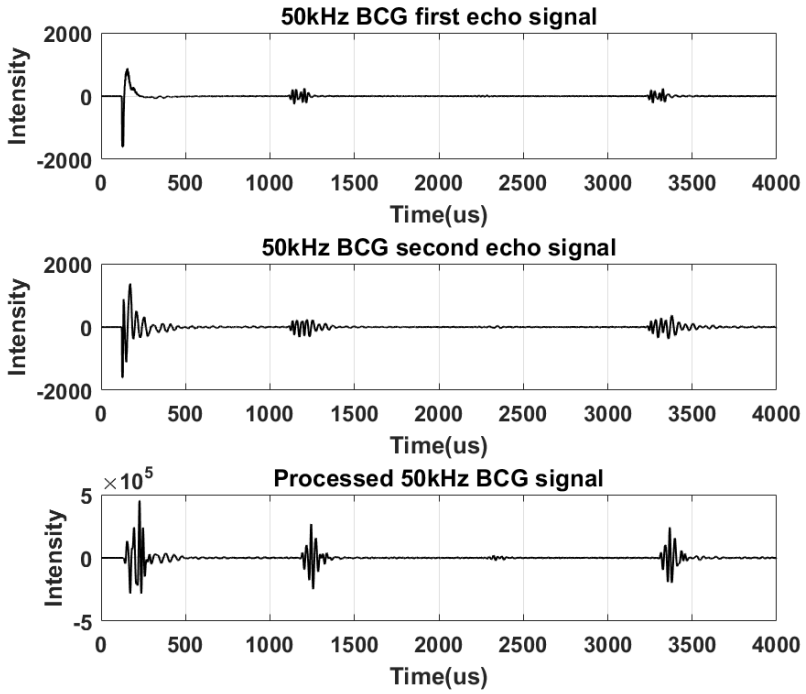

Figure 4.16: 50 kHz BCG code pair original echo signal pairs and processed result.

Figure 4.17 shows the zoom in of processed front 30 kHz, 35 kHz, 40 kHz, 45 kHz and 50 kHz 6-bit BCG code echo signal. In laboratory testing, the central frequency of the

piezoelectric transducers is 40 kHz. From the results, the intensity of 40 kHz processed signal from front side is the highest of the different frequency results. There is a good agreement between the experimental results and the central frequency of the transducers. For the selection of frequency range, the front side result shows that 40 kHz is an appropriate testing frequency.

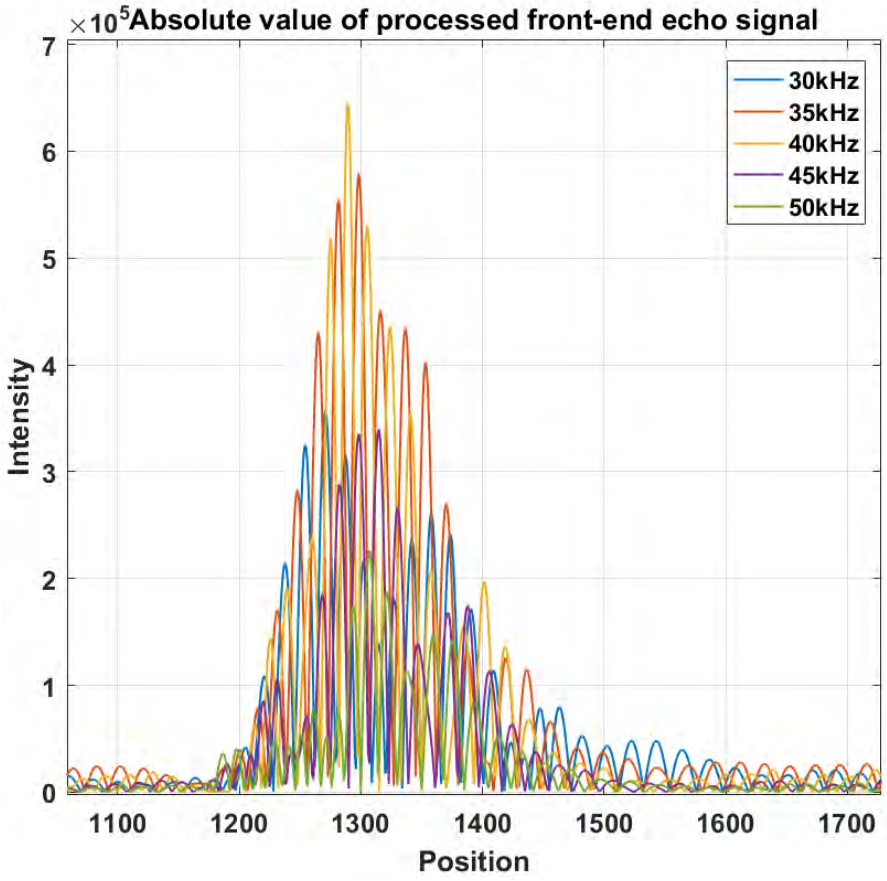

Figure 4.17: Absolute value of processed BCG front-end echo signal.

4.4.2 Testing of different frequency Barker code

In order to verify the performance of the Barker code method at different frequencies, a variety of frequency tests were implemented. Figure 4.18, Figure 4.19, Figure 4.20, Figure 4.21 and Figure 4.22 show the original Barker code echo signals and processed Barker code signals at the frequency of 30 kHz. Due to the different length of transmitted signals, the processed results showed that the intensities can be improved as the length increases. However, the longer length of transmitted signal the longer the duration time, causing low resolution. By observing the echo signal, the processed echo signals changed as the length of code sequence varied. The processed echo signals from front side and

back side can be improved by the increased length of code sequence.

The increment of SNR of front side 3-bit Barker code signal is 16.7 dB compared to sine wave at frequency 30 kHz, and the peak side lobe level of this signal is -11.8 dB. The increment of SNR of back side processed 3-bit signal is 19.1 dB compared to sine wave at frequency 30 kHz, and the peak side lobe level of this signal is -13.3 dB. The increment of SNR and peak side lobe level of 5-bit Barker code are better than 3-bit Barker code. The SNR was improved by 2.6 dB at front side and by 1.2 dB at back side, the peak side lobe level was decreased by 2.8 dB at front side and by 4.9 dB at back side. As the code length increases, 7-bit Barker code, 11-bit Barker code and 13-bit Barker code have a significant improvement in SNR. The average increment of SNR for 7-bit Barker, 11-bit Barker code and 13-bit Barker code is 21.7 dB, 23.6 dB and 24.2 dB compared to sine wave. However, the peak side lobe level of these codes have not significantly improved or even dropped. The reason for this may be due to the length of the code.

Table 4.4: SNR and PSL of various length Barker code from front and back side at 30 kHz

Code bit	**Front SNR (dB)**	**Front PSL(dB)**	**Back SNR(dB)**	**Back PSL(dB)**
3	16.7	-11.8	19.1	-13.3
5	19.3	-14.6	20.3	-18.2
7	20.9	-18.7	22.4	-20.8
11	22.9	-18.2	24.3	-21.2
13	23.6	-19.1	24.8	-22

Table 4.4 shows the SNR and side lobe level of the various Barker codes at 30 kHz frequency. Through the experimental data, the length of Barker code will affect both the SNR and peak side lobe level. When the excitation code is selected, the length of the code needs to be considered.

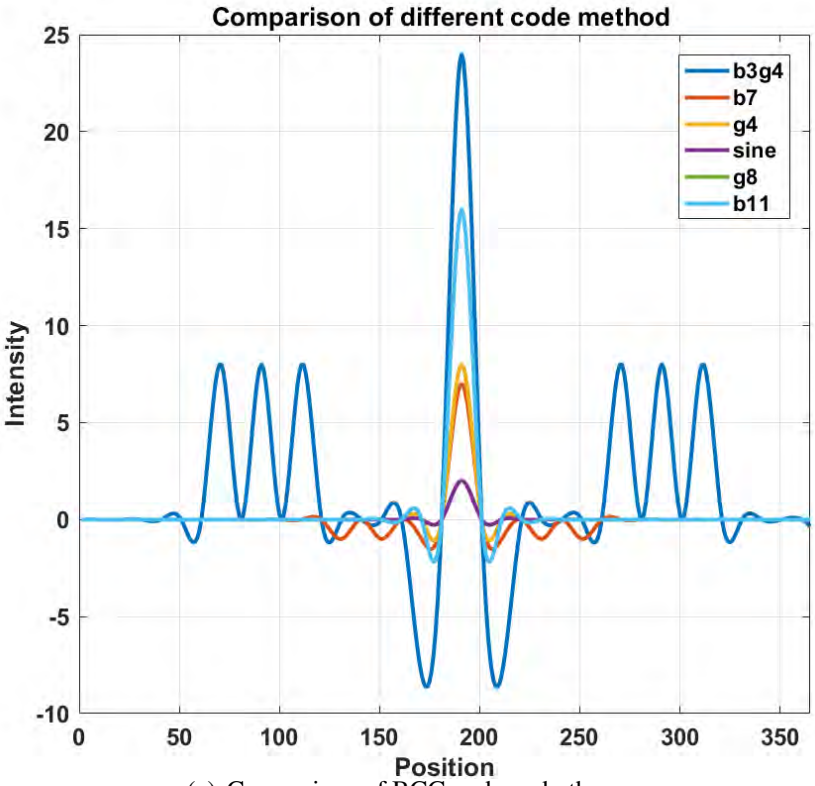

(a) Comparison of BCG code and others

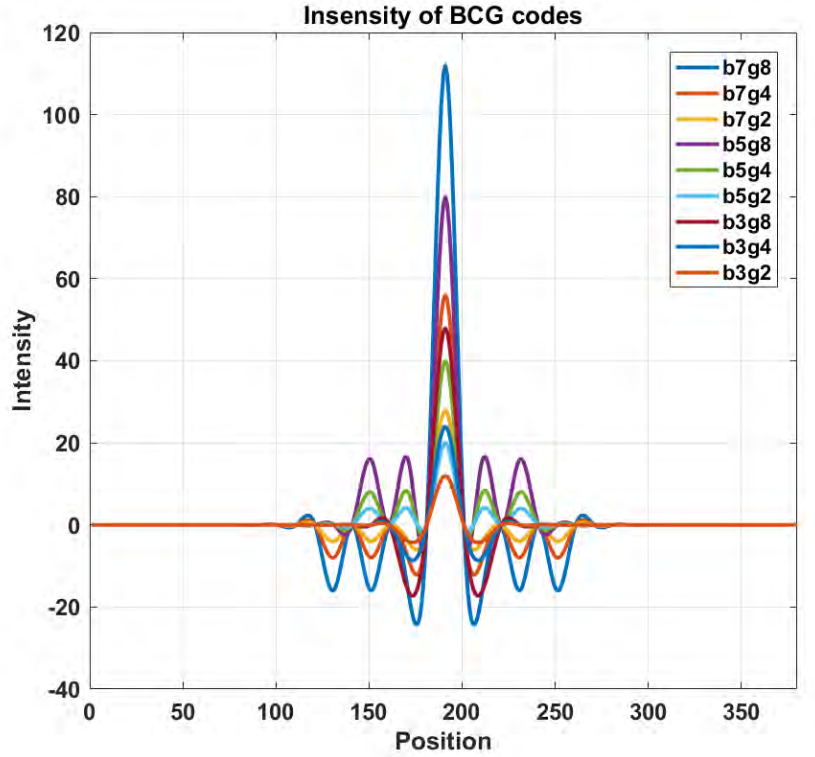

(b) Intensities of different BCG codes after matched filter

Figure 4.5: The theoretical simulation results. (**a**) The 3-bit Barker code combined 4-bit Golay code compared to simple pulse, 7-bit Barker code, 11-bit Barker code, 4-bit Golay code and 8-bit Golay code. (**b**) the theoretical intensity comparison of 15 different types BCG code.

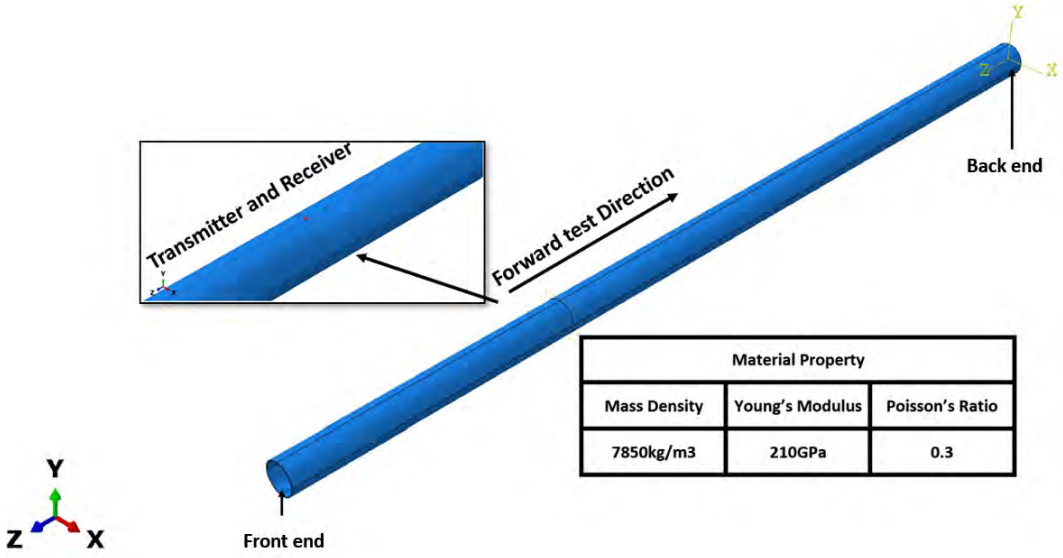

Figure 4.6: Setup of FEM model for a 8-inch steel pipe, the transmitter and receivers are located at the 2600 mm from the back end.

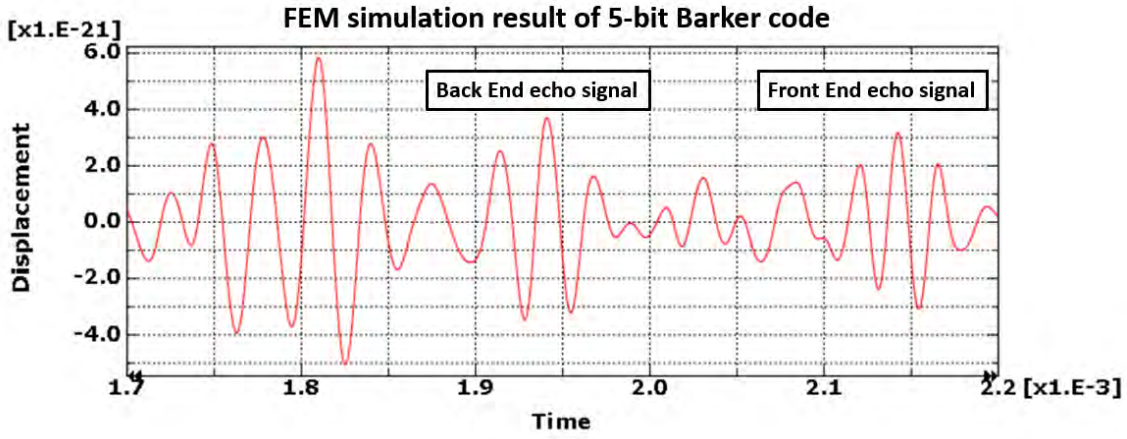

Figure 4.7: The displacement/time plot of Barker code echo signal from receiver in FEM model of the simulation.

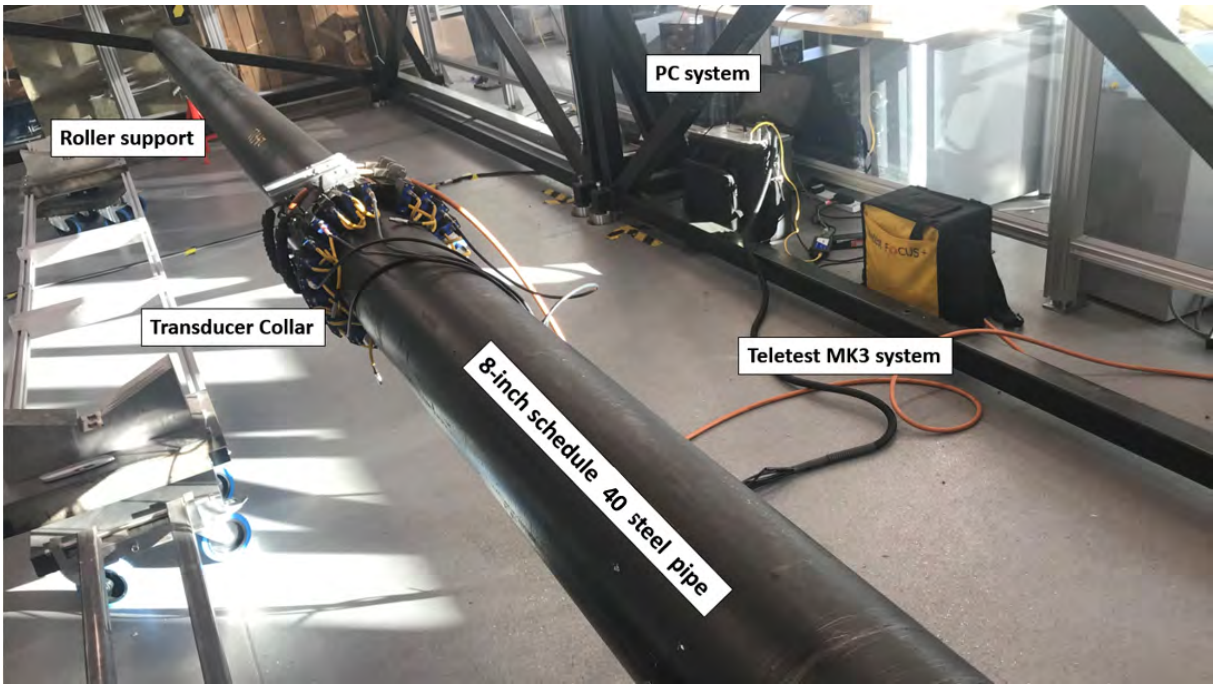

Figure 4.9: Real pipeline experiment set-up which used different torsional waves T (0,1) of coded excitation.

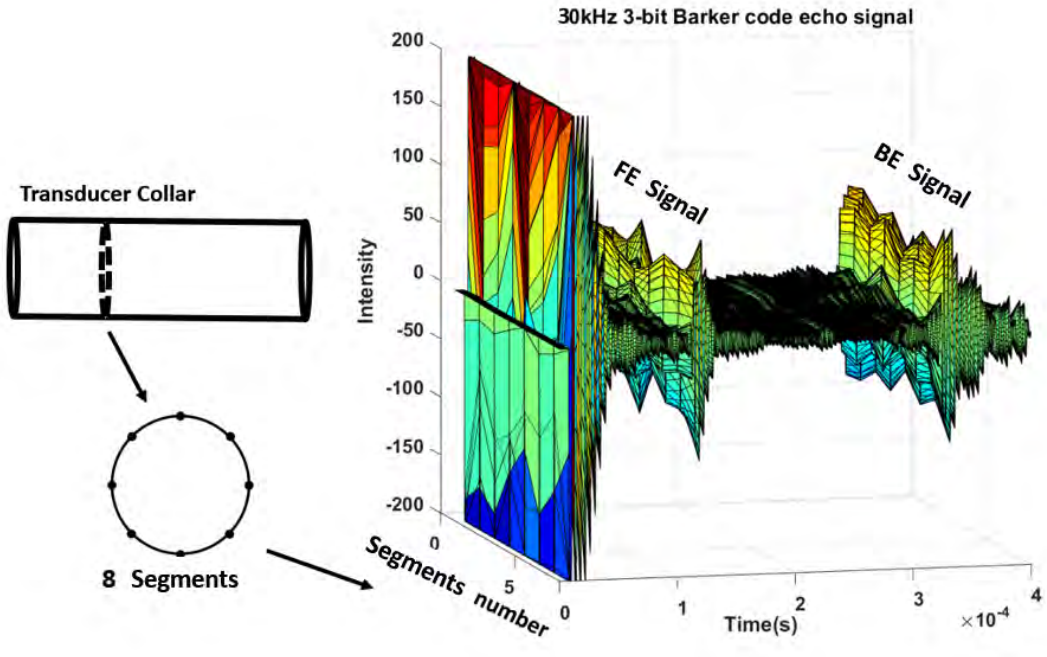

Figure 4.11: The real test echo signals of 30 kHz 3-bit Barker code from Teletest 8 segments.

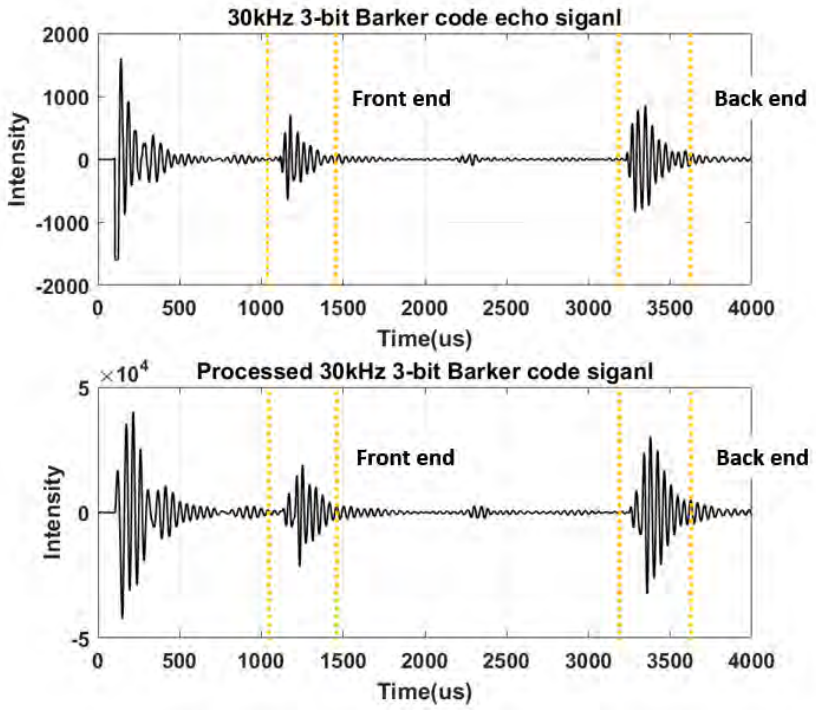

Figure 4.18: 30 kHz 3-bit Barker code pair original echo signal pairs and processed result.

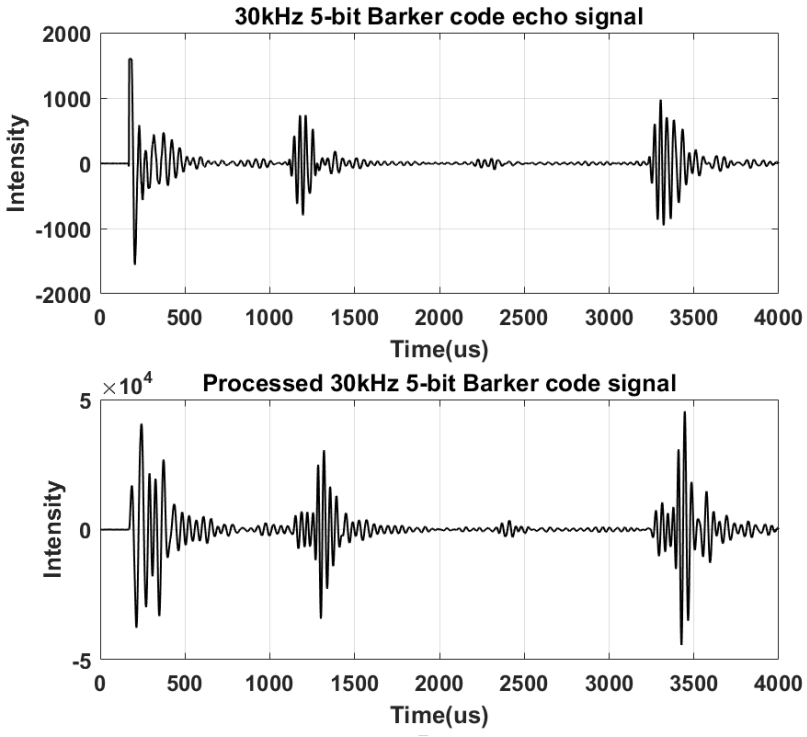

Figure 4.19: 30 kHz 5-bit Barker code pair original echo signal pairs and processed result.

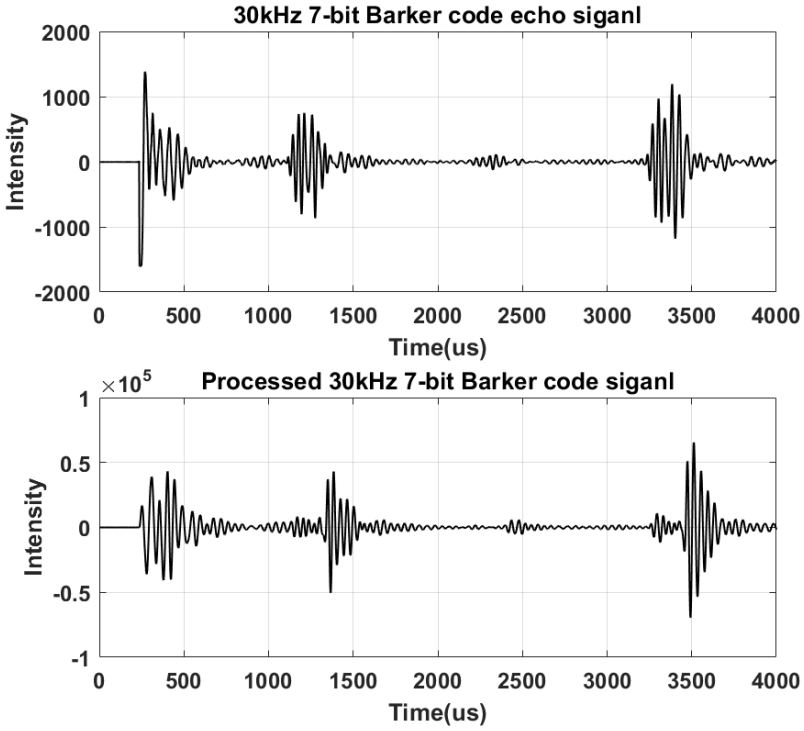

Figure 4.20: 30 kHz 7-bit Barker code pair original echo signal pairs and processed result.

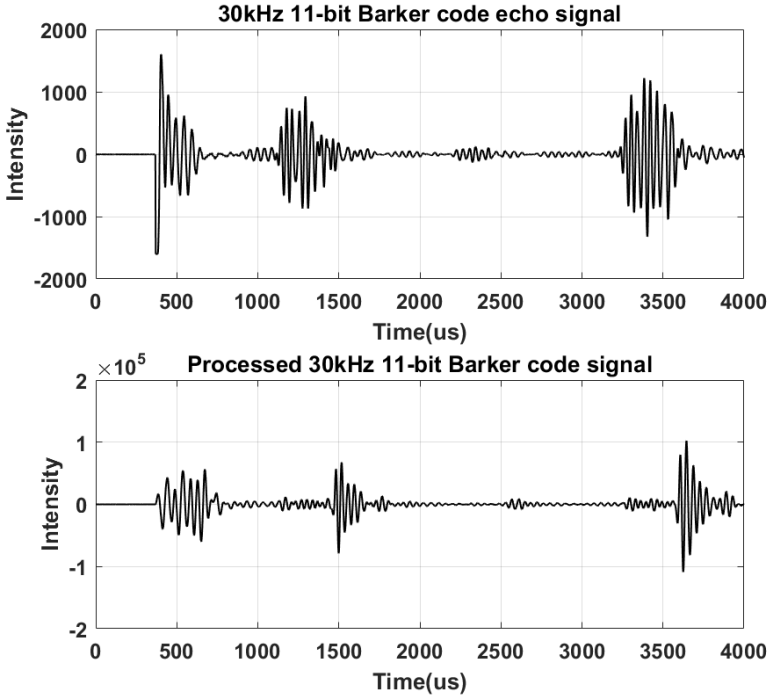

Figure 4.21: 30 kHz 11-bit Barker code pair original echo signal pairs and processed result.

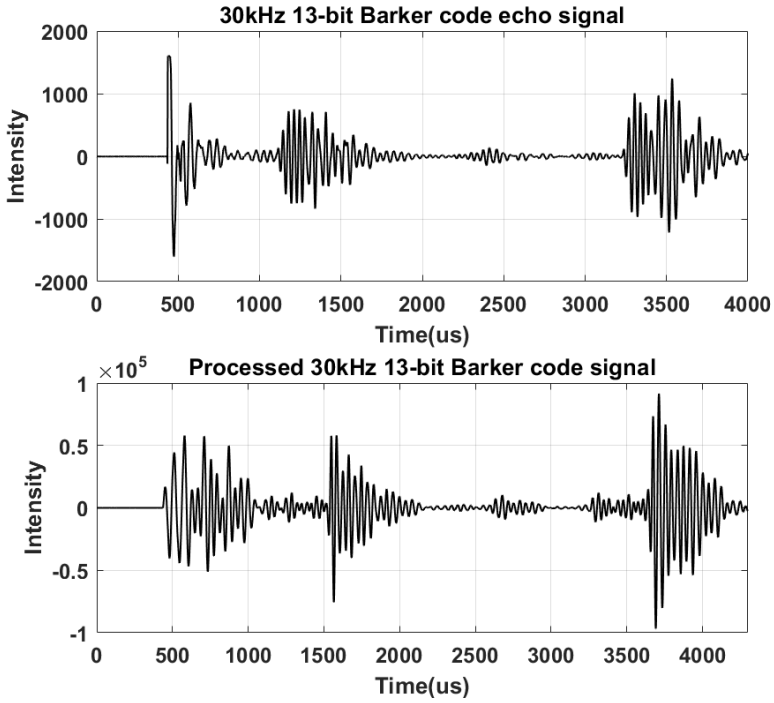

Figure 4.22: 30 kHz 13-bit Barker code pair original echo signal pairs and processed result.

Figure 4.23, Figure 4.24, Figure 4.25, Figure 4.26 and Figure 4.27 show the original Barker code echo signals and the processed Barker code signals at the frequency of 35 kHz. The experimental data show that the length of Barker code increased can improve both the echo SNR and PSL. Therefore, the length of the code needs to be considered when the excitation code is selected.

As with results of the Barker signal at 35 kHz, the SNR and peak side lobe level have been significantly improved. The increment of SNR of front side 3-bit Barker code signal is 16.6 dB compared to sine wave at frequency of 35 kHz, and the peak side lobe level of this signal is -13.7 dB. The increment of SNR of back side processed 3-bit signal is 17.4 dB compared to sine wave at frequency of 35 kHz, and the peak side lobe level of this signal is -13 dB. The improvement of SNR and peak side lobe level of 5-bit Barker code is is not obvious.The SNR was improved by 1.2 dB at front side and by 1.4 dB at back side, the peak side lobe level was decreased by 1.3 dB at front side and by 3.6 dB at back side. As the code length increases, 7-bit Barker code, 11-bit Barker code and 13-bit Barker code have a significant improvement in SNR. The average increment of SNR for 7-bit Barker, 11-bit Barker code and 13-bit Barker code is 20.2 dB, 21.5 dB and 22.6 dB compared to sine wave. However, the peak side lobe level of these codes have not significantly improved or even dropped. These results are similar to the results of Barker code at 30 kHz. The reason for this may be due to the length of the code.

Table 4.5: SNR and PSL of various length Barker code from front and back side at 35 kHz

Code bit	**Front SNR (dB)**	**Front PSL(dB)**	**Back SNR(dB)**	**Back PSL(dB)**
3	16.6	-13.7	17.4	-13
5	17.8	-15	18.8	-16.6
7	19.5	-13.9	20.8	-18.3
11	20.7	-16.2	22.4	-17.5
13	21.9	-21.8	23.4	-18.7

Table 4.5 shows the SNR and side lobe level of the various Barker codes at 35 kHz frequency. The values of the increased SNR of the Barker code at 35 kHz from the front and back pipe ends are almost the same in the experiment. It can be concluded from experimental results that the length of Barker code is an important factor affecting both the SNR and peak side lobe level.

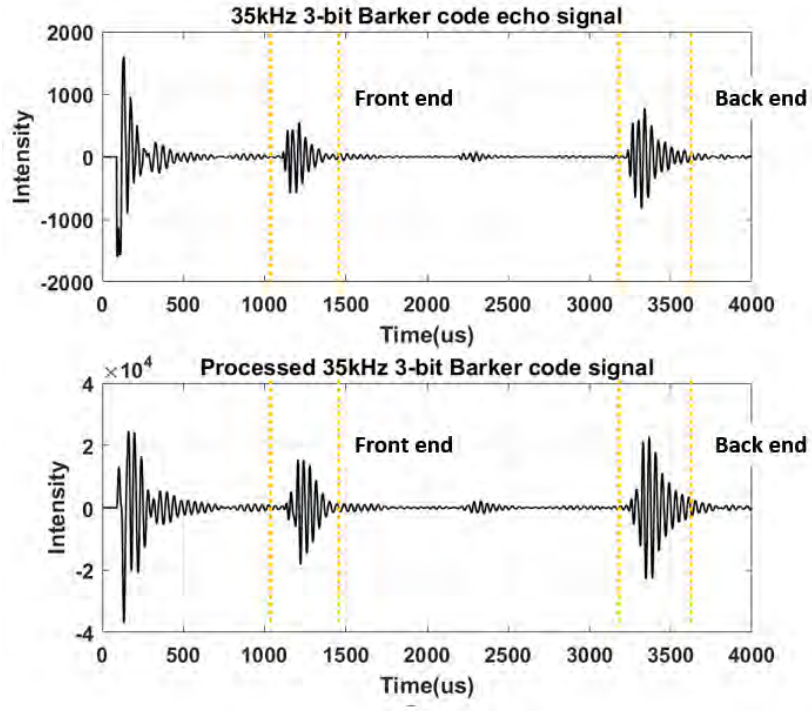

Figure 4.23: 35 kHz 3-bit Barker code pair original echo signal pairs and processed result.

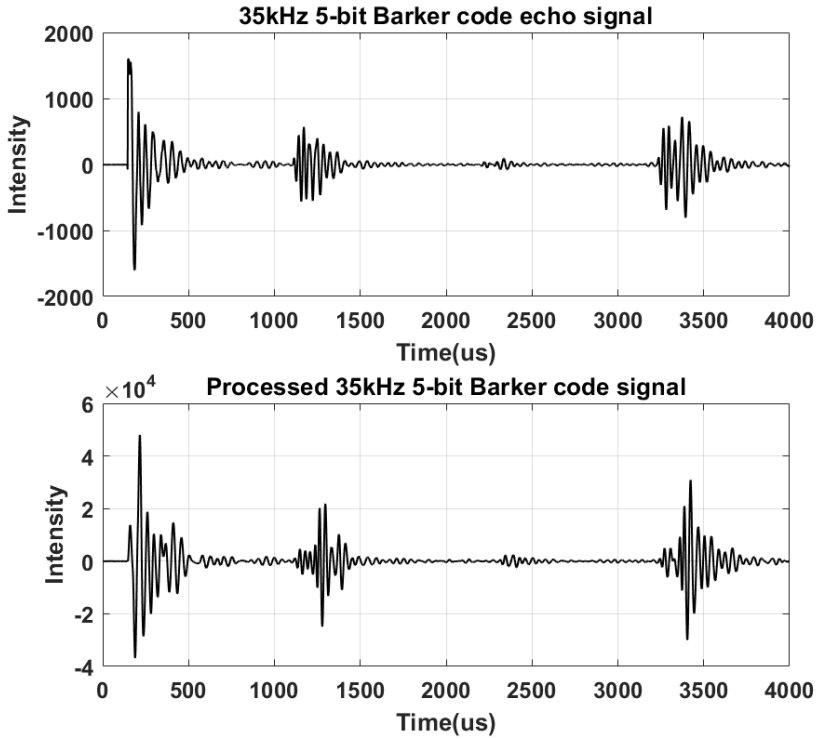

Figure 4.24: 35 kHz 5-bit Barker code pair original echo signal pairs and processed result.

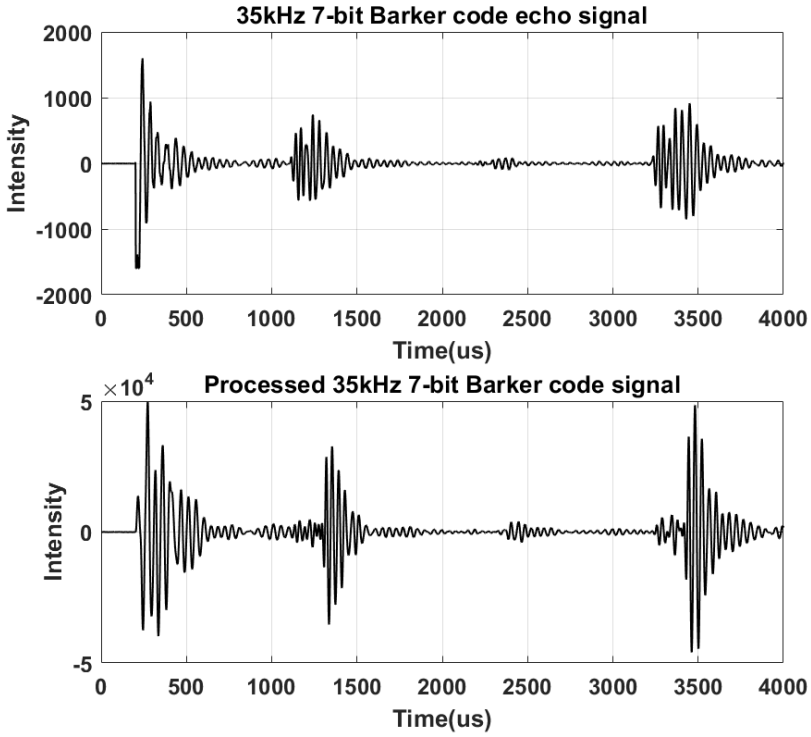

Figure 4.25: 35 kHz 7-bit Barker code pair original echo signal pairs and processed result.

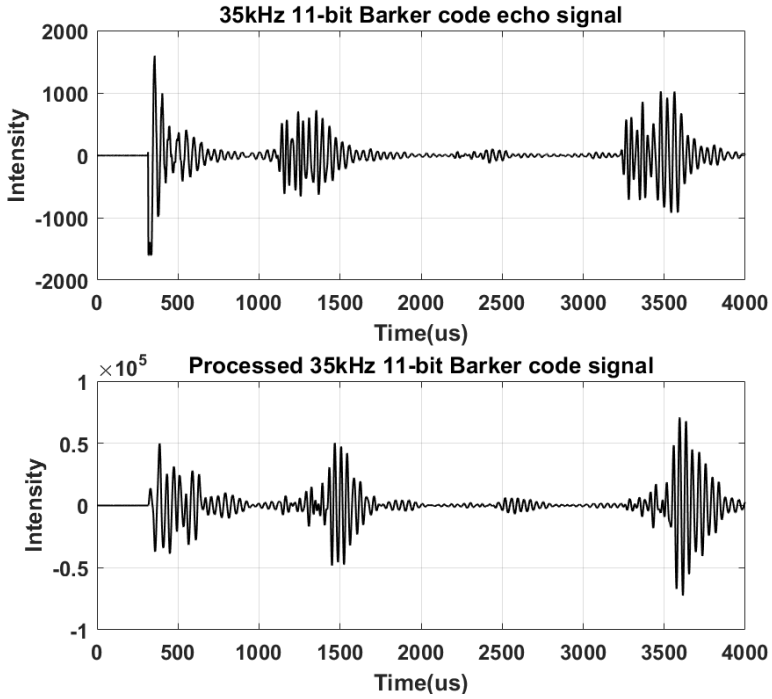

Figure 4.26: 35 kHz 11-bit Barker code pair original echo signal pairs and processed result.

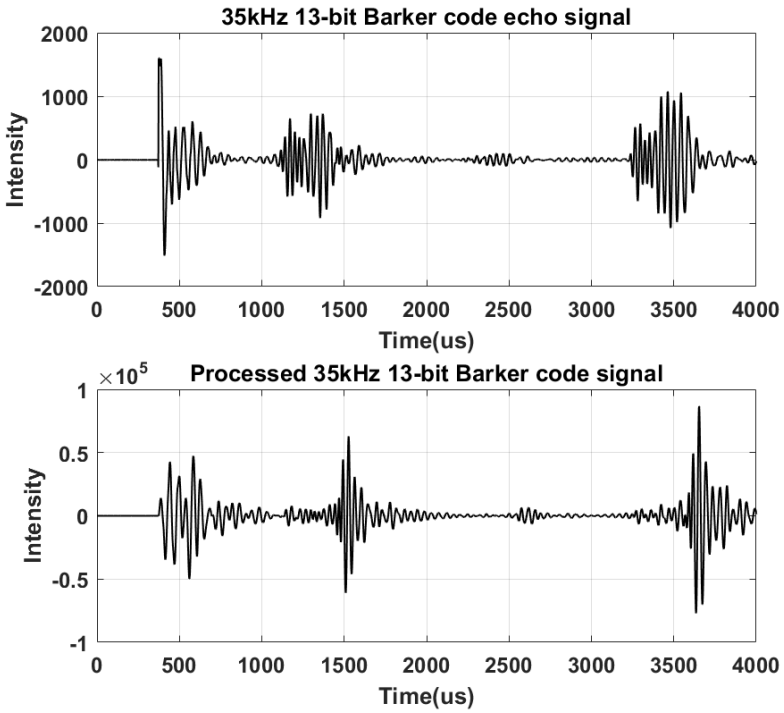

Figure 4.27: 35 kHz 13-bit Barker code pair original echo signal pairs and processed result.

Figure 4.28, Figure 4.29, Figure 4.30, Figure 4.31 and Figure 4.32 show the original Barker code echo signals and processed Barker code signals at the frequency of 40 kHz. Like the transmission signal at 30 kHz and 35 kHz, the length of the code affects the SNR and side lobe level of the detection results. However, the longer length of transmitted signal the longer duration time, causing the low resolution. By observing the echo signals, the processed echo signals change as the frequency changes.

The increment of SNR for 3-bit Barker code, 5-bit Barker code, 7-bit Barker code, 11-bit Barker code and 13-bit Barker code front side processed signal is 17.3 dB, 18.7 dB, 20.7 dB, 22.6 dB and 23.2 dB at frequency of 40 kHz, respectively. The increment of SNR for 3-bit Barker code, 5-bit Barker code, 7-bit Barker code, 11-bit Barker code and 13-bit Barker code back side processed signal is 17.8 dB, 19.6 dB, 21.4 dB, 23.2 dB and 23.8 dB at frequency of 40 kHz respectively, which is nearly the same as the results from the front side. The average peak side lobe level of 3-bit Barker code, 5-bit Barker code, 7-bit Barker code, 11-bit Barker code and 13-bit Barker code processed signal is -13.9 dB, -17 dB, -25.5 dB, -22.8 dB and -19.5 dB at frequency of 40 kHz.

Table 4.6: SNR and PSL of various length Barker code from front and back side at 40 kHz

Code bit	**Front SNR (dB)**	**Front PSL(dB)**	**Back SNR(dB)**	**Back PSL(dB)**
3	17.3	-14.9	17.8	-12.8
5	18.7	-17.9	19.6	-16.1
7	20.7	-25.9	21.4	-25
11	22.6	-25	23.2	-20.6
13	23.2	-21	23.8	-18

Table 4.6 shows the SNR and side lobe level of the various Barker codes at 40 kHz frequency. According to the experimental data, the length of Barker code will affect both the SNR and peak side lobe level. The effects of code length can not be neglected When choosing the excitation code. The SNR and side lobe level results at 40kHz frequency is better than the results at 30 kHz and 35 kHz.

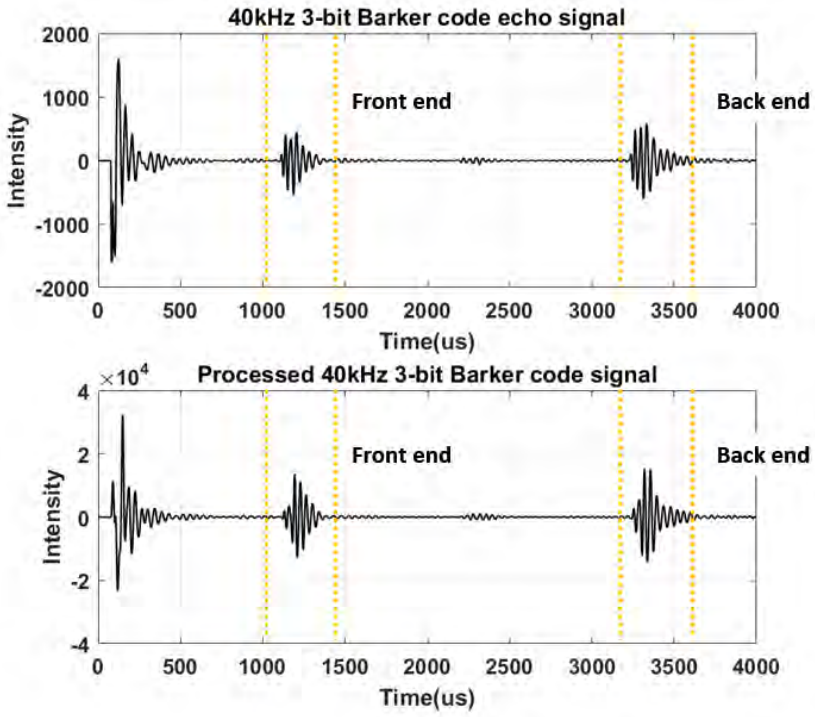

Figure 4.28: 40 kHz 3-bit Barker code pair original echo signal pairs and processed result.

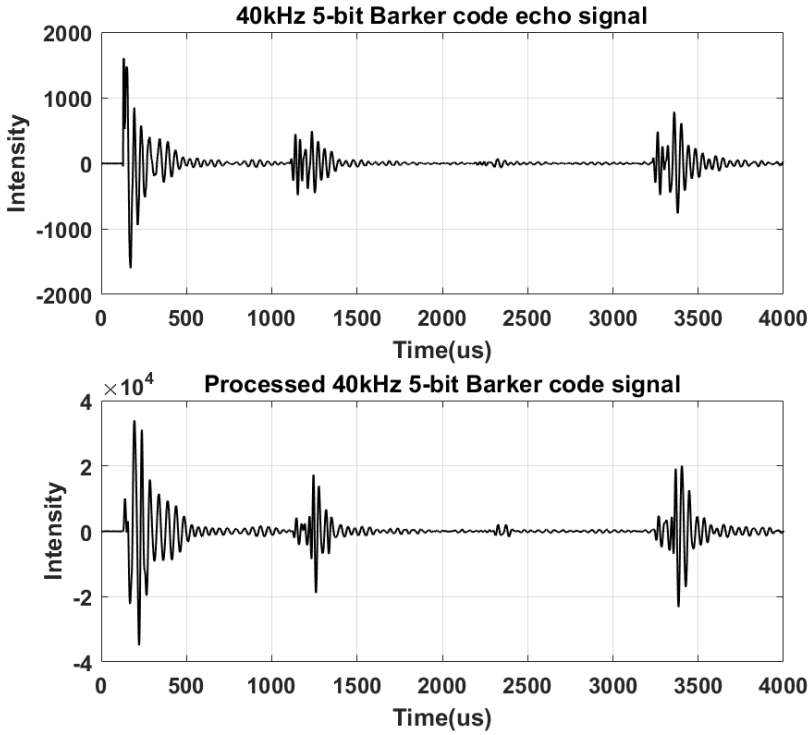

Figure 4.29: 40 kHz 5-bit Barker code pair original echo signal pairs and processed result.

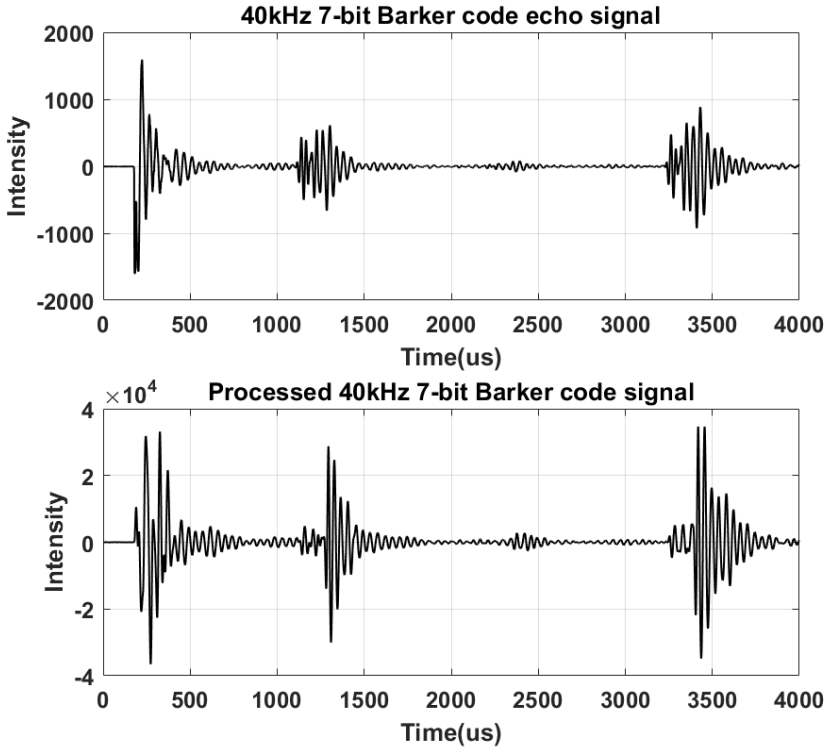

Figure 4.30: 40 kHz 7-bit Barker code pair original echo signal pairs and processed result.

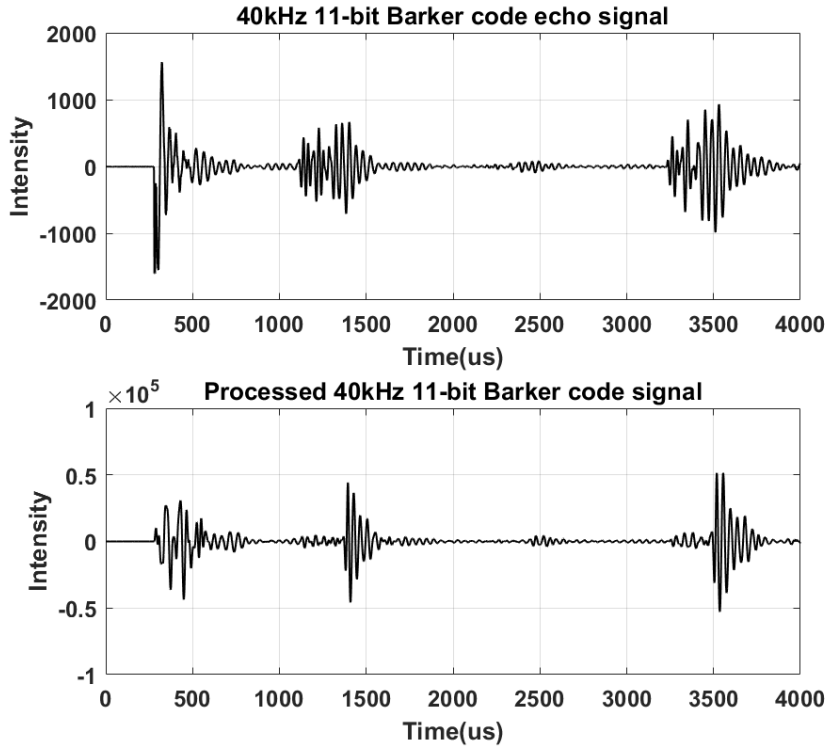

Figure 4.31: 40 kHz 11-bit Barker code pair original echo signal pairs and processed result.

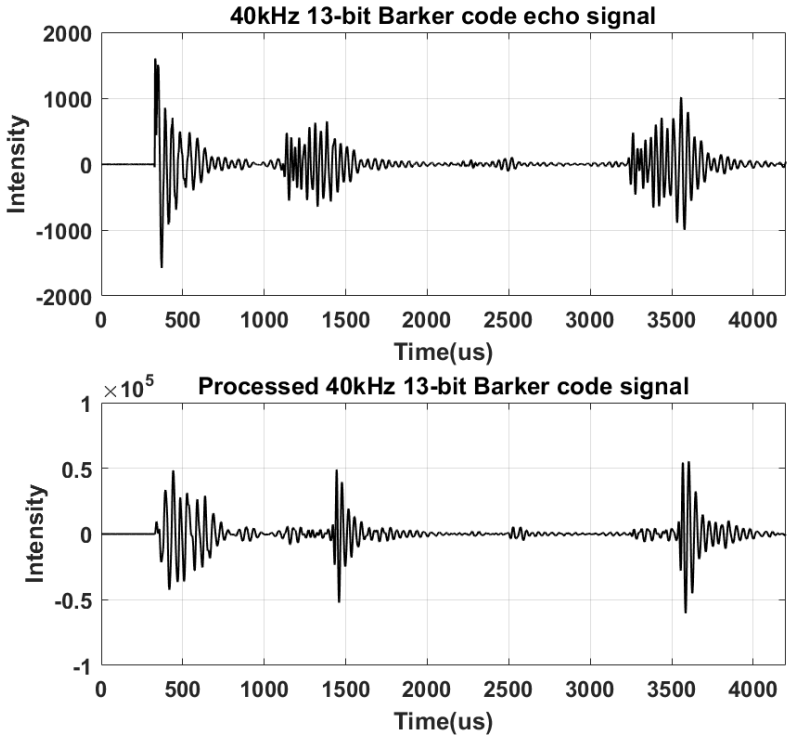

Figure 4.32: 40 kHz 13-bit Barker code pair original echo signal pairs and processed result.

Figure 4.33, Figure 4.34, Figure 4.35, Figure 4.36 and Figure 4.37 show Barker code echo signals and processed Barker code signals at the frequency of 45 kHz. As the frequency of the transmission signal increases, the SNR and peak side lobe level performance of the echo signal with the same code length decreases. This is caused by the inherent performance of the experimental instrument hardware. The center frequency of the collar's piezoelectric transducer is 40 kHz. By observing the echo signal, the processed echo signal changes as the frequency changes. The processed echo signal from front side and back side are increased by frequency.

The increment of SNR and peak side lobe level at 45 kHz Barker code are lower than the performance at 40 kHz overall. The increment of SNR for 3-bit Barker code, 5-bit Barker code, 7-bit Barker code, 11-bit Barker code and 13-bit Barker code front side processed signal is 14 dB, 15.6 dB, 17.9 dB, 19.8 dB and 20.2 dB at frequency of 45 kHz compared to sine wave, respectively. The increment of SNR for 3-bit Barker code, 5-bit Barker code, 7-bit Barker code, 11-bit Barker code and 13-bit Barker code back side processed signal is 13.5 dB, 16.5 dB, 17.7 dB, 19.7 dB and 20.7 dB at frequency of 45 kHz compared to sine wave, respectively which are almost the same with the front side results. The average peak side lobe level of 3-bit Barker code, 5-bit Barker code, 7-bit Barker code, 11-bit Barker code and 13-bit Barker code processed signal is -15.4 dB, -15.9 dB, -17.6 dB, -19.9 dB and -20.6 dB at frequency of 45 kHz.

Table 4.7: SNR and PSL of various length Barker code from front and back side at 45 kHz

Code bit	**Front SNR (dB)**	**Front PSL(dB)**	**Back SNR(dB)**	**Back PSL(dB)**
3	14	-12.4	13.5	-18.4
5	15.6	-16.2	16.5	-15.7
7	17.9	-19.6	17.7	-15.6
11	19.8	-20.4	19.7	-19.3
13	20.2	-17.9	20.7	-23.3

Table 4.7 shows the SNR and side lobe level of the various Barker codes at 45 kHz frequency. The intensities of the signal echos from the front and back pipe ends are significantly increased after the echos are processed by fitted matched filter. According to the experimental data, the length of the Barker code affects both the SNR and the peak side lobe level. When selecting an excitation code, the length of the code must be considered.

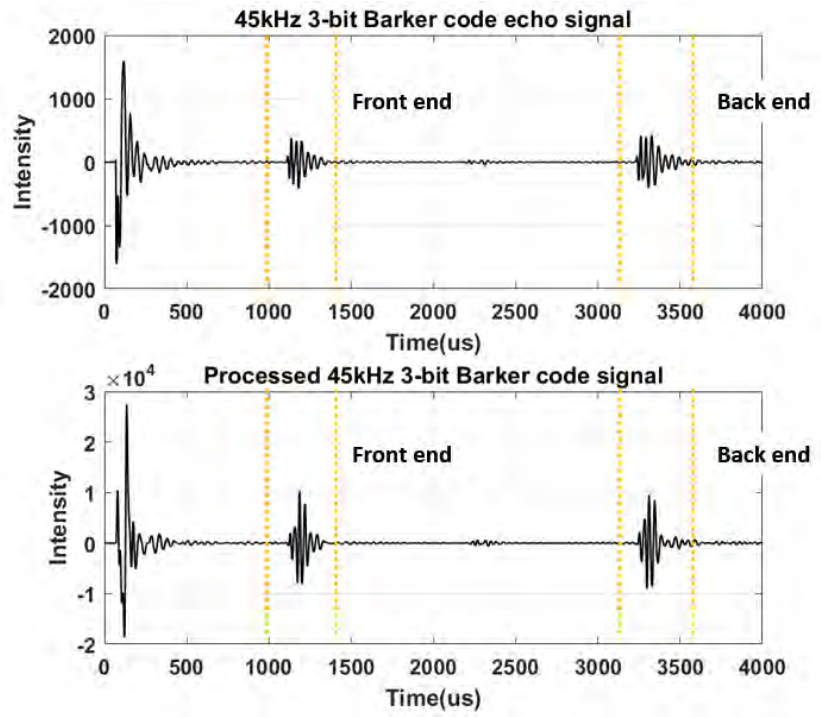

Figure 4.33: 45 kHz 3-bit Barker code pair original echo signal pairs and processed result.

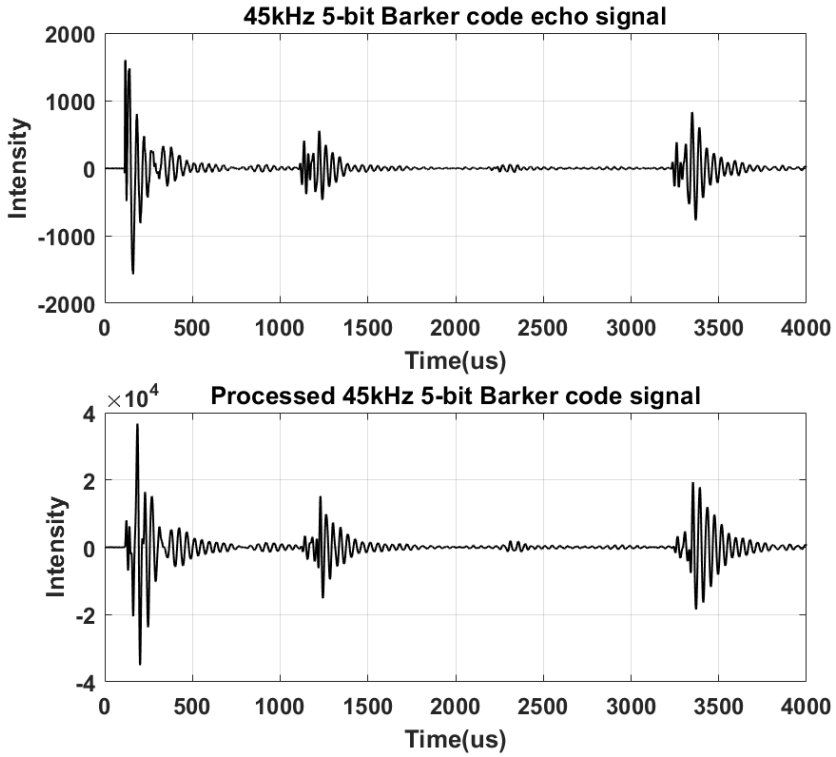

Figure 4.34: 45 kHz 5-bit Barker code pair original echo signal pairs and processed result.

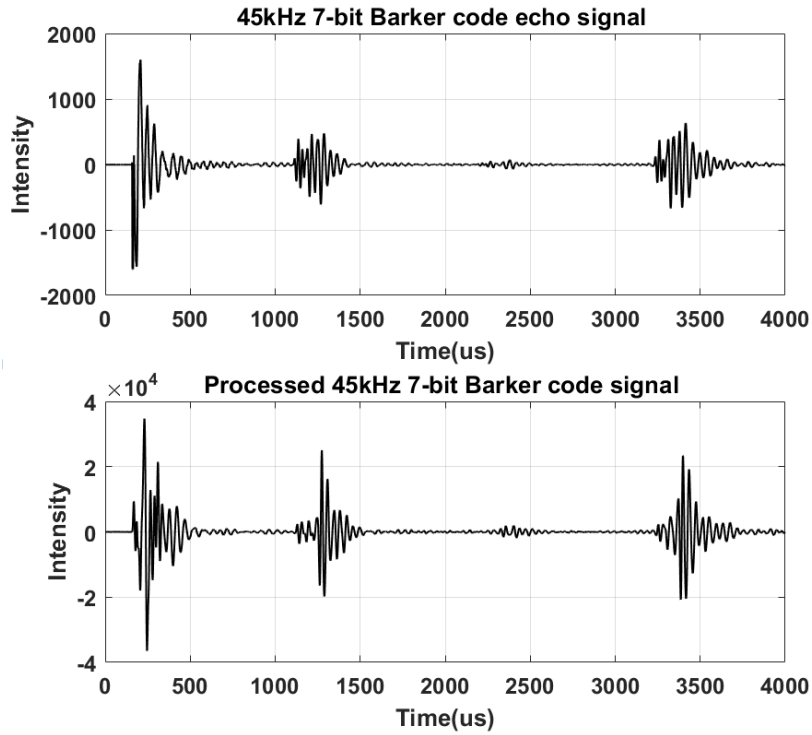

Figure 4.35: 45 kHz 7-bit Barker code pair original echo signal pairs and processed result.

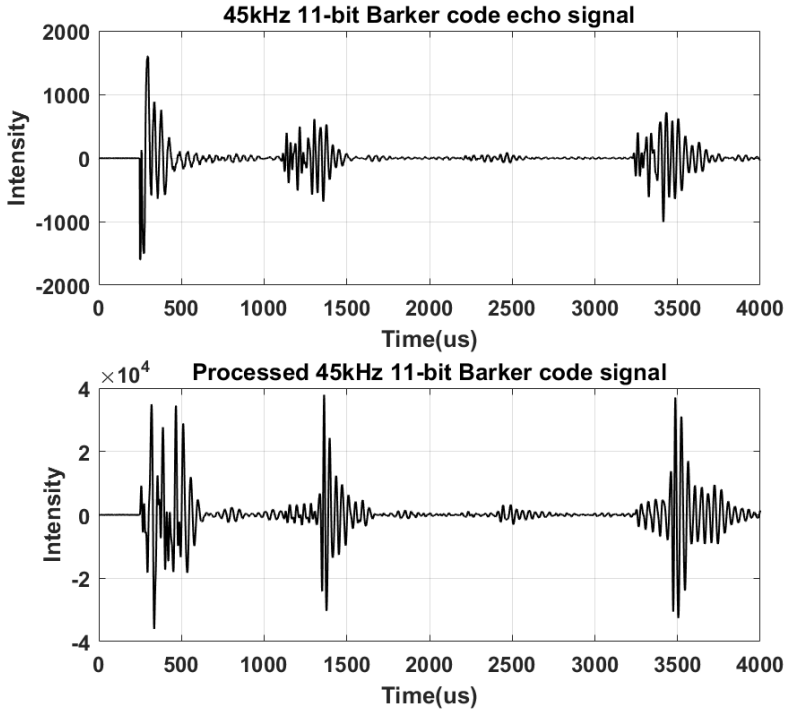

Figure 4.36: 45 kHz 11-bit Barker code pair original echo signal pairs and processed result.

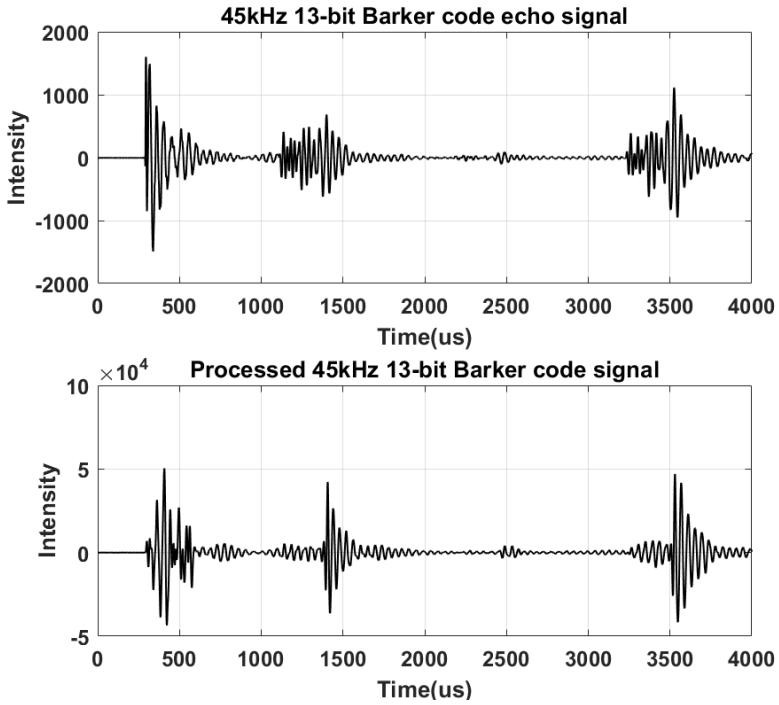

Figure 4.37: 45 kHz 13-bit Barker code pair original echo signal pairs and processed result.

Figure 4.38, Figure 4.39, Figure 4.40, Figure 4.41 and Figure 4.42 show the original Barker code echo signals and processed Barker code signal at the frequency of 50 kHz. Due to the different length of transmitted signal, the processed results show that the intensities increase with the length. However, the longer length of transmitted signal, the longer the duration time, that will cause the low resolution. By observing the echo signal, the processed echo signal changes as the frequency changes. The processed echo signal from front side and back side are increased by frequency.

The performance of Barker code at 50 kHz is the worst compared to others. The average increment of SNR for 3-bit Barker code, 5-bit Barker code, 7-bit Barker code, 11-bit Barker code and 13-bit Barker code processed signal is 12.4 dB, 15.9 dB, 16.4 dB, 18.4 dB and 19.8 dB at frequency 50 kHz, respectively which are almost the lower 2 dB than the 45 kHz Barker code results overall. The average peak side lobe level of 3-bit Barker code, 5-bit Barker code, 7-bit Barker code, 11-bit Barker code and 13-bit Barker code processed signal is -14.5 dB, -15.6 dB, -14.2 dB, -17.6 dB and -19.7 dB at frequency 50 kHz which are almost the higher 2 dB than the 45 kHz Barker code results overall.

Table 4.8: SNR and PSL of various length Barker code from front and back side at 50 kHz

Code bit	Front SNR (dB)	Front PSL(dB)	Back SNR(dB)	Back PSL(dB)
3	12.8	-11.9	12.1	-17.1
5	15.5	-12.5	16.4	-18.6
7	16.7	-13.9	16.1	-14.5
11	18.6	-19	18.1	-16.3
13	19.4	-20.1	20.1	-19.3

Table 4.8 shows the SNR and side lobe level of the various Barker codes at 50 kHz frequency. The length of the Barker code was found to affect both the SNR and the peak side lobe level in the experimental data. The Barker coded excitation method for a pure wave mode T(0,1) generation and prorogation has more effective behaviour in the circumferential direction.

4.4.3 Pulse modulated Barker code signal

In laboratory testing, the pulse modulated various length Barker codes have been used as transmitted signals. Figure 4.43, Figure 4.44, Figure 4.45, Figure 4.46 and Figure 4.47 show pulse modulated Barker code echo signals and processed Barker code signals at the frequency of 40 kHz. Table 4.9 shows the SNR and PSL of pulse modulated various

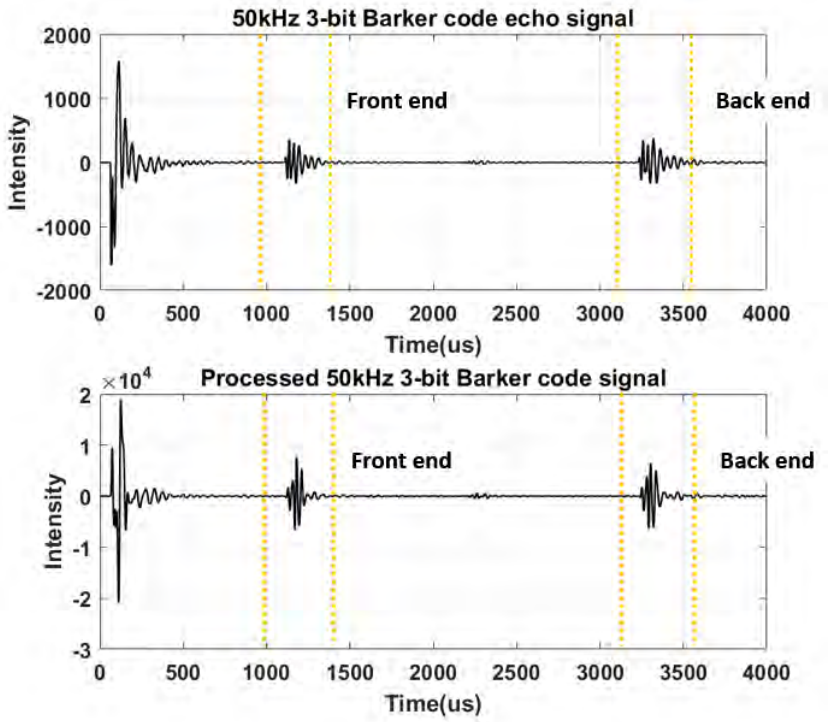

Figure 4.38: 50 kHz 3-bit Barker code pair original echo signal pairs and processed result.

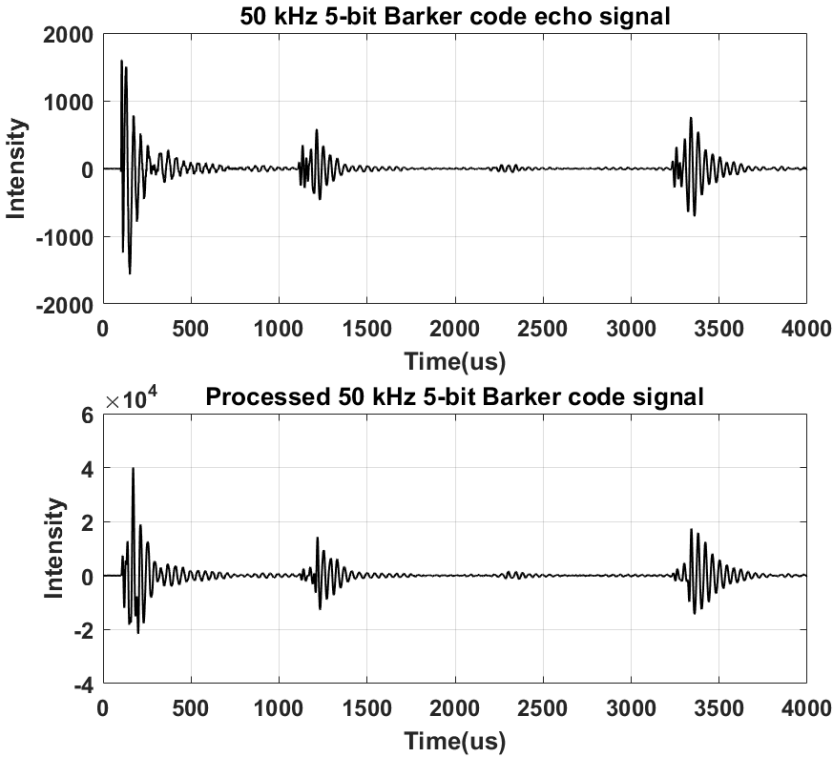

Figure 4.39: 50 kHz 5-bit Barker code pair original echo signal pairs and processed result.

length Barker code from front and back side at frequency of 40 kHz. Compared with the sine modulated Barker code, the results of SNR were decreased around 2 dB in most code

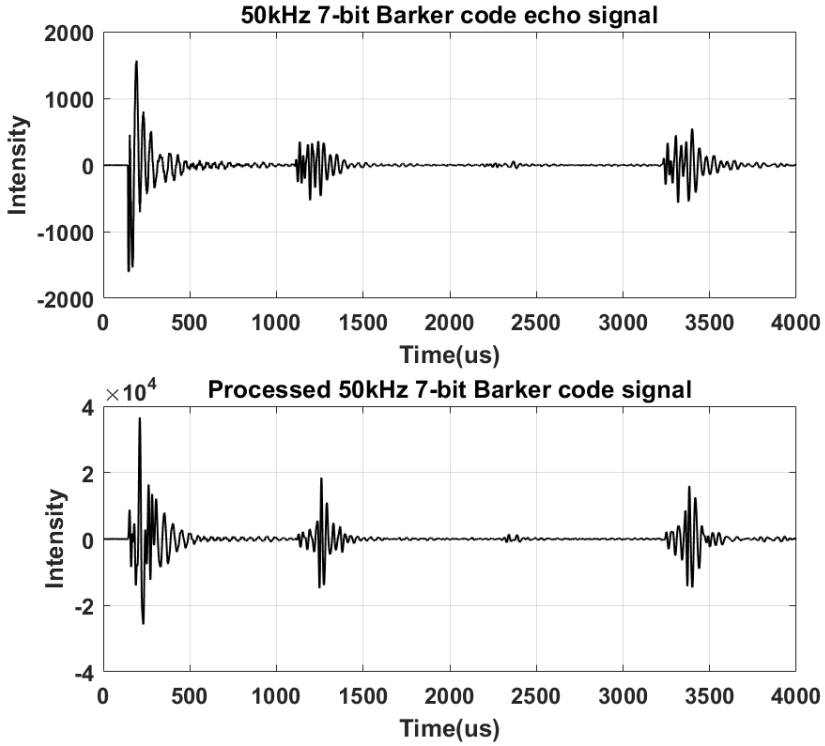

Figure 4.40: 50 kHz 7-bit Barker code pair original echo signal pairs and processed result.

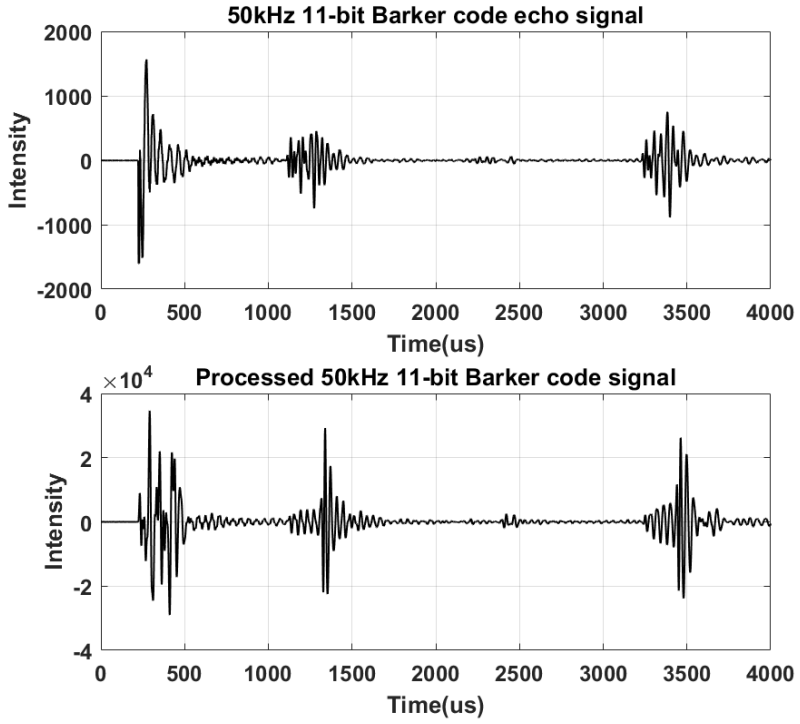

Figure 4.41: 50 kHz 11-bit Barker code pair original echo signal pairs and processed result.

length at frequency of 40 kHz and the PSL of the pulse modulated signals are similar with the sine modulated results at frequency of 40 kHz.

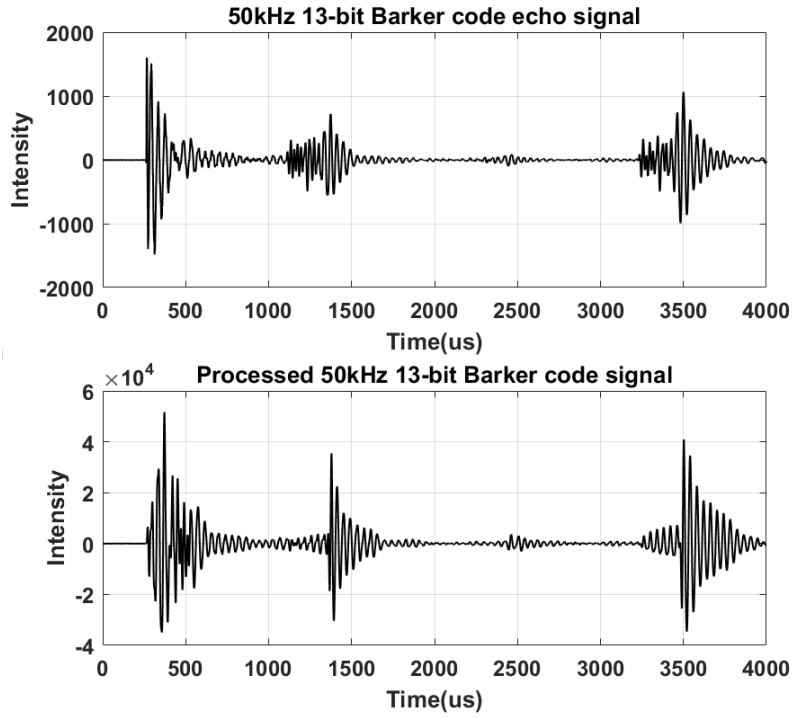

Figure 4.42: 50 kHz 13-bit Barker code pair original echo signal pairs and processed result.

Table 4.9: SNR and PSL of pulse modulated various length Barker code from front and back side at 40 kHz

Code bit	Front SNR (dB)	Front PSL(dB)	Back SNR(dB)	Back PSL(dB)
3	14	-14.8	15.2	-17.7
5	15.2	-20.4	17.8	-21.1
7	17.8	-16.6	19.4	-21.2
11	19.5	-23.7	21.2	-23.2
13	18.6	-18.6	21.4	-17.6

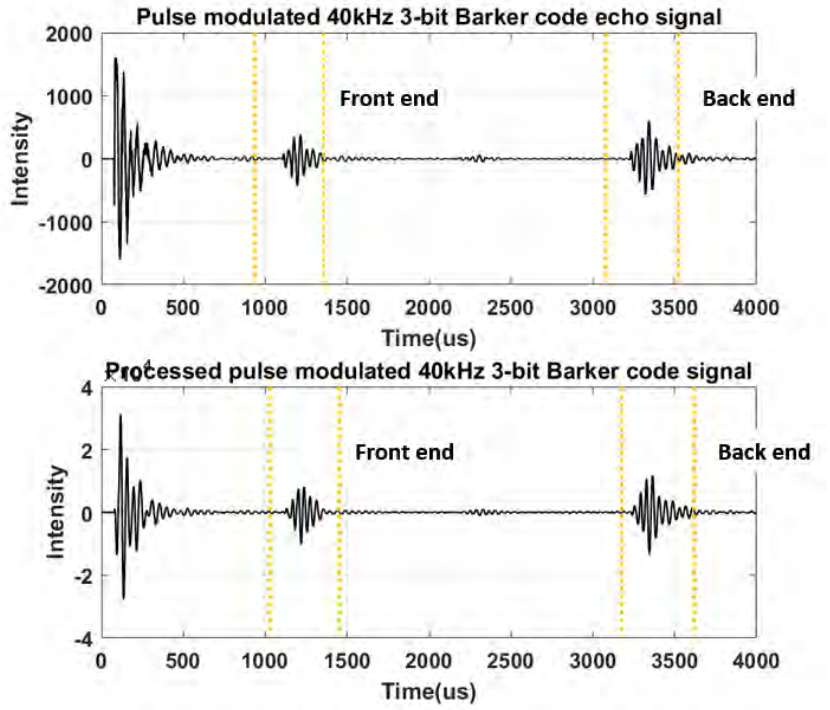

Figure 4.43: Pulse modulated 40 kHz 3-bit Barker code pair original echo signal pairs and processed result.

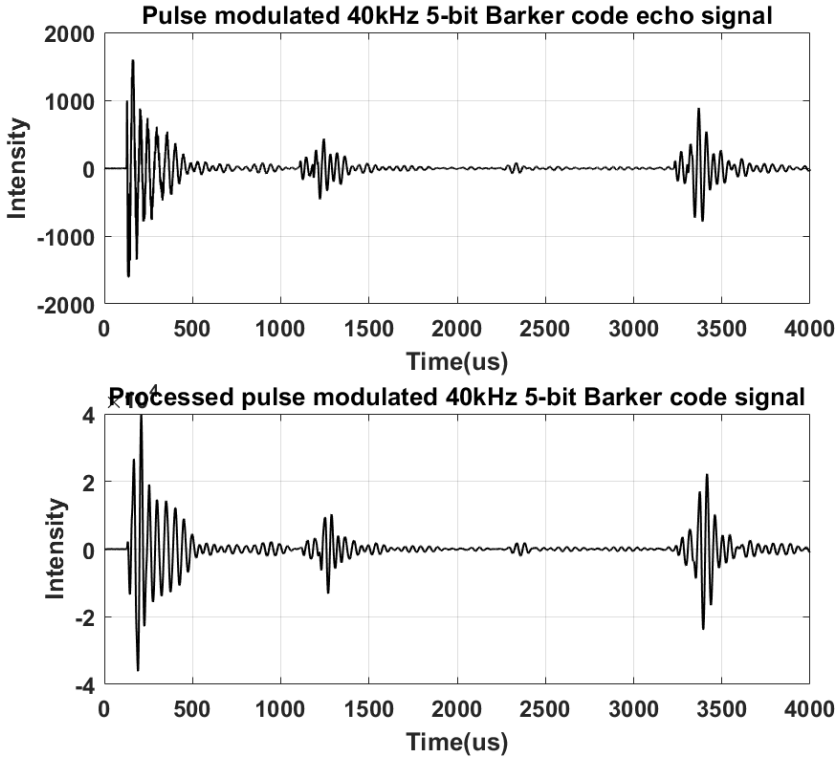

Figure 4.44: Pulse modulated 40 kHz 5-bit Barker code pair original echo signal pairs and processed result.

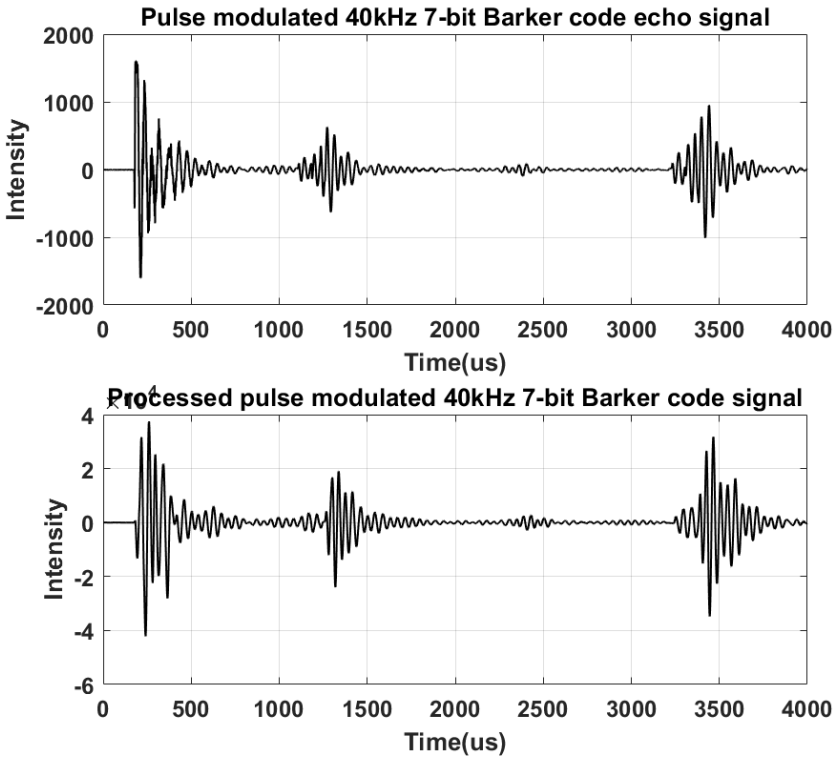

Figure 4.45: Pulse modulated 40 kHz 7-bit Barker code pair original echo signal pairs and processed result.

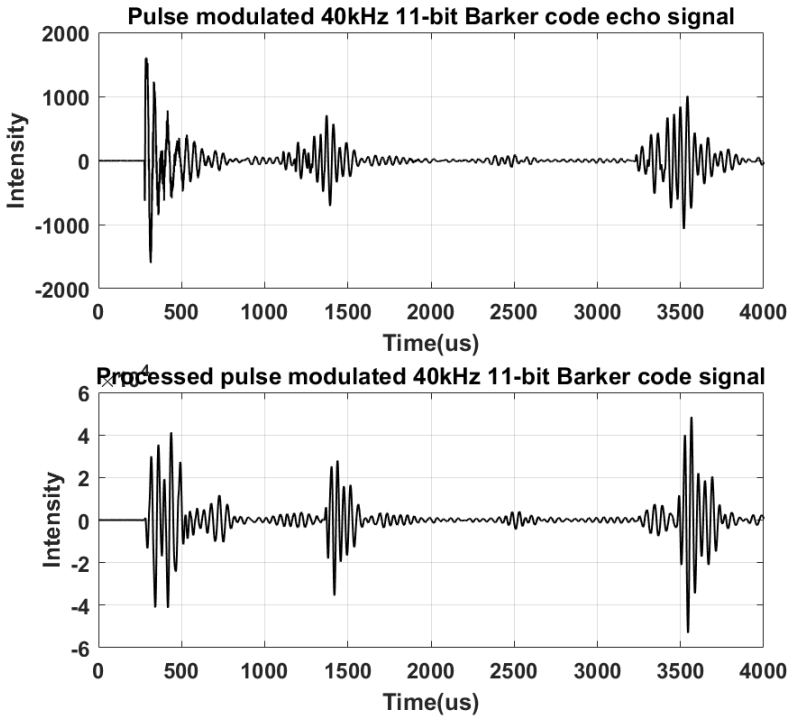

Figure 4.46: Pulse modulated 40 kHz 11-bit Barker code pair original echo signal pairs and processed result.

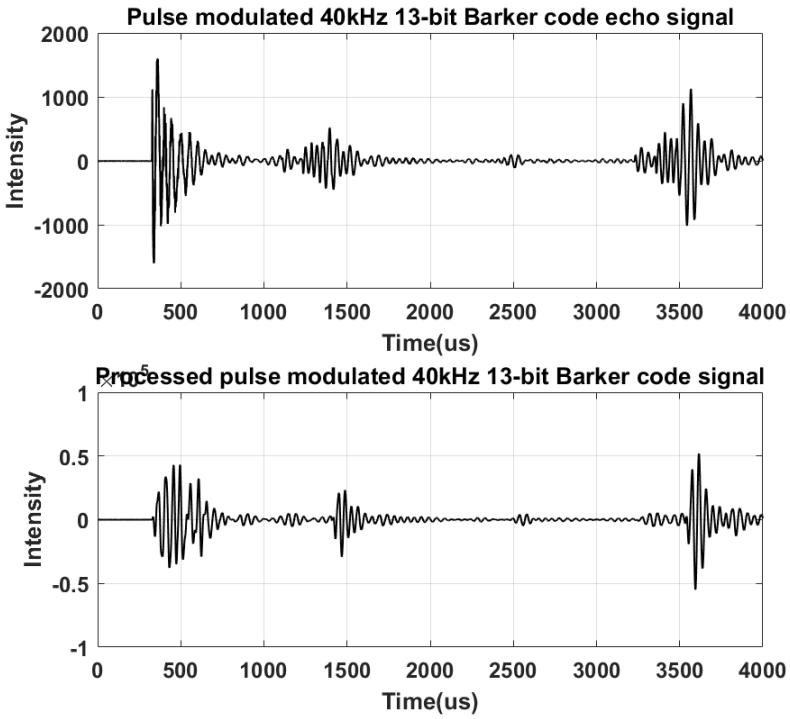

Figure 4.47: Pulse modulated 40 kHz 13-bit Barker code pair original echo signal pairs and processed result.

4.4.4 Results analysis

Firstly, this part compares SNR and peak side lobe level of FEM simulation and laboratory testing at 40 kHz. The FEM simulation and laboratory testing comparison as for SNR improvement is shown in Figure 4.48. The development of SNR for different codes from FEM simulation and testing are basically the same at the frequency of 40 kHz. The development of SNR for echo signals compared to the sine wave can be observed at different coding lengths as expected. Due to different code excitation length, the duration of the excited signals is different. The front side results are as same as the back side results. The results of SNR development of FEM simulation and testing are very close. The variation trend of back end increasing SNR is the same as front end SNR. The trend is agreed with the theoretical results.

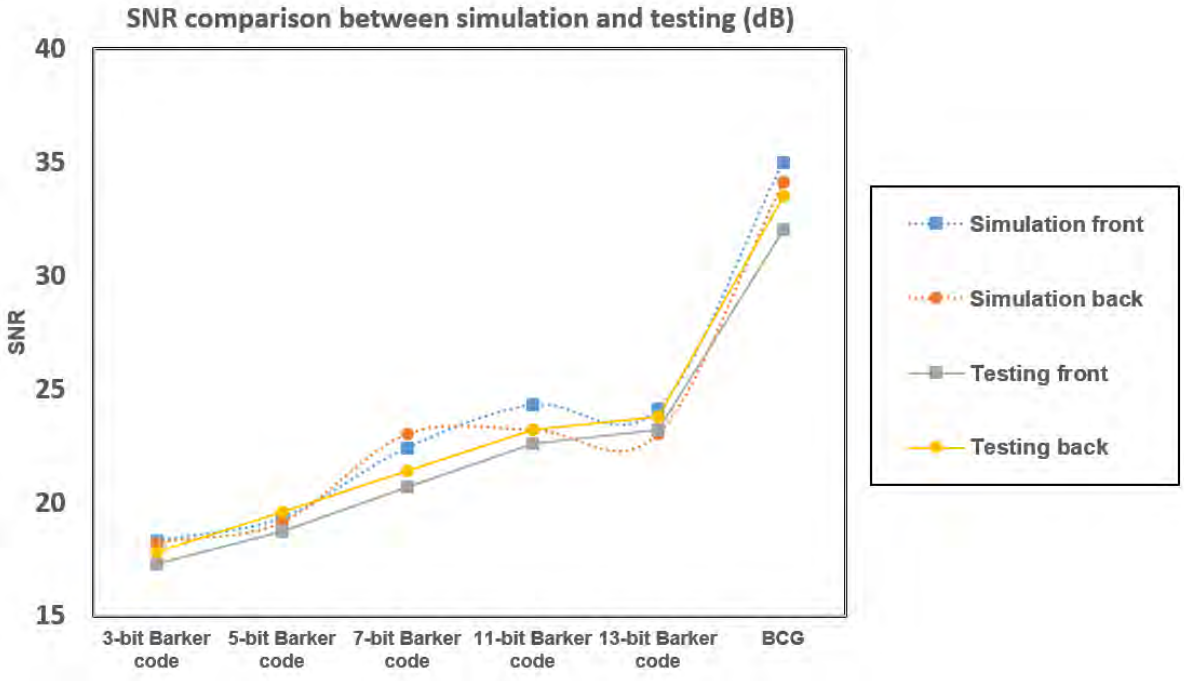

Figure 4.48: The increasing SNR of FEM simulation and laboratory testing from back side and front side.

The FEM simulation and laboratory testing peak side lobe level comparison is shown in Figure 4.49. The peak side lobe level of different codes from FEM simulation and testing are basically the same at the frequency 40 kHz. The peak side lobe level of echo signals changes with the length of transmitted method. The proposed method behave the best peak side lobe level. Due to different code excitation length, the duration of the excited signals is different. The front side results are a bit better than the back side results. That may be caused by the system coherent noise. The peak side lobe level results of FEM

simulation and testing are very close. The trend is agreed with the theoretical.

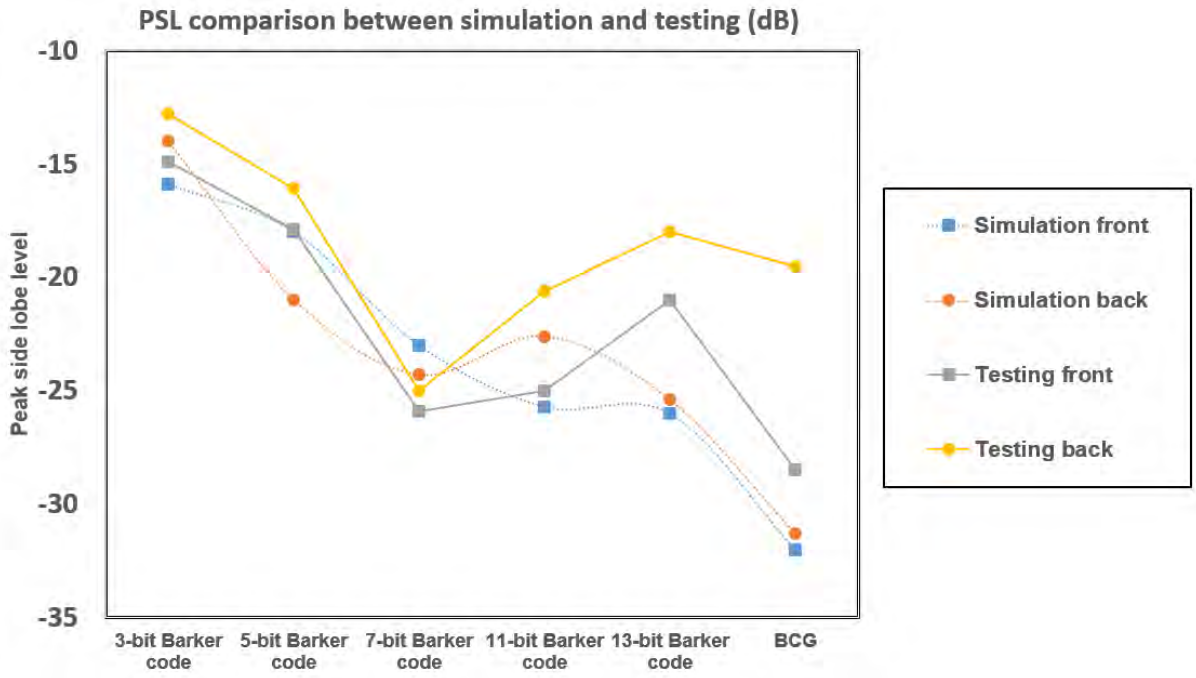

Figure 4.49: The peak side lobe level of FEM simulation and laboratory testing from back side and front side.

The cross-correlation result of echo signals from front end are shown in Figure 4.50. The Figure 4.50 (a) contains the results of 40 kHz different bits of Barker code, different bits of Golay code and BCG code. It is obvious from the figure that the main lobe of the BCG code is the largest as expect. The BCG code ability to increase the intensity of echo signal is much better than other code methods. Figure 4.50 (b) shows the Fast Fourier Transform of the echo signals.

Secondly, this part compares the result under different frequencies in laboratory testing. Figure 4.51 and Figure 4.52 show the increment of SNR for all processed echo signals from both side. Figure 4.51 is the results from the front side, and it demonstrates that the proposed method which is sine wave modulated BCG code have the largest SNR at all frequencies (30 kHz-50 kHz). The average increment of SNR is around 10 dB compared with other methods. The highest increment of SNR is 32 dB at the frequency of 40 kHz. Depending on comparison and analysis, it can be found that the best frequency to improve the SNR in this system is 40 kHz. Figure 4.52 shows the increment of SNR from the back side at different frequencies. The results shows that the average SNR of the Barker code signals is decreased 11.1 dB compared to the proposed method, which is perfect agreed with the theoretical results 10.7 dB. The increment of SNR from the back side is the same

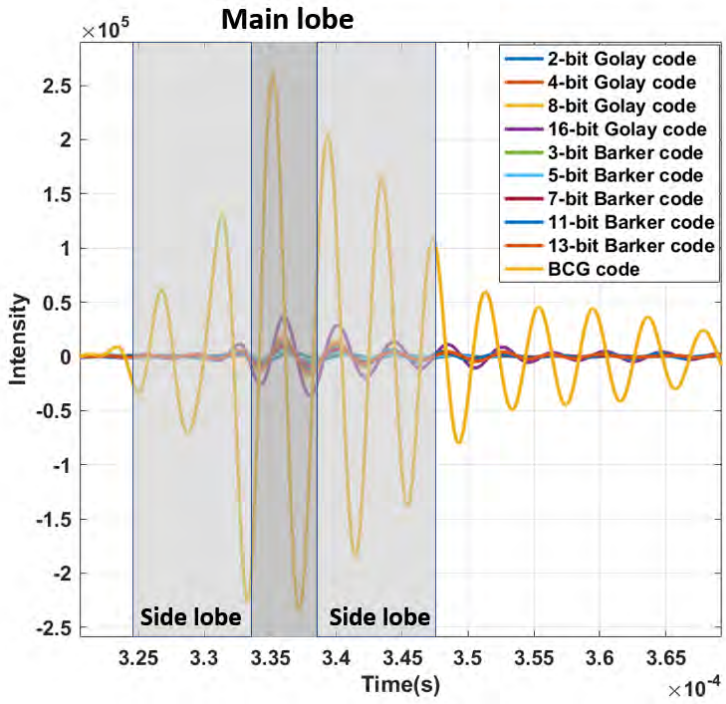

(a) Intensities of different codes after cross-correlation

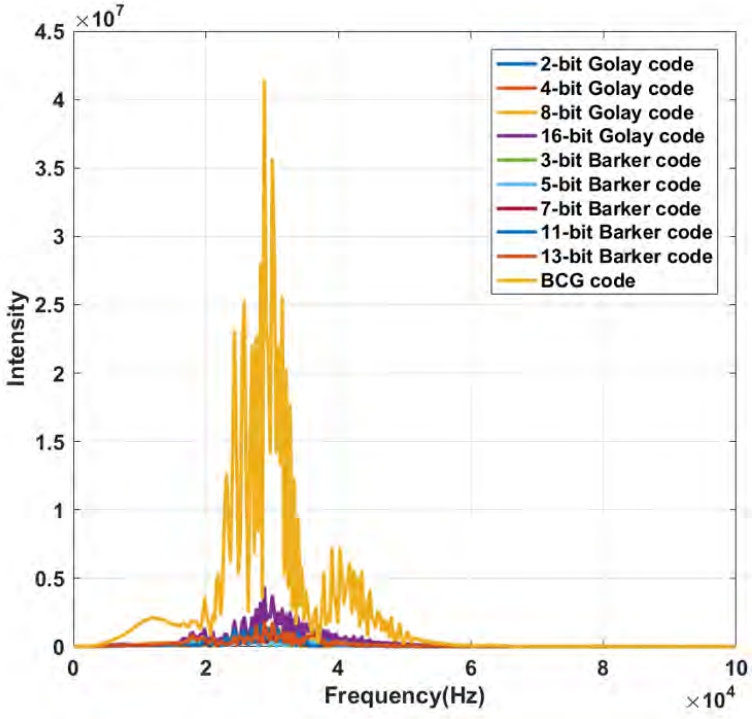

(b) Fast Fourier Transform of the different codes

Figure 4.50: Comparison of cross-correlation BCG code and others result (**a**) The different bits of Barker code, different bits of Golay code and BCG code intensity results comparison (**b**) The different bits of Barker code, different bits of Golay code and BCG code Fast Fourier Transform results comparison

as the value from front side. The best performance signal appeared at the frequency of 40 kHz. That is because the central frequency of the piezoelectric transducer in testing

device is around 40 kHz, which the trend is the same as the expected results.

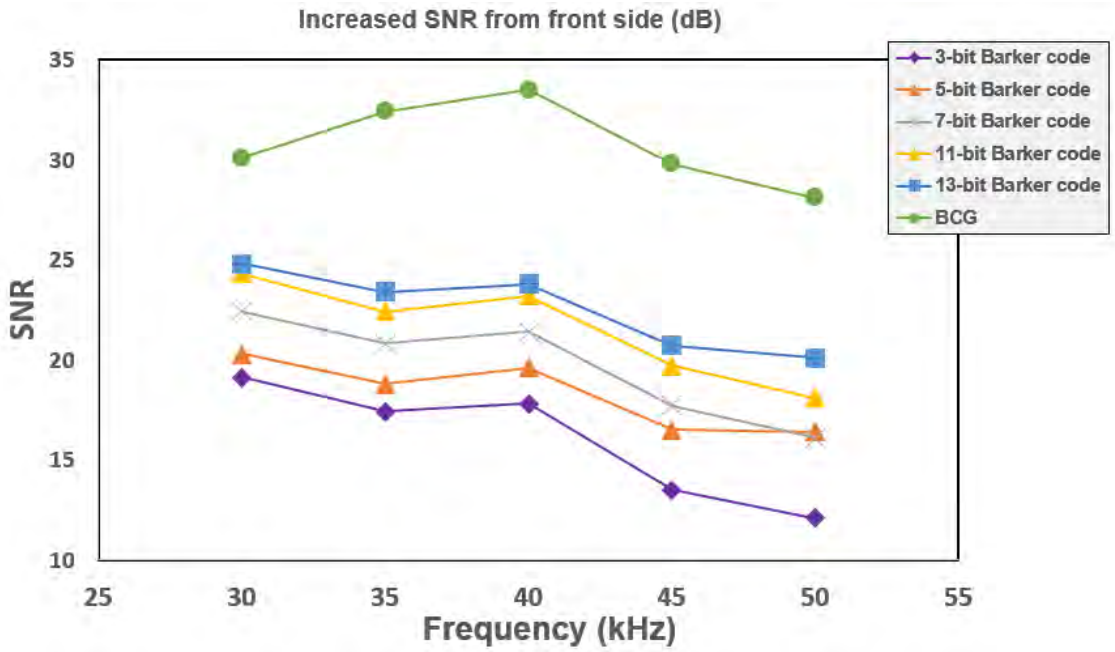

Figure 4.51: The increasing SNR of all echo signals from front side.

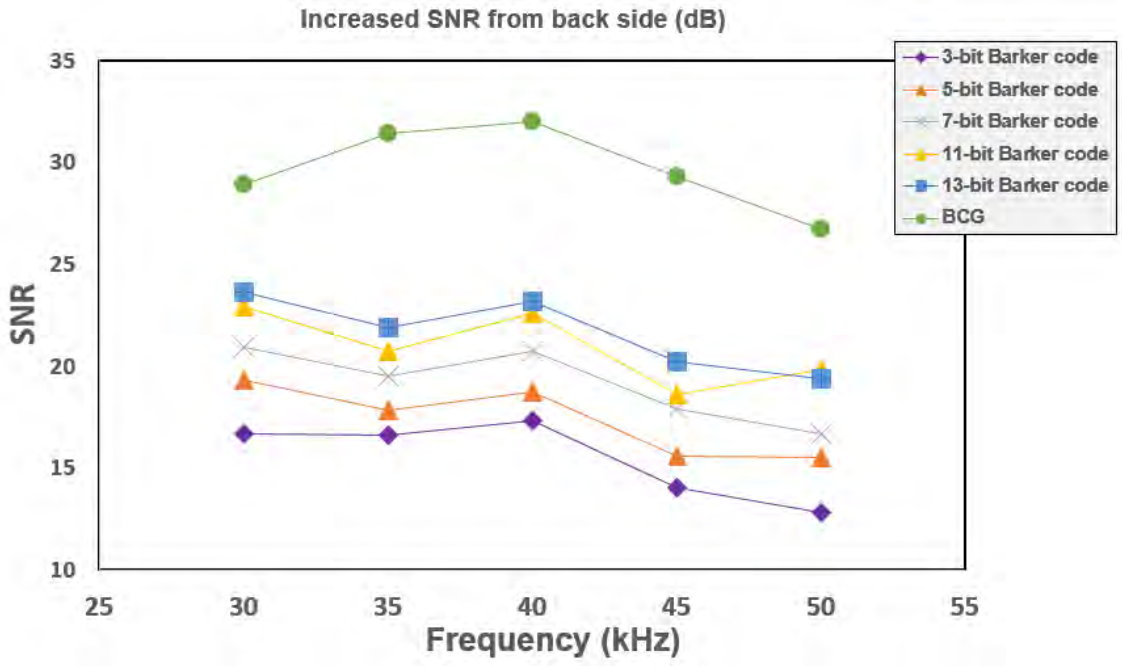

Figure 4.52: The increasing SNR of all echo signals from back side.

Figure 4.53 and Figure 4.54 show the peak side lobe level of all processed echo signals from both side. Figure 4.53 is the results from the front side and it shows that the pro-

posed method which is sine wave modulated BCG code have the lowest peak side lobe level -28.5 dB at the frequency of 40 kHz. The peak side lobe level of this method at 30 kHz is not ideal, which is slightly better than 3-bit Barker code. The average peak side lobe level of the proposed method is lower around 5.41 dB than other methods. Through comparison and analysis, it can be found that the best frequency for side lobe level in this system is 40 kHz. Figure 4.54 shows the side lobe level from the back side at different frequencies. Since the peak side lobe level results are under different frequency (from 30 kHz to 50 kHz), the average result is used to compared the performance of the results.

The results show that the average peak side lobe level of the Barker code signals from both side is decreased -17.6 dB, which is basically matched the theoretical results of -19 dB. However, the peak side lobe level of BCG code from the back side is not as same as the value from front side. The value is higher than expected. The reason of the undesirable value could be caused by the coherent noise in the system. Based on all the results of the front side and the back side, signals with 40 kHz frequency is an optimal choice for transmission.

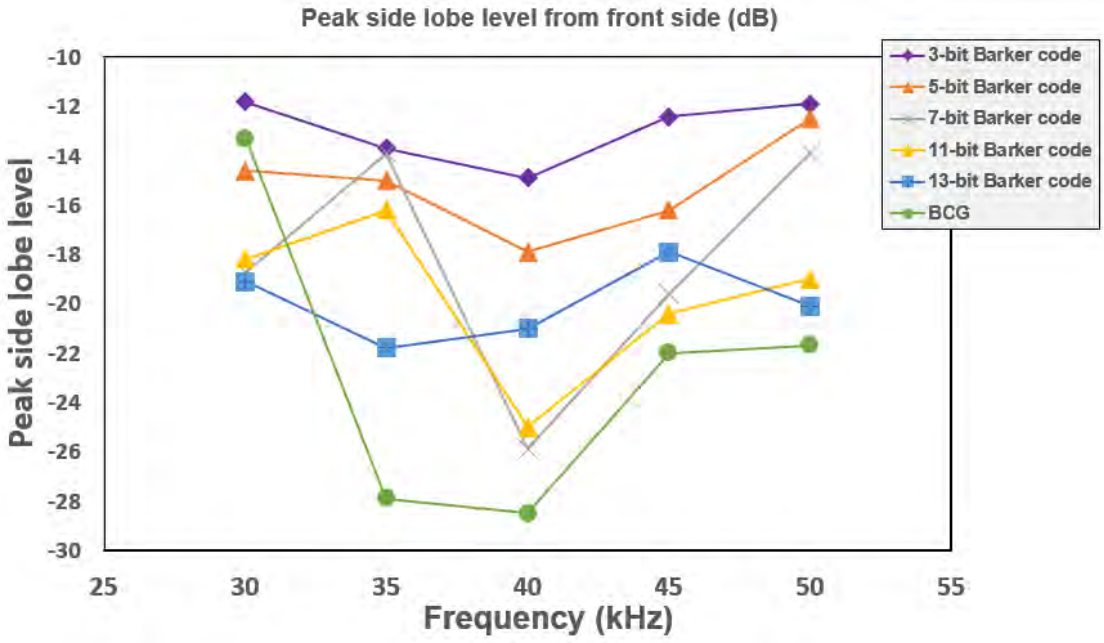

Figure 4.53: The peak side lobe level of all echo signals from front side.

Finally, this part compares the sine wave modulated results and the pulse modulated results. Figure 4.55 and Figure 4.56 show the SNR comparison and peak side lobe level comparison between pulse modulation and sine modulation at 40 kHz. The increasing SNR of sine modulated method is higher than pulse modulated method in all code sequences. The increasing SNR by using sine modulation is around 2-3 dB higher com-

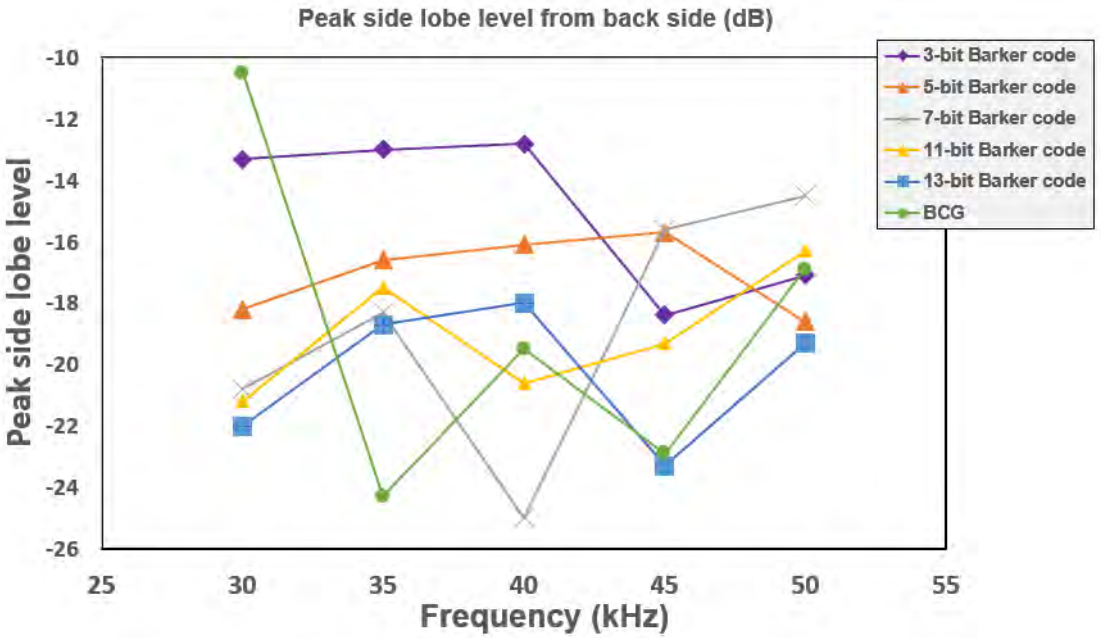

Figure 4.54: The peak side lobe level of all echo signals from back side.

pared to pulse modulation method. The peak side lobe level of the sine modulated signal behave better in long code length. The best peak side lobe level appeared at 7-bit length, which is -25.9 dB. Through a comprehensive analysis of these two modulation methods, it is found that sine modulation is slightly better than pulse modulation in this system. Due to the signal quality criterion, the BCG code has higher main lobe and the peak side-lobe level is lower at the same time. Based on these results, there is a good agreement between the simulated FE results and experimental results. Based on these results, further research on FEM modelling can be performed to use FE models with T (0,1) excitation. The 40 kHz sine modulated signal behaves the best in the system. It is considered as the transmitted signal in next chapter. The new BCG coded excitation method of T (0,1) has more effective behaviour in the circumferential direction.

4.5 GWT system for defect detection

Section 4.5 shows that the BCG code has the ability to increase SNR in guided wave testing. An defect detection has been done on pipeline. Figure 4.57 shows the schematic diagram of practical testing experiment. Figure 4.58 show the photograph of experimental set-up. Figure 4.59 shows the actual appearance of the defect. The specimen was a 11.6 m long, 8-inch (219.1 mm outer diameter) schedule 120 (14.27 mm wall thickness)

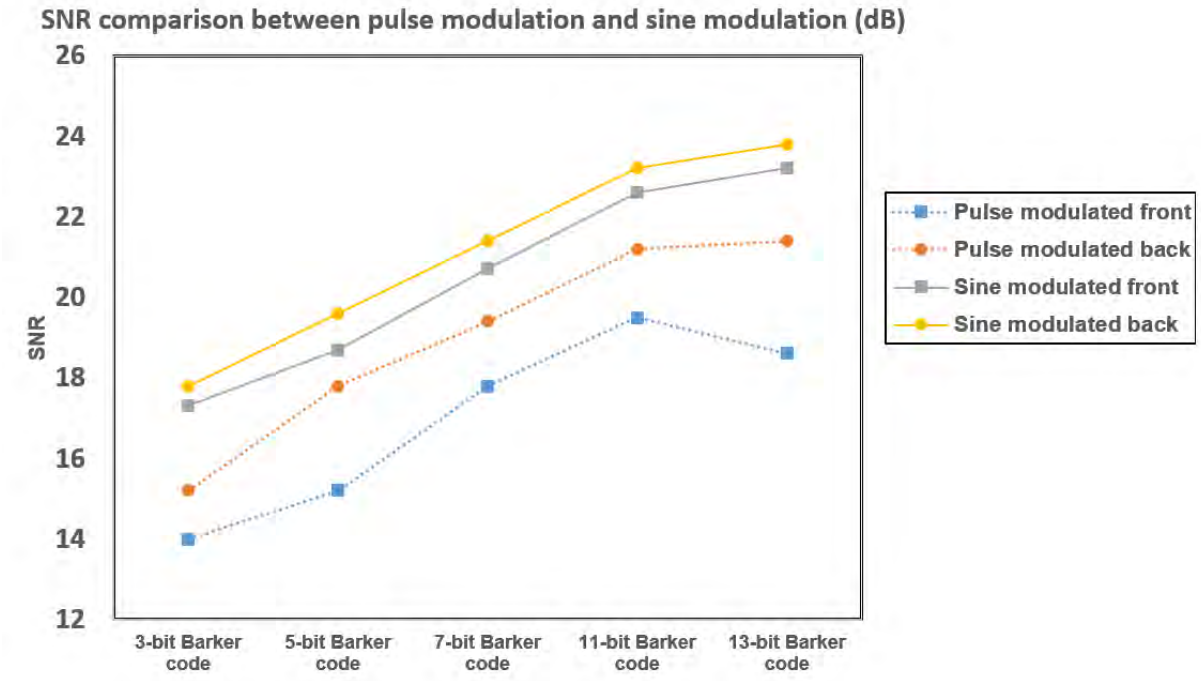

Figure 4.55: The increasing SNR of pulse modulated and sine modulated testing from back side and front side.

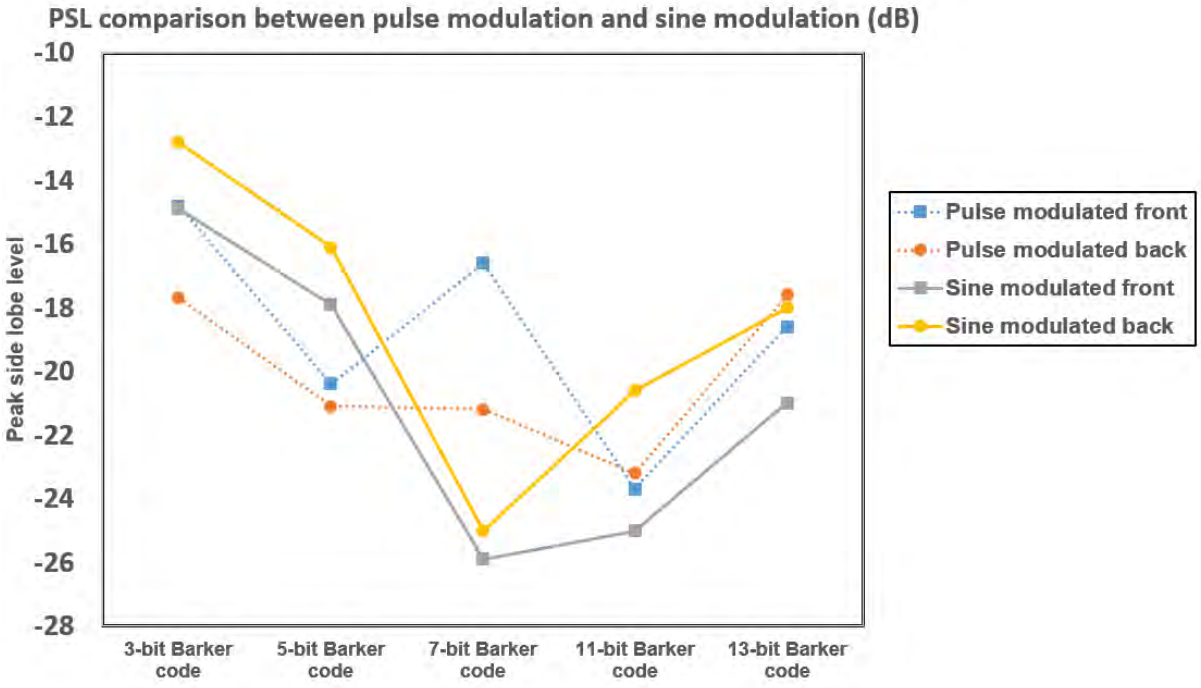

Figure 4.56: The peak side lobe level of pulse modulated and sine modulated testing from back side and front side.

steel pipe. A 3 mm thickness outer notch appeared at 3.5 m from the guided wave transducer collar. The inspection system with 8 segments of transducers was placed at 5.3 m from the pipe end showing as in Figure 4.57. The wave mode T(0,1) was generated in the circumferential direction and the excitation region of each patch is $13mm \times 3mm$. The transducer collar which was driven by Teletest MK3 has 8 segments and each segment has three transducers. The pulse echo signal from the notch and pipe ends was received by using transducers. Figure 4.59 shows the actual appearance of the defect on the circumference of pipe.

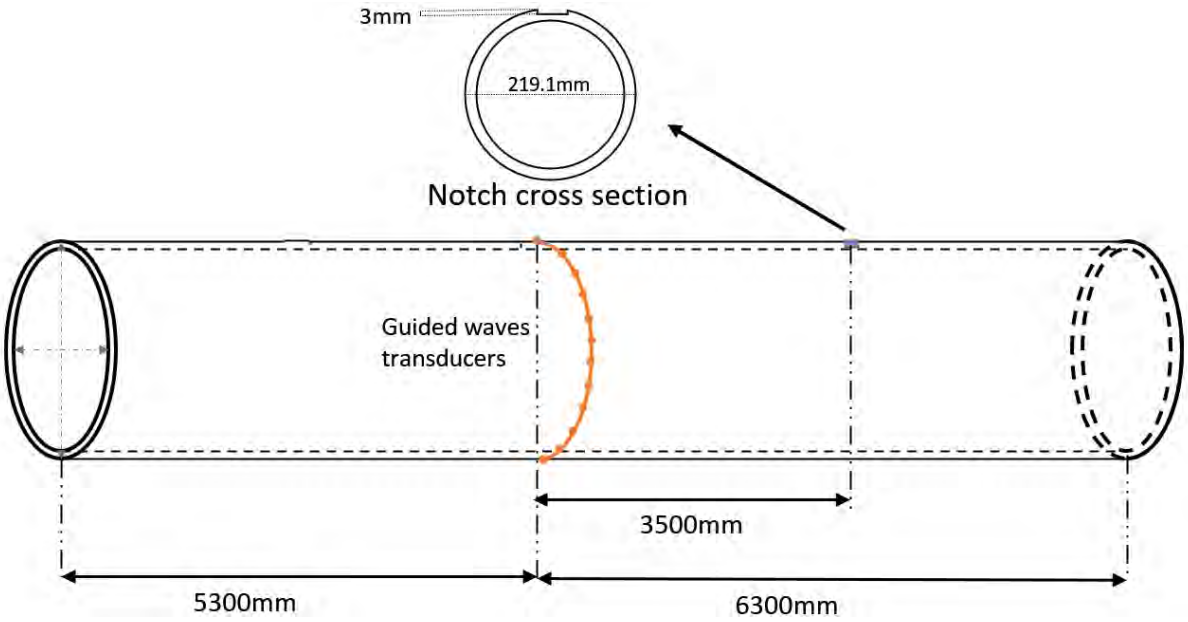

Figure 4.57: Schematic diagram of practical testing experiment.

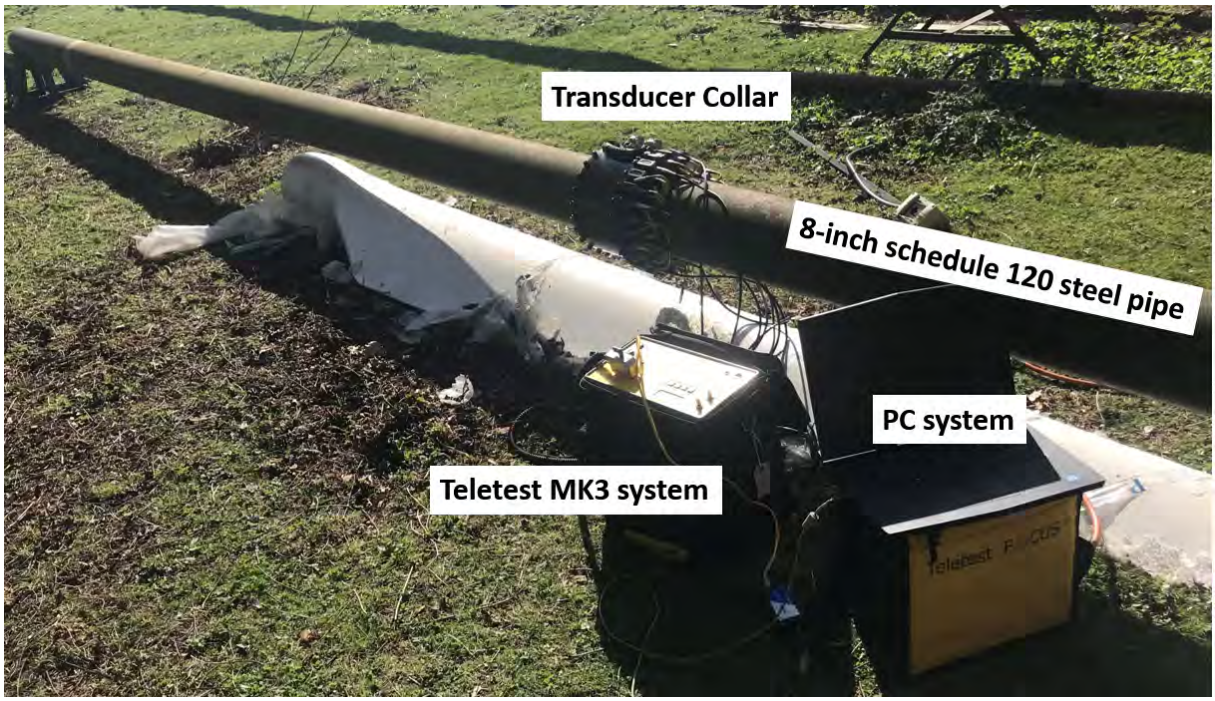

Figure 4.58: Photograph of practical testing experiment.

Figure 4.59: The actual appearance of the defect.

Due to the experimental results from the front side, the section chose 40 kHz as transmitted frequency. The transducers were excited by commercial simple sine pulse, 8-bit golay code pair, 7-bit Barker code and 3-bit Barker code convolution 4-bit Golay code pair at 40 kHz frequency. Signal is digitized at 1 MHz sampling rate.

Figure 4.60 shows the practical testing results inspired by simple pulse. The fundamental wave mode T(0,1) was generated in the circumferential direction. The echo signals include the reflected signal from notch, front side and back side. In the practical testing, it is easy to be ignored due to the small defect which is only 2 mm depth. The defect in the echo signal is hardly to be recognized. The reason comes from environmental noise and the inherent characteristics of piezoelectric transducers. In guided wave detection, it is very difficult to obtain a pure T(0,1) mode wave, so the influence of coherent noise is very huge. The resolution of the torsional wave mode T(0,1) is not up to the requirement.

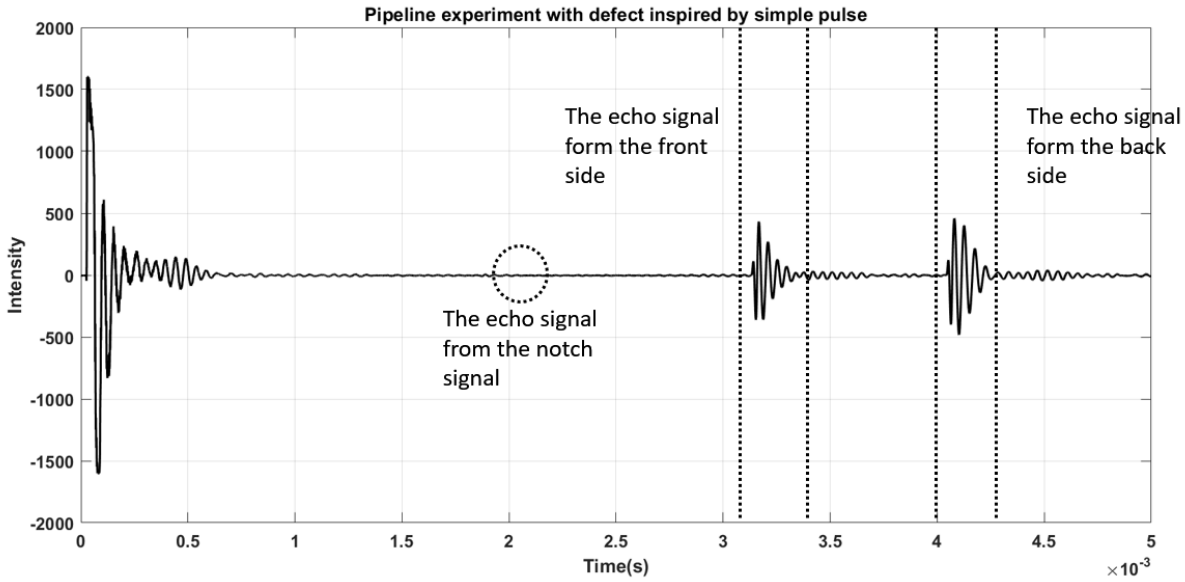

Figure 4.60: The pipeline testing result inspired by simple pulse.

Figure 4.61 shows that the practical testing results inspired by the 7-bit Barker code sequence. Figure 4.61 (a) shows the original echo signal, and Figure 4.61 (b) shows the echo signal processed by a spacial matched filter. The reflected signal from the front and back sides has increased significantly. However, the echo signal from the notch is still hard to recognize. Figure 4.62 shows that the real world testing results inspired by 8-bit Golay code pair sequences. Figure 4.62 (a) shows the original echo signal pair and Figure 4.62 (b) shows the echo signal processed by a spacial matched filter. The situation is the same as the Barker code sequence, although the processed signal is the result of 8-bit Golay code pair superposition. The displacement amplitude of pulse echo signal from the notch is still very clear.

Figure 4.63 shows that the real world testing results inspired by 8-bit Golay code pair sequences. Figure 4.63 (a) shows the original echo signal pair and Figure 4.63 (b) shows the

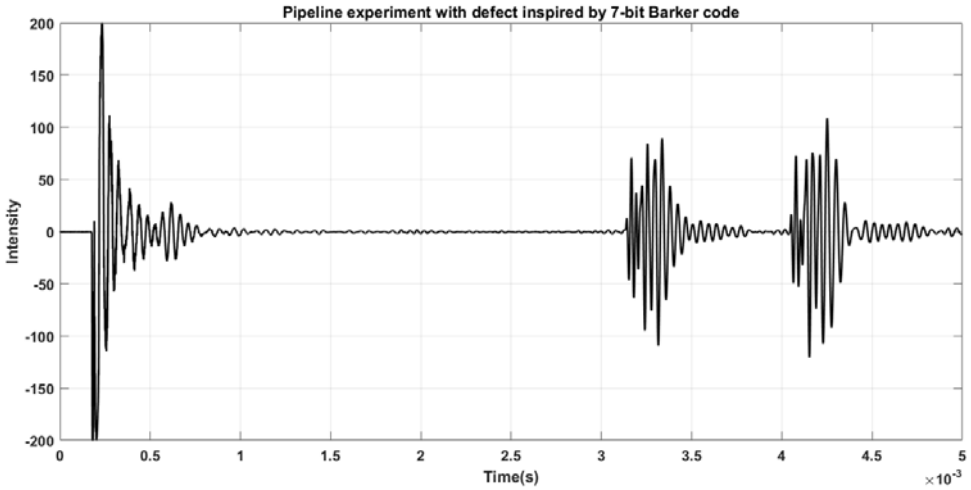

(a) The original echo signal of pipeline testing inspired by 7-bit Barker code sequence

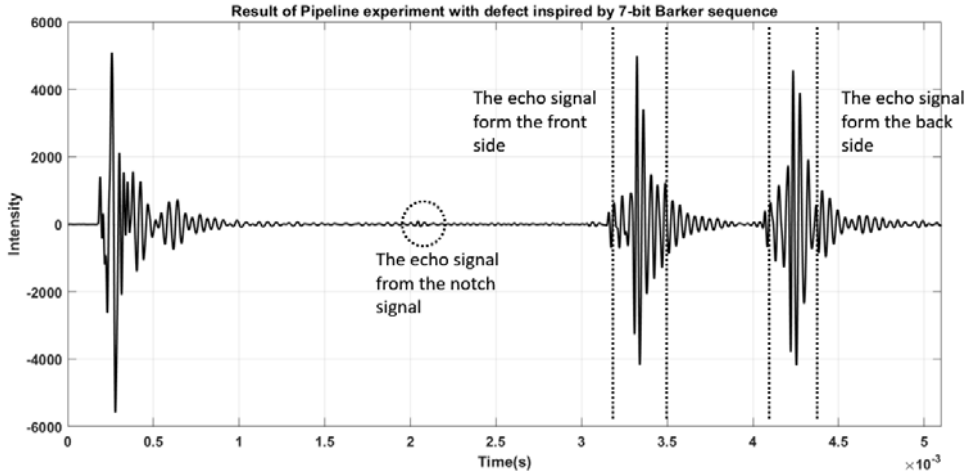

(b) The processed signal of pipeline testing inspired by 7-bit Barker code sequence

Figure 4.61: testing result inspired by 7-bit Barker code sequence (**a**) The original echo signal of pipeline testing inspired by 7-bit Barker code sequence (**b**) The processed signal of pipeline testing inspired by 7-bit Barker code sequence

echo signal processed by spacial matched filter. Although the echo signals from the notch are still very small in original reflected signals. The intensity of the echo signal from the notch has been increased in processed signal significantly. Figure 4.64 is the zoom in of the reflect signal from the 2 mm depth notch. The increment of intensity is 6 dB, which has excellent agreement between experimental and simulated results.

From experimental studies, some summaries are noted: the proposed method is a feasible method to excite the T(0,1) wave mode propagation with its significant purity for ultrasonic guided wave testing on pipes. This method can effectively improve the echo SNR when the inspection system device transmits the wave mode T(0,1). The theoretical and experiential testing results of the SNR and PSL have a good agreement. The increasing SNR of the BCG code has significant improvement and the PSL of the developed BCG

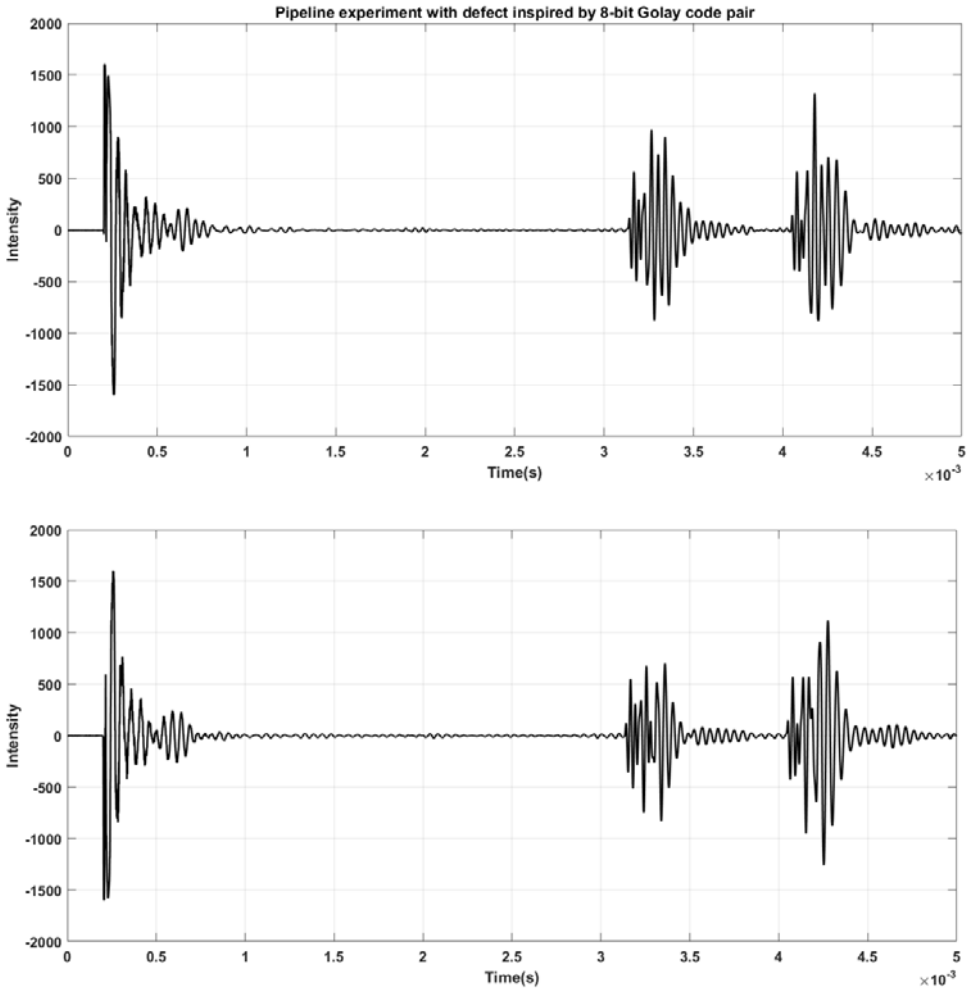

(a) The original echo signal of pipeline testing inspired by 8-bit Golay code pair sequence

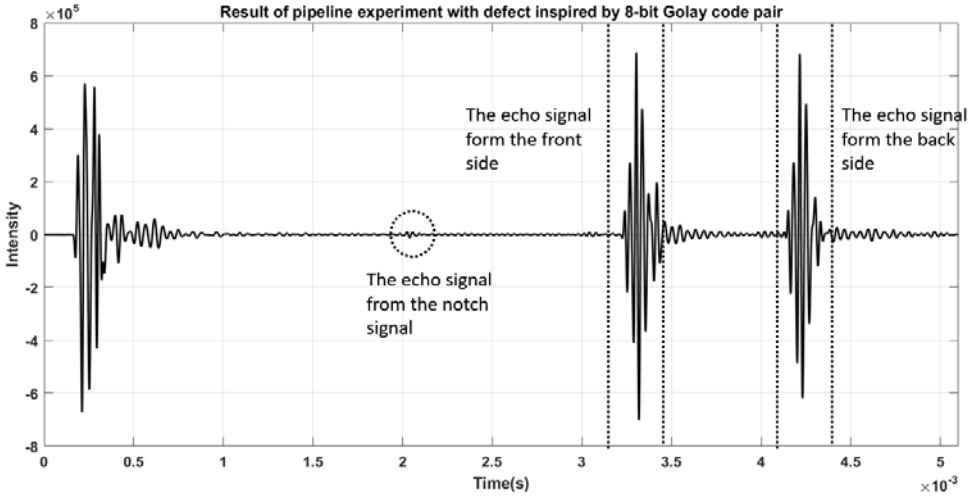

(b) The processed signal of pipeline testing inspired by 8-bit Golay code pair sequence

Figure 4.62: The testing result inspired by 8-bit Golay code pair sequence (**a**) The original echo signal of pipeline testing inspired by 8-bit Golay code pair sequence (**b**) The processed signal of pipeline testing inspired by 8-bit Golay code pair sequence

code is smaller than Barker code. The performance of BCG code is much better than the traditional coded excitation without changing the code length. Therefore, the proposed coded method, as a developed technique, is able to use in guided wave testing and many other potential applications for improving the echo SNR.

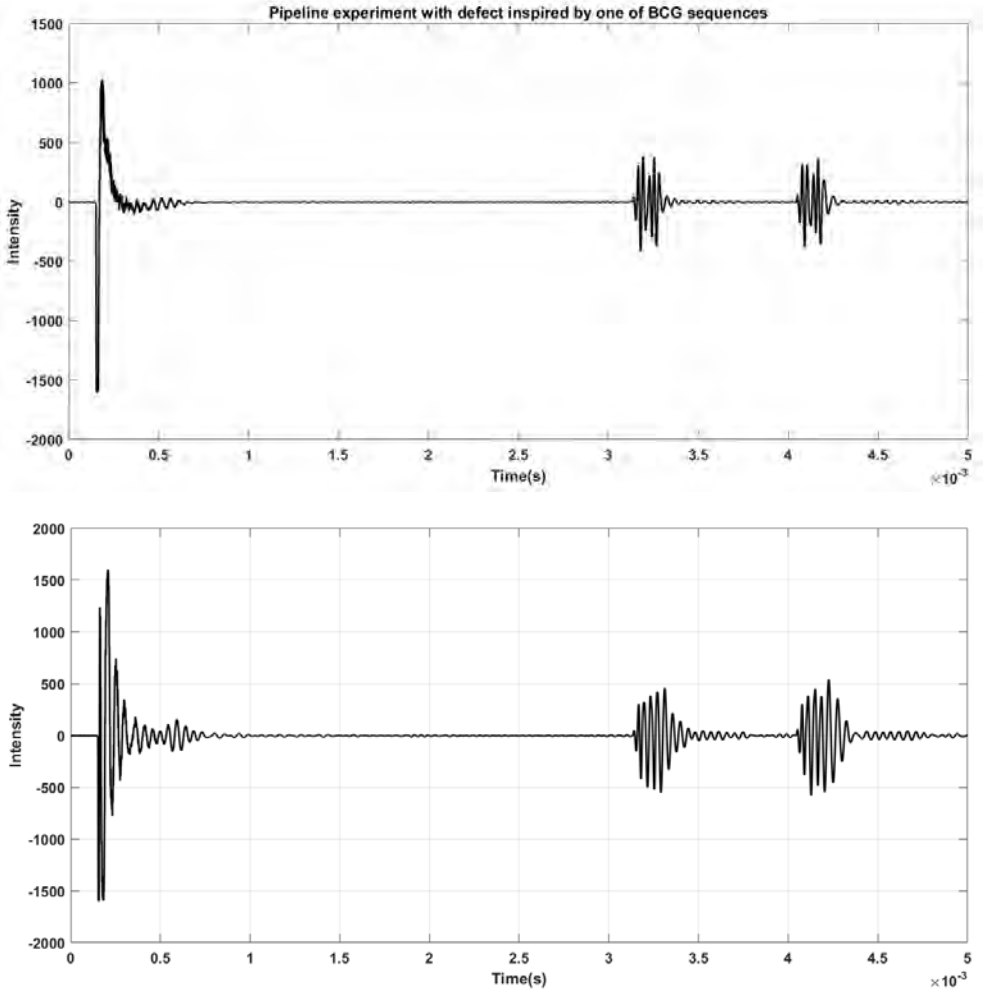

(a) The original echo signal of pipeline testing inspired by BCG code pair sequence

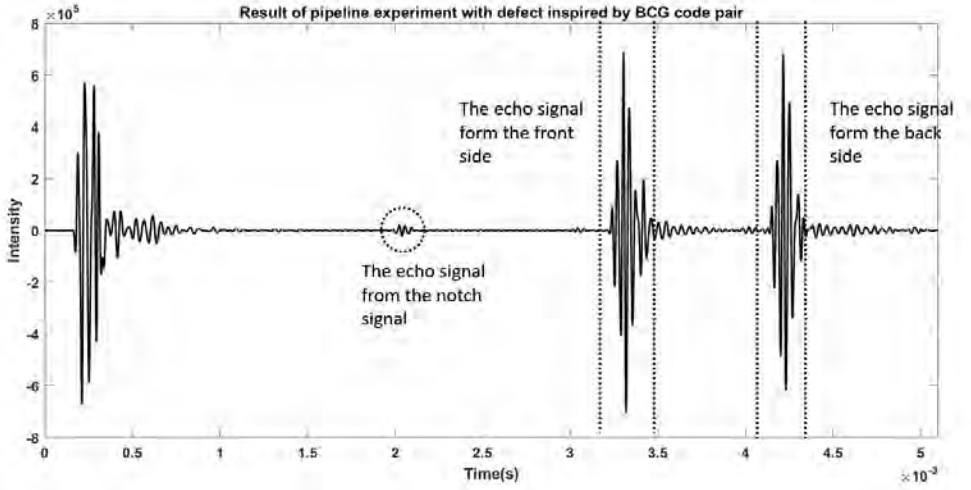

(b) The processed signal of pipeline testing inspired by BCG code pair sequence

Figure 4.63: The testing result inspired by BCG code pair sequence (**a**) The original echo signal of pipeline testing inspired by BCG code pair sequence (**b**) The processed signal of pipeline testing inspired by BCG code pair sequence

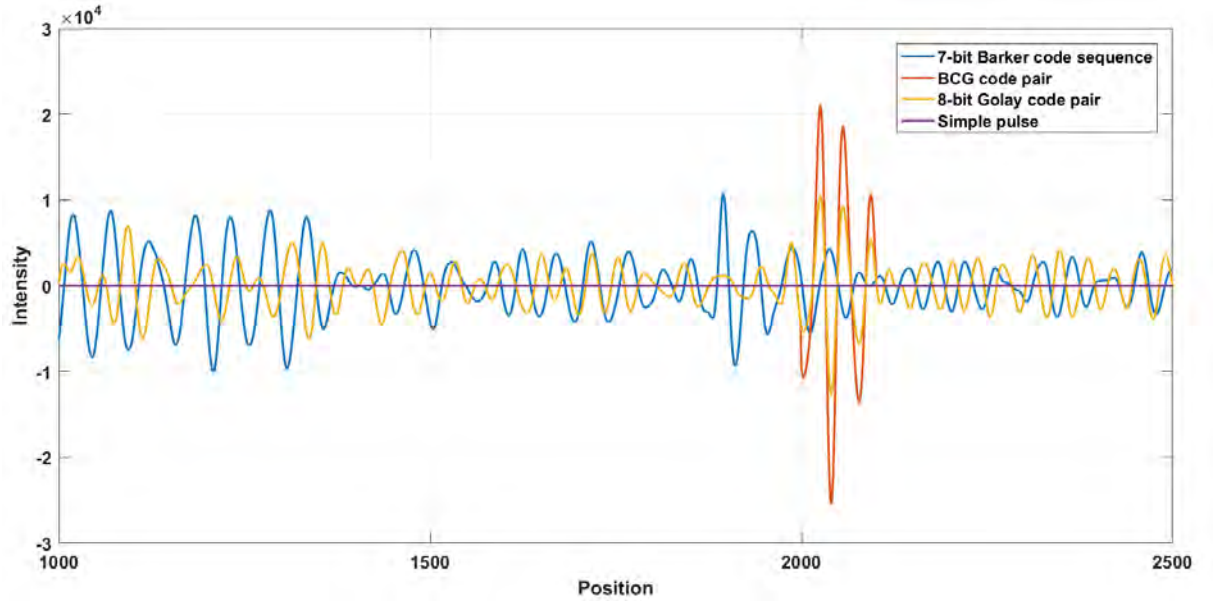

Figure 4.64: The comparison of defect echo signal results.

4.6 Summary

The proposed novel coded excitation method which combined the phase coded excitation has applied in this chapter. The purpose of the method is to reduce the noise to improve the SNR of echo signals. Laboratory tests were implemented on a 7 m long 8-inch schedule 40 steel pipe. Sine wave, Barker code, and BCG code of the torsional wave mode T(0,1) are among the transmitted signals. These signals have central frequencies of 30 kHz, 35 kHz, 40 kHz, 45 kHz and 50 kHz. The coded method was also practically tested. The results showed that the BCG code can improve the main lobe intensity significantly. The average increment of SNR is 30.2 dB compared to sine wave and the average peak side lobe level is -20.8 dB. By comparing the echo signals of different frequencies, it is found that all signals have the best SNR performance at 40 kHz in this GWT system. The defect detection testing used the 40 kHz proposed method on a 11.6 m long 8-inch schedule 120 steel pipe. By comparing the amplitude of the echo signal, it is clear that the defect echo of the proposed signal has a significant gain. The defect signal has an SNR that is approximately 6 dB higher than Barker signal.

The proposed method is a viable way to excite the T(0,1) wave mode with high purity for ultrasonic guided wave testing. When transmitting the T(0,1) wave mode, this method effectively improves the SNR. The results of the FEM simulation and the actual testing are matched. The increasing SNR of the BCG code has resulted in a noticeable improvement, and the peak-side lobe of the BCG code is smaller than that of the Barker code. The performance of BCG code is much better than the traditional coded excitation with-

out changing the code length. Therefore, the proposed coded method, as a developed technique, is able to use in guided wave testing and many other potential applications for improving the echo SNR.

Chapter 5

Non-linear Modulated Coded Excitation method for Ultrasound Imaging Application

5.1 Introduction

The hybrid pulse compression methods were used in the UT system and the GWT system in Chapters 3 and 4. The experimental and simulation results show that the novel method is feasible in an A-scan ultrasound system. As a result, the novel technology is being considered to be used in ultrasound imaging systems.

Ultrasound imaging is becoming more popular as a testing method in imaging and nondestructive testing systems. Figure 5.1 depicts the fundamental principles of the ultrasound imaging technique. The method is based on the physical properties of an ultrasound wave as it propagates through a medium. When compared to other imaging modalities, ultrasound imaging has several advantages, including being less expensive and more convenient. This method can also be used to detect in real time. Ultrasound imaging systems utilize a variety of ultrasound transducers based on multiarray configuration, including linear sequential arrays, curvilinear arrays, linear phased arrays, and phased arrays for object detection.

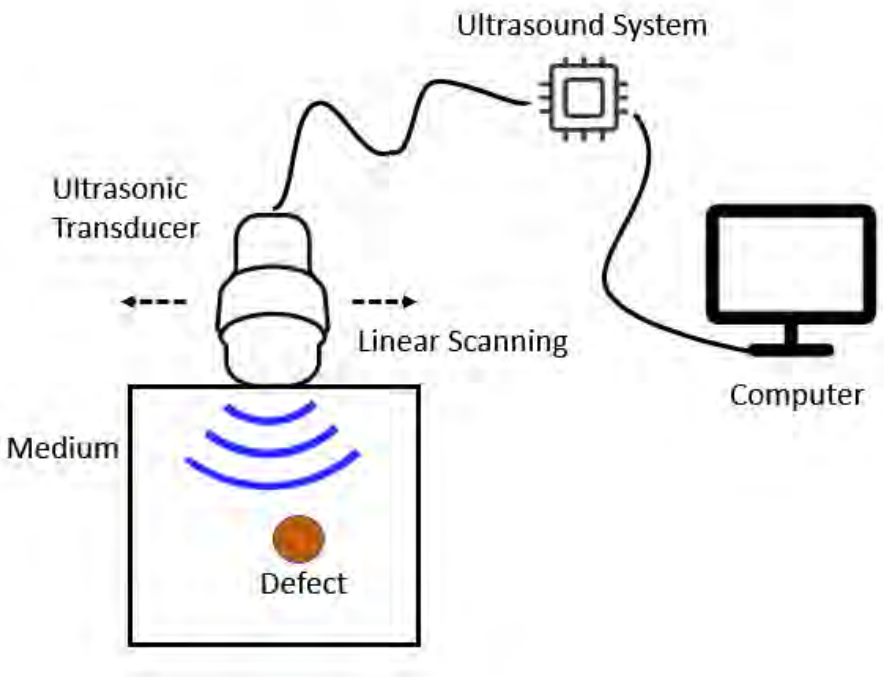

Figure 5.1: The fundamental principles of the ultrasound imaging technique.

In an ultrasound imaging system, SNR is a parameter that reflects the compression between the power of the output imaging signal and the power of the noise signal. The imaging effect improves with a greater SNR in theory. Axial resolution is a parameter that measures the ability to identify a defect or tissue between two shortest distances distributed along the axis of an ultrasound beam. With a high axial resolution, the UI system can more precisely identify the location of the object.

To improve the quality of ultrasound imaging, a very effective method of increasing SNR and axial resolution must be invested in. However, because of the high bandwidth of the sidelobe, the ultrasound imaging system has a low axial resolution. There are some methods for removing noise from ultrasonic signals, such as the wavelet transform. Because the strength of the filter result is poor in some applications, the wavelet transform is difficult to satisfy the SNR requirements in those cases. [82].

As mentioned before, pulse compression has widely been used in radar and medical ultrasound imaging. This method uses a long sequence to get a high main lobe energy while also getting a low and short sidelobe energy. There are two modulation methods in this method: frequency modulation and phase modulation. The linear-frequency chirp is a common method of frequency modulation. The frequency of the chirp signal rises (or falls) over time. Barker code has been primarily used to increase SNR in radar for many years. [108] This technique is an efficient method to increase SNR in UI systems.

In this chapter, a non-linear modulation method based on the Zak transform is used to modulate the hybrid coded excitation. And the novel hybrid signal is applied to ultrasound imaging systems. The method combines the advantages of the coding methods and the modulation method. The performance of the method will be evaluated by SNR and peak sidelobe level of the processed signal. The main contributions of this chapter are presented below.

- The non-linear frequency based on the Zak transform modulated hybrid coded excitation technique is applied for ultrasound imaging device for the first time.
- The theoretical analysis results proved that the proposed method can eliminate the limit of code length, not like other methods that have a certain value of length.
- The cyst simulations provided that the proposed method has the ability to increase SNR and penetration compared to the other code methods and modulation methods in ultrasound imaging systems. This work promotes the ultrasound imaging system of the proposed technique.

The rest of this chapter is organized as follows. In Section 5.2, the related work of ultrasound imaging has been reviewed. The methodology and analysis its superiority are also in Section 5.3. The theoretical analysis results are described in Section 5.4 and the experiment set-up and the cyst testing results are described in Section 5.5. Finally, the summary is given in Section 5.6.

5.2 Related works

Katamaneni *et al*. [137] studied the axial resolution comparison between LFM and NLFM, the main lobe width in NLFM reduced that can increase the axial resolution. Wang *et al*. [114] used the pseudo chirp signal as a carrier signal to modulate the Barker-Golay code. The ultrasound imaging simulation results in FIELD II showed that the combined code can increase the SNR and axial resolution in ultrasound imaging. Juan *et al*. [138] used the LFM to modulate the Barker code to increase the axial resolution in ultrasound imaging. NLFM can attenuate the sidelobes without any SNR-robbing sidelobe filtering or window functions [139]. To improve the SNR and axial resolution, the NLFM-various signals which are non-linear frequency modulated various codes are applied in this thesis.

Kang J *et al*. [140] proposed a new dynamic pulse compressed method based on chirp-code excitation to improve the SNR while compensating for tissue attenuation in medical ultrasound imaging. Kumru, Y *et al*. [141] applied Golay coded pair to obtain improved detection of 50 m breast microcalcifications in ultrasound mammography. The coded excitation improves signal to noise ratio, increases penetration depth and provides images with better resolution.

The aim of this chapter was to expand the use of the pulse compression technology in ultrasonic imaging equipment to improve image quality. This chapter discusses the performance of various theoretical modulation basic methods in ultrasound imaging applications, the limitations of research and comparison, and the hybrid modulation method that overcomes the current disadvantages. The frequency modulation ultrasound imaging application, phase modulation ultrasound imaging application, and hybrid method ultrasound imaging application were all put to the test.

5.3 Methodology

Pulse compression techniques are widely used in radar and ultrasonic signal processing, which use reference signals for correlation with received signals to increase SNR without changing average transmission power. There are two main methods concerned with this technique, which are the frequency modulation method and the phase modulation method. Barker code sequence and Golay code pair are applied in this chapter as the phase modulation method. The Zak transform is used to process the NLFM signal synthesis method in this chapter. This section contains the generation and processing of Barker code, NLFM and NLFM-various sequence.

5.3.1 Phase modulation sequence

Barker code sequence is a typical phase modulation method in pulse compression technique. The advantage of the Barker code sequence is the low sidelobe level, which is constant equal to one. Due to the unique property, the lengths of the Barker code sequence are only 2,3,4,5,7,11 and 13. Table 5.1 shows all the existing Barker code sequences.

The longer the Barker code sequence, the more accurately the data can be processed and errors due to distortion can be omitted. However, the long transmitted sequences cause

the low resolution. The 5-bit Barker code sequence and the 7-bit Barker code sequence are used as synthesis code methods in this chapter.

Table 5.1: All types of Barker code sequence

Barker code length	Code	MLI	SLL(dB)
2	(+1,-1),(+1,+1)	2	-6
3	+1,+1,-1	3	-9.5
4	(+1,-1,+1,+1),(+1,-1,-1,-1)	4	-12
5	+1,+1,+1,-1,+1	5	-14
7	+1,+1,+1,-1,-1,+1,-1	7	-16.9
11	+1,+1,+1,-1,-1,-1,+1,-1,-1,+1,-1	11	-20.8
13	+1,+1,+1,+1,-1,-1,-1,+1,+1,-1,+1,-1,+1	13	-22.3

Golay code is defined as a pair of equal finite length composed elements, where the number of identical element pairs in one sequence equals the number of different element pairs in another at any given interval [120]. An optimum pulse compression result with no sidelobes is attained by mixing matched pairs of echoes produced by broadcasting a pair of complimentary sequences.

Defined there are a pair of Golay complementary pair sequence G_a(n) and sequence G_b(n). Each element of G_a(n) and G_b(n) is either 1 or -1. Due to the property of Golay code pair, the auto-correlations of sequence G_a(n) and sequence G_b(n) are shown in Equation 5.1. $\delta(n)$ is a Dirac delta function. $*$ is the symbol of convolution.

$$G_a(n) * G_a(-n) + G_b(n) * G_b(-n) = 2N * \delta(n) \tag{5.1}$$

When use the coded excitation in ultrasonic testing or imaging, sequence G_a(n) and sequence G_b(n) are used instead of the traditional single-pulse excitation to stimulate the ultrasound transducer sequentially. The echoes from the same stationary object in the ultrasound field are represented by e_a(n) and e_b(n).

$$e_a(n) = y_t(n) * G_a(n) * y_r(n) \tag{5.2}$$

$$e_b(n) = y_t(n) * G_b(n) * y_r(n) \tag{5.3}$$

Where y_t(n) and y_r(n) are the impulse response of the ultrasound transmitter and receiver. If the receiver and transmitter have the same element, y_r(n) =y_t (n) the cross-correlation

between e_a (n) and sequence G_a(n) is

$$e_a(n) * G_a(-n) = y_t(n) * G_a(n) * G_a(-n) * y_r(n) \tag{5.4}$$

And the cross-correlation between e_b(n) and sequence G_b(n) is

$$e_b(n) * G_b(-n) = y_t(n) * G_b(n) * G_b(-n) * y_r(n) \tag{5.5}$$

Sum the two cross-correlation results,

$$g(n) = e_a(n) * G_a(-n) + e_b(n) * G_b(-n) = 2N(y_t(n) * \delta(n) * y_r(n)) \tag{5.6}$$

$g(n)$ is the result of pulse compression of Golay code pair. It shows that the amplitude of $g(n)$ is equal to 2N times the echo amplitude of a single-pulse simulation.

Because of their peculiar properties, Golay code pairs can be used as ultrasonic transmitter input signals, and the sidelobes of the echo signal after decoding are eliminated.

5.3.2 Linear frequency modulation

The Linear frequency modulation (LFM) method, which has another name, chirp signal, is widely used in radar and sonar systems. The instantaneous frequency of chirp signal linearly increases or decreases with time. The quadratic phase coefficient k makes the phase function of the LFM signal. The Equation 5.7 shows the description waveform of LFM $s(t)$.

$$s(t) = \begin{cases} e^{j2\pi(f_c t - \frac{1}{2}kt^2)}, -\tau/2 \leq t \leq \tau/2 \\ 0, elsewhere \end{cases} \tag{5.7}$$

where fc is the carrier frequency of the transmitted waveform, k is the chirp rate or the sweep rate of the waveform. Equation 5.8 shows the description of bandwidth.

$$B = k\tau \tag{5.8}$$

The instantaneous frequency $f(t)$ can be obtained by differentiating the argument of the exponential in Equation 5.9,

$$f(t) = f_c + kt \tag{5.9}$$

The quadratic phase coefficient k produces a linear frequency during the duration of the signal. Since the frequency bandwidth of chirp signals is much higher than the information bandwidth, the large gain of a system can be easily obtained. This method is readily generated and can be processed by a matched filter.

LFM increases the bandwidth and subsequently improves the range resolution of the signal by a factor equal to the time bandwidth product. However, relatively high sidelobes remain in the autocorrelation function. Such an autocorrelation function is unacceptable in some radar applications, where more than one target is present, giving rise to echo of different amplitudes. Time domain weighting is equal to the amplitude modulation of the transmitted signal. However, such implementation will lead to a reduction in transmitted power, and therefore the SNR will be decreased. Frequency domain weighting spectrum shaping methods are used in well known weighting windows such as Hanning and Hamming. However, the implementation of weighting windows may lead to the penalty of mainlobe broadening. The NLFM waveform is designed such that its matched filter response satisfies the sidelobe requirements. Since the receiver is matched to the signal shape, , there are no mismatch losses in time domain weighting and frequency domain weighting. Figure 5.2 shows an example of the LFM waveform. The frequency character of the example is from 1 MHz to 3 MHz.

5.3.3 Non-Linear frequency modulation

Because the auto-correlation function of the LFM waveform exhibits a sine function shape and the sidelobe structure has the same problem that can reduce axial resolution. The commonly used methods to reduce the sidelobe of compression output are accomplished by linear filtering or by applying window functions. This additional filter can help to decrease sidelobes. However, since the cumulative filtering is no longer precisely matched to the signal, it will reduce output SNR by 1-2 dB.

The frequency ramp of nonlinear frequency modulation (NLFM) is non-linear. This method is no attenuation of the signal. In this chapter, the NLFM signal synthesis method

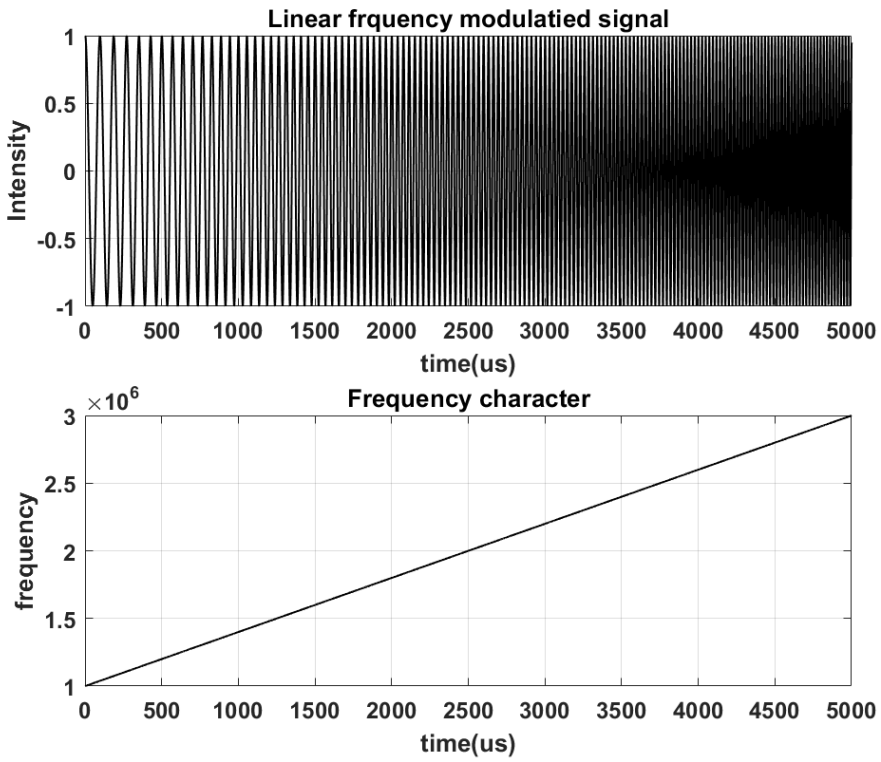

Figure 5.2: Example waveform of LFM signal.

based on the Zak transform is applied. Gelfand invented and applied the Zak transform to a differential equations problem [142]. The Zak transform is extremely popular in engineering.

The NLFM s(t) could be expressed as Equation 5.10.

$$s(t) = Arect[\frac{t-\frac{t_i}{2}}{t_i}]e^{2\pi j\theta(t)} \tag{5.10}$$

Where A is the amplitude of the signal, ti is the signal duration time and $\theta(t)$ is the angle modulation function. To find the relationship between time and the instantaneous signal frequency, the sub-pulse number and the number of the frequency component in the sub-pulse number in the sub-pulse train model should be found. To simplify the problem, the most common way is to set the rank of norm equal to 2. When the rank of norm is equal to 2, Equation 5.11 shows the angle modulation function of the NLFM signal.

$$\theta(t) = k - \sqrt{k^2 - (t-k)^2} \tag{5.11}$$

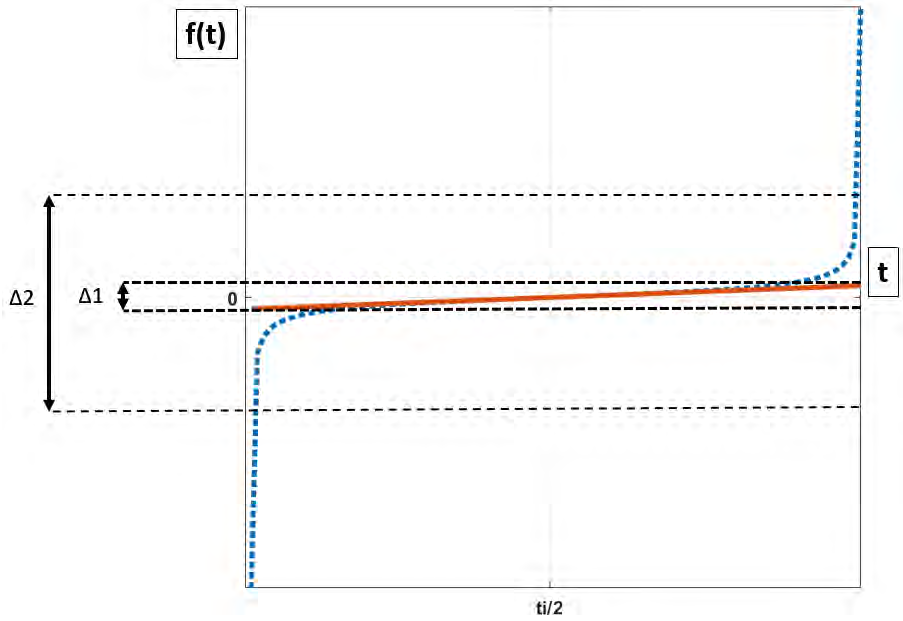

Figure 5.3: Example of instantaneous frequency of NLFM signal.

And

$$f(t) = \frac{t-k}{\sqrt{k^2-(t-k)^2}} \tag{5.12}$$

The instantaneous frequency of NLFM can be described by Equation 5.12, when rank of norm equal to 2. Figure 5.3 shows the instantaneous frequency of the NLFM signal. The linear instantaneous frequency change interval $\triangle_1$ and instantaneous frequency change interval $\triangle_2$ are the main lobe width and the auto correlation function of the NLFM signal side lobe level separately. The $\triangle_1$ can be described in Equation 5.13.

$$\triangle_1 = \frac{2\triangle_2\sqrt{\triangle_2^2+4}}{\triangle_2^2+4} \tag{5.13}$$

Figure 5.4 shows an example of the real part NLFM waveform which is processed by Zak transform.

5.3.4 NLFM-Barker hybrid method

Due to the property of Barker code and NLFM, the hybrid method can combine the advantages of these two methods. The Barker code can be expressed as a convolution of carrier signal with an over-sampled Barker code sequence. The NLFM-Barker signal can be expressed as Equation 5.14.

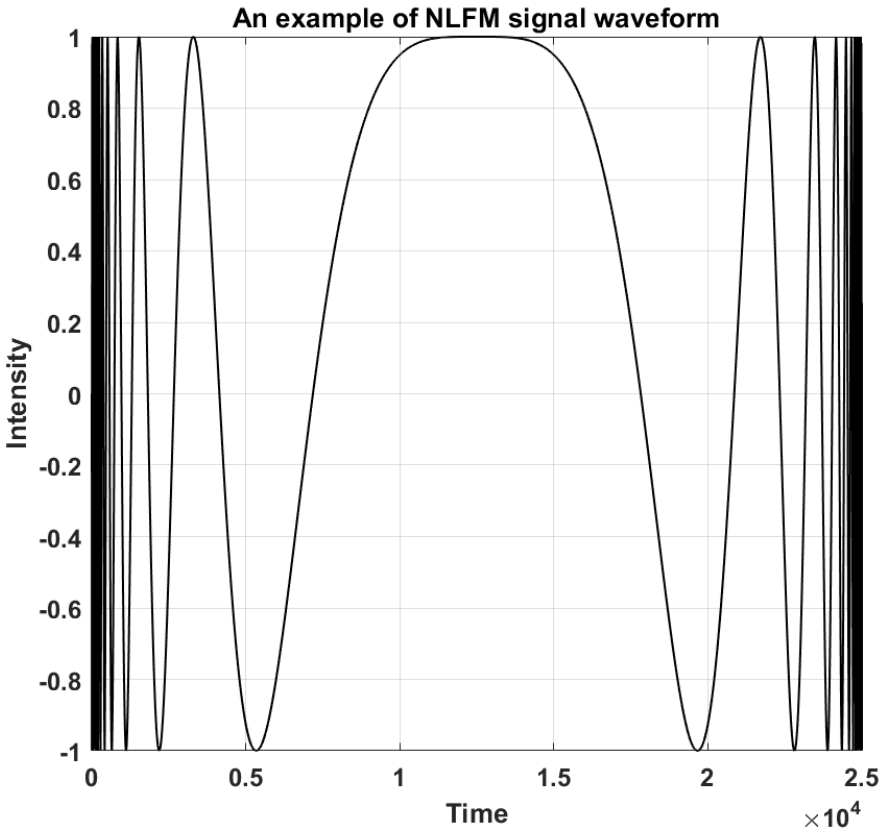

Figure 5.4: Example real part waveform of NLFM signal.

$$c(t) = s(t) \times b(n) \tag{5.14}$$

Where $b(n)$ is the over-sampled Barker sequence, $s(t)$ is the carrier signal and $c(t)$ is the NLFM-Barker signal. Figure 5.5 shows the generation and compression of the NLFM-Barker code signal.

The NLFM-Barker code signal is generated by the convolution Barker code sequence with the NLFM signal. The hybrid transmitted sequence transmits in medium, and the received signal will be processed by the NLFM matched filter and the Barker code matched filter. Figure 5.6 shows an example of the compressed NLFM-Barker result. It can be easily seen that the pulse width of the main lobe and side lobes are very narrow.

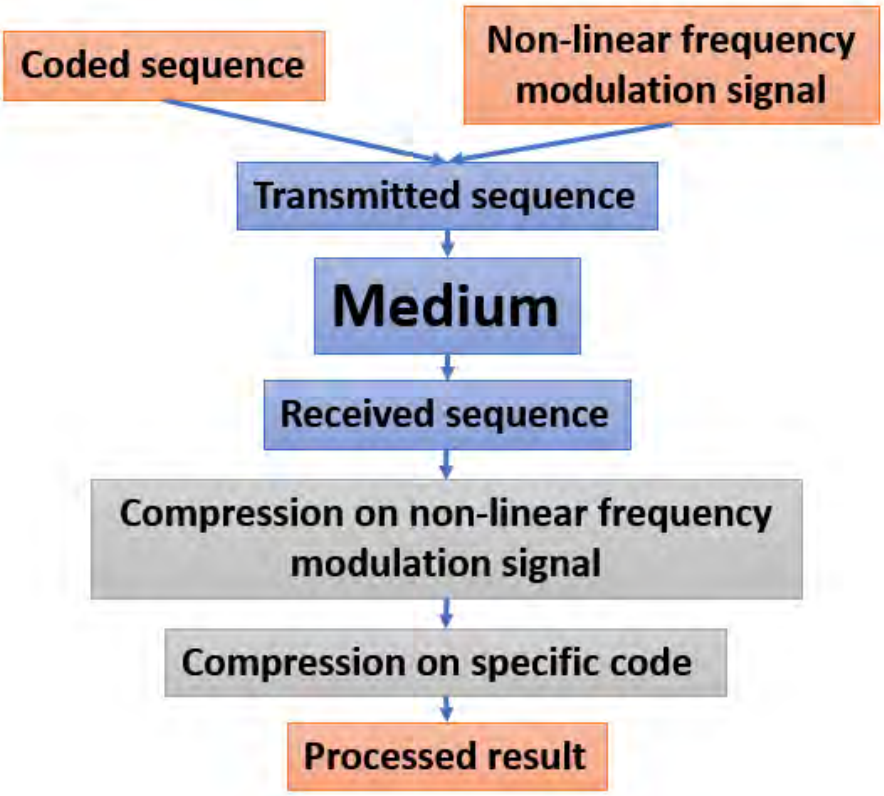

Figure 5.5: Generation and compression of NLFM-Barker code signal.

5.4 Theoretical analysis

The NLFM signal and hybrid method are generated by Zak transform. The theoretical study analyzed the performance of the NLFM signal by comparing the auto-correlation function of the NLFM signal.

The phase characteristic in radians of the synthesised NLFM signal is shown in Figure 5.7. The phase characteristic of the applied NLFM signal changes fast in the early stage, slow in the middle stage, and fast in the later stage. The ACF of both signals are shown in Figure 5.8. The frequency axis is normalized by the sampling frequency. It is easy to notice that the ACF side lobes level and their structure is much better in the case of the NLFM signal than in the case of the LFM signal, despite the main lobe broadening. The side lobe level suppression is achieved thanks to the main lobe duration broadening. It is measured at the maximum of the first side lobe level.

In order to evaluate the performance of the NLFM-Barker code, the theoretical study on axial resolution compared to other methods should be tested. The important indicator of axial resolution is the width of the compressed pulse. Figure 5.9 compared the compression results of 7-bit Barker code sequence, LFM, NLFM and NLFM-Barker code

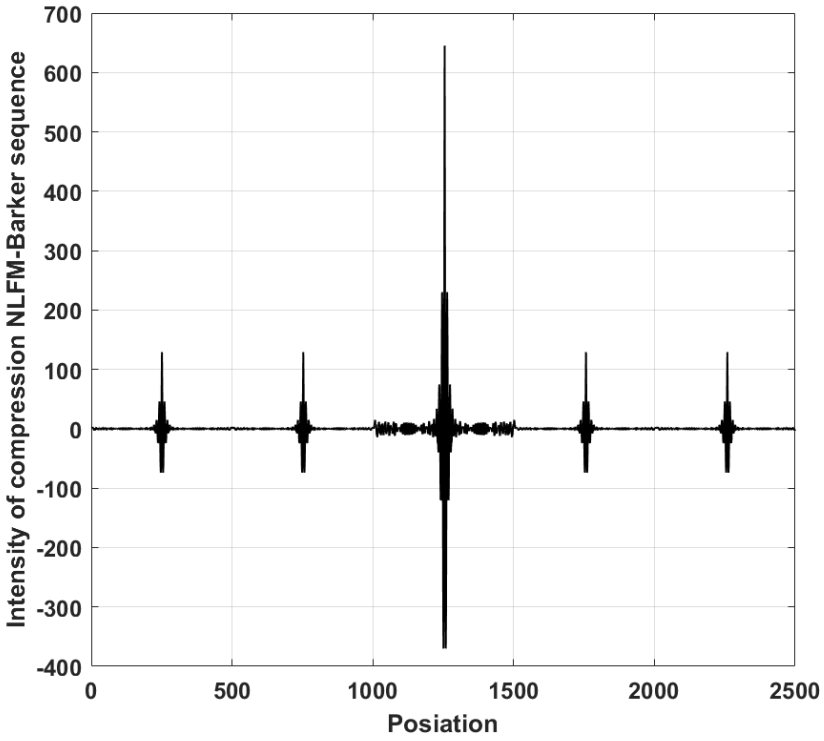

Figure 5.6: Echo signal of NLFM-Barker code after pulse compression.

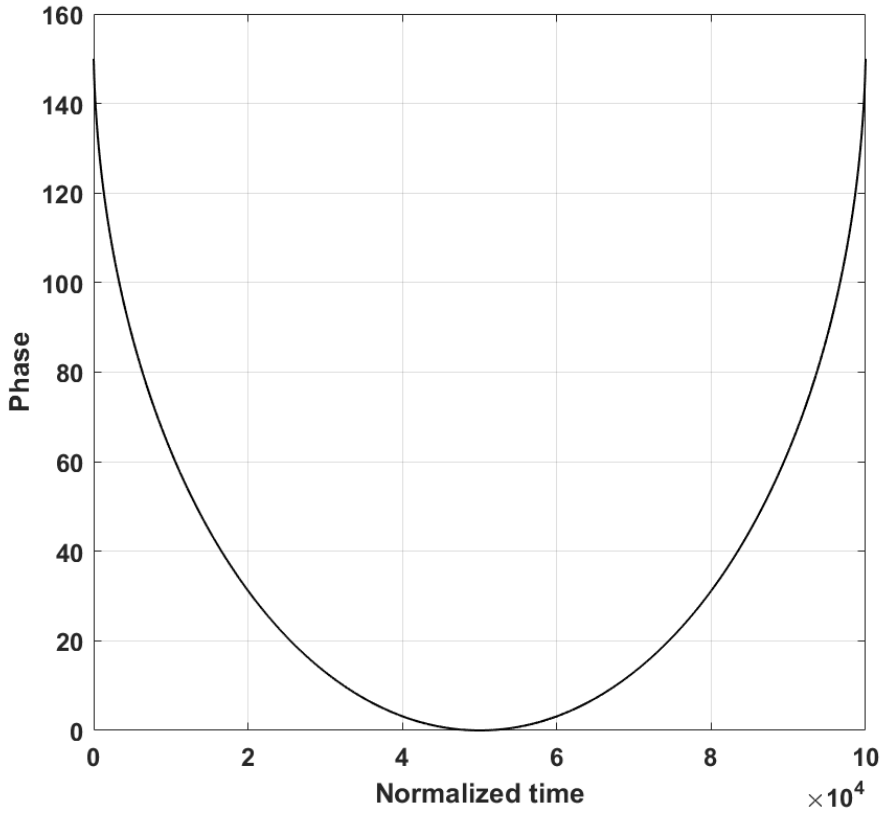

Figure 5.7: Phase characteristic of the NLFM signal.

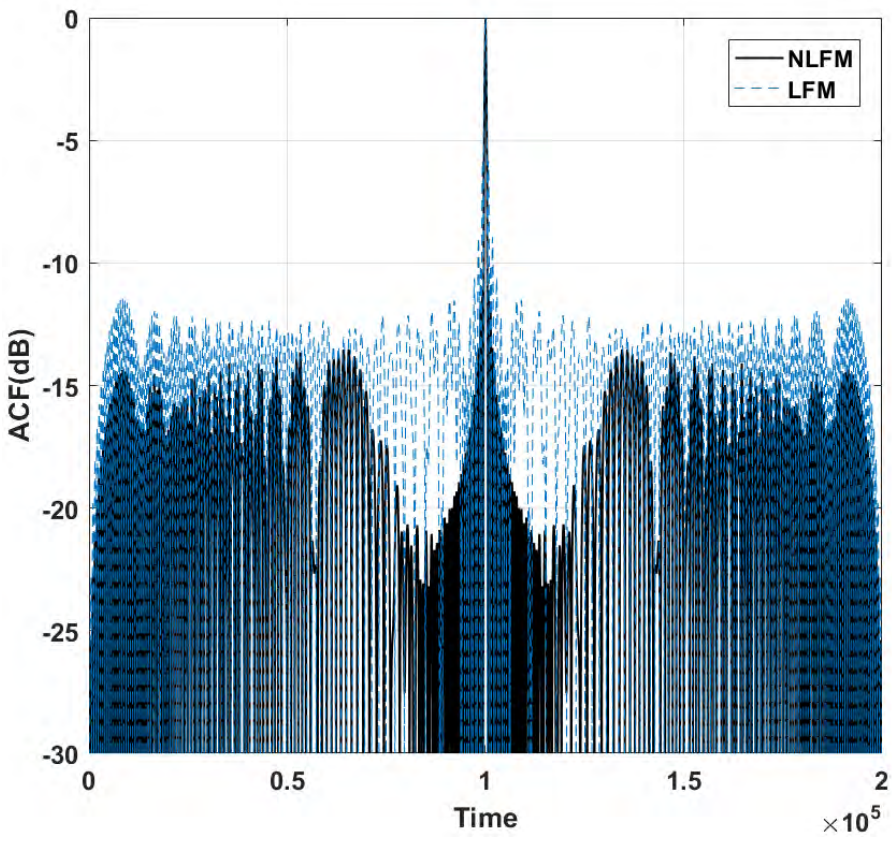

Figure 5.8: ACF of the NLFM and LFM signals.

sequence. The auto-correlation waveform of applied code method and other methods are normalized. The width of the main lobe is very narrow. Figure 5.10 shows the zoom in of the main lobe in Figure 5.9,which contains Barker code, LFM, NLFM and Barker NLFM. Due to the normalization, the main lobe amplitude of the NLFM-Barker code is the same as others, but the main lobe width of the correlation pattern has been reduced compared to other code methods.

As the main lobe width is very small, the sensitivity of discrimination is high. The nearby target in the range between the main lobe width can be easily distinguished. The sidelobe level of the NLFM-Barker sequence is the same as the Barker code sequence, but the sidelobe width of the applied method is much smaller than the Barker code sequence. Since the applied method has the property of reducing the width of the main lobe and side lobes, the axial resolution can be increased without using the window function and other methods. This method avoids the reduced SNR of echo signal. Due to this advantage, the NLFM-Barker code sequence is considered in the ultrasound imaging area. The BCG code has better performance than the Barker code, so it is also considered in the ultrasound imaging system.

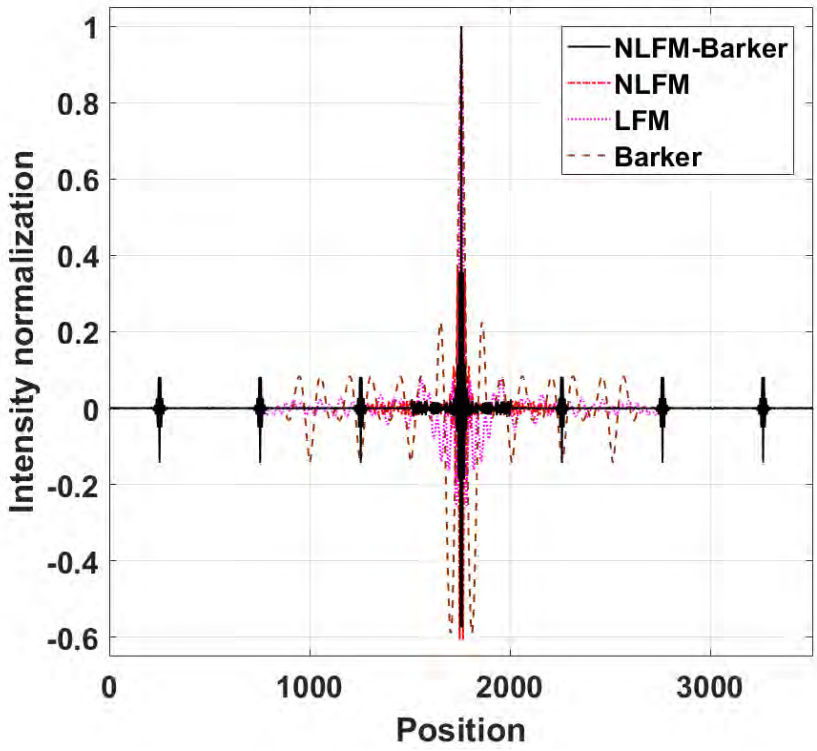

Figure 5.9: Auto-correlation function of 7-bit NLFM-Barker, NLFM, LFM and 7-bit Barker code sequence waveform.

5.5 Simulation

The theoretical study in section 5.4 indicated that the NLFM-Barker code has the best performance in axial resolution than other methods. This proposed method can be used in ultrasound imaging. The phantom simulations in MATLAB have been setup in this section by using the FIELD II toolbox. The linear array transducer has 192 elements which are 5 mm in height, 440 um in width and 5 mm in kerf. The transmit and receive focus are fixed. There are 50 scan lines in this simulation model. The center frequency of the transducer is 3.6 MHz and the sampling frequency is 100 MHz.

Figure 5.11 shows the scatterers used in the experiment. The cyst phantom, which consists of 10000 points, is designed in MATLAB. These points were randomly distributed with two $5 \times 5 \times 5$ mm cubes. Figure 5.12, Figure 5.13, Figure 5.13, Figure 5.14, Figure 5.15 and Figure 5.16 show the cyst phantom images obtained by simple pulse, LFM, NLFM, NLFM-Barker code sequence and NLFM-BCG code sequence.

In order to compare the performance of each method, contrast ratio (CR) and SNR are used intuitively to contrast the performance of the applied method and simple pulse. CR can be expressed as Equation 5.15.

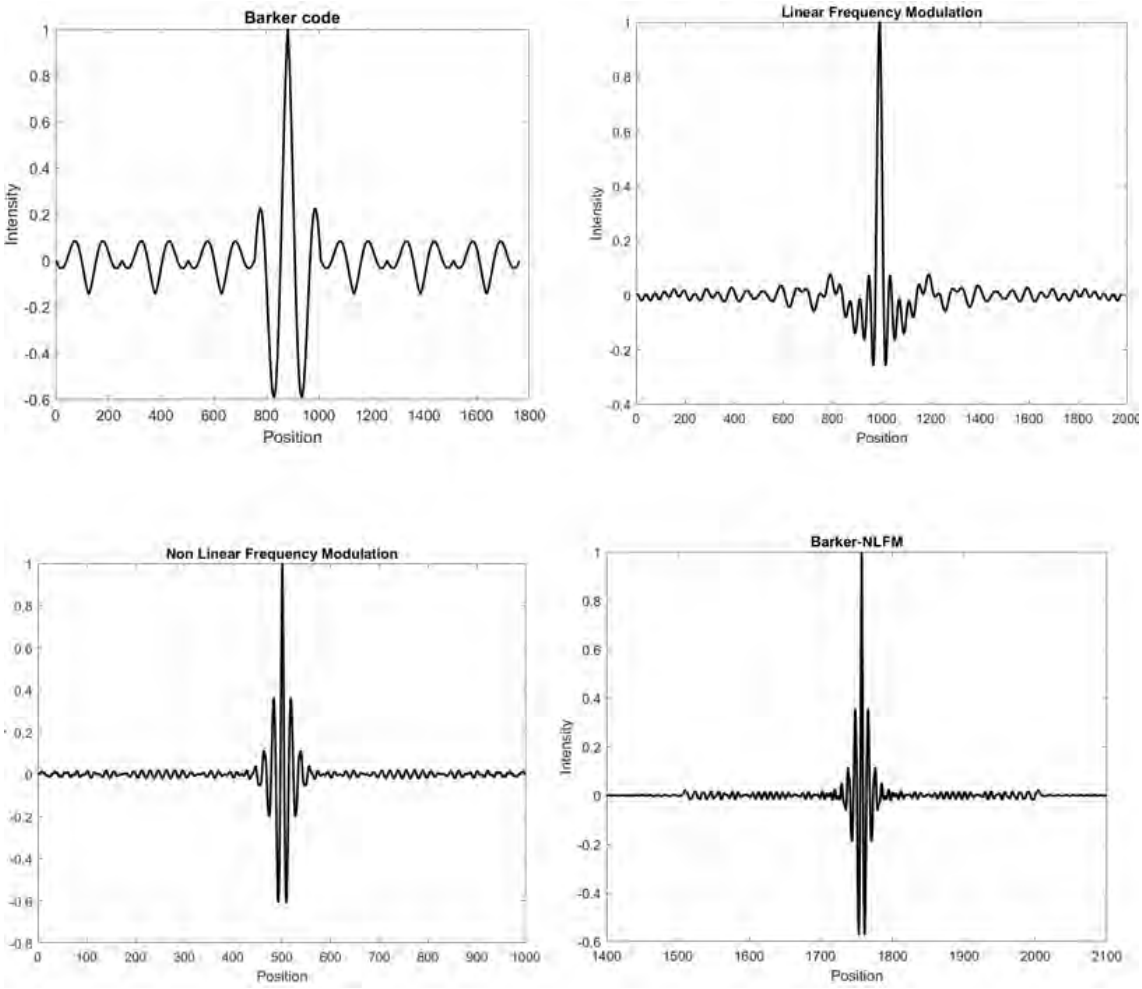

Figure 5.10: Zoom in of the main lobe and width of NLFM-Barker and other code methods.

$$CR = 20log_{10}\frac{\mu_{in}}{\mu_{out}} \tag{5.15}$$

Where μ_{in} is the mean intensity of the cyst inside and μ_{out} is the mean intensity of the cyst outside. Table 5.2 shows the contrast ratio of these methods.

The CR of NLFM-BCG method is 34.22 dB, which is higher than the simple pulse. The scan lines on the right of Figure 5.12, Figure 5.13, Figure 5.13, Figure 5.14, Figure 5.15 and Figure 5.16 show that the duration time of NLFM-BCG method is smaller than the simple pulse, that can increase the axial resolution of ultrasound imaging. The performance of NLFM-BCG sequence in cyst phantom simulation agreed with the results of theoretical studies. Figure 5.17 shows the SNR results of the different transmitted signals.

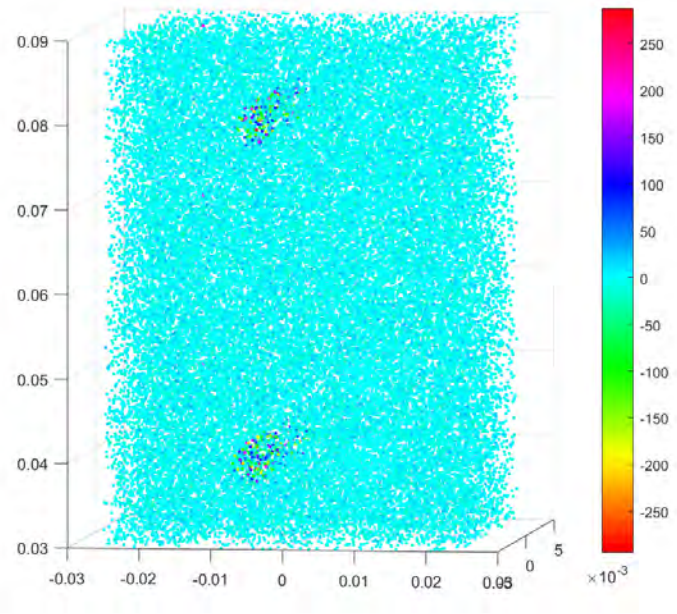

Figure 5.11: Simulation of scatterers used in the experiment.

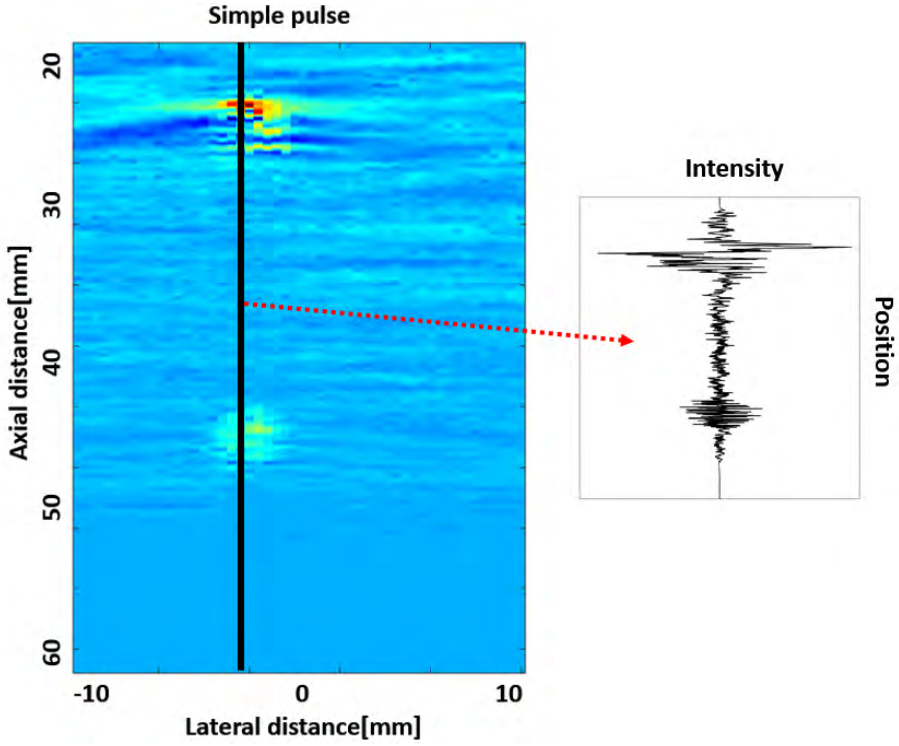

Figure 5.12: The simulated cyst phantom by using simple pulse and the scan line.

Due to the complicated of NLFM method, there are various NLFM-Barker code sequences. But the property of NLFM is the ability to reduce the width of the main lobe and side lobes. All the NLFM-Barker code sequences can increase the axial resolution more than other methods without losing SNR. Table 5.2 shows the CR results of different codes.

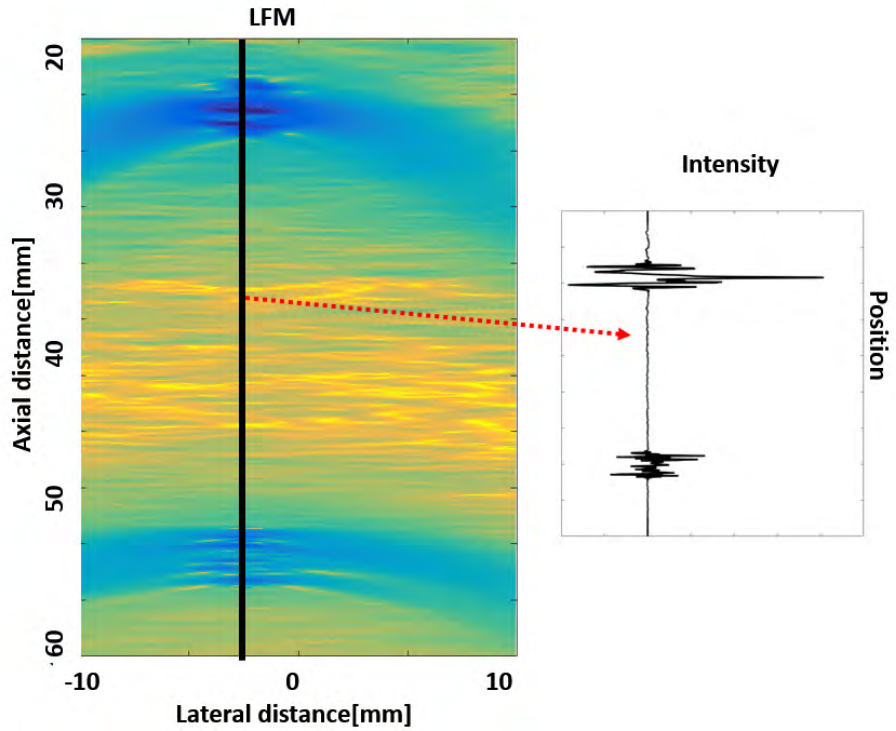

Figure 5.13: The simulated cyst phantom by using LFM code sequence and the scan line.

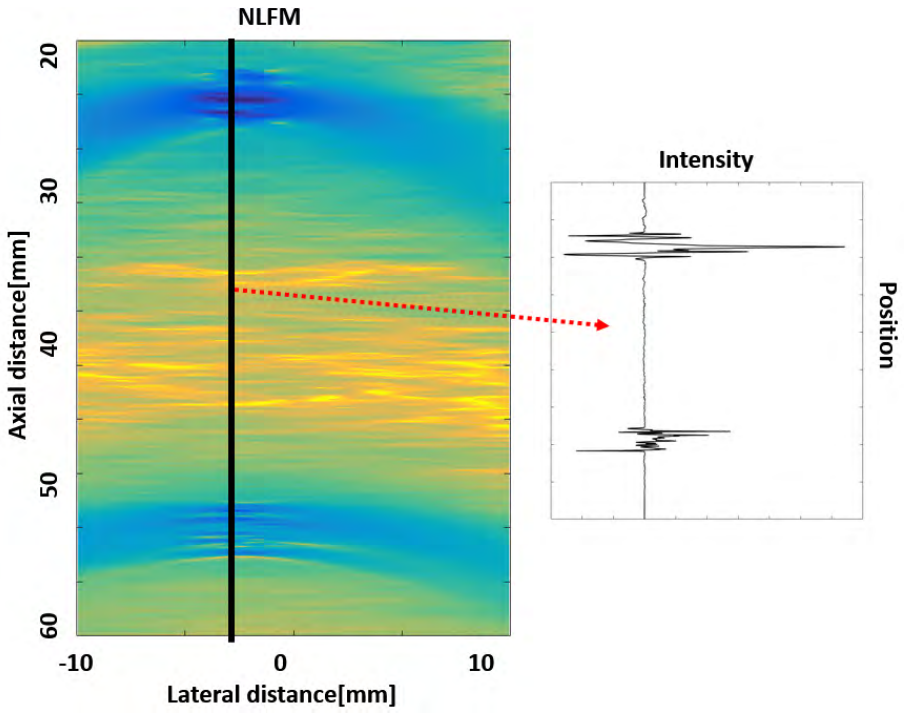

Figure 5.14: The simulated cyst phantom by using NFLM and the scan line.

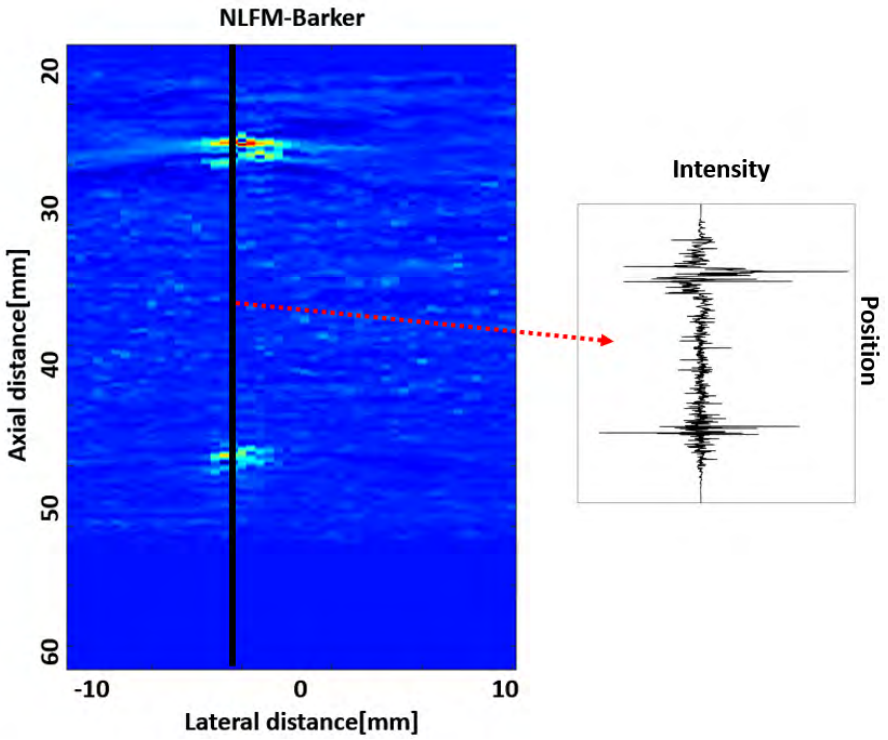

Figure 5.15: The simulated cyst phantom by using NLFM-Barker code sequence and the scan line.

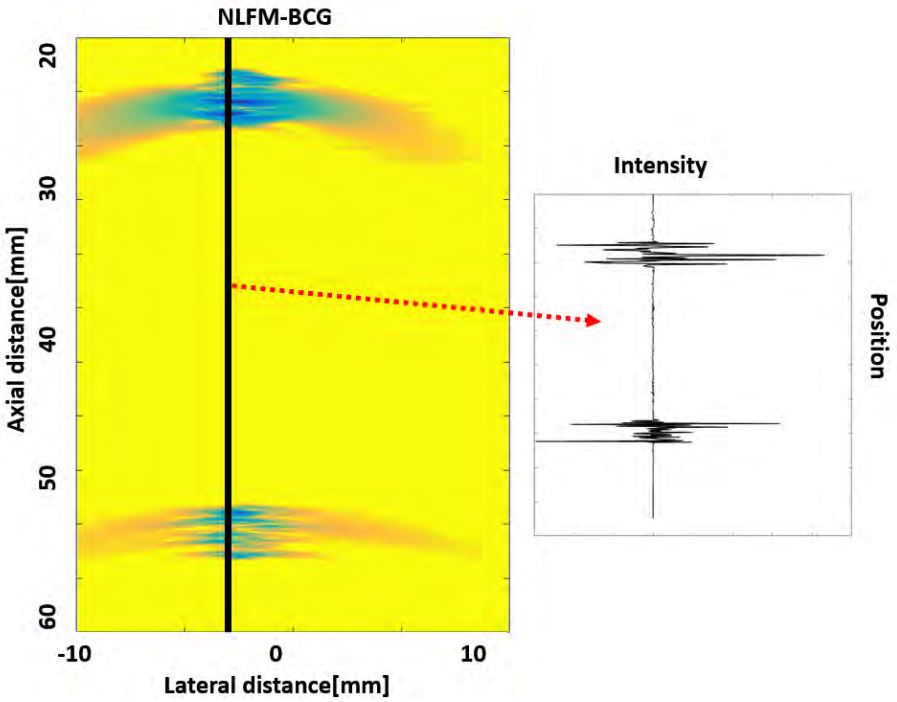

Figure 5.16: The simulated cyst phantom by using NLFM-BCG code sequence and the scan line.

Table 5.2: Contrast ratio of different codes

Code method	MI of inside cyst	MI of outside cyst	CR(dB)
Simple pulse	6.1	0.7	18.26
LFM	7.4	0.6	21.82
NLFM	8.8	0.7	21.98
NLFM-Barker 3	12.1	0.9	22.66
NLFM-Barker 5	18.3	1.2	23.7
NLFM-Barker 7	31.2	1.4	26.72
NLFM-Barker 11	97.2	3.5	28.6
NLFM-Barker 13	165.3	4.2	31.9
NLFM-Golay 4 pair	23.3	1.2	25.7
NLFM-Golay 8 pair	100.3	3.2	29.9
NLFM-BCG	**329.2**	**6.4**	**34.22**

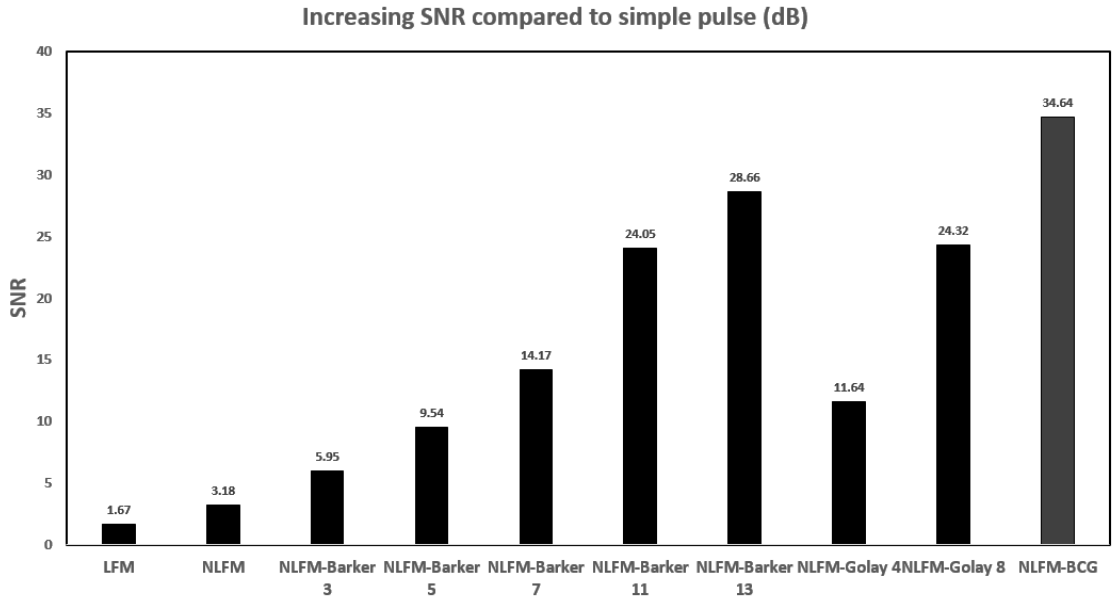

Figure 5.17: Increasing SNR results by using various code methods.

Figure 5.17 depicts the increasing SNR results of various transmitted signals compared to a simple pulse. The method of combining nonlinear frequency modulation and hybrid coded excitation performs better than other methods when comparing and analysing the imaging SNR of different excitation signals. This means that this technique has the potential to be used in clinical ultrasound. This technique is simple to use, low in cost, safe for the human body, and effective.

5.6 Summary

This chapter used the non-linear frequency modulated hybrid phase coded excitation signal as the excitation signal in the ultrasound imaging system. The signal resolution will be greatly improved after nonlinear frequency modulation, and the coded signal of coded excitation will have a very high SNR. The proposed method combines these two benefits. Theoretical analysis of this signal reveals that the proposed signal has unrivalled advantages in improving the SNR and CR when compared to other commonly used signals. The comparison in the theoretical study shows that the proposed method can reduce the width of the main lobe and side lobe without reducing the SNR of the echo signal. The proposed method was used in cyst phantom simulation. The experimental results show that the proposed method has a very high internal signal intensity. The CR of proposed signal is 15.96 dB higher than the sine wave, and its SNR is 36.64 dB higher than the sine wave's. This is a significant advancement in ultrasound imaging systems. The findings of this study will help to advance the clinical use of the ultrasound coded excitation technique.

Chapter 6

Conclusion and Future Works

6.1 Conclusion

This study looked into the possibility of using an ultrasound pulse compression technique to detect structural integrity in high frequency short range UT system, low frequency long range GWT system and ultrasound imaging system.

To transmit signals in the high-frequency UT system, various types of coded excitation methods are used. In the UT system, unlike other systems that use traditional methods, a novel hybrid pulse compression technique is applied and implemented. The Barker code method, the Golay code pair method, and the Barker code convolution Golay code pair method are the most studied. The proposed BCG method is obtained by convolving Barker code and Golay code pair that combine the advantages of the two coding methods. The hybrid codes share the same sidelobe as the baker code, and their main lobe is associated with one of the Barker code and Golay code pairs that are used. It combines the features of a high main lobe Barker code and no side lobe Golay code pair. There is no need to change the UT system's hardware to improve SNR by using this method. The proposed method has been theoretically analysed and then tested in extensive simulation experiments. The experimental results showed that the intensity of the code produced by the convolution of Barker code and Golay is much higher than the intensity of the simple pulse, and the PSL of the code is lower than the traditional Barker code, which is the same as the theoretical analysis results. This method can achieve an extremely high SNR. The B13G8 code produces the best results in the experiment, with a SNR of 38.5 dB higher than the sine wave. This method solves the shortcomings of poor or unusable detection results of ultrasonic equipment under low voltage conditions. UT device can be used in

low voltage situations for a variety of applications by using the proposed method.

The GWT system is subjected to a novel coded excitation method that combines phase coded excitation. For long-range distance testing, accurate positioning of results and defects is very important. The goal of this method is to reduce noise in order to increase the SNR of the echo signal. The theoretical analysis proved the feasibility and superiority of the proposed hybrid method. The hybrid code excitation method can get a very narrow main lobe width and a very high main lobe intensity after matched filtering processing to obtain a very high resolution. The laboratory pipeline test results show that the proposed coded signal outperforms other methods in the torsional wave mode T(0,1) at different frequencies. When using the same transmission signal, the SNR improvement of different frequencies varies slightly. The system has the best improved SNR and PSL in this study when using a frequency of 40 kHz. The BCG code outperformed all others in laboratory tests. The BCG code's SNR was increased to 33.5 dB at 40kHz, and the PSL was -28.5 dB. The traditional method and the proposed method are used in the defect detection field testing. By comparing testing results, the proposed method can clearly detect the defect signal, whereas the defect signal of other methods is not obvious. The defect signal of the proposed method is 6 dB higher than the SNR of the Barker code. The performance of BCG code is significantly better than that of traditional coded excitation without changing the code length. The proposed method can improve the GWT system's signal-to-noise ratio and thus its accuracy.

Theoretical research and verification in FIELD II simulation were used to carry out ultrasound imaging testing experiments. The SNR and resolution indicators are very critical for ultrasound imaging systems. In an ultrasound imaging system, a nonlinear frequency modulated hybrid phase modulated signal is used as an excitation signal. The comparison in the theoretical study shows that the proposed method can reduce the width of the main lobe and side lobe without reducing the SNR of the echo signal. In cyst phantom simulation, the applied method was used. Because of the signal's properties, the axial resolution and CR have significantly improved over other code methods. The proposed signal's CR is 15.96 dB higher than the sine wave's, and its SNR is 36.64 dB higher. The applied signal performs well in terms of increasing axial resolution. This represents a significant step forward in ultrasound imaging systems.

In summary, theoretical analysis and experimental results show that the novel hybrid pulse compression method can significantly improve the system's SNR and resolution. Through theory, simulation, and experiments, it is found that the longer the code applied in the process of using the proposed method, the higher the improved SNR. The proposed method fills the gap in the code length of the traditional coding excitation method, and can apply

codes of various lengths more flexibly in the process of using the method. This method only requires changing the transmitted signal without changing the ultrasound system hardware. This method can be used for a variety of ultrasound applications in a more convenient, cost-effective, and efficient manner. It is precisely because of the superior performance of the proposed method that it can be applied to most ultrasound systems to improve their performance, especially in future portable devices. The proposed method can be used not only in ultrasonic detection equipment but also in applications like mechanical waves and light.

6.2 Future works

Future works could be done from the following aspects to improve the performance of ultrasound applications.

The UT system tests performed in the current study are in Matlab Field II simulation, but there will be other factors as a result of impression echo in the actual test. More practical tests will be required to analyse and evaluate this method's ability to improve SNR. The proposed technology can be combined with commercial UT equipment to improve the efficiency and accuracy of the equipment.

The guided wave experiment demonstrated the feasibility of the proposed method in the system. However, only the pipeline's outer wall defect test was carried out during the actual inspection process. This method's dependability can be demonstrated using a broader range of defects. This method can theoretically be applied to low-voltage guided wave equipment, but more experiments are needed to confirm the feasibility.

The benefits of the proposed method are only verified in simulation in the ultrasound imaging system. The proposed method can be combined with existing ultrasound imaging machines to perform more actual measurements, resulting in better test results. Portable ultrasound imaging equipment is lightweight and requires little power. Portable ultrasound imaging equipment is still in its early stages, and its stability and imaging quality are unsatisfactory. As a result, the proposed method can be used to improve the performance of these devices.

Bibliography

[1] NTS Board. Columbia gas transmission corporation pipeline rupture, 2014.

[2] Shiwei Liu, Yanhua Sun, Min Gu, Changde Liu, Lingsong He, and Yihua Kang. Review and analysis of three representative electromagnetic NDT methods. *Insight-Non-Destructive Testing and Condition Monitoring*, 59(4):176–183, 2017.

[3] Samuel Chukwuemeka Olisa, Muhammad A Khan, and Andrew Starr. Review of current guided wave ultrasonic testing (gwut) limitations and future directions. *Sensors*, 21(3):811, 2021.

[4] Daniel A Kiefer, Michael Fink, and Stefan J Rupitsch. Simultaneous ultrasonic measurement of thickness and speed of sound in elastic plates using coded excitation signals. *IEEE transactions on ultrasonics, ferroelectrics, and frequency control*, 64(11):1744–1757, 2017.

[5] Peter W Tse and Xiao Juan Wang. Semi-quantitative analysis of defect in pipelines through the use of technique of ultrasonic guided waves. In *Key Engineering Materials*, volume 413, pages 109–116. Trans Tech Publ, 2009.

[6] Prawin Kumar Sharan, S Sheethal, Sri Krishna Chaitanya, and Hari Kishore Maddi. Long range ultrasonic testing-case studies.

[7] Jonathan M Cannata, Jay A Williams, Qifa Zhou, Timothy A Ritter, and K Kirk Shung. Development of a 35-mhz piezo-composite ultrasound array for medical imaging. *IEEE transactions on ultrasonics, ferroelectrics, and frequency control*, 53(1):224–236, 2006.

[8] Xiaohua Jian, Zhile Han, Pengbo Liu, Jie Xu, Zhangjian Li, Peiyang Li, Weiwei Shao, and Yaoyao Cui. A high frequency geometric focusing transducer based on 1-3 piezocomposite for intravascular ultrasound imaging. *BioMed research international*, 2017, 2017.

[9] Kevin L Rens, Terry J Wipf, and F Wayne Klaiber. Review of nondestructive evaluation techniques of civil infrastructure. *Journal of performance of constructed facilities*, 11(4):152–160, 1997.

[10] Louis Cartz. Nondestructive testing. 1995.

[11] ZD Wang, Y Gu, and YS Wang. A review of three magnetic ndt technologies. *Journal of Magnetism and Magnetic Materials*, 324(4):382–388, 2012.

[12] Misac N Nabighian, VJS Grauch, RO Hansen, TR LaFehr, Y Li, Jonathan W Peirce, Jeffrey D Phillips, and ME Ruder. The historical development of the magnetic method in exploration. *Geophysics*, 70(6):33ND–61ND, 2005.

[13] JB Nestleroth. Circumferential mfl in-line inspection for cracks in pipelines. Technical report, Battelle Memorial Institute (US), 2003.

[14] Robin James, Mohammad Faisal Haider, Victor Giurgiutiu, and David Lilienthal. A simulative and experimental approach toward eddy current nondestructive evaluation of manufacturing flaws and operational damage in cfrp composites. *Journal of Nondestructive Evaluation, Diagnostics and Prognostics of Engineering Systems*, 3(1):5, 2020.

[15] Damhuji Rifai, Ahmed N Abdalla, Ramdan Razali, Kharudin Ali, and Moneer A Faraj. An eddy current testing platform system for pipe defect inspection based on an optimized eddy current technique probe design. *Sensors*, 17(3):579, 2017.

[16] Peipei Zhu, Yuhua Cheng, Portia Banerjee, Antonello Tamburrino, and Yiming Deng. A novel machine learning model for eddy current testing with uncertainty. *NDT & E International*, 101:104–112, 2019.

[17] SF Dmitriev, VN Malikov, AM Sagalakov, and LI Shevtsova. Flaw inspection of welded joints in titanium alloys by the eddy current method. *Welding International*, 31(8):608–611, 2017.

[18] Chunyan Xiao and Yanhua Zhang. A method of magnetic scanning imaging for detecting defects in ferromagnetic materials. *Measurement Science and Technology*, 22(2):025503, 2011.

[19] Junbiao Fei, Xianzhang Zuo, Yunze He, Guiyun Tian, and Tao Zhang. The extraction of characteristic quantity of shallow defects in pulsed magnetic flux leakage signal. In *The 17th International Conference on Automation and Computing*, pages 225–229. IEEE, 2011.

[20] M Ricci, A Ficola, ML Fravolini, L Battaglini, V Brunori, A Palazzi, M Pastorelli, P Burrascano, P Valigi, and L Appolloni. Machine vision and magnetic imaging NDT for the on-line inspection of stainless steel strips. In *2012 IEEE International Conference on Imaging Systems and Techniques Proceedings*, pages 415–420. IEEE, 2012.

[21] Chai Xiuli, Lu Yang, Gan Zhihua, and Zhao Jianjun. Structure and character analysis of a new type of steel wire rope non-destructive testing detector apparatus. In *2009 International Conference on Mechatronics and Automation*, pages 4095–4099. IEEE, 2009.

[22] S Evanson, RJP Bain, GB Donaldson, G Stirling, and G Hayward. A comparison of the performance of planar and conventional second-order gradiometers coupled to a squid for the NDT of steel plates. *IEEE Transactions on Magnetics*, 25(2):1200–1203, 1989.

[23] Muhammad Ahsan Pasha and Tariq Mairaj Khan. A pipeline inspection gauge based on low cost magnetic flux leakage sensing magnetometers for non-destructive testing of pipelines. In *2016 International Conference on Emerging Technologies (ICET)*, pages 1–5. IEEE, 2016.

[24] Chandra S Angani, Helena G Ramos, Tiago J Rocha, and Artur L Ribeiro. Svm classification of thickness and lift-off using transient eddy current oscillation method. In *2016 IEEE International Instrumentation and Measurement Technology Conference Proceedings*, pages 1–6. IEEE, 2016.

[25] Tiezhu Qiao. A study of steel cord belt magnetic memory testing system. In *2009 ISECS International Colloquium on Computing, Communication, Control, and Management*, volume 2, pages 564–566. IEEE, 2009.

[26] Yong-Kai Zhu, Gui-Yun Tian, Rong-Sheng Lu, and Hong Zhang. A review of optical NDT technologies. *Sensors*, 11(8):7773–7798, 2011.

[27] Y Tian, K Shimazoe, X Yan, O Ueda, T Ishikura, T Fujiwara, M Uesaka, M Ohno, H Tomita, and Y Yoshihara. High energy x-ray photon counting imaging using linear accelerator and silicon strip detectors. *Nuclear Instruments and Methods in Physics Research Section A: Accelerators, Spectrometers, Detectors and Associated Equipment*, 830:251–255, 2016.

[28] Joris Degrieck, Wim De Waele, and Patricia Verleysen. Monitoring of fibre reinforced composites with embedded optical fibre bragg sensors, with application to filament wound pressure vessels. *NDT & E International*, 34(4):289–296, 2001.

[29] Yanhua Peng, Guixiong Liu, Yanming Quan, and Qilin Zeng. The depth measurement of internal defect based on laser speckle shearing interference. *Optics & Laser Technology*, 92:69–73, 2017.

[30] Terumi Inagaki, Toshimitsu Ishii, and Toshikatsu Iwamoto. On the NDT and E for the diagnosis of defects using infrared thermography. *NDT & E International*, 32(5):247–257, 1999.

[31] Sanjeevareddy Kolkoori, Norma Wrobel, Uwe Zscherpel, and Uwe Ewert. A new x-ray backscatter imaging technique for non-destructive testing of aerospace materials. *NDT & E International*, 70:41–52, 2015.

[32] HM Cho, HS Cho, KS Kim, HW Lim, SY Park, SR Lee, KC Kim, UK Je, YO Park, and DK Hong. Experimental study on the application of a compressed-sensing (cs)-based deblurring method in x-ray nondestructive testing and its image performance. *NDT & E International*, 75:1–7, 2015.

[33] Paul A Rometsch, Daniele Pelliccia, Dacian Tomus, and Xinhua Wu. Evaluation of polychromatic x-ray radiography defect detection limits in a sample fabricated from hastelloy x by selective laser melting. *NDT & E International*, 62:184–192, 2014.

[34] Anton du Plessis, Stephan Gerhard le Roux, and Anina Guelpa. Comparison of medical and industrial x-ray computed tomography for non-destructive testing. *Case Studies in Nondestructive Testing and Evaluation*, 6:17–25, 2016.

[35] Lewis Fry Richardson. Apparatus for warning a ship of its approach to large objects in a fog. *British Patent*, 9423, 1912.

[36] Paul G Newman and Grace S Rozycki. The history of ultrasound. *Surgical clinics of north America*, 78(2):179–195, 1998.

[37] S Sokoloff. Ultrasonic oscillations and their application. *Techn Physics (USSR)*, 2:522–544, 1935.

[38] Mark R Jolly, Arun Prabhakar, Bogdan Sturzu, K Hollstein, Rajendra Singh, S Thomas, Peter Foote, and Andy Shaw. Review of non-destructive testing (NDT) techniques and their applicability to thick walled composites. *Procedia CIRP*, 38:129–136, 2015.

[39] Sivaram N Ramadas, Joseph C Jackson, Jerzy Dziewierz, Richard O'Leary, and Anthony Gachagan. Application of conformal map theory for design of 2-D ultrasonic array structure for NDT imaging application: A feasibility study. *IEEE*

transactions on ultrasonics, ferroelectrics, and frequency control, 61(3):496–504, 2014.

[40] Wei-can Guo, Jian-feng Shi, and Dong-sheng Hou. Research on phased array ultrasonic technique for testing butt fusion joint in polyethylene pipe. In *2016 IEEE Far East NDT New Technology & Application Forum (FENDT)*, pages 1–5. IEEE, 2016.

[41] Sylvie Legendre, Daniel Massicotte, Jacques Goyette, and Tapan K Bose. Neural classification of lamb wave ultrasonic weld testing signals using wavelet coefficients. *IEEE Transactions on Instrumentation and Measurement*, 50(3):672–678, 2001.

[42] Nasim Moallemi and Shahram Shahbazpanahi. A distributed reflector localization approach to ultrasonic array imaging in non-destructive testing applications. *IEEE transactions on signal processing*, 62(15):3863–3873, 2014.

[43] Marco Ricci, Luca Senni, and Pietro Burrascano. Exploiting pseudorandom sequences to enhance noise immunity for air-coupled ultrasonic nondestructive testing. *IEEE Transactions on Instrumentation and Measurement*, 61(11):2905–2915, 2012.

[44] Jorge Camacho, Jorge F Cruza, Jose Brizuela, and Carlos Fritsch. Automatic dynamic depth focusing for NDT. *IEEE Transactions on Ultrasonics, Ferroelectrics, and Frequency Control*, 61(4):673–684, 2014.

[45] Honggang Li and Zhenggan Zhou. Application of p4 polyphase codes pulse compression method to air-coupled ultrasonic testing systems. *Ultrasonics*, 78:57–69, 2017.

[46] Dominik Flore, Konrad Wegener, Herwig Mayer, Ulrike Karr, and Claus C Oetting. Investigation of the high and very high cycle fatigue behaviour of continuous fibre reinforced plastics by conventional and ultrasonic fatigue testing. *Composites Science and Technology*, 141:130–136, 2017.

[47] A Cavuto, M Martarelli, G Pandarese, GM Revel, and EP Tomasini. Experimental investigation by laser ultrasonics for high speed train axle diagnostics. *Ultrasonics*, 55:48–57, 2015.

[48] HG Tattersall. The ultrasonic pulse-echo technique as applied to adhesion testing. *Journal of Physics D: Applied Physics*, 6(7):819, 1973.

[49] OR Gericke. Determination of the geometry of hidden defects by ultrasonic pulse analysis testing. *The Journal of the Acoustical Society of America*, 35(3):364–368, 1963.

[50] Adnan Aydin. Upgraded isrm suggested method for determining sound velocity by ultrasonic pulse transmission technique. *Rock mechanics and rock engineering*, 47(1):255–259, 2014.

[51] Shyamal Mondal and T Sattar. An overview tofd method and its mathematical model. *NDT. net*, 5(4), 2000.

[52] A Hecht. Time of flight diffraction technique (tofd)–an ultrasonic testing a method for all applications. *NDT Journal*, 2(9), 1997.

[53] P Wilcox, M Evans, B Pavlakovic, D Alleyne, K Vine, P Cawley, and M Lowe. Guided wave testing of rail. *Insight-Non-Destructive Testing and Condition Monitoring*, 45(6):413–420, 2003.

[54] Philip W Loveday, Craig S Long, and Dineo A Ramatlo. Ultrasonic guided wave monitoring of an operational rail track. *Structural Health Monitoring*, 19(6):1666–1684, 2020.

[55] Salisu El-Hussein, John J Harrigan, and Andrew Starkey. Long range guided waves for detecting holes in pipelines. *Journal of Structural Integrity and Maintenance*, 5(2):113–126, 2020.

[56] Premesh Shehan Lowe, Habiba Lais, Veena Paruchuri, and Tat-Hean Gan. Application of ultrasonic guided waves for inspection of high density polyethylene pipe systems. *Sensors*, 20(11):3184, 2020.

[57] Xudong Niu, W Duan, Hua-Peng Chen, and HR Marques. Excitation and propagation of torsional T (0, 1) mode for guided wave testing of pipeline integrity. *Measurement*, 131:341–348, 2019.

[58] Paul Fromme, Paul D Wilcox, Michael JS Lowe, and Peter Cawley. On the development and testing of a guided ultrasonic wave array for structural integrity monitoring. *IEEE transactions on ultrasonics, ferroelectrics, and frequency control*, 53(4):777–785, 2006.

[59] Eli Leinov, Michael JS Lowe, and Peter Cawley. Investigation of guided wave propagation and attenuation in pipe buried in sand. *Journal of Sound and Vibration*, 347:96–114, 2015.

[60] Renaldas Raišutis, Rymantas Kažys, Liudas Mažeika, Egidijus Žukauskas, Vykintas Samaitis, and Audrius Jankauskas. Ultrasonic guided wave-based testing technique for inspection of multi-wire rope structures. *NDT & E International*, 62:40–49, 2014.

[61] Thomas Clarke, Peter Cawley, Paul David Wilcox, and Anthony John Croxford. Evaluation of the damage detection capability of a sparse-array guided-wave shm system applied to a complex structure under varying thermal conditions. *IEEE transactions on ultrasonics, ferroelectrics, and frequency control*, 56(12):2666–2678, 2009.

[62] Howard Matt, Ivan Bartoli, and Francesco Lanza di Scalea. Ultrasonic guided wave monitoring of composite wing skin-to-spar bonded joints in aerospace structures. *The journal of the acoustical society of america*, 118(4):2240–2252, 2005.

[63] DN Alleyne, T Vogt, and P Cawley. The choice of torsional or longitudinal excitation in guided wave pipe inspection. *Insight-Non-Destructive Testing and Condition Monitoring*, 51(7):373–377, 2009.

[64] Houman Nakhli Mahal, Kai Yang, and Asoke K Nandi. Detection of defects using spatial variances of guided-wave modes in testing of pipes. *Applied Sciences*, 8(12):2378, 2018.

[65] Mehmet K Yücel, Sina Fateri, Mathew Legg, Adam Wilkinson, Vassilios Kappatos, Cem Selcuk, and Tat-Hean Gan. Coded waveform excitation for high-resolution ultrasonic guided wave response. *IEEE Transactions on Industrial Informatics*, 12(1):257–266, 2015.

[66] Hossein Taheri, Jikai Du, and Fereidoon Delfanian. Experimental observation of phased array guided wave application in composite materials. *Materials Evaluation*, 75(10):1308–1316, 2017.

[67] Vincent Chan and Anahi Perlas. Basics of ultrasound imaging. In *Atlas of ultrasound-guided procedures in interventional pain management*, pages 13–19. Springer, 2011.

[68] Kirsten Christensen-Jeffries, Olivier Couture, Paul A Dayton, Yonina C Eldar, Kullervo Hynynen, Fabian Kiessling, Meaghan O'Reilly, Gianmarco F Pinton, Georg Schmitz, and Meng-Xing Tang. Super-resolution ultrasound imaging. *Ultrasound in medicine & biology*, 46(4):865–891, 2020.

[69] Libertario Demi, Marcello Demi, Renato Prediletto, and Gino Soldati. Real-time multi-frequency ultrasound imaging for quantitative lung ultrasound–first clinical results. *The Journal of the Acoustical Society of America*, 148(2):998–1006, 2020.

[70] Haowei Tai, Mawia Khairalseed, and Kenneth Hoyt. Adaptive attenuation correction during h-scan ultrasound imaging using k-means clustering. *Ultrasonics*, 102:105987, 2020.

[71] Shujaat Khan, Jaeyoung Huh, and Jong Chul Ye. Deep learning-based universal beamformer for ultrasound imaging. In *International Conference on Medical Image Computing and Computer-Assisted Intervention*, pages 619–627. Springer, 2019.

[72] Johannes F De Boer, Barry Cense, B Hyle Park, Mark C Pierce, Guillermo J Tearney, and Brett E Bouma. Improved signal-to-noise ratio in spectral-domain compared with time-domain optical coherence tomography. *Optics letters*, 28(21):2067–2069, 2003.

[73] MJ Firbank, A Coulthard, RM Harrison, and ED Williams. A comparison of two methods for measuring the signal to noise ratio on mr images. *Physics in Medicine & Biology*, 44(12):N261, 1999.

[74] Xiaolan Yan, Donglai Zhang, and Fei Zhao. Improve the signal to noise ratio and installation convenience of the inductive coil for wire rope nondestructive testing. *NDT & E International*, 92:221–227, 2017.

[75] Yu Bilik, M Haridim, and D Bilik. Application of NDT methods to improve the detection of underground linear objects. *NDT & E International*, 91:129–138, 2017.

[76] Kumar Anubhav Tiwari, Renaldas Raisutis, and Vykintas Samaitis. Signal processing methods to improve the signal-to-noise ratio (snr) in ultrasonic non-destructive testing of wind turbine blade. *Procedia Structural Integrity*, 5:1184–1191, 2017.

[77] A Bernieri, L Ferrigno, M Laracca, A Rasile, and M Ricci. Ultrasonic NDT on aluminum bars: An experimental performance comparison of excitation and processing techniques. *Measurement*, 128:393–402, 2018.

[78] Nadav Levanon and Eli Mozeson. *Radar signals*. John Wiley & Sons, 2004.

[79] Bahman Lashkari, Kaicheng Zhang, Edem Dovlo, and Andreas Mandelis. Coded excitation waveform engineering for high frame rate synthetic aperture ultrasound imaging. *Ultrasonics*, 77:121–132, 2017.

[80] Che-Chou Shen, Jun-Kai Peng, Chi Wu, and Chia-Yuan Liu. Orthogonal golay excitation for range side lobe elimination in dual-frequency harmonic imaging. *Biomedical Signal Processing and Control*, 18:386–393, 2015.

[81] Che-Chou Shen and Tai-Yu Shi. Third harmonic transmit phasing for snr improvement in tissue harmonic imaging with golay-encoded excitation. *Ultrasonics*, 51(5):554–560, 2011.

[82] Zhenggan Zhou, Baoquan Ma, Jingtao Jiang, Guang Yu, Kui Liu, Dongmei Zhang, and Weiping Liu. Application of wavelet filtering and barker-coded pulse compression hybrid method to air-coupled ultrasonic testing. *Nondestructive Testing and Evaluation*, 29(4):297–314, 2014.

[83] Pilsu Kim, Eunji Jung, Sua Bae, Kangsik Kim, and Tai-kyong Song. Barker-sequence-modulated golay coded excitation technique for ultrasound imaging. pages 1–4, 2016.

[84] Julio Isla and Frederic Cegla. Coded excitation for pulse-echo systems. *IEEE transactions on ultrasonics, ferroelectrics, and frequency control*, 64(4):736–748, 2017.

[85] Sheng Zhou, Xiaochun Wang, Jianjun Ji, and Yanqun Wang. Ophthalmological ultrasound biometer using Golay-coded pulse excitation. In *2014 7th International Conference on Biomedical Engineering and Informatics*, pages 76–80. IEEE, 2014.

[86] Jose R Sanchez, Emma Keating, Sam Muir, Jacob Sandlund, and James Irwin. An fpga-based coded excitation system for ultrasonic imaging using a second-order, one-bit sigma-delta modulator. In *IEEE International Conference on Electro-Information Technology, EIT 2013*, pages 1–6. IEEE, 2013.

[87] Almog Lahav, Yuval Ben-Shalom, Tanya Chernyakova, and Yonina C Eldar. Coded excitation ultrasound: Efficient implementation via frequency domain processing. In *2016 IEEE International Conference on Acoustics, Speech and Signal Processing (ICASSP)*, pages 674–678. IEEE, 2016.

[88] Juan Fu, Gang Wei, Qinghua Huang, Fei Ji, and Yizhi Feng. Barker coded excitation with linear frequency modulated carrier for ultrasonic imaging. *Biomedical Signal Processing and Control*, 13:306–312, 2014.

[89] Feifei Zhao, Ling Tong, Qiong He, and Jianwen Luo. Coded excitation for diverging wave cardiac imaging: A feasibility study. *Physics in Medicine & Biology*, 62(4):1565, 2017.

[90] Hu Peng, XueMei Han, and Jianyu Lu. Study on application of complementary golay code into high frame rate ultrasonic imaging system. *Ultrasonics*, 44:e93–e96, 2006.

[91] Hui Peng and Juhong Tie. Ultrasound elasticity imaging using golay code. In *BIO Web of Conferences*, volume 8, page 03017. EDP Sciences, 2017.

[92] Zhiping Zhang, Michael J Nowak, Michael Wicks, and Zhiqiang Wu. Bio-inspired rf steganography via linear chirp radar signals. *IEEE Communications Magazine*, 54(6):82–86, 2016.

[93] Philippe Lasaygues, Andrés Arciniegas, and Loïc Brancheriau. Use of a chirp-coded excitation method in order to improve geometrical and acoustical measurements in wood specimen. *Physics Procedia*, 70:348–351, 2015.

[94] Hui Peng and Dong C Liu. Enhanced ultrasound strain imaging using chirp-coded pulse excitation. *Biomedical Signal Processing and Control*, 8(2):130–141, 2013.

[95] Changhan Yoon, Wooyoul Lee, Jae Hee Song, Jin Ho Chang, Tai-kyong Song, and Yangmo Yoo. New baseband pulse compression for chirp coded excitation. In *2013 IEEE International Ultrasonics Symposium (IUS)*, pages 906–909. IEEE, 2013.

[96] AI Meriläinen, V Kananen, C Fridlund, J Eskelinen, E Hæggström, and K Raum. GHz ultrasonics with arbitrary code excitation. In *2013 IEEE International Ultrasonics Symposium (IUS)*, pages 703–706. IEEE, 2013.

[97] Tahereh Kahookar Toosi and Hamid Behnam. Combined pulse compression and adaptive beamforming in coded excitation ultrasound medical imaging. In *2009 International Conference on Signal Processing Systems*, pages 210–214. IEEE, 2009.

[98] Jonathan Mamou and Jeffrey A Ketterling. Coded excitation and annular arrays for high-frequency ultrasound imaging. In *2006 International Conference of the IEEE Engineering in Medicine and Biology Society*, pages 2408–2411. IEEE, 2006.

[99] Ulrike Dackermann, Roman Elsener, Jianchun Li, and Keith Crews. A comparative study of using static and ultrasonic material testing methods to determine the anisotropic material properties of wood. *Construction and Building Materials*, 102:963–976, 2016.

[100] Ranjeet Kumar, Anil Kumar, and Girish Kumar Singh. Electrocardiogram signal compression using singular coefficient truncation and wavelet coefficient coding. *IET Science, Measurement & Technology*, 10(4):266–274, 2016.

[101] Yongmin Li and Cheung-Fat Chan. Code excited sample-by-sample gain adaptive coding for lossless compression of audio signals. In *2010 18th European Signal Processing Conference*, pages 482–486. IEEE, 2010.

[102] Qiyu Peng and Li-Qun Zhang. High-resolution ultrasound displacement measurement using coded excitations. *IEEE transactions on ultrasonics, ferroelectrics, and frequency control*, 58(1):122–133, 2011.

[103] Martin P Mienkina, Claus-Stefan Friedrich, Nils C Gerhardt, Wilko G Wilkening, Martin R Hofmann, and Georg Schmitz. Experimental evaluation of photoacoustic coded excitation using unipolar golay codes. *IEEE transactions on ultrasonics, ferroelectrics, and frequency control*, 57(7):1583–1593, 2010.

[104] Simon Triger, Jean-Francois Saillant, Christine EM Demore, Sandy Cochran, and David RS Cumming. Low-voltage coded excitation utilizing a miniaturized integrated ultrasound system employing piezoelectric 2-D arrays. *IEEE transactions on ultrasonics, ferroelectrics, and frequency control*, 57(2):353–362, 2010.

[105] Sheng-Wen Huang and Pai-Chi Li. Arbitrary waveform coded excitation using bipolar square wave pulsers in medical ultrasound. *IEEE transactions on ultrasonics, ferroelectrics, and frequency control*, 53(1):106–116, 2006.

[106] Sergio Malo, Sina Fateri, Makis Livadas, Cristinel Mares, and Tat-Hean Gan. Wave mode discrimination of coded ultrasonic guided waves using two-dimensional compressed pulse analysis. *IEEE transactions on ultrasonics, ferroelectrics, and frequency control*, 64(7):1092–1101, 2017.

[107] Christopher Charles Henry Guyott, P Cawley, and RD Adams. The non-destructive testing of adhesively bonded structure: a review. *The Journal of Adhesion*, 20(2):129–159, 1986.

[108] Richard Y Chiao and Xiaohui Hao. Coded excitation for diagnostic ultrasound: A system developer's perspective. *IEEE transactions on ultrasonics, ferroelectrics, and frequency control*, 52(2):160–170, 2005.

[109] Merrill I Skolnik. Introduction to radar. *Radar handbook*, 2:21, 1962.

[110] Steven G Kanzler and Michael L Oelze. Improved scatterer size estimation using backscatter coefficient measurements with coded excitation and pulse compression. *The Journal of the Acoustical Society of America*, 123(6):4599–4607, 2008.

[111] Y Takeuchi. An investigation of a spread energy method for medical ultrasound systems: Part one: Theory and investigation. *Ultrasonics*, 17(4):175–182, 1979.

[112] Matthew O'Donnell. Coded excitation system for improving the penetration of real-time phased-array imaging systems. *IEEE transactions on ultrasonics, ferroelectrics, and frequency control*, 39(3):341–351, 1992.

[113] Jonathan Jedwab and Matthew G Parker. A construction of binary golay sequence pairs from odd-length barker sequences. *Journal of Combinatorial Designs*, 17(6):478–491, 2009.

[114] Mingquan Wang, Shan Cong, and Shi Zhang. Pseudo chirp-barker-golay coded excitation in ultrasound imaging. In *2018 Chinese Control And Decision Conference (CCDC)*, pages 4035–4039. IEEE, 2018.

[115] Norman Katz, Mark Nelson, Michael Goldbaum, S Chaudhuri, and S Chatterjee. Detection of blood vessels in retinal images using two-dimensional matched filters. *IEEE Trans. Med. Imaging*, 8(3):263–269, 1989.

[116] Merrill Ivan Skolnik. Introduction to radar systems. *New York, McGraw Hill Book Co., 1980. 590 p.*, 1980.

[117] John C Bancroft. Introduction to matched filters. *CREWES Research*, 2002.

[118] RH Barker. Group sysnchronizing of binary digital systems. *Communication theory*, pages 273–287, 1953.

[119] R Turyn. On barker codes of even length. *Proceedings of the IEEE*, 51(9):1256–1256, 1963.

[120] Marcel Golay. Complementary series. *IRE Transactions on Information Theory*, 7(2):82–87, 1961.

[121] OP Sahu and Anil K Gupta. Measurement of distance and medium velocity using frequency-modulated sound/ultrasound. *IEEE Transactions on Instrumentation and Measurement*, 57(4):838–842, 2008.

[122] Imre Török and Rudolf Seller. Pulse compression in search radar. *Periodica Polytechnica Electrical Engineering*, 42(4):391–408, 1998.

[123] Mike JS Lowe, David N Alleyne, and Peter Cawley. Defect detection in pipes using guided waves. *Ultrasonics*, 36(1-5):147–154, 1998.

[124] Houman Nakhli Mahal, Peter Mudge, and Asoke K Nandi. Comparison of coded excitations in the presence of variable transducer transfer functions in ultrasonic guided wave testing of pipelines. In *Proceedings of the 9th European Workshop on Structural Health Monitoring, Manchester, UK*, pages 10–13, 2018.

[125] Peter Cawley, MJS Lowe, DN Alleyne, B Pavlakovic, and P Wilcox. Practical long range guided wave inspection-applications to pipes and rail. *Mater. Eval*, 61(1):66–74, 2003.

[126] Xiaojun Song, Dean Ta, and Weiqi Wang. A base-sequence-modulated golay code improves the excitation and measurement of ultrasonic guided waves in long bones. *IEEE transactions on ultrasonics, ferroelectrics, and frequency control*, 59(11):2580–2583, 2012.

[127] Zeng Fan, John Rudlin, Giorgos Asfis, and Hongying Meng. Convolution of barker and golay codes for low voltage ultrasonic testing. *Technologies*, 7(4):72, 2019.

[128] Jeena Joy, Salice Peter, and Neetha John. Denoising using soft thresholding. *International Journal of Advanced Research in Electrical, Electronics and Instrumentation Engineering*, 2(3):1027–1032, 2013.

[129] TH Gan, DA Hutchins, DR Billson, and DW Schindel. The use of broadband acoustic transducers and pulse-compression techniques for air-coupled ultrasonic imaging. *Ultrasonics*, 39(3):181–194, 2001.

[130] PJ Mudeg. Field application of the teletest; long-range ultrasonic testing technique. *Insight*, 43(2):74–77, 2001.

[131] MJS Lowe and P Cawley. Long range guided wave inspection usage–current commercial capabilities and research directions. *Department of Mechanical Engineering, Imperial College London: London, UK*, 2006.

[132] MG Silk and KF Bainton. The propagation in metal tubing of ultrasonic wave modes equivalent to lamb waves. *Ultrasonics*, 17(1):11–19, 1979.

[133] Ruiqi Guan, Ye Lu, Wenhui Duan, and Xiaoming Wang. Guided waves for damage identification in pipeline structures: A review. *Structural Control and Health Monitoring*, 24(11):e2007, 2017.

[134] Paul D Wilcox. A rapid signal processing technique to remove the effect of dispersion from guided wave signals. *IEEE transactions on ultrasonics, ferroelectrics, and frequency control*, 50(4):419–427, 2003.

[135] Wenbo Duan and Ray Kirby. A numerical model for the scattering of elastic waves from a non-axisymmetric defect in a pipe. *Finite Elements in Analysis and Design*, 100:28–40, 2015.

[136] A Demma, P Cawley, M Lowe, and AG Roosenbrand. The reflection of the fundamental torsional mode from cracks and notches in pipes. *The Journal of the Acoustical Society of America*, 114(2):611–625, 2003.

[137] Sridevi Katamaneni and D Elizbath Rani. Mainlobe width reduction using linear and nonlinear frequency modulation. In *2009 International Conference on Advances in Recent Technologies in Communication and Computing*, pages 918–920. IEEE, 2009.

[138] Juan Fu, Gang Wei, and Qinghua Huang. Barker coded excitation using lfm carrier for improving axial resolution in ultrasound imaging. In *2013 ICME International Conference on Complex Medical Engineering*, pages 150–153. IEEE, 2013.

[139] Armin Walter Doerry. Generating nonlinear fm chirp waveforms for radar. Technical report, Sandia National Laboratories, 2006.

[140] Jinbum Kang, Yeajin Kim, Wooyoul Lee, and Yangmo Yoo. A new dynamic complex baseband pulse compression method for chirp-coded excitation in medical ultrasound imaging. *IEEE transactions on ultrasonics, ferroelectrics, and frequency control*, 64(11):1698–1710, 2017.

[141] Yasin Kumru, Kerem Enhoş, and Hayrettin Köymen. Pulse coding with complementary golay sequences for signal to noise ratio improvement in ultrasound mammography. In *Proceedings of Meetings on Acoustics 176ASA*, volume 35, page 020002. Acoustical Society of America, 2018.

[142] C Leśnik. Nonlinear frequency modulated signal design. *Acta Physica Polonica A*, 116(3):351–354, 2009.

Appendix A.

Appendix

```
file1= dir(fullfile(root, '*.TIM'));
fset1 = zeros(length(file1), 1);
for ii = 1:length(file1)
fname = file1(ii).name;
fset1(ii) = str2num(fname(1:end-4));
end
[ifset1] = sort(fset1);
for ii = 1:length(ifset1)
cur_index_r1 = ifset1(ii);
cur_name_r1 = fullfile(root1, file1(cur_index_r1).name);
r_1(:, ii)= dlmread(cur_name_r1, '', 0, 0);
end
fileR1 = fopen('R1.TIM','w');
fprintf(fileR1,'%1s\r\n','User specified excitation file -
   Ring1.tim');
fprintf(fileR1,'%1s\r\n','8');
fprintf(fileR1,'%1s\r\n','1');
fprintf(fileR1,'%1s\r\n','0');
fprintf(fileR1,'%1s\r\n','1');
fprintf(fileR1,'%1s\r\n','0.2');
fprintf(fileR1,'%1s\r\n','251');
nbytes_r1 = fprintf(fileR1,'%1.10f %2.10f %3.10f %4.10f
   %5.10f %6.10f %7.10f %8.10f\n',r_1');
fclose(fileR1);
```